LBL-20446
c.2

Lawrence Berkeley Laboratory
UNIVERSITY OF CALIFORNIA

CHEMICAL BIODYNAMICS DIVISION

RECEIVED
LAWRENCE
BERKELEY LABORATORY

OCT 13 1986

LIBRARY AND
DOCUMENTS SECTION

DEVELOPMENT AND APPLICATION OF A HIGH POWER,
BROADLY TUNABLE, PICOSECOND SOURCE

H. Nathel
Ph.D. Thesis

June 1986

TWO-WEEK LOAN COPY
This is a Library Circulating Copy
which may be borrowed for two weeks.

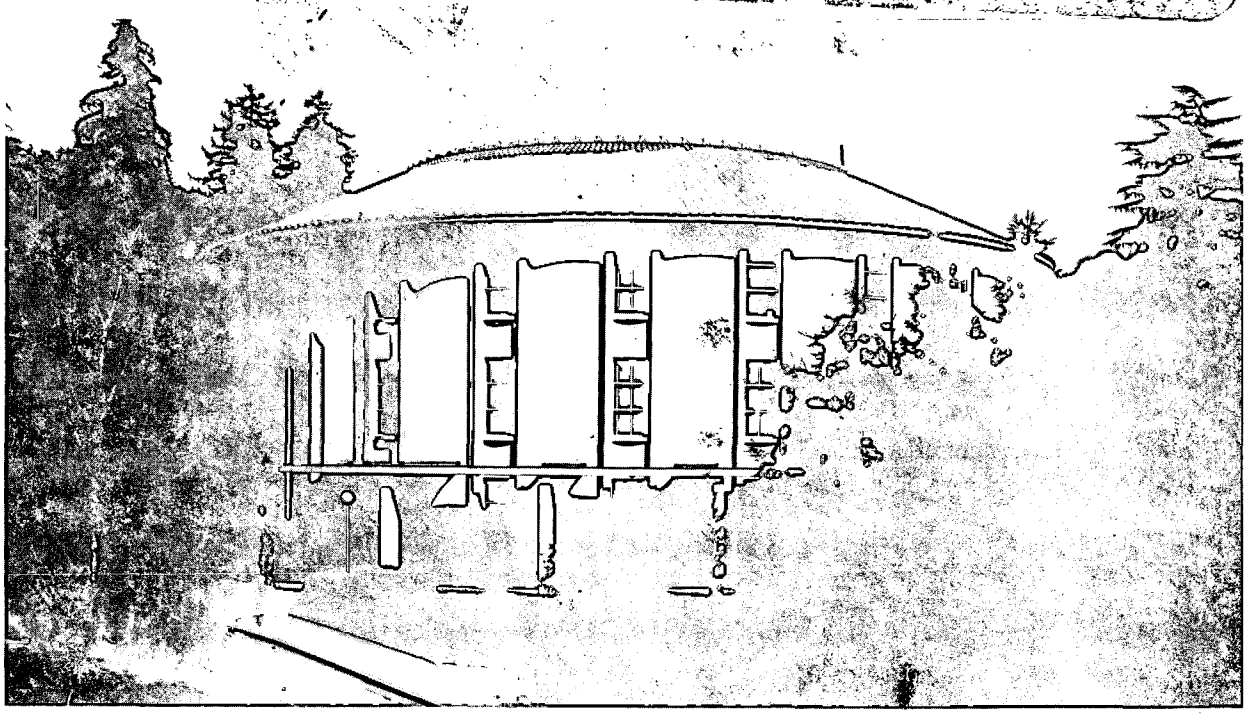

Prepared for the U.S. Department of Energy under Contract DE-AC03-76SF00098

LBL-20446
c.2

DISCLAIMER

This document was prepared as an account of work sponsored by the United States Government. While this document is believed to contain correct information, neither the United States Government nor any agency thereof, nor the Regents of the University of California, nor any of their employees, makes any warranty, express or implied, or assumes any legal responsibility for the accuracy, completeness, or usefulness of any information, apparatus, product, or process disclosed, or represents that its use would not infringe privately owned rights. Reference herein to any specific commercial product, process, or service by its trade name, trademark, manufacturer, or otherwise, does not necessarily constitute or imply its endorsement, recommendation, or favoring by the United States Government or any agency thereof, or the Regents of the University of California. The views and opinions of authors expressed herein do not necessarily state or reflect those of the United States Government or any agency thereof or the Regents of the University of California.

DEVELOPMENT AND APPLICATION OF A HIGH POWER, BROADLY TUNABLE, PICOSECOND SOURCE

Howard Nathel
Ph.D. Thesis

Lawrence Berkeley Laboratory
University of California
Berkeley, California 94720

June 1986

This work was supported by the Assistant Secretary for Energy Research, Office of Basic Energy Sciences, Division of Chemical Sciences of the U.S. Department of Energy under Contract Number DE-AC03-76SF00098.

DEVELOPMENT AND APPLICATION OF A HIGH POWER, BROADLY TUNABLE, PICOSECOND SOURCE

Howard Nathel

Abstract

The development of a pulsed, active/passive, mode-locked, Nd:YAG laser system is described in detail. The careful design and construction of the system resulted in very reliable and stable operation. A full appreciation for the mode-locking process aided in the understanding of important factors that contributed to the excellent performance of the system, especially the implementation of active mode-locking.

Careful spectral and temporal characterization of the single pulses as a function of position in the mode-locked pulse train resulted in exciting discoveries. Transform-limited behavior of the output pulses of the system was attained in two ways. Pulses selected early in the mode-locked pulse train exhibityed near transform-limited behavior. Use of an intracavity etalon resulted in true transform-limited behavior for these pulses while also affording the experimenter the choice of higher spectral or temporal resolution. By selecting pulses early in the pulse train, nonlinear effects such as self-phase modulation, which destroys the coherence of the mode-locked pulses, could be avoided.

The phenomenon that as the frequency spread of the pulses, after the peak of the mode-locked pulse train, exceeded the gain-bandwidth of the lasing medium, pulse shortening was discovered. Eventually,

pulses at the extreme end of the mode-locked pulse train, with pulse durations as short as 2ps to 3ps were measured. The corresponding spectral bandwidths of these pulses were between 6.0 cm^{-1} and 6.5 cm^{-1}. These pulses are at or near the Fourier transform-limit for Gaussian pulses and are the shortest pulses ever observed from a mode-locked Nd:YAG laser without external pulse compression techniques being employed. The idea of intracavity, nonlinear pulse compression has been proposed to explain these gain-bandwidth limited pulses. The method involves the nonlinear index of refraction of materials inside the laser cavity feeding energy into frequency elements outside the gain-bandwidth of the lasing medium via self-phase modulation. This results in a frequency sweep (i.e. chirp) of the pulse and only those freqency elements that lie under the gain-bandwidth of the amplifying medium are amplified in time (i.e. those frequency elements at the center of the pulse). As the frequency sweep continues to increase, the pulse duration decrease until the limit of the Fourier transform of the gain-bandwidth is reached. This explanation describes the observed phenomenon quite adequately.

Taking advantage of the high peak powers attainable from the laser system, a simple third harmonic (355nm) pumped, single pass, travelling wave, optical parametric source (OPS) was constructed in order to extend the tunability of such a system across nearly the entire visible and near infrared spectral regions. Spectral, temporal, and spatial characterizations were performed on the output pulses of the device, and conditions leading to transform-limited

operation were ascertained. A detailed systematic study had never been performed to date on such a system. Our results could be explained by the theories of optical parametric fluorescence and amplification.

The broad, continuous tunability of the OPS was exploited in the study of the wavelength dependence of rotational reorientation dynamics of rhodamine 6G (R6G) in ethanolic solutions using picosecond time-resolved, fluorescence depolarization techniques. It was determined that wavelength had no effect on the rotational reorientation dynamics of the system under investigation on timescales equivalent to or much less than the rotational lifetime of the solute. This seemingly negative result addresses the role of vibronic excitation and librational motions in such studies, and also lends support to the validity of the compartability of results determined by different experimental techniques.

TABLE OF CONTENTS

Abstract 1

Acknowledgments iii

Chapter I. Introduction 1

A. Motivation 1

B. Laser Development Effort 6

C. Experiments Using the Improved Picosecond Laser Sources 11

Chapter II. Pulsed, Active/Passive Mode-Locked, Nd:YAG Laser System 20

A. Background 20

B. Passive Mode-Locking 27

C. Active Mode-Locking 39

D. Resonator Design 50

E. Operation and Performance 87

F. Amplification 124

Chapter III. Temporal and Spectral Characterization of the Pulsed, Active/Passive Mode-Locked, Nd:YAG Laser 132

A. Background 132

B. Experimental 146

C. Results and Discussions 153

D. Interpretation, Conclusions, and Comparisons . . . 183

Chapter IV. Optical Parametric Source 201

A. Background 201

B. Nonlinear Optical Crystal Configurations 207

C. Experimental 214

D. Results 221

E. Discussion 245

F. Conclusion 266

Chapter V. Rotational Reorientation Dynamics of Rhodamine 6G as a Function of Excitation Wavelength 274

A. Introduction 274

B. Experimental 277

C. Results and Discussion 285

D. Conclusion 292

Appendix I 293

References 294

ACKNOWLEDGMENTS

I view the culmination of my graduate work as a collaborative effort. The collaboration begins with my parents. They have supported me in every way possible. My father's interest in my work and success, as well as the pride he has taken in me, have been a great boom to my ego. From my mother, I have inherited an appreciation of nature and beautiful things, very important characteristics of a successful scientist. My grandparents have instilled a heritage in me. One of which I am proud. They have also shown me that hard work is rewarding and that adversities are surmountable. I thank my brothers for showing me that there are other things in life outside of science. I thank Glenn Gold and Anne Hecht for being like family to me for the past twelve years, disregarding the distance between us.

Throughout my graduate student career, I have had the pleasure of working and interacting with many interesting and unique characters. My research director, John Clark, through his continous encouragement, helped me dispell all of my insecurities which gave me the confidence to become a sound experimentalist. I owe much of how I conduct myself in a laboratory to the influence of Dennis Guthals. I have always emulated his approach to practical problems. Laura Philips and Steve Webb played an instrumental role in the study of the excitation wavelength dependence of rotational reorientation dynamics of rhodamine 6G in solution. More importantly, Laura and Steve have been a constant source of friendship and companionship despite my ups and downs. Doug Anthon collaborated with me on the development of the

laser system and optical parametric source. I thank him for "making a big deal" about things I would not have. Sheila Yeh was of great assistance in characterizing the sources. More recent additions to the group who helped to liven things up were Marion Helfand and Steve Finkel, both of whom performed many thankless tasks such as figure preparations.

Many members of Professor Yuan Lee's research group have become good friends and collaborators. In particular Tim Minton added a new dimension (his tongue) to working hard. Paul Weiss, Rick Brudzynski, Gary Robinson, Bob Continetti, Kerry Busarow, Alec Wodtke, Barbara Balko, Mike Covinsky, and Eric Hintsa were not only good friends, but lousy softball players. To Gil Nathanson and Marion Helfand, I wish good luck and look forward to future collaborations. Special thanks go to Ann Weightman for encouragement, friendship, and assistance in completing this manuscript.

I would like to thank Professors Yuan Lee and Roger Falcone for demonstrating their confidence in my technical abilities. I look forward to future collaborations with both of them. I would also like to thank Mark Maestre for showing me that there did indeed exist a more cynical scientist than myself.

This thesis could not have been completed without the love and support from my wife's family, especially her parents. Their tolerance of my eccentricities is greatly appreciated.

Special thanks go to my best pal, Mathilde, whose unending love and devotion are an inspiration at all times.

Last, but most important of all, I wish to thank my wife, Lisa. Her ability to put things in the proper perspective have helped me to get through what I thought were difficult times. To her, this thesis, as am I, are dedicated.

I. Introduction

A. Motivation

Over the past two decades, the continuing quest for ultrashort laser pulses as probes of ultrafast chemical, biological, and physical events has led to the development of many new laser sources. Both novel technical achievements as well as refinements of existing technologies have aided in these developments. One of the earliest and most commonly used picosecond laser source has been the pulsed, mode-locked, Nd:YAG laser. The popularity of such mode-locked, solid-state lasers is due in part to the fact that a large amount of the developmental work necessary for the design and construction of these sources has been carried out as part of the substantial research and development efforts in the laser fusion program.

A major disadvantage of pulsed, mode-locked, solid-state lasers is the occurrence of large-scale amplitude fluctuations in the output of passively mode-locked laser oscillators. These fluctuations are a direct result of the intrinsic randomness of the passive mode-locking process (see Chapter II). Even when a great effort is made to stabilize the laser cavity, well mode-locked pulse trains typically are not produced more than 80 percent of the time.

In order to conduct picosecond time resolved spectroscopic experiments in an accurate and consistent fashion, it is important to have a reliable laser system with reproducible output pulses. When this work was begun six years ago, the choice of picosecond excitation sources were between pulsed, mode-locked, solid-state lasers, the newly

developed synchronously-pumped dye laser, and passively mode-locked dye lasers. The choice of a pulsed, mode-locked, solid-state laser was made with the notion that sufficient expertise existed to avoid the substantial development effort typically associated with the application of emerging technologies Nd:YAG (Yttrium Aluminum Garnet doped with Neodymium) (Nd:$Y_3Al_5O_{12}$) was chosen over Nd:glass as the lasing medium because higher repetition rates (10 Hz as opposed to one pulse per minute) were of greater value than shorter pulses (30 ps as opposed to 5 ps) for the planned experiments.

At the time, the only commercially available high repetition rate pulsed, mode-locked, Nd:YAG laser was the Quantel model YAG 400. Unfortunately, it turned out that this lower suffered from all the problems that are inherent in a purely passively mode-locked system. A major effort was required to construct a reliable laser system. Most of the electrical components and laser heads of the YAG 400 laser system were retained. All other components were either designed and constructed in our laboratory or purchased from other vendors.

One of the main reasons requiring the stabilization of the laser was that the system was to be used to pump various optical parametric sources (OPS). These OPS would serve to extend the spectral coverage of the laser far beyond the harmonics of the Nd:YAG (fundamental = 1064nm, 2nd = 532nm, 3rd = 355nm, and 4th = 266nm) and provide continuous tunability. Because the parametric interaction is a nonlinear optical process, fluctuations in the pump laser intensity are greatly amplified in the output of the OPS. In order for proper

characterization and utilization in various experiments, these sources needed to be as stable as possible. In certain experiments, the picosecond spectroscopic technique employed involved nonlinear optical processes as well. The desire to use such techniques as coherent anti-stokes Raman spectroscopy (CARS) and multiphoton ionization (MPI) imposed stringent stability requirements on the laser system.

One of the major advantages of using a pulsed, mode-locked, solid-state laser is the high peak intensity available, allowing the use and study of nonlinear optical processes. However, if proper care is not taken, these high peak intensities become a disadvantage. The proper handling of these peak powers is an extremely difficult task. Large scale amplitude fluctuations in the output of the oscillator make the task even more difficult. The suppression of certain nonlinear optical processes is necessary if other processes are to be observed and used in experiments. One such process that not only ruins experiments but also destroys the experimental apparatus is optical damage.

When working with high intensity picosecond pulses, one quickly learns the limitations imposed by optical damage. If proper generation and manipulation of the radiation is to be achieved, and if the observation of weak nonlinear effects in materials and samples is to be successful, then optical damage must be eliminated. The peak power available from mode-locked laser systems can greatly exceed that of Q-switched and other longer-pulsed lasers. However, because the energy per pulse and pulse duration of mode-locked lasers are significantly less, the threshold for optical damage in most materials is consider-

ably higher with picosecond pulses than with longer pulses.[1,2] This has enabled the observation of many higher order nonlinear effects that would have been difficult to observe using other laser sources. However, there is a fine line between the threshold conditions for many nonlinear optical interactions and the onset of optical damage. Fluctuations in the output of picosecond lasers blurr this fine line, so it is important to reduce these amplitude fluctuations.

Great care must be employed when using such high peak power sources. Not only must the laser output itself be very stable, but also the cleanliness and basic maintenance of all optics, laser rods, and nonlinear optical materials must be impeccable. Optical damage results from four basic phenomena: thermal damage in strongly absorbing materials; damage arising from absorptions at inclusions, other impurities, or bulk defects; surface damage due to dirt, cracks, scratches, or other surface imperfections; and intrinsic bulk damage in transparent materials due to avalanche or multiphoton ionization, usually accompanied by self-focusing.[2]

Self-focusing is caused by the nonlinear index of refraction. At very high optical intensities the index of refraction of materials become a function of the electric field. An intense optical beam with a Gaussian beam profile will produce an incremental index change that is a maximum at the center of the beam and tapers off to zero at the edge of the beam. This can cause a lens-like effect that can lead to self-focusing of the beam. Self-focusing is a twofold problem,

destroying both experiments and apparatus. Moreover, once self-focusing begins, it is an uncontrollable effect that can cause damage to all optical components down line from the point of initiation. For high repetition rate picosecond lasers any observation of self-focusing usually means that damage has already occurred. Therefore elimination of self-focusing should be a top priority. With the appropriate maintenance of optical equipment and by always ensuring that all laser-beam diameters are sufficiently large to avoid filament formation upon passage through materials, self-focusing can be controlled.

Since the effects of even a small degree self-focusing is to drastically change the intensity profile of the laser beam, characterization of nonlinear optical effects becomes even more difficult. For example, different nonlinear optical effects often have similar thresholds. Stimulated Raman scattering is often accompanied by self-focusing and self-phase modulation. This can complicate the outcome of an experiment, making the interpretation of results more difficult. A carefully designed experiment will attempt to isolate the desired effect, or at least control other competing effects in a predictable way. As will be pointed out later in the study of self-phase modulation of ultrashort light pulses, self-focusing makes a complete analysis difficult and is often the limiting factor in exploiting the modulation in a positive way.

Thus, in order to conduct a wide variety of nonlinear optical experiments and developmental projects it was necessary to improve and

stabilize the available laser system. Once the system was designed, constructed, and stabilized, the system was carefully characterized. The characterization led to the observation of a number of novel, useful, and interesting effects.

B. Laser Development Effort

A major part of this thesis (Chapter II) will describe the development of a reliable pulsed mode-locked Nd:YAG laser-amplifier system. This thesis also includes a detailed description of how the high peak powers attainable from this laser system enabled the extension of the temporal resolution and spectral ranges normally associated with such a system (Chapters III and IV). These extensions helped to overcome many of the shortcomings typically associated with mode-locked, Nd:YAG lasers such as relatively long pulsewidths, and the limitation of available frequencies to the harmonics of the fundamental of the Nd:YAG. These developments, when combined with the well known advantages of mode-locked Nd:YAG lasers, such as high peak powers, moderately high repetition rates, transform-limited operation with the use of intracavity etalons,[3,4] and a high degree of amplitude stability[4,5,6] when active and passive mode-locking are utilized, make the system described here a very attractive source for a wide range of picosecond spectroscopic investigations.

The techniques and results decribed in Chapter II enable the problem of amplitude stability in the output of the mode-locked, Nd:YAG laser oscillator to be solved. Once this problem was overcome

the laser development effort concentrated on improved techniques for the handling and manipulation of high power optical pulses. The establishment of expertise in the handling and manipulation of high peak power picosecond pulses was necessary if proper use and thorough characterization of the system were to be carried out. The laser system described in this work is an ideal source for many different chemical physics and nonlinear optics experiments because of the high degree of energy amplitude stability of the pulse trains (less than two percent shot-to-shot variation) and the high peak intensities (greater than 10^{13} watts/cm^2 when focused to a 0.1mm spot diameter) achievable.

A common phenomenon occurring in high-power solid-state, mode-locked lasers is self-phase modulation.[3,4,7-13] Self-phase modulation results from the interaction of high-intensity, picosecond pulses with the nonlinear index of refraction of materials inside the laser cavity, especially the lasing medium. Self-phase modulation is known to produce progressive spectral and temporal broadening of successive laser pulses in the mode-locked pulse train. The spectral broadening is typically due to a frequency sweep (i.e., chirp) imposed on the laser pulseby the self-phase modulation process.

Measurements tht involved the simultaneous characterizaton of the spectral and temporal properties of the output pulses of the Nd:YAG laser developed here lead to some unique results. It was observed that as the frequency spread of a mode-locked pulse approaches and exceeds the gain-bandwidth of the lasing medium, there occurs a

narrowing of the pulse duration for each successive round trip transit through the laser cavity. These observations formed the basis for a novel, intracavity nonlinear pulse compression scheme. It has been demonstrated that pulses as short as 2 to 3 ps with spectral bandwidths of $6.0cm^{-1}$ to $6.5cm^{-1}$ (near transform-limited) can be generated from the Nd:YAG laser system described in this thesis simply by selecting a single pulse late in the mode-locked pulse train.

In the past, self-phase modulated pulses have been a hindrance in the study of coherent phenomena. In the present work, self-phase modulation has been constructively exploited to produce pulses with duration close to the theoretical limits available using Nd:YAG as the active medium. It should be noted that the technique is extremely simple to implement. It does not require the use of the technique (adapted from radar technology) of inducing a positive frequency sweep in a picosecond pulse and subsequent pulse compression by propagation through a negatively dispersive delay line. The technique that is most commonly used to achieve optical pulse compression.[14-22] Because single mode optical fibers and grating pairs are avoided, the technique discovered in this work offers considerable advantages for the compresion of high-energy pulses. Chapter III will elaborate on how the thorough temporal and spectral characterization of the laser system led to the discovery of the pulse compression scheme. An explanation of the physical mechanisms responsible for the pulse shortening is also given.

Once the design, construction, stabilization, and characterization of the pulsed active/passive mode-locked, Nd:YAG oscillator-amplifier was completed, it became feasible to use and exploit the high peak intensities of single amplified picosecond pulses. Construction of a simple, single pass, optical parametric source (OPS) that could be continuously tuned throughout nearly the entire visible spectrum became the next goal of the research described in this thesis (Chapter IV). Owing to the high peak intensities from the laser system used to pump the device, useful output energies could be generated upon a single pass of the pump pulse through two nonlinear optical crystals. Unlike optical parametric oscillators[24,25] (OPO) which use the output of Q-switched lasers as the pump source, there was no need to build an external resonator to obtain suitable conversion efficiencies. Need for an external resonator would have destroyed the simplicity of the device by complicating the alignment and tuning. The use of an external resonator would have also required a variety of broadband dichroic mirrors to allow passage of the pump wavelength and output coupling of the desired OPS wavelength, eliminating the ability to rapidly tune across the entire visible spectrum. The OPS is much simpler than the various dye laser alternatives that might have been attempted. With a single pump wavelength at an OPS, greater continuous tunability can be achieved with a single set of nonlinear crystals than can be achieved with many different pump frequencies and a number of dyes.

The broadly tunable source is based on spontaneous optical parametric fluorescence and high gain optical parametric amplification[26-34] in potassium dihydrogen phosphate (KDP) pumped by single, picosecond, third harmonic (λ_3 = 355nm) pulses derived from the pulsed, active/-passive mode-locked, laser-amplifier system. Broad spectral bandwidth spontaneous parametric fluorescence is produced by the generation of photon pairs at frequencies ω_1 and ω_2 such that $\omega_3 = \omega_1 + \omega_2$. Parametric fluorescence colinear with the pump beam is amplified and spectrally narrowed via optical parametric amplification in Type II phase-matched KDP. Pump power densities necessary for stable operation are 2×10^9 watts/cm^2, which is easily achievable from the laser system. Visible light continuously tunable from 650nm to 450nm and near infrared light tunable from 780nm to 1675nm have been achieved from this device via simple angle tuning. This scheme is surely one of the simplest, efficient, broadly tunable picosecond sources demonstrated to date. With one or two more nonlinear conversion steps, the tunability of such a system can be extended to provide pulses which are nearly continuously tunable over the spectral range from 220nm to 1675nm.

A large portion of Chapter IV is devoted to a description of the construction and characterization of the OPS. Optimum nonlinear optical crystal configurations, both for efficient third harmonic conversion and optical parametric conversion, are discussed in detail. Certain observed performance characteristic, and conditions leading to them are explained and discussed. Emphasis should be

placed on the fact that once a stable diffraction limited pumping source is available, the spectral, temporal, and spatial qualities and tunability achievable with an OPS is excellent. The output of such a device can be used to conduct a variety of picosecond time resolved fluorescence and nonlinear optical experiments.

C. Experiments Using the Improved Picosecond Laser Sources

the major part of this thesis is dedicated to a detailed discussion of the development and characterization of the pulsed active/passive mode-locked Nd:YAG laser-amplifier system and of the OPS. The overall system in its final form has been the work horse of the laboratory in which the present work was conducted. Not only was it used in the developmental project, discussed in this thesis, but was also used on the excitation source for a picosecond, time-resolved emission apparatus[35] that employs an ultrafast streak camera for fluorescence detection and temporal analysis.

The ultrafast streak camera also provides a convenient means for immediate and direct observation of picosecond laser pulses. Single pulse temporal measurements, when performed simultaneously with single pulse spectral measurements, provide the opportunity to directly observe the quality of picosecond laser pulses as evidenced by their approach to transform-limited behavior. The laser performance can be conveniently optimized since the temporal and spextral behavior of the output pulses can be monitored in real time. The discovery of intracavity nonlinear pulse compression was made possible because of

the simultaneous, real time temporal and spectral measurements allowed by this system. Also, the effects of various operating conditions on the performance of the OPS were studied using this apparatus.

Many of the time-resolved emission experiments performed using this apparatus used only the harmonics of the 1064nm Nd:YAG fundamental output for sample excitation. These investigations include "Picosecond Studies of Excited-State Proton-Transfer Reactions"[36] and "Picosecond Studies of Electronically Excited Molecules in Solution."[37] However, the broad, continuous tunability of the OPS over nearly the entire visible spectrum, when combined with the excellent time resolution and sensitivity of the streak camera detector, allowed for other unique and novel experiments. The OPS was used a the study of the effect of excess excitation energy in excited electronic states of molecules in solution,[38] in particular Rhodamine 6G in ethanol. From the results of these experiments it was possible to determine the effect of the relaxation and dissipation of excited state vibrational energy on the rotational reorientation time and anisotropy. The influence of vibrational excitation on the direction of the excited state emission transition moment and the effect of local solvent heating have been evaluated. Details and results of these experiments are discussed in Chapter V.

The broad spectral range covered by the OPS was also used in the study of energy flow in phycobilisomes.[39] The photosynthetic antenna system known as a phycobilisome consists of a macromolecular complex containing many chromophores. This antenna system funnels light to

the photosynthetic reaction center, in which light is converted to chemical potential energy. Energy transport in these systems is complex. One series of experiments was designed to measure interdisk energy transfer between the two specific structural units of the WT6701 phycobilisome, phycoerythrin, and physocyanin. A comparative study was conducted using the WT6701 phycobilisomes and mutant CM25 phycobilisomes. Using the second harmonic of the mode-locked Nd:YAG laser as the excitation source, the rise time of emission from the terminal emitter of the phycobilisome was measured, allowing the energy transfer time to the terminal emitter in each phycobilisome to be determined. Because the mutant does not contain any phycoerythrin subunits, whereas the WT6701 phycobilisome contains an average of 1.6 phycoerythrin discs, the CM25 phycobilisome has a shorter channel for excitation transfer to the terminal emitter. The shorter pathway in the CM25 is manifested as a faster rise time of the emission from the terminal accepting unit.

A second series of experiments involved only the WT6701 phycobilisome. The experiment exploited the tunability of the OPS to avoid any excitation of the phycoerythrin chromophores. The experiment was virtually the same as the comparative study between WT6701 and CM25 phycobilisome, but relied solely on the study of the WT6701 phycobilisome. In both cases, the results were similar, and the transfer time was determined to be 25 ps between the phycoerythrin and phycocyanin.

Knowing the energy transfer times between the two chromophores, and again utilizing the tunable output of the OPS, further investigations were conducted to determine the rate and mechanism of energy flow within a single phycobilisome unit, in this case phycoerythrin. Instantaneous rise times of the emission from phycoerythrin independent of the nature of absorbing chromophore were observed. The data suggests very rapid internal energy transfer within a single phycoerythrin subunit. These results confirmed that the rate-limiting step of energy flow processes in phycobilisomes is interdisk rather than intradisk energy transfer.

As mentioned earlier, a certain amount of expertise must be developed to properly handle the high peak powers associated with pulsed, mode-locked solid-state lasers. Problems arising from both thermal lensing of laser rods and self-focusing in optical materials must be eliminated or controlled if optical damage is to be avoided. Four projects that will not be described in this thesis contributed to the expertise developed in the routine handling and manipulation of the high peak intensity pulses. Normal fundamental (1064nm) pulse energies used for experiments ranged from 5mJ to 15mJ. In the four projects to be briefly described fundamental pulse energies ranged from 50mJ to 100mJ.

The first project was the design and construction of a colinear, double-pass amplifier based on a polarization rotation method.[4] Amplification factors of 200 were achievable with this method with maintenance of very good beam quality. Details of the amplifier will

be discussed in Chapter II. The other projects used multiple amplifiers placed in series to achieve high output energies. The first of these projects, conducted jointly with Quantel International of Santa Clara, California required generations of 60mJ of second harmonic (532nm) light to pump a short cavity dye laser-amplifier system.[40] Maintenance of excellent beam quality was necessary to ensure optimal performance of the system and prevent optical damage to both pump laser and dye laser-amplifier components.

The other developmental project requiring high energy outputs of the fundamental, second, and third harmonic of the laser was the demonstration of a laboratory scale picosecond soft x-ray source conducted jointly with Dr. David J. Nagel of the Naval Research Laboratory.[41] The picosecond soft x-ray source was produced via a laser generated plasma. Intensities in the range of 10^{12} to 10^{13} watts/cm^2 were necessary for efficient production of the x-rays. Ultrashort x-ray bursts with energies up to 1.5 Kev were generated by focusing any of the three harmonics of the laser-amplifier system onto a solid aluminum target. The spectral and spatial characteristics of the x-ray bursts were monitored using various crystal and grating spectrographs and x-ray pinhole cameras, respectively. Despite the fact that such x-ray bursts are not coherent, picosecond x-ray generation could lead to important developments in x-ray lithography, picosecond x-ray absorption and emission spectroscopy, and picosecond, time-resolved EXAFS.

In experimental studies of unimolecular reaction dynamics performed in conjunction with Professor Yuan T. Lee's group the laser-amplifier system has been arranged in its present and perhaps final form. The amplified, single, 1064nm pulse is beam split and amplified again in independently controllable beam lines to provide pump and probe pulses at different wavelengths. The pump and probe beams are time delayed with respect to one another via an optical delay line. The first experiments along these lines required generation of large quantities of third harmonic (355nm) light as a detection probe (using nonresonant, multiphoton ionization) for toluene produced by the isomerization of cycloheptatriene (CHT) following excitation of the CHT with fourth harmonic (266nm) light. It was the goal of this research to directly observe the rate of isomerization of excited cycloheptatriene to toluene. Work is presently being continued along these lines in the study of secondary dissociation reactions and unimolecular reaction dynamics of radicals. Both the harmonics of the laser and the tunable outputs of various OPS's are being used as excitation and detection wavelengths. Resonant multiphoton ionization of atoms is being employed as the detection probe.

From the above, the brief discussion of the developmental projects and scientific investigations carried out using the laser system described in this thesis, it should be obvious that the system has developed into an extremely versatile tool. In order to emphasize the versatility of the system a comparison with other available picosecond

laser systems is of interest. Any form of ultrashort pulse formation can be a very trying and difficult task because of the great care and patience that must be employed with such state-of-the-art systems. The main advantage of a pulsed active/passive mode-locked, Nd:YAG laser is that extremely high peak intensities can be generated with great amplitude spectral, and temporal stability at moderate repetition rates. Therefore simple Type I and Type II optical parametric conversion schemes[29-31,42,43] using the harmonics of the laser can be employed to expand the tunability of such a system across the infrared, near infrared, visible, and near ultraviolet regions of the spectrum. The tunability can be extended even further into the ultraviolet by mixing the outputs of such devices with the harmonics and Raman shifted output of the harmonics in other nonlinear optical crystals.[44,45] Great care is necessary for the spatial qualities of such output beams to be sufficient for high conversion efficiencies. With good beam quality conversion efficiencies of approximately 10 percent leading to outputs of hundreds of microjoules can be achieved. For picosecond pulse durations, such pulses energies are certainly high enough to permit many types of experiments.

In contrast, picosecond dye laser systems, which typically produce pulses with shorter pulse widths, cannot provide the same energies as the Nd:YAG, OPS systems. Both synchronously pumped dye lasers[46-48] and short cavity dye lasers[40] require sophisticated dye amplifier systems to achieve pulse energies greater than 1mJ. Such amplifiers systems often require a separate, high-power laser system as the

amplifier pumping system, necessitating a large equipment expenditure. Complicated timing and synchronization equipment, both electrical and optical, is required to minimize the jitter between the oscillator and amplifier chains. The argument that the repetition rate of a synchronously pumped dye laser (~100 MHz) is a great advantage over a pulsed solid-state system is not entirely valid. Because of the trade off between output energy and repetition rate, unless the amplifier chain is pumped by a metal vapor laser or complicated regenerative amplifier,[49] high output energy operation of these dye lasers is limited to the tens of Hertz repetition rates of the Q-switched solid-state lasers used to pump the amplifiers.

The difficulty in achieving stable, single-mode, narrow-linewidth operation from an amplified short cavity dye laser makes it an unattractive alternative for applications that require these characteristics. Mode walk off and multimode operation are difficult to suppress. Picosecond dye laser pulses with energies in the millijoule range[40] can be generated with such a system. However, the repetition rate is no greater than the pulsed mode-locked Nd:YAG laser-amplifier system used as the pump source. Also, as is the case with all dye lasers, the tuning range for any one dye and pump wavelength is never greater than fifty nanometers in contrast to the several hundred nanometer range of an OPS.

The major limitation of pulsed mode-locked Nd:YAG laser systems, once the problem of amplitude instability is overcome, is the longer pulse durations generated from such systems. Typical pulse widths are

approximately 30ps. Both mode-locked Nd:Glass laser systems and certain dye laser systems can produce pulses as short as 2ps to 5ps. Employing intracavity pulse compression techniques,[22,23] subpico-second pulses can be generated. The shortest pulses reported from amplified, pulsed mode-locked Nd:YAG laser systems have been 5ps from a regenerative amplifier with a saturable absorber placed in the resonator,[50] 12ps from passively mode-locked oscillator with an intracavity etalon,[3] and 7ps from a self-injected Nd:YAG laser with a saturable absorber placed in the cavity.[51] Other than the intracavity etalon technique, the other two techniques require sophisticated alignment procedures with numerous extra optical components and electrical timing circuits. The discovery of intracavity nonlinear pulse compression in the laser system described in this thesis is a far simpler method of generating shorter, less than 10ps pulses from a pulsed mode-locked Nd:YAG laser. Pulse durations between 2ps to 5ps have been observed. These are the shortest pulses reported to date from this type of laser, and were achieved without the use of any extra complicated devices.

Hopefully, future experiments will exploit the discoveries and developments described in this thesis. Researchers who use pulsed mode-locked, Nd:YAG laser-amplifier systems should view these systems with new vigor. These systems are certainly far from being obsolete. They can be extremely versatile and unique if appropriate care is taken in their design, construction, and operation.

II. Pulsed, Active/Passive Mode-Locked, Nd:YAG Laser System

A. Background

Pulses of picosecond duration are obtained from solid-state lasers by mode-locking, a technique by which the longitudinal modes of the laser cavity are locked in phase with one another. Theoretically, pulse widths on the on the order of the Fourier Transform of the gain bandwidth of the laser should be attainable.[52]

The output of a free running laser consists of both longitudinal and transverse modes. These oscillations have no fixed amplitude or phase relationship with respect to one another. The radiation emitted from such a free running laser is thus the result of constructive and destructive interference between all the oscillating modes. For the sake of simplicity, consider the axial mode properties only for the TEM_{00} (lowest order transverse electric-magnetic field) tranverse mode of the laser resonator. In a typical laser cavity, with Nd:YAG as the amplifying medium, there are several thousand axial modes that fall within the frequency bandwidth for which operation is above the threshold for lasing (i.e. where the gain of the medium exceeds the losses of the resonator).

In order to be complete, the discussion of laser emission must take place in both the frequency and time domain. In the frequency domain, the intracavity laser radiation consists of many discrete spectral lines determined by the axial mode spacing c/2L, where c is the speed of light and L is the length of the resonator. For a free running laser, oscillation of such modes is independent of one another

and the phase relationships between them are random. In the time domain, laser emission is characteristic of thermal noise.

Forcing the oscillating modes to maintain a fixed phase relationship with respect to one another causes the output of the laser to vary in a well-defined manner. Such a laser is said to be "mode-locked" or "phase locked", and exhibits an intensity versus output frequency spectrum that has a Gaussian distribution. In the time domain the output pulse also has a Gaussian distribution. The behavior of an ideally mode-locked laser is shown in Figure 1.[1] Another way to view mode-locking is that it consists of the correlation of spectral amplitudes and phases. By eliminating the initial randomness associated with the spectral composition of the output of the free running laser, the correlation of the modes is complete. The radiation becomes localized, resulting in a single pulse. The single pulse circulates inside the laser cavity, and with each successive transit a portion of the pulse is coupled outside the cavity. The result is the appearance of a single pulse at a rate of c/2L. Therefore mode-locking results in a train of pulses with a repetition period that is equal to the round-trip cavity transit time.

In order to understand the temporal and spectral properties of each pulse in the mode-locked pulse train as well as to gain a general understanding of the peak powers available from such a laser, some simplifying assumptions should be made. An optical pulse can be completely described in terms of a phase and an intensity. It is immaterial whether reference is made to the time or frequency domain,

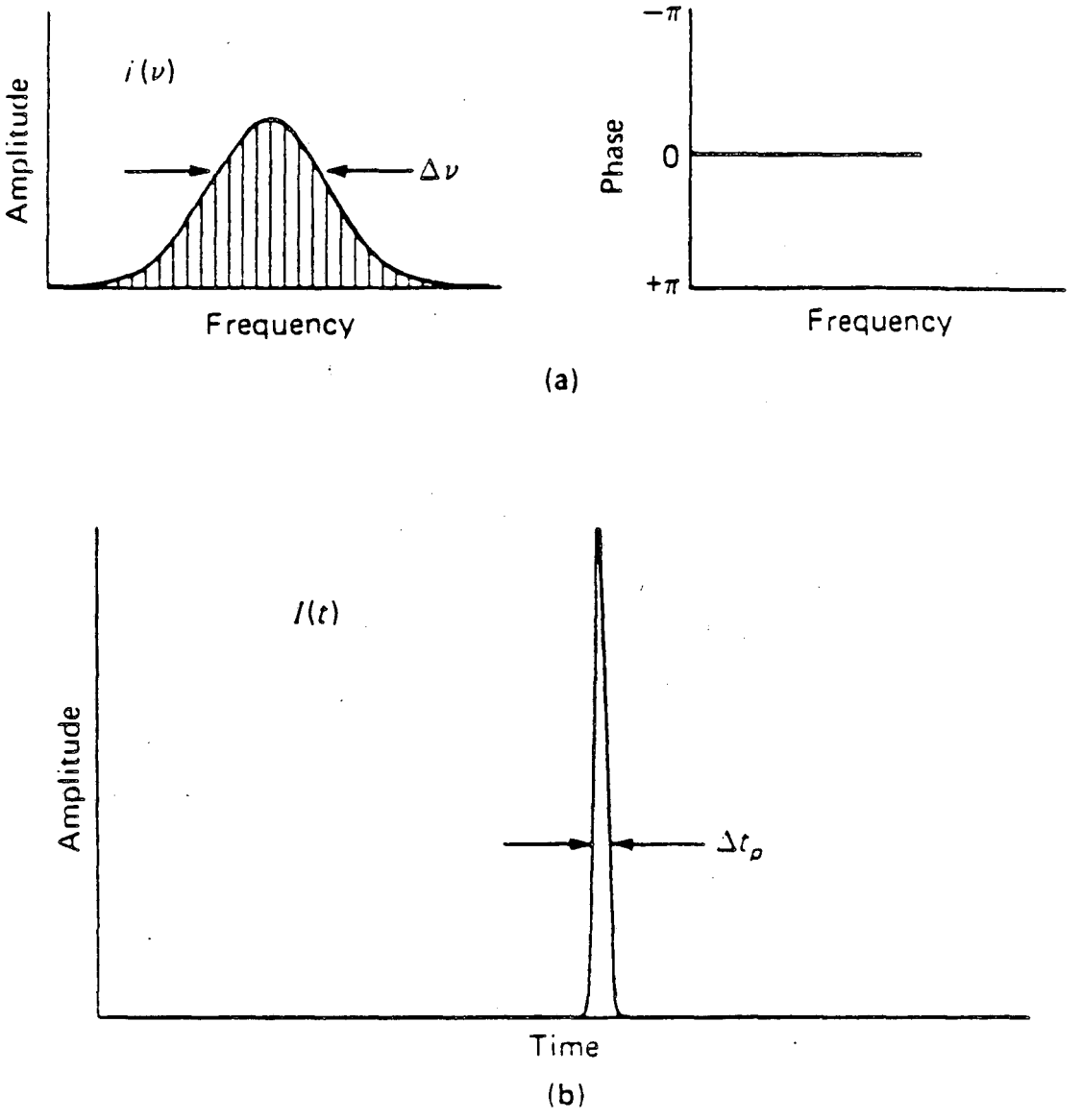

XBL 863-975

Fig. 1. Signal structure for an ideally mode-locked laser. (a) The spectral intensities have a Gaussian distribution, while the spectra phases are identically zero. (b) In the time domain, the signal is a transform limited, Gaussian pulse (from reference 1).

since they are related by the Fourier transform. Because the temporal and spectral intensities, I(t) and i(ν) respectively, depend not only on one another but also on a phase function, there is no one-to-one correspondence between the two. The only general relationship between the two is a form of the Heisenberg uncertainty principle

$$\Delta\nu\Delta\tau \geq K \tag{1}$$

where $\Delta\tau$ and $\Delta\nu$ are the full width at half maximum (FWHM) of I(t) and i(ν) respectively, and K is a constant on the order of unity.

The uncertainty principle dictates that the duration of the shortest possible pulse obtainable for a given spectral bandwidth is

$$\Delta\tau = \frac{K}{\Delta\nu} . \tag{2}$$

The shortest possible pulse out of a given laser therefore results when the laser emission fills the entire gain bandwidth of the lasing medium, $\Delta\nu_L$. The number of axial modes which are contained within the oscillating bandwidth is $N = \Delta\nu_L \Delta\tau_r$, where $\Delta\tau_r = 2L/c$ is the round trip transit time in the optical resonator. The duration of an ideal mode-locked pulse is therefore

$$\Delta\tau \approx \frac{1}{\Delta\nu_L} \approx \frac{\Delta\tau_r}{N} . \tag{3}$$

Equation (3) not only reiterates the uncertainty principle result that the narrower the pulse width the larger the bandwidth required to generate the pulse, but also points out that the pulse width of a mode-locked pulse is roughly equal to the cavity round trip transit time divided by the number of excited axial modes.

Assuming spectral intensities and therefore temporal profiles to have Gaussian distributions, the most general expression for an optical pulse is given by

$$E(t) = \frac{E_0}{2} \exp(-\alpha t^2) \exp[j(2\pi\Delta\nu_p t + \beta t^2)], \tag{4}$$

where the term α determines the Gaussian envelope of the pulse and the term $j\beta t$ is a frequency sweep during the pulse (i.e., chirp). The pulsewidth at the half intensity points is

$$\Delta\tau_p = \left[\frac{2\ln 2}{\alpha}\right]^{1/2}, \tag{5}$$

and the bandwidth taken at the half intensity points of the pulse spectrum is

$$\Delta\nu_p = \frac{1}{\pi}\left[2\ln 2\left(\frac{\alpha^2 + \beta^2}{\alpha}\right)\right]^{1/2}. \tag{6}$$

For future reference and discussion, it should be noted how the frequency sweep contributes to the total spectral width of the optical pulse. The pulsewidth-bandwidth product is a parameter often used as a figure of merit of how well a mode-locked laser is working. For Gaussian pulses, the pulsewidth-bandwidth product is given by

$$\Delta\tau_p\Delta\nu_p = \left(\frac{2\ln 2}{\pi}\right)\left[1 + \left(\frac{\beta}{\alpha}\right)^2\right]^{1/2}. \tag{7}$$

When no frequency sweep is present (i.e. $\beta = 0$, coherent pulse generation), equation (7) yields $K = \Delta\tau_p\Delta\nu_p = 0.441$.

Extremely high peak powers are generated from pulsed, mode-locked, solid-state lasers because the energy that would have been contained

in the entire output of the unmode-locked laser is now contained within the ultrafast pulse. These lasers are therefore very attractive to inertial confinement fusion researchers. For example, the duty cycle (i.e. the ratio of the pulse-on-to-pulse-off time) is $\frac{\Delta\tau_p}{\Delta\tau_r} \approx \frac{1}{N}$. Therefore the peak power of a pulse is approximately N times the average pulse when the laser is not mode-locked. By correlating the phases of the axial modes in a Nd:YAG resonator, peak powers can be as high as 10^3 times the average power when the modes are incoherently phased.

The (longitudinal) coupling of the axial modes required to generate mode-locked pulses is achieved experimentally by placing inside the laser cavity either an externally driven loss or phase modulator (active mode-locker), or a passive device that exhibits saturable absorption (passive mode-locker), or the combination of both. Saturable absorption is the preferred way of generating mode-locked output high peak power from a pulse pumped solid-state laser if the shortest possible pulses are desired. Saturable dyes simultaneously Q-switch and mode-lock the laser emission. A passively mode-locked laser generates a relatively short train of mode-locked pulses. The envelope of the train of pulses approximate the duration of a regular dye Q-switched pulse. However, due to the intrinsic randomness of passive mode-locking, purely passive systems are subject to large fluctuations in the energy, spectral widths, and durations of the output pulses. Other problems include incomplete mode-locking and

poor threshold conditions. All of these problems combine to make the output sufficiently inconsistent enough so that passively mode-locked lasers are difficult to use in many picosecond experiments.

By combining active mode-locking, which was developed for the generation of short pulses at high repetition rates from continuous wave (CW) lasers, with passive mode-locking, stable output as well as high peak powers can be obtained.[4,5,6] This combination makes pulse pumped solid-state lasers a very productive laboratory tool. In order to understand the intrinsic problems of passively mode-locked, solid-state lasers, and to appreciate how the addition of active mode-locking helps alleviate these problems, a qualitative presentation of both passive and active mode-locking theory is necessary.

B. Passive Mode-Locking

The first successful use of a saturable absorber to simultaneously Q-switch and mode-lock a solid-state laser was accomplished in 1965.[53,54] Computer simulations of the evolution of a mode-locked pulse train from noise aid in the discussion of pulse formation in a passively mode-locked laser. One such simulation is depicted in Figure 2.[55] The transformation of irregular pulses into a single mode-locked pulse is shown in this figure. Figures 2a-d show that noise like fluctuations are linearly amplified via successive passes through the gain medium. Both a smoothing of the pulse substructure and a broadening in time of the noise spikes is manifested. Figures 2e-g show that the amplitude fluctuations amongst the random noise-like bursts have increased, and that only the amplitude of the strongest noise burst has been successfully amplified. Eventually all the background pulses have been suppressed, as seen in Figure 2h.

The understanding of passive mode-locking in solid-state lasers was vastly enhanced by the time domain description of Letokhov.[56] This model states that the simultaneous Q-switched and mode-locked pulse evolution from noise-like bursts can be divided into three stages. These are linear amplification, nonlinear absorption, and nonlinear amplification.

In the initial stage, because the intensity is low, population inversion of the lasing transition and the transmission of the saturable dye are not affected by the radiation circulating within the laser cavity. Therefore both the amplification and the absorption

Fig. 2. Computer simulation of the evolution of a mode-locked pulse from noise. (a-d) Region of linear amplification and linear dye absorption; (e-g) nonlinear absorption in the dye cell (h) regime of nonlinear amplification, dye completely bleached (from reference 55).

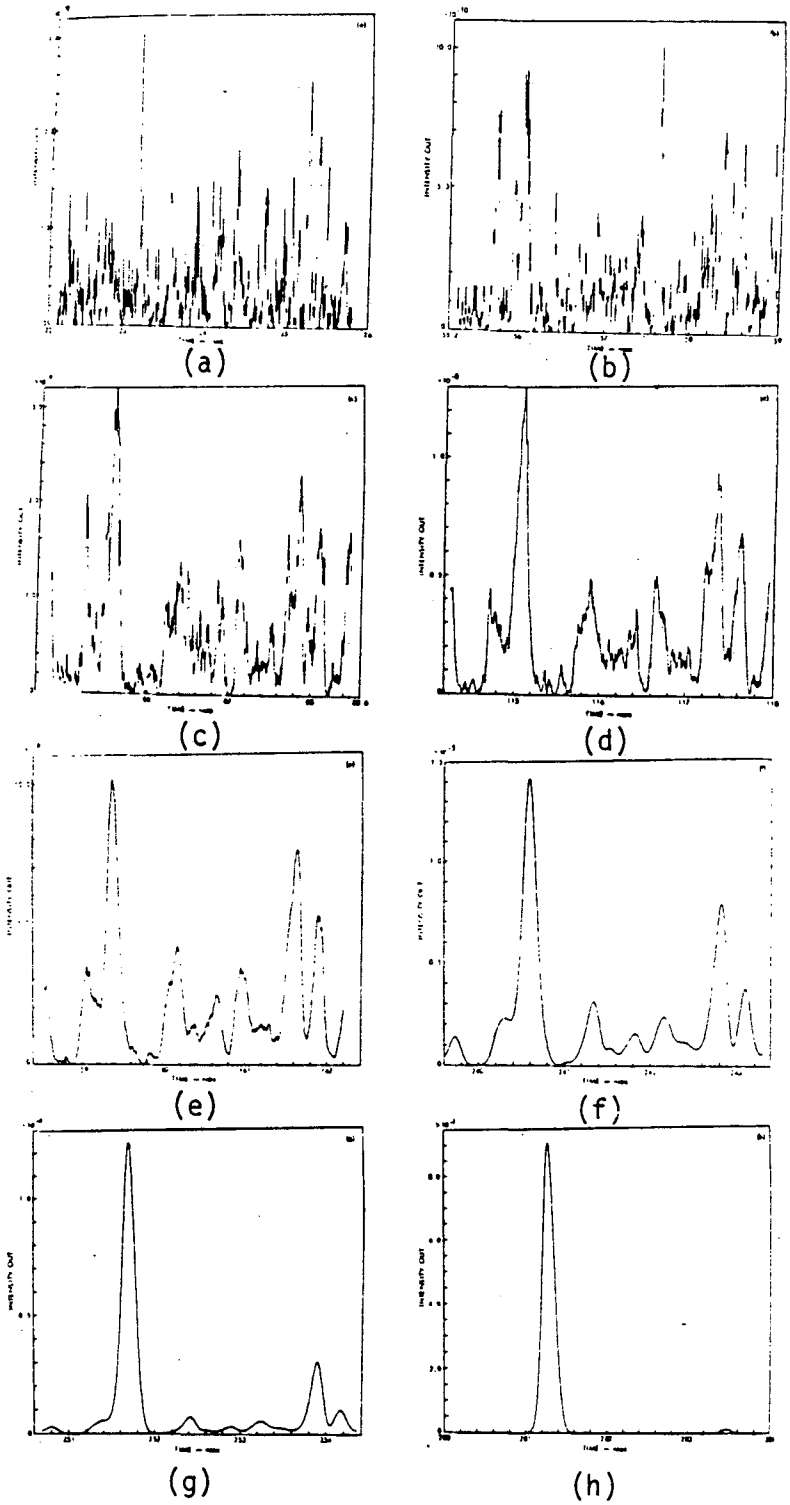

XBL 866-2186

Fig. 2

processes can be considered to be linear. The emission modes are random with no phase correlation. Hence, the intensity pattern is similar to that of amplified spontaneous emission. Since the emission is a random function of time, the total emission is similar to incoherent radiation. In this regime there has been excitation of sufficient axial modes that the laser radiation has a spectral content about equal to the fluorescence bandwidth of the active medium. Each noise spike has a temporal width inversely proportional to that bandwidth. The intensity fluctuations are therefore very short in time. The random sequence of such fluctuations is depicted in Figure 2a.

Initially the laser emission lacks periodicity. However, as the radiation is amplified over the noise background some periodicity is exhibited. This becomes apparent as the number of round trips within the cavity increases. Also, natural mode selection occurs in the region of linear development due to the amplifying medium. The frequency dependent gain favors cavity modes at the center of the fluorescence line. Thus the amplification process results in spectral narrowing. In the time domain this leads to a smoothing and a broadening of the intensity fluctuations in the time domain as already pointed out in Figures 2a-d.

For a passively mode-locked Nd:YAG laser, the linear amplification process can be viewed with the aid of the following numerical example. The fluorescence line width in Nd:YAG is $6.5 cm^{-1}$, corresponding to approximately 195 GHz.[3] For a typical Nd:YAG laser cavity with a 10ns round trip transit time, almost 2×10^3 cavity modes are

initially excited. This bandwidth also implies that the duration of the intensity of spontaneous emission is approximately 2ps at the beginning of the linear amplification stage. Assuming a constant linear amplification of 1.2 times per pass, calculations[3] show that the frequency width of the emission reduces to between $0.3cm^{-1}$ and $0.6cm^{-1}$. This corresponds to an increase in a typical fluorescence spike duration to between 50ps and 100ps.

In the second phase of pulse evolution depicted in Figures 2e-g, the gain in the amplifying medium is still linear, but the absorption of the dye is nonlinear because the intensity peaks in the laser cavity approach the values of the saturation intensity, I_s, of the dye (see Figure 3, $I_s = \frac{h\nu}{\sigma_D \tau_D}$; for Eastman Kodak 9740 in 1,2-dichloroethane $\tau_D = 11 \times 10^{-12}$sec, so $I_s \approx 4 \times 10^7$ W/cm^2). Two effects take place simultaneously in the nonlinear absorption regime. First, there is "survival of the fittest" of the pulses, that is there is a naturally selective process determined by the intensity and spectral content of the pulses. The most intense fluctuations that were built up during the linear amplification regime preferentially bleach the dye and grow rapidly in intensity. However, since the absorption process is frequency dependent, the selection of the "strongest" pulse is not only on the basis of amplitude alone. The "weaker" pulses encounter larger absorptions in the dye cell and are suppressed. For ideal mode-locking (i.e. complete), the number of pulses per round trip should be reduced to one. The elimination of almost all background pulses is depicted in Figure 2h.

The second effect taking place in the nonlinear absorption stage is the narrowing of the circulating pulses in time. Consequently the frequency spectrum is broadened. The pulse shape is affected by the nonlinear absorption of the dye. The wings of the pulse are more strongly absorbed than the peak according to Figure 3.[1] However, this effect is partly negated because of the tendency of the linear amplifying medium to narrow the spectrum due to the natural mode selection at the center of the gain profile. The second stage is complete when the absorbing transition of the dye is completely saturated (i.e. bleached). At this point the transmission of the dye should be close to unity (i.e. transparent).

The preceding discussion obviates certain characteristics of a mode-locking dye. They include: (1) an absorption line at the laser wavelength; (2) an absorption linewidth greater than or equal to the laser linewidth; (3) a recovery time shorter than the round trip time for a pulse to circulate between the two mirrors defining the laser cavity; and (4) a recovery time shorter than the pulse duration of the intensity spikes at the end of the linear amplification stage.

For a passively mode-locked Nd:YAG laser operating in the nonlinear absorption region, the theoretical expectation of pulses with durations somewhere between an upper limit imposed by the saturable absorber recovery time and a lower limit defined by the inverse of the gain bandwidth of the lasing medium is never experimentally observed. Q-switch dyes are available with recovery times as short as 11ps (Eastman Kodak 9740 in 1,2-dichloroethane).

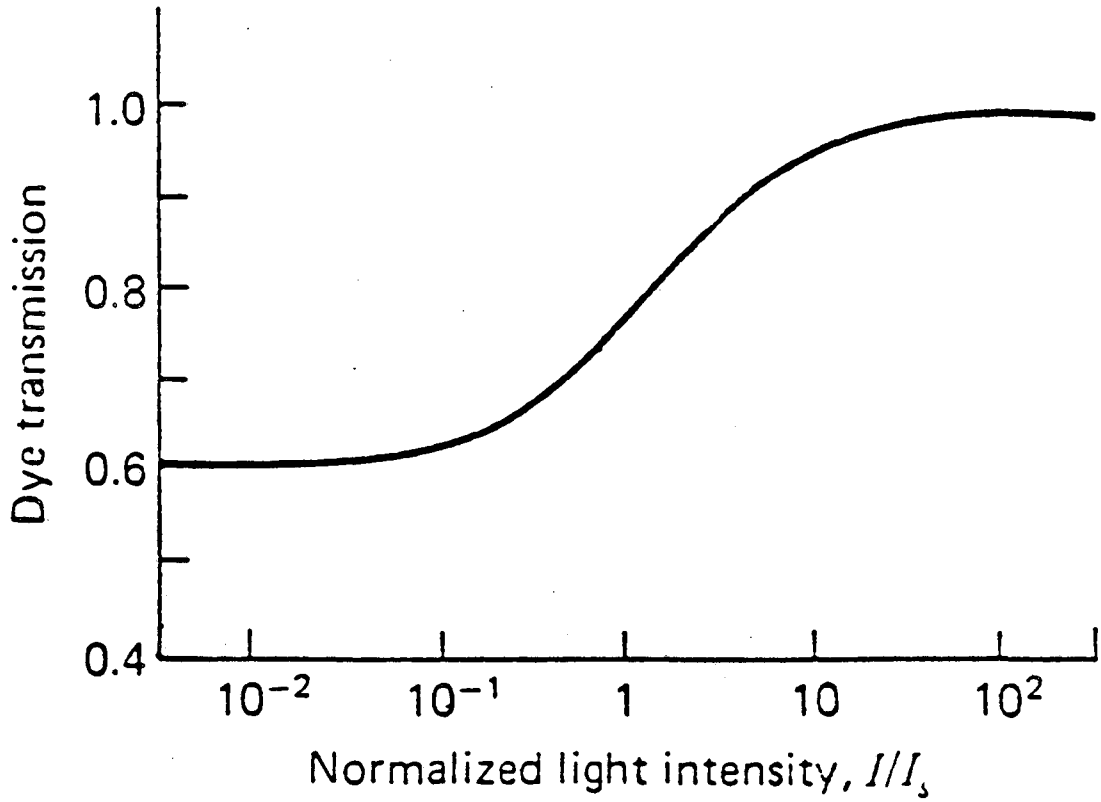

XBL 863-976

Fig. 3. Nonlinear transmission of a saturable absorber versus light intensity in units of the saturation intensity, I_s, of the dye (from reference 1).

However, pulse widths are rarely below 20ps. This is consistent with model calculations showing constant pulse shortening in this region of 2.5.[3] The independence of the shortening on the boundary conditions mentioned above is due to the natural spectral gain narrowing in the Nd:YAG amplifying medium. This mechanism is therefore a decisive mechanism in determining the final pulse duration.

The concluding third phase of pulse evolution begins when the intracavity intensity is sufficiently high to bleach the nonlinear absorber transition. Amplification is now nonlinear and a region of high peak power is achieved. In a Nd:YAG laser, during the nonlinear amplification stage, pulse intensities quickly rise to gigawatts per square centimeter levels within ten round-trip transits of the laser cavity. As depicted in Figure 2h, at this stage there remains only one pulse. Successive passage of the high intensity pulse through the laser cavity results in the appearance of pulse train at the output of the laser. A typical mode-locked pulse train is shown in Figure 4. Eventually, the population inversion is depleted and the pulse train decays away.

The expectation that the nonlinear amplification would broaden the pulse spectrum and consequently reduce the pulse duration is not observed. This is seen in a comparison of Figures 2g and 2h. Nonlinear pulse width narrowing associated with most high gain processes should occur after the passage of the pulse through long path lengths of amplifying medium. However, in the case of a laser resonator, the path is folded back and forth upon itself. Therefore,

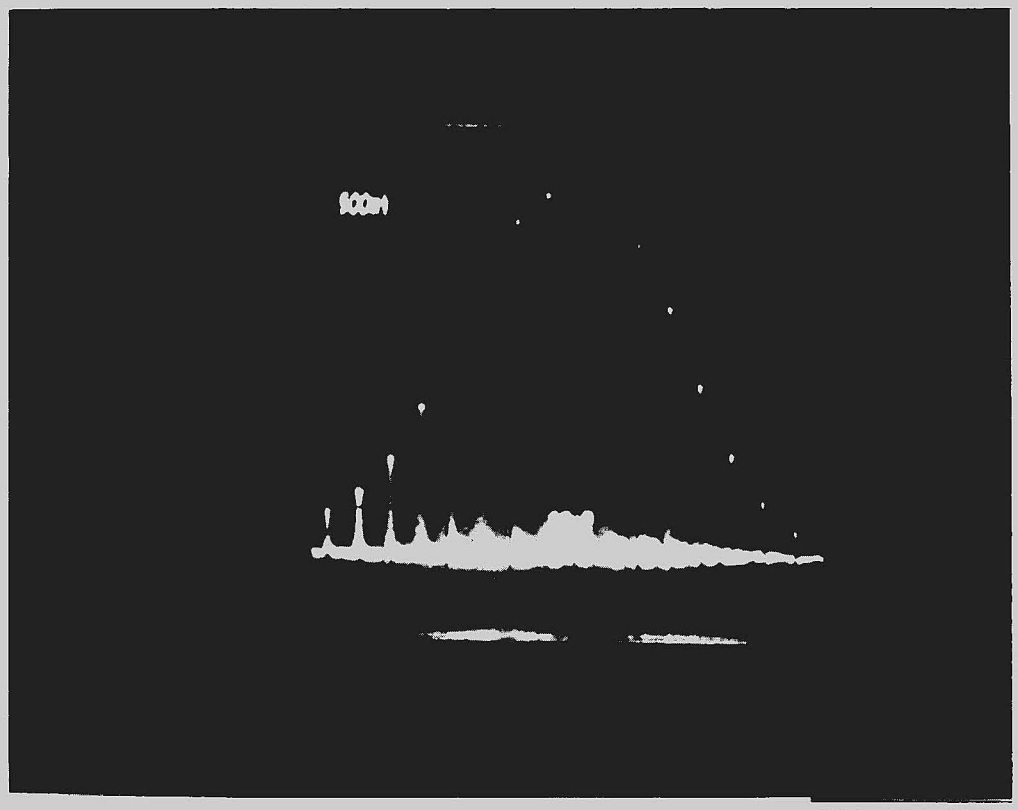

XBB 863-1638

Fig. 4. Oscilloscope photograph of typical mode-locked pulsed train with pulse separations of 10 ns.

the nonlinear pulse shaping processes are reduced because the pump cannot restore the population inversion lost during each pass through the amplifying medium before the light is reflected back.[55] In other words, constant gain cannot be maintained.

In addition to the reasons mentioned above, the onset of new, nonlinear porocesses also lead to the fact that in high-powered, mode-locked, solid-state lasers, the final pulse width never reaches the theoretical limit imposed by the inverse of the gain bandwidth of the amplifying medium. These new processes cause the high-intensity pulses to evolve into complicated spectral and temporal structures. At these high intensities, various nonlinear effects occur which severely alter the coherent nature of the pulse. Pulse width measurements consistently yield pulses with durations longer than the reciprocal of the gain bandwidth. Observation of broad pulse spectrum with substructure is very typical.

Treacy[15] was the first to observe pulses characteristic of self-phase modulation. Pulses generated by a mode-locked Nd:Glass laser at 1.06μm were observed to have a measured spectral width of 100Å and a pulse duration of 4ps. Spectral widths of this magnitude should lead to pulse duration an order of magnitude shorter than what was observed. An interferometric instrument was constructed to measure the time resolved spectrograms of these pulses. Treacy detected a quadratic term in the time dependent phase of the pulse corresponding to a sweep of the carrier frequency (i.e. chirp). Compression of these pulses by the measuring instrument itself

occurred because the frequency sweep was linear and positive. With the compression technique, pulses having durations of 0.4ps were generated. Since then many authors have claimed observations of spectral broadening typical of self-phase modulation.[3,4,7-13] These reports will be discussed in detail in Chapter III as a background to and for comparison with the results observed here.

During the high-intensity stage of the pulse development, the characteristics of the output pulses are in part determined by the intensity dependent index of refraction (i.e. the nonlinear index of refraction, n_2) of the laser rod and other optical components in the cavity. This causes a change in the index of refraction of those components at high powers. Self-phase modulation resulting from the varying index of refraction can cause a frequency sweep of the laser pulse. This frequency sweep can cause many different phenomenon observed in lasers such as pulse compression[4,15] or the breakup of a pulse into a burst with characteristics of the intensity spikes observed in the early stages of the mode-locking process.[8,10] If the problem of self-focusing does not become an issue, self-phase modulation will continue throughout the pulse train and the spectral shifts will become significant compared to the gain bandwidth of the lasing medium. Measurements of individual pulses as a function of position in the mode-locked pulse train clearly show the change of pulse properties as a function of the number of round trip cavity transits.[3,4,7-13] Pulses positioned early in the pulse train exhibit behavior closest to transform-limited.

From the foregoing discussion of passive mode-locking in solid-state lasers, it is evident that the inherent chaotic nature of the process (pulse buildup from noise fluctuations) leads to great instabilities in such a laser. Many of these problems can be curtailed if a more reliable form of mode-locking is used, that of active mode-locking. However, high peak powers associated with passive mode-locking cannot be generated solely with the active form. Therefore combining both forms is necessary for stable generation of high peak power pulse trains.

C. Active Mode-Locking

In order to produce short, high-peak-power pulses from solid-state lasers, simultaneous Q-switching and mode-locking is a necessity. The simplest method to achieve both Q-switching and mode-locking is through the use of a saturable absorber. However, purely passive mode-locking of solid-state lasers suffers from satellite pulse formation, missed shots, and large shot-to-shot variations in pulse duration and energy. The lack of reproducibility of a purely passive system is due to the buildup of the pulse from statistical fluctuations in the initial spontaneous emission. The increasing complexity and accuracy of experimental investigations involving picosecond lasers has led to the need for more reliable and more stable picosecond sources. An improvement in the stability of a passively mode-locked, Nd:YAG laser can be achieved by the addition of active mode-locking, so that the buildup of the pulse is no longer initiated from the statistical fluctuations associated with the initial spontaneous emission. Because the modulation produced by the active mode-locker is always present during the flashlamp pulse, the buildup of the passively mode-locked pulse is from the well-defined pulse resulting from the transmission window of the active mode-locker.

The addition of active Q-modulation (mode-locking) and an active Q-switch to a passively mode-locked laser was reported as early as 1974.[57] The electrooptic modulator was a Pockels cell that required a high radio-frequency (RF) driver at 100 MHz. The availability of simple, high-frequency acoustooptic modulators has led to simpler

experimental setups employing active mode-locking. Operation of active/passive mode-locked Nd:Glass lasers with pulse train amplitude stabilities down to ±5 percent have been reported.[58,59] Descriptions of Nd:YAG laser systems combing active and passive mode-locking may be found in the literature.[4,5,6] Pulse train amplitude fluctuations routinely better than ±3 percent and as good as ±1 percent are achievable.

Active mode-locking is accomplished in one of two ways. Placement of either a phase modulator (FM) or an amplitude modulator (AM) inside a laser cavity, driven at exactly the frequency of the axial mode spacing, causes the laser to generate a train of mode-locked pulses with a pulse repetition rate of c/2L. Both electrooptic and acousto-optic modulators have been employed.

As is the case with passive mode-locking, active mode-locking should be viewed in both the frequency and time domains. In the frequency domain, introducing a time varying transmission, T(t), at a repetition rate of $f_m = c/2L$ (or a harmonic of f_m) using an amplitude modulator inside the laser resonator creates side bands on each oscillating axial mode that overlap adjoining axial modes. Initially, the axial mode with frequency ν_o nearest the peak of the laser gain profile begins to oscillate. If the loss modulator is operating at a frequency f_m, then the carrier frequency develops side bands at $\pm f_m$. Because the modulation frequency is chosen to coincide with the frequency separation of the axial modes, the upper $(\nu_o + f_m)$ and lower $(\nu_o - f_m)$ side bands will have the same

frequency as the adjacent axial modes that are resonant in the laser cavity. These modes are therefore coupled to the original oscillating mode. As the $\nu_0 + f_m$ and $\nu_0 - f_m$ oscillating modes pass through the modulator, side band formation will result in coupling to the $\nu_0 \pm 2f_m$ modes. Injection locking effects caused by the creation of weak side bands on the oscillating axial modes causes a well defined amplitude and phase relationship amongst the modes. This strong mode coupling or mode-locking phenomenon is similar to what happens in passive mode-locking. The side band production, mode-coupling process will continue until all the modes above the threshold for oscillation, i.e. those falling within the gain bandwidth of the laser, are coupled.

In the time domain, the same intracavity modulation element, with modulation period equal to the round trip transit time, 2L/c, can reshape the internal circulating field distribution repeatedly on each successive found trip inside the cavity. Radiation incident at the modulator during a certain part of the modulation cycle will again be incident at the same time during the next cycle after one round trip in the laser cavity. The light subject to the loss at one time will again suffer a loss on the next round trip. Hence, all the light in the resonator will experience loss except the light which passes through the modulator when the modulator loss is zero, as shown in Figure 5a.[1] At the low loss time intervals (extrema of the modulation cycle) the radiation will build up in a narrow pulse. The modulation effect can be accumulated over many passes so as to be much stronger

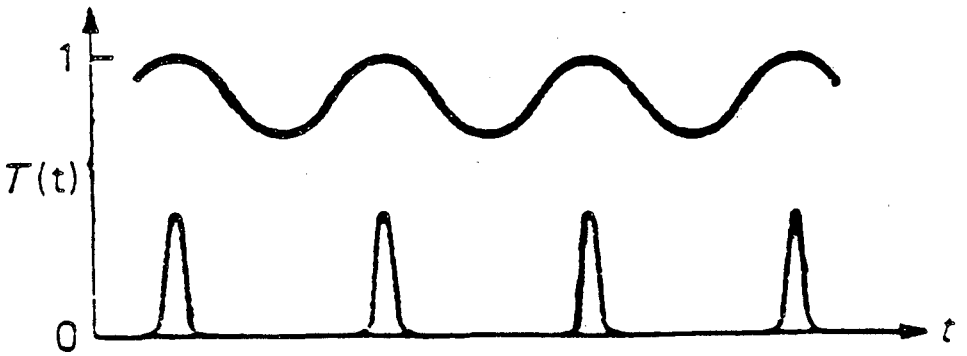

(a) AM mode locking

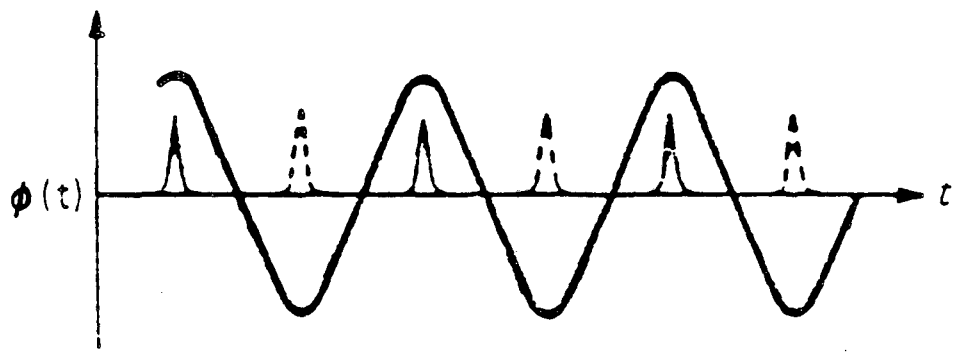

(b) FM mode locking

XBL 863-977

Fig. 5. Mode-coupling behavior in the case of (a) active AM mode-locking, and (b) FM mode-locking (from reference 1).

than the single pass modulation strength. The pulse narrowing is the result of the repeated superposition of the transmission function.

Siegman and Kuizenga[60] developed an analysis of active mode-locking in homogeneously broadened lasers (such as Nd:YAG) by following a single mode-locked pulse through one round trip around the laser cavity. In a homogeneous laser, in the absence of mode coupling, oscillation occurs in only a few axial modes near the center of the gain profile. In this case, mode-locking is the result of a competition between the side band generation of the active modulator and the spectrally narrow band bass of the laser gain curve. The active mode-locker acts to push energy outward from the central axial modes into axial modes away from the frequency of maximum gain. The laser gain curve continually acts to narrow the oscillation spectrum and broaden the mode-locked pulse width. The analysis, which requires a self-consistent solution, is carried out on a Gaussian pulse. The result is a simple expression that shows the dependence of the mode-locked pulse width on laser linewidth, modulation frequency, depth of modulation, and saturated gain.

For an acoustooptic, AM modulator operating as a traveling wave Bragg device as well as for an electrooptic AM modulator, the single pass transmission function is

$$T(t) = \cos(\delta_{AM} \sin\omega_m t), \tag{8}$$

where δ_{AM} is the modulation depth and $\omega_m = 2\pi f_m$ is the angular frequency of the modulation. If the laser cavity length is exactly matched to the modulation frequency, then the pulse passes through the

modulator at the instant of maximum transmission. This occurs twice in every period of the modulation signal ω_m, and therefore the modulator is driven at a frequency equal to one half the axial mode spacing of the laser. Expanding equation (8) about the transmission maximum at t = 0 yields the round trip modulation function

$$T(t) = \exp(-\delta_{AM}^2 \omega_m^2 t^2), \tag{9}$$

which results in a pulse width for an AM active mode-locked laser[60] of

$$\Delta\tau_p(AM) \approx \frac{(g\ell)^{1/4}}{2\delta_{AM}^{1/2}} \frac{1}{f_m \Delta\nu_L}^{1/2}, \tag{10}$$

where g is the saturated gain coefficient at the laser line center, $\Delta\nu_L$ is the gain bandwidth of the laser, and ℓ is the length of the active medium. The AM active mode-locked pulses have no frequency chirp (i.e., $\beta = 0$ in equation (4)). The pulse width is inversely proportional to the quartic root ($\Delta\tau_p(AM) \propto P_M^{-1/4}$) of the modulator drive power because the modulation depth is directly proportional to the square root of the drive power. Therefore increasing the drive power does not have a large effect on the pulse width.

When an active mode-locker is used as a phase modulator (FM mode-locking), light passing through an electrooptic or acoustooptic mode-locker will be up or down shifted from the carrier frequency unless it passes through when the modulation cycle is at either of the two extrema. The energy circulating inside the cavity passing through the FM modulator at times other than the extrema is Doppler shifted.

The shift is proportional to the slope of the phase change with respect to time, and repeated shifts or successive passes through the device eventually push the energy outside the spectral range over which gain is available from the laser medium. The interaction of the spectrally broadened circulating power with the narrow laser gain bandwidth results in a reduction in gain for most frequency components. In this sense the phase modulator becomes similar to the loss modulator and FM mode-locking can be treated in the same way as AM mode-locking.

Figure 5b[1] demonstrates the case of FM mode-locking. The existence of two extrema in phase per modulation cycle causes a phase uncertainty in the mode-locked pulse position, since the pulse can occur at either of the two equally probable phases relative to the modulating signal. Another characteristic of FM active-mode-locking (as is the case with all FM mode-locking) is that the quadratic variation of the phase perturbation about the pulse arrival time introduces a frequency chirp in the mode-locked pulses (i.e., $\beta \neq 0$ in equation (4)).

The FM phase modulator introduces a sinusoidally varying phase perturbation such that the single pass transmission function through the modulator is

$$T(t) = \exp(j\delta_{FM}\cos\omega_m t). \tag{11}$$

The round trip transmission function can be expanded as

$$T(t) \approx \exp[\pm j2\delta_{FM}(1-\pi_m^2\, t^2/2)]. \tag{12}$$

If the constant phase factor is dropped, the transmission function can be expressed as

$$T(t) \approx \exp(\pm j\delta_{FM}\omega_m^2 t^2/2). \tag{13}$$

The plus/minus sign corresponds to the two possible phase positions at which the pulse can pass through the modulator. With the above in mind, and the same analysis as prescribed in reference 54 for the AM mode-locking case, the pulse width for an FM mode-locked pulse is given by

$$\Delta\tau_p(FM) \approx \frac{(g\ell)^{1/4}}{2(\delta_{FM})^{1/4}\,(f_m\Delta\nu_L)^{1/2}}\,. \tag{14}$$

For FM active mode-locking, the pulse width is even less sensitive to modulator drive power than the AM case.

The laser system to be described here utilizes AM active mode-locking. An acoustooptic, traveling wave Bragg deflector is used as the loss modulator. A detailed description including performance characteristics will be provided in the next two sections. It is interesting, however, to discuss the effect that the modulator has on the pulse width and to evaluate whether passive or active mode-locking is more important in the determination of the pulse width of a mode-locked pulse.

A transient description of the buildup of AM active mode-locking has been developed for the case where the laser field initially starts out as noise.[61,62] For an AM modulator with modulation function according to equation (8), a transient solution of the active mode-locking process yields

$$\Delta\tau_p = \frac{\Delta\tau_{p_o}}{[\tanh(M/M_o)]^{1/2}} \cdot \tag{15}$$

An estimation of the pulse width of an active/passive mode-locked laser involves the separate evaluation of the effects of each process. If the results show the effects are of the same magnitude, then determination of which has a greater influence is necessary. For a typical pulsed, mode-locked Nd:YAG laser with 100 MHz axial mode spacing and a modulator drive power to yield a 50 percent modulation depth, buildup time to steady-state requires between 500 and 1000 round trip cavity transits. Thus, according to equation (15), pulse widths from the purely actively mode-locked system will range between 120ps and 170ps. These durations are relatively long compared with the final pulse lengths found in the output of a purely passive system, which typically range from 20ps to 50ps.

Following the approach of Albrecht and Bunkenberg[63] of considering each mode-locking process separately, and then combining the two effects on pulse duration according to

$$\Delta\tau_{a/p} = \frac{1}{\sqrt{\left(\frac{1}{\Delta\tau_a}\right)^2 + \left(\frac{1}{\Delta\tau_p}\right)^2}} \tag{17}$$

leads to the conclusion that the effect of active mode-locking is negligible compared to the effect of passive mode-locking. However, recalling the discussion of passive mode-locking from the last section leads to another interpretation. During the linear amplification stage of pulse development the pulse length of the initial noise pulse

first increases due to the bandwidth narrowing effect of the laser gain medium. By the end of this stage pulse durations of 50ps to 100ps with frequency spreads of 0.3 cm^{-1} to 0.6 cm^{-1} are typically observed. Subsequently, during the nonlinear absorption phase the pulse width decreases down to its final value of approximately 25ps and remains relatively constant through the nonlinear amplification stage.

Applying the same theory of pulse evolution to the active/passive system provides insight into the mechanism of laser stabilization and a different interpretation than the results obtained following the formalism of reference 63. At the beginning of the nonlinear absorption stage the length of the pulse due to purely active mode-locking can be in the same range as the pulse lengths of the purely passive system. This can have two different effects. First, because the transmission window of the modulator is always present, the pulse does not evolve from a statistical noise spike as is the case in the purely passive system, but evolves from an already well defined pulse with a stable amplitude and duration determined by the transmission function of the modulator. This results in improved shot-to-shot stability in pulse energy and duration.

Second, at the onset of the nonlinear regions of pulse development in the active/passive system (i.e. upon addition of mode-locking dye) longer pulses are present than in the purely passive system. Equation (15) gives an approximate pulse duration of 150ps for pulse buildup times of 750 round trip cavity transits (which is the case for the

system described presently). Subsequently, during the nonlinear absorption and amplification stages, the effects of the active modulator can be neglected, and pulse shortening proceeds in the way as in the purely passive system. The pulse shortening is initiated with a longer pulse (150ps) than in the purely passive system (50ps to 100ps) resulting in longer final pulse duration in the active/passive system. This explanation is in good agreement with what has been experimentally observed.[4,5] The active/passive system described in the next section typically generates pulses between 20 and 30 percent longer than the equivalent system without active modulation.

D. Resonator Design

Even though the design and construction of most mode-locked solid-state laser oscillators is relatively simple, the output of such systems tend to be very unpredictable. Unless very careful adjustments are provided for dye concentration, optical pumping intensity (flashlamp voltages), and resonator alignment, average pulse durations from one mode-locked pulse train to the next change drastically, and the pulse train envelopes are not reproducible.[64] Early designs of mode-locked solid-state lasers were lucky to produce optimum mode-locking at a rate of ten percent.

An operational definition of optimum mode-locking or reliable generation of ultrashort pulses is the ability to produce clean (i.e. zero interpulse intensity), high signal-to-noise (i.e. ratio between the peak intensity of the principal pulses separated by 2L/c and the background radiation between the principal pulses) pulse trains with maximum probability and stability. Maximum probability and stability implies that the laser must fire a completely mode-locked pulse train — each time the flashlamps fire with a minimum of shot-to-shot energy amplitude fluctuations. Also included in this definition is that no satellite pulses should be observed due to parasitic resonator reflections inside the cavity. When single mode-locked pulses are amplified to high energy levels, any radiation preceding or following the main pulse is extremely undesirable.

Performance levels suitable to carry out reliable high-energy experiments can be achieved with carefully designed systems that are

operated close to threshold. When the proper saturable absorber and a well devised optical system are employed, clean mode-locked pulse trains free of satellite pulses can be generated 60 to 70 percent of the time in a purely passive system. When extreme care is taken, which involves the optimization of each individual component of the system, and careful alignment of the cavity, reliable output can occur 80 to 90 percent of the time.[65,66] Implementation of active mode-locking can result in 100 percent optimum mode-locking with mode-locked pulse train amplitude fluctuations as good as one percent.[4-6,63]

Of particular interest to the design of a mode-locked system are the resonator configuration, including mechanical stability, the type of dye and solvent used for passive mode-locking, the thickness and construction of the dye cell, thermal stabilization of those components that are temperature sensitive, and the quality of other optical elements including the active mode-locker. In this section, a discussion of these elements and their influence on the oscillator output will be featured. Of prime importance are the effects of these elements on pulse energy and duration, interpulse energy and satellite pulse suppression, and shot-to-shot reproducibility.

A schematic diagram of the pulsed active/passive mode-locked Nd:YAG oscillator is shown in Figure 6. All the optical mounts from the original Quantel YAG 400 system were replaced with home designed optical mounts constructed by the U.C. Berkeley Chemistry Department Machine Shop. These mounts were more stable and easier to align than

Fig. 6. Schematic diagram of the pulsed, active/passive mode-locked, Nd:YAG oscillator.

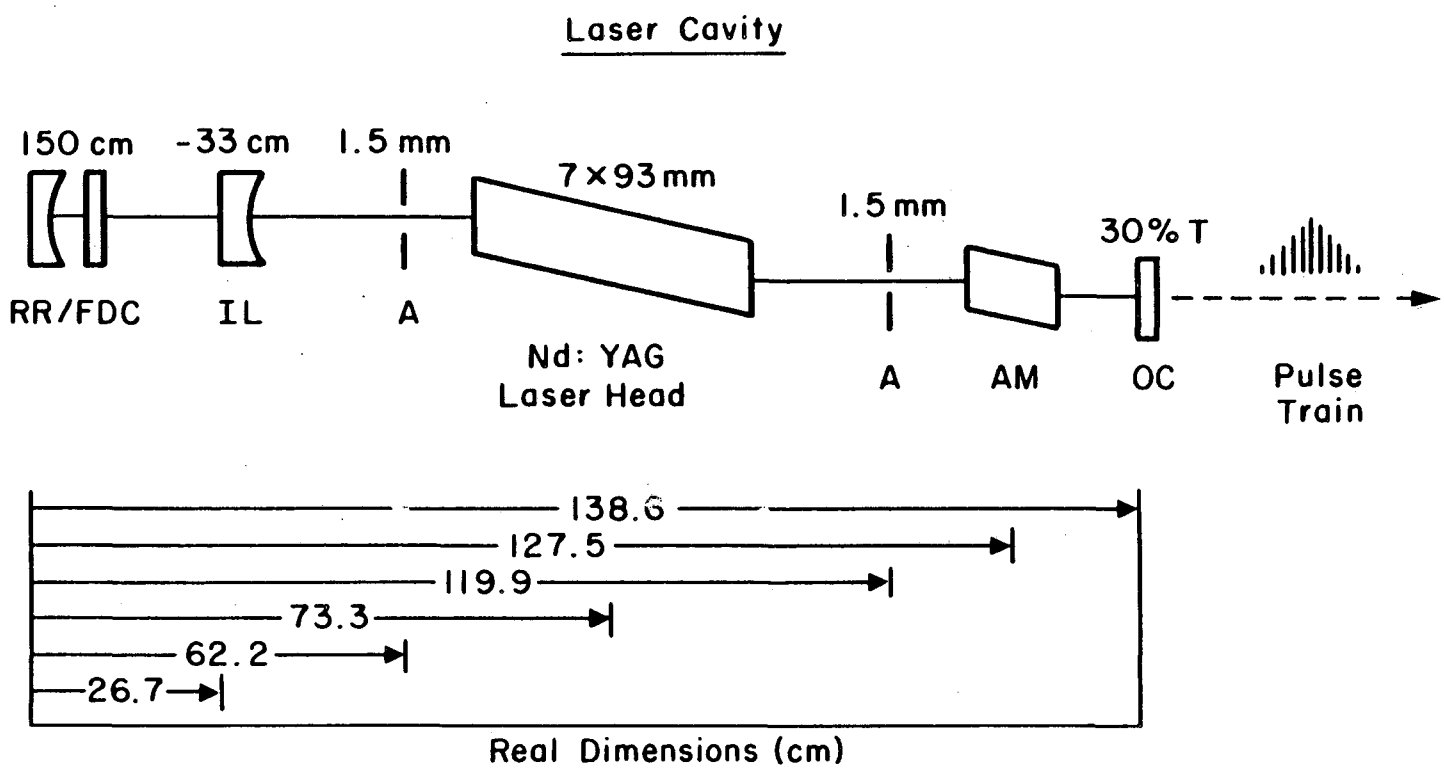

RR/FDC: Rear Reflector/Flowing Dye Cell
IL: Intracavity Lens
A: Aperture
AM: Active Mode-Locker
OC: Output Coupler

Fig. 6

XBL 863-982

the originally supplied mounts. They were also designed to provide the exact adjustments necessary to attain proper performance from the oscillator. These mounts were used throughout the laboratory for all optical systems. All of the cavity components were mounted on optical rail plates that in turn were rigidly attached to a floating Invar support rail system. The rail system was mounted on a vibration isolated optical table (NRC Model No. RS-48-8 or RS-410-8). Invar was used because of its mechanical rigidity and low coefficient of thermal expansion ($4 \times 10^{-7}\,^{\circ}C^{-1}$), making it insensitive to slight changes in ambient temperature (attempts were made to maintain laboratory temperature to $\pm 1.0^{\circ}C$). The rail plates contacted the rails at three points ensuring kinematic reproducibility in the case that optical components had to be removed during the course of alignment or maintenance. The optical rail system allowed for the independent translation of any optical element along the axis of laser beam propagation. The flexibility afforded by this degree of freedom proved to be invaluable in the initial setup of various systems, in particular in the optimization of intracavity lenses and certain extracavity beam expanding or beam reducing optics. Also, it was very important in determining where laser heads and apertures should be positioned inside the cavity.

The pulsed, active/passive mode-locked, Nd:YAG oscillator is a special case of a plano-concave resonator design known as a hemispherical resonator. The hemispherical resonator shown in Figure 7 has one flat mirror ($R_2 = \infty$) and one curved mirror. The

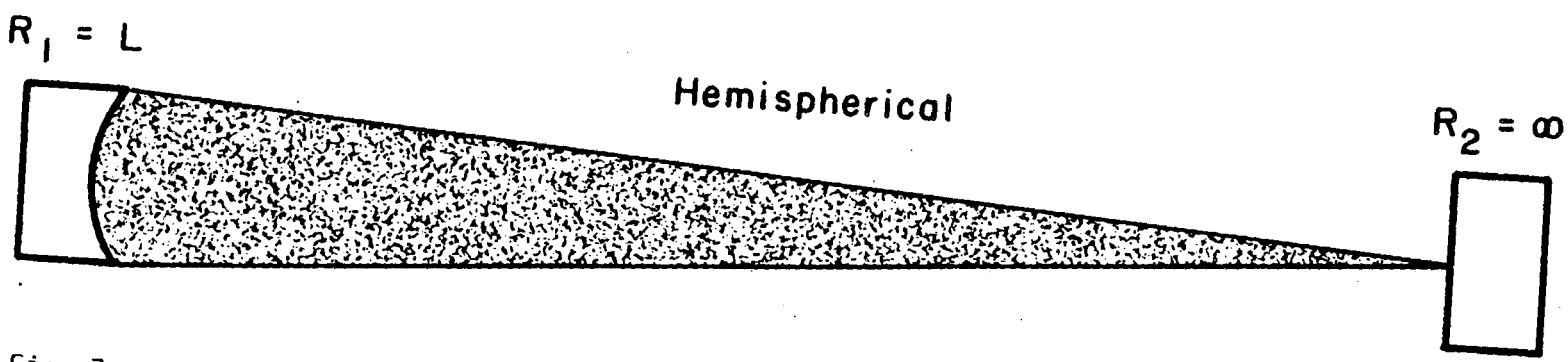

Fig. 7. Schematic diagram of a plano-concave resonator design known as a hemispherical resonator.

XBL 863-983

flat mirror is placed approximately one focal length distance away from the spherical mirror. The resultant beam of such a laser resonator has a relatively large diameter at the curved mirror and focuses to a diffraction-limited spot at the reflective surface of the flat mirror (output coupler). The beam propagates from the output coupler of the laser as if it came from a diffraction-limited point initiated at the reflective surface of the front mirror. The reasoning behind the choice of design of the resonator is twofold. Besides the desire for diffraction-limited mode behavior, in a passively mode-locked laser it is preferable to have the beam as large as possible on its transit through the mode-locking dye cell. Lower intensities of light in the dye cell prolong the lifetime of the dye solution and help reduce the occurrence of burning of optics in contact with the dye solution. The cavity described presently employs a contacted flowing dye cell to the back 100 percent (at 1064nm) reflector, as seen in Figure 6.

An important consideration in the design of a mode-locked laser resonator is the elimination of all reflections that might occur from components located between the two mirrors defining the laser cavity. Reflections from an optical surface that is parallel to the cavity mirrors will act as a second resonator. The main mode-locked pulse is thus split into several pulses that circulate inside their respective resonators with different round-trip transit times. Outputs from the oscillator become very erratic and usually consist of two or more superimposed pulse trains or extra pulses in the train. With the use

of optical surfaces at Brewster's angle, antireflection (AR) coatings on surfaces parallel to the resonator mirrors, and optical surfaces tilted away from the resonator's optical axis, parasitic resonator transients can be avoided and the occurrence of satellite pulses can be suppressed.

In the system depicted in Figure 6, the elimination of coupled resonator structures like those resulting from unwanted reflections was accomplished in the following ways: both the laser rod and acoustooptic modulator were at Brewster's angle; both the output coupler and back mirror were AR coated at 1064nm and on their nonreflective surface had a 30 min of arc wedge between the two surfaces; and the intracavity lens and dye cell window were AR coated at 1064nm on both sides and one side respectively. All optics from the original Quantel design were replaced by optics purchased from Optics for Research Corporation and coated by CVI Corporation. Similar precautions were taken in order to avoid stray back reflections into the cavity and amplifiers. Any stray reflection passing through a laser head could be amplified and cause catastrophic optical damage. In general, all mirrors were AR coated and had a 30 min of arc wedge on their nonreflecting side. All lenses and other polarizing optics (such as waveplates) that were used in amplifier chains and nonlinear optical conversion schemes were AR coated at the appropriate wavelengths. Nd:YAG amplifier rods were both AR coated at 1064nm and had surfaces tilted two degrees away from the normal to the direction of beam propagation.

The fact that the laser rod and active mode-locker were placed at Brewster's angle served not only to eliminate intracavity reflections, but also ensured that the laser output would be linearly polarized. Because the laser rod and active modulator were tilted in the plane parallel to the table top, the Brewster angle selectively favors p-polarized radiation (light horizontally polarized). Therefore, single pulse selection could be carried out using the Pockels effect, which is based on electrooptical polarization rotation in a birefringent medium. The other criterion for being able to use the Pockels effect for single pulse selection is that the cavity length be long enough (150 cm) so that interpulse spacings are long enough (10ns) to allow the use of conventional high voltage pulse forming electronics. Details of the single pulse selector will be discussed later.

Another way to reduce the number of reflective surfaces in the laser cavity was to have the mode-locking dye cell combined with the back reflector of the resonator. As shown in Figure 6, a 100 percent, 1064nm reflector with a focal length of 150 cm (radius of curvature of 300 cm) in direct contact with the flowing dye solution was incorporated into the passive mode-locking cell. A saturable absorber dye cell with the dye in contact with a cavity mirror not only produces the most reliable mode-locked pulse trains, but also yields the shortest pulses.[11,79]

Four major criteria must be considered when designing a dye cell for mode-locking purposes. Placing the dye cell in contact with one

of the cavity mirrors has already been mentioned. The other three requirements are: the dye should be circulated through a laminar flow system; the dye cell should be temperature controlled; and the optical path through the dye should satisfy the condition $\ell \leq c\tau_D/2n$, where ℓ is the dye thickness, c is the speed of light, τ_D is the relaxation time of the dye, and n is the refractive index of the dye solution.

It has been demonstrated that the thermal effects in the saturable absorbers used for mode-locking of solid-state lasers can cause severe limitations on pulse-to-pulse stability for lasers with repetition rates in excess of one pule per second.[67] Thermalization of the energy absorbed by the dye (Eastman Kodak Q-switch Dye 9740 dissolved in Eastman Kodak Q-switch Grade 1,2-Dichloroethane) causes a time-dependent negative lens formed in the volume of the dye that has been heated by the Nd:YAG laser pulses Gaussian intensity profile. The large-scale refraction by the negative lens causes a time dependent loss or gain mechanism that can lead to optical distortion from shot-to-shot and results in large scale amplitude fluctuations. This can lead to an increased mode-locking threshold or to the appearance of higher order transverse modes and possible damage to laser components. Nonuniform laser output occurs if repetition rates exceed the thermal time constants of the dye solution which have been measured to be about one second.[67]

To eliminate the thermal distortion, a closed-cycle, flowing dye cell should be incorporated into the system. The flow velocity has to be adjusted so that fresh solution is exposed to each laser pulse. A

large reservoir of dye solution is necessary to replenish the recirculating system. For a 10Hz system, a flow velocity of 5 cm/sec is adequate to ensure the heated volume of dye is swept away before the next laser pulse[67] (assuming a 5mm beam diameter in the dye cell). Design of the cell should provide for laminar flow so that optical distortions due to movement of the solution between the mirror and output window are kept to a minimum. Pumping action through the cell from a large volume assures uniform mixing of the dye and keeps the dye concentration constant over extended periods of time.

Because of the unstable nature of mode-locking dyes, materials used in construction of a flowing dye cell and reservoir system should be limited to stainless steel, teflon, and glass. Eastman Kodak 9740 is also extremely sensitive to ultraviolet radiation and suffers from severe degradation upon exposure. Therefore to prevent dye decomposition, the glass dye reservoir should be shielded from room lights, teflon tubing used to pump the dye solution through the cell should be black, and the aperture in the dye cell should be small. Further filtering of the ultraviolet light can be accomplished if BK-7 glass is used as the output window of the dye cell.

Strict attention must also be paid to the temperature control of the dye solution for two reasons. First, the absorption characteristics of Eastman Kodak 9740 change significantly with temperature. The absorption variation of this particular dye is one percent per degree Celsius in a dilute solution.[68] Second, because the index of refraction of the dye solution is also temperature dependent, the

temperature must be precisely maintained in order to prevent optical distortions within the dye cell. Therefore it is best to control the dye reservoir to ±0.1°C.

Final and most important of all considerations is the use of a narrow path dye cell in contact with one of the cavity mirrors. The pulse width, spectral, and spatial qualities of individual pulses in a mode-locked pulse train have a direct relationship to the optical path length of the dye cell. Dye cell thickness is related to low-light level transmission, T_0, as follows

$$\ell = \ln(1/T_0)/2\alpha, \quad \alpha = \sigma_D N_0, \tag{18}$$

where σ_D is the absorption coefficient and N_0 is the molecular concentration. Mode-locking dye solutions typically have a low-light level transmission ranging from 50 to 80 percent. The exact low-light level transmittance of the saturable absorber solution is a function of cavity conditions. However, better mode-locking generally occurs at higher transmittance. If higher output powers are desirable, then the range of transmittance should be 50 to 60 percent.

Since the dye concentration is inversely proportional to the optical path length of the cell, a shorter pathlength requires an increased dye concentration. The condition

$$\ell \leq \frac{c\tau_D}{2n} , \tag{19}$$

when combined with the low-light transmission levels that are suitable for proper mode-locking (equation (18)) places constraints not only on dye concentration but on cell thickness. The fact that these two

effects to consider are inversely proportional to one another means a delicate balance between the two must be considered when designing a mode-locking dye cell.

The design considerations imposed by equation (19) arise from the theoretical explanation of the maximum emission principle.[69] In very simplistic terms, it is desirable for the round trip transit time in the contacted dye cell to be less than the relaxation time of the dye, the main reason being that it is undesirable to have the same pulse bleach the saturable absorber more than once in any given transit through the dye cell. If the dye needed to be bleached more than once, a higher laser intensity would be necessary. The threshold for lasing would thus be increased. The higher intensities could lead to intensity dependent effects such as self-phase modulation, self focusing, and optical damage, all of which are typically unwanted effects in mode-locked lasers.

Another reason for a short path length contacted dye cell is due to the "colliding pulse" theory. The "colliding pulse" theory states that due to the nonlinear absorption characteristics of saturable absorbers, the overlap of portions of a pulse in time inside the dye cell leads to pulse shortening. The higher the absorption of the wings of the overlapped pulses relative to the center, more intense part of the pulse results in shorter pulses.

The design of the mode-locking dye cell provided with the original Quantel system (Quantel Mode-locking Dye Cell MS400) satisfied only one of four of the stringent requirements necessary for optimal

mode-locking. Even though the concave 150 cm focal length, 100 percent 1064nm back reflector was in optical contact with the dye solution, the dye cell was stirred with a magnetic stir bar. There was no provision for a laminar flow system from a large dye reservoir. No attention was paid to temperature control of the dye solution and the optical path (2mm) through the cell was much too long to satisfy equation (19). Performance of the oscillator using the MS400 dye cell was very erratic. Missed shots, large shot-to-shot energy instability, and frequent burning of the dye cell window and back reflector were common occurrences. The dye reservoir (the cell itself) was constructed from anodized aluminum and not stainless steel required to keep the dye solution free of contaminates. Stirring of the dye solution was accomplished by coupling a teflon coated bar magnet to another bar magnet attached to the shaft of a 24 volt motor. Solvent often leaked into the motor dissolving electrical insulation leading to short circuiting of the motor. Turbulence caused by the stirring motion also contributed to the less than acceptable performance of the system.

The final design of the mode-locking dye cell used in the oscillator depicted in Figure 6 is shown in Figure 8. The simplicity of its design was the key to its success. The back piece of the cell was designed to hold a concave 1 in. diameter, 0.375 in. thick, 100 percent reflector at 1064nm which had a 300 cm radius of curvature. The front piece of the cell was designed to hold a 1 in. diameter, 0.375 in. thick output window made from BK-7 glass and AR coated at

Fig. 8. Schematic diagram of the design of the laminar flow, short optical pathlength, mechanically stable dye cell.

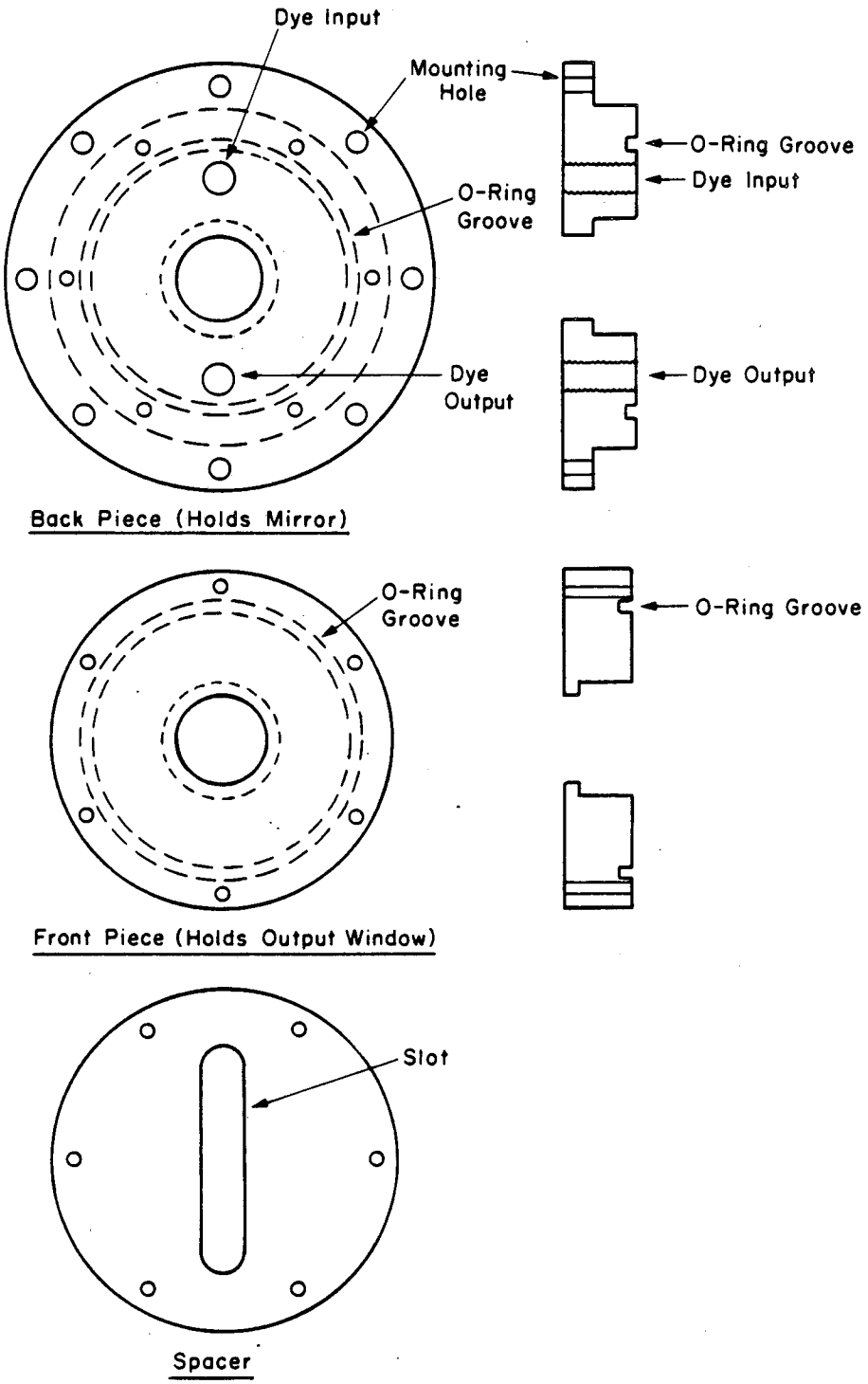

XBL 863-979

Fig. 8

1064nm on the outer surface. The window had a 30 min. of arc wedge in order to avoid etalon effects. The two pieces were constructed from stainless steel and are held together by an eight hole bolt circle with a 2.625 in. diameter. The two pieces compress a 2.25 in. diameter by 1/16 in. thick teflon coated viton O-ring sitting in a groove. Leak tight seals are made between the outer surfaces of the optical components and the 0.75 in. lips machined on the two pieces using 0.875 in. diameter by 1/16 in. thick teflon coated viton O-rings. When assembled the main body of the cell is 2.990 in. in diameter by 1.210 in. thick. Laminar flow is accomplished by having two drilled and tapped 1/16 in pipe thread holes opposite one another within the 2.25 in. diameter O-ring groove on the back piece. These holes serve as the input and output ports for the dye solution. The inner thickness of the cell is determined by using various thicknesses of 2.990 in. diameter stainless steel shim stock machined with a 0.375 in. wide by 2.0 in. long slot for optical clearance. The spacers were also machined to have the same bolt pattern that is used to hold the front and back pieces of the cell together. The back piece was designed to have a 0.250 in. thick by 3.75 in. outer diameter lip with a 3.375 in. diameter bolt circle to allow proper mounting of the cell onto a modified, home designed, two inch diameter mirror mount. The mount provides the appropriate vertical (ϕ) and horizontal (θ) micrometer adjustments necessary in laser cavity alignment.

The ease of construction, relatively small number of parts, leak-tight, laminar flow design, and variable-thickness spacer all contribute to making the dye cell very reliable for optimum mode-locking. Only when O-rings became vitrified or when optical components were burned and needed to be replaced was disassembly required. Equation (19) requires that given the relaxation time of Eastman Kodak Q-switch Dye No. 9740 of 11ps[70] and a solvent refractive index of 1.4, the dye thickness should be no greater than 1.2mm. It is a well known fact that shorter dye path lengths yield shorter pulse lengths in passively mode-locked lasers.[11,69] The lower limit on dye thickness is determined by the onset of turbulence in the flowing dye. No systematic study was performed on the relationship between dye cell path length and laser performance. However, no measurable difference in the output of the laser was observed when either 100 micron or 250 micron spacers were used. Another nice feature of the dye cell-mirror mount configuration was that in the event of a burn on either the window or back reflector, the dye cell could be rotated 180 degrees within the mirror mount. This allowed for easy repositioning and minimal realignment of the laser cavity in the event of a burn.

Dye transport to and from the dye reservoir and flow through the cell were accomplished using a micropump (Micropump Corp. Model No. 81152) that had a variable speed control. Linear flow rates in the neighborhood of 5 cm/sec[67] were maintained to ensure the heated volume of dye was swept away before the next laser pulse. An in-line filter holder (Valin Corp. or Nucleopore Corp.) with a membrane filter

was used to ensure removal of all particulate matter from the flow system. The dye was carried between all components of the flowing system in 0.250 in. outer diameter, black teflon tubing. Connections were made with 0.250 in. Swagelock connectors and 1/16 in. pipe thread adapters, all made from stainless steel. To prevent heating of the dye solution due to the action of the micropump and to maintain a dye solution stable temperature, the glass dye reservoir was placed in a water bath. The water was recirculated, cooled, and temperature controlled by a Neslab Model No. RTE5 Endocal Refrigerated Recirculating Bath. The temperature of the bath was maintained at 25.0°C ± 0.1°C.

Use of a curved (concave) back reflector not only gives the resonator the desired hemispherical character (in conjunction with the flat output coupler), but in general reduces the stringent requirement of cavity stability and facilitates optical alignment. Figure 7 shows that this resonator configuration maintains a beam with a diameter that is large in the dye cell and small at the output coupler. However, introduction of the laser rod into the cavity has a perturbing effect on this arrangement as demonstrated in Figure 9.[71] The positive thermal lens of the laser rod requires compensation if lowest order transverse mode (TEM_{00}) operation is to be achieved. Therefore, a -33 cm focal length, BK-7 lens, AR coated on both surfaces at 1064nm was placed inside the cavity 26.7 cm from the back reflector. The optimum lens position was determined while the laser was free running (non-mode-locked). The final location was based on maximum output

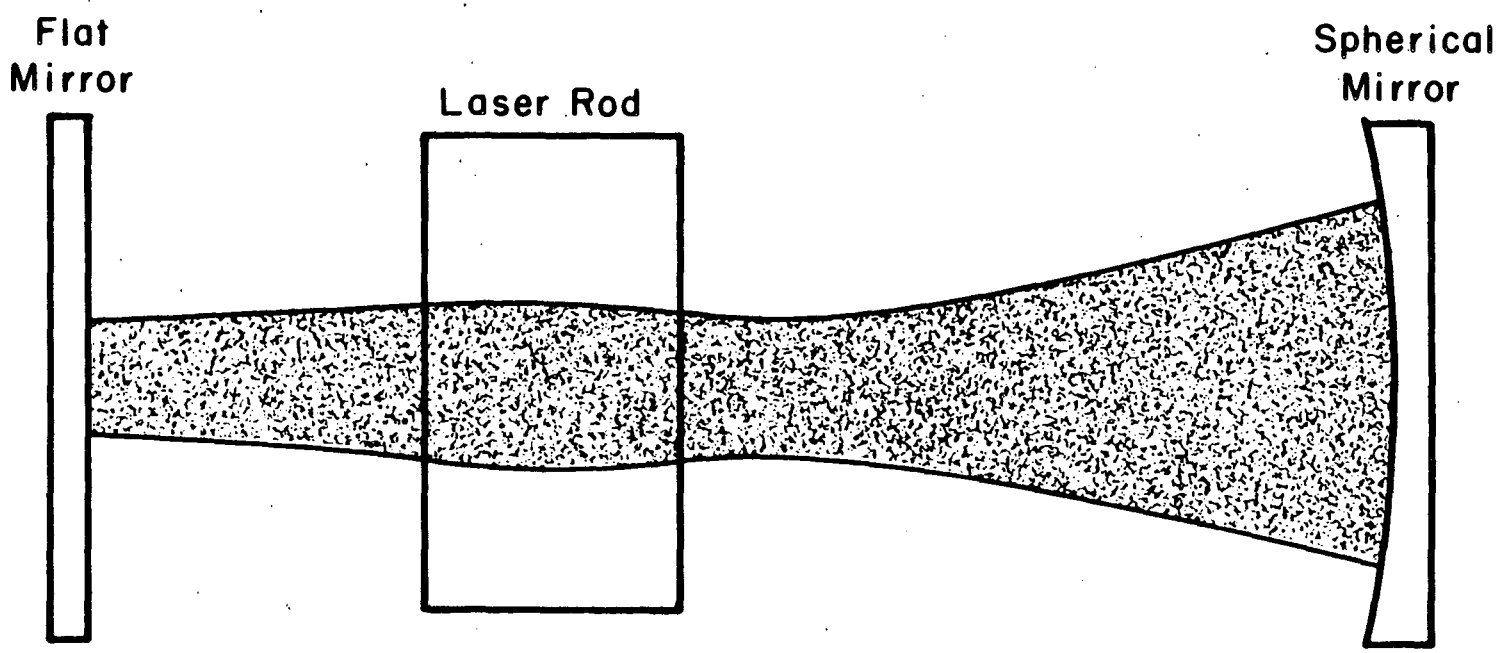

Fig. 9. Schematic diagram of the radiation field behavior within a hemispherical cavity accounting for the effect of the thermal lensing of the laser rod.

XBL 863-988

power during the alignment procedure. Essential adjustments for this lens included vertical and horizontal displacement with respect to the beam propagation axis. Two NRC Model No. 450 Mini-Translation Stages were used for this purpose in conjunction with a home designed lens holder that placed the lens at the correct beam height.

Compensation for the positive thermal lens of the laser rod is necessary for two reasons. First, generation of a diffraction-limited Gaussian TEM_{00} spatial profile is very important. Nonlinear optical methods such as harmonic generation and parametric interactions require homogeneous spatial profiles. Second, the introduction of a positive thermal lens inside the cavity causes the beam to be smaller at the dye cell and laser rods than would normally be expected in the hemispherical resonator. A higher probability of burning the dye cell window or reflector therefore exists due to the reduced beam size resulting in an increased optical power density. Also, less gain can be extracted from the laser gain medium if a smaller beam passes through the rod. Figure 9[71] demonstrates the intracavity field behavior without thermal lens compensation. There is clear evidence of the existence of two beam wastes as opposed to one in the case of true hemispherical character as seen in Figure 7. Beam divergence and mode quality of such a resonator would be more difficult to understand and control.

Introduction of a compensating lens within the laser cavity relaxes some of the critical requirements of laser head positioning. Initially, the laser head was placed approximately in the center of

the cavity. The beam size through the rod was empirically tailored to extract maximum gain and fit hemispherical requirements by sliding the lens along the optical rail system.

The schematic diagram of the laser oscillator in Figure 6 shows two 1.5mm apertures placed 62.2 cm and 119.9 cm away from the rear mirror. These apertures ensured TEM_{00} output. TEM_{00} mode operation is preferable not only for reasons mentioned previously, but because of the reduction of intermode interference effects and the avoidance of component damage that frequently accompanies multitransverse-mode operation due to large localized power densities. The apertures were constructed from a machinable ceramic (MACOR) and were placed in mounts identical to that used for the intracavity lens. When intracavity apertures were machined from steel shim stock, observation of burns around the opening were noticed. To ensure no irregularities in the mode pattern, MACOR was substituted.

The size of the aperture was chosen to correspond to the smallest size that permitted proper alignment of the cavity. Use of larger apertures resulted in increased output power. However, the implementation of active mode-locking created more stringent requirements in the alignment procedure. It became much more critical to make sure the beam was propagating parallel to the optical rails. Smaller apertures were essential in fulfilling this requirement. Also, if the apertures became too large, the beam quality began to deteriorate.

To ensure TEM_{00} output, the apertures should act as a spatial filter, and therefore should be placed at or near a beam waist. In a true hemispherical resonator, the beam waist is at the reflective surface of the output coupler as depicted in Figure 7. Therefore, in principle only the second aperture should be necessary in the cavity. However, because of the effect of the positive thermal lens of the laser rod, a second beam waist exists between the dye cell and the laser head shown in Figure 9.[71] The use of the -33 cm focal length lens should restore true hemispherical character to the resonator and only the second aperture should be required. However, operation of the laser without the first aperture resulted in a decrease in energy amplitude stability from less than two percent to greater than five percent. Also, a degradation in beam quality was noticed. These observation led to the conclusion that a spatial filter was needed before the laser head to filter out higher order transverse modes. A mild beam waist must be present even with the compensating lens.

The laser head is placed between the two mode selecting apertures and 73.3 cm from the rear reflector. The laser head is a Quantel Model No. SF408-07[72] and was used without modification. The module contained a 7mm diameter by 93mm long Nd:YAG (Neodymium 3+ ion doped into Yttrium Aluminum Garnet, $Nd^{3+}:Y_3Al_5O_{12}$) rod cut and polished at Brewster's angle. The oscillator rod was doped to a level of 1.1 percent by atomic weight with neodymium ions. The Nd:YAG laser is a four-level system. The laser transition having a wavelength of

1064nm originates from the R_2 component of the $^4F_{3/2}$ level and terminates at the Y_3 component of the $^4I_{11/12}$ level.

The SF408-07 has two linear quartz flashlamps filled with two atmospheres of Krypton (EG and G Electrooptics Model No. SKQS273-3) situated above and below the laser rod. Krypton filled flashlamps are used as the excitation source of the Nd^{3+} ions because the emission of these lamps best matches the absorption spectrum of the Nd^{3+} ion doped in YAG. The pumping geometry is surrounded by a high reflectivity magnesium oxide diffuser that homogenizes the output of the lamps. The discharge system used to fire the flashlamps uses a negative critically damped pulse (-1.8KV maximum) of duration 250 μsec (FWHM).[72] The lamps are short circuited by ionizing the Krypton with a short trigger pulse. The trigger pulse comes from a high voltage silicon controlled rectifier (SCR) triggering circuit.[72] The SCR pulse is voltage doubled in a transformer and creates a 17KV voltage spike. The flashlamps ionize before this voltage is reached. The ionized flashlamps discharge the 30μF capacitor in the capacitor bank causing the high intensity light flash.[72] The maximum pumping energy deliverable to the laser head is thus 27J per lamp in 250μsec at 10Hz.

The control unit, power supplies, and capacitor banks which control the firing order of the laser heads, supply power to the capacitor banks, and store energy for the flashlamps are Quantel Model Nos. CU401, PU420 and 430, and CB430 respectively.[72] Early in the use of the Quantel components the discovery was made that the original

SCR used in the trigger circuit (CS-14603) was not robust enough for this application and its lifetime was severely limited under these operating conditions. Subsequently the old SCR was replaced with a GEC158PB SCR.

Between 20 and 27 Joules per pulse per laser head must be dissipated and carried away when such a laser system is in operation. This large thermal load coupled with the strong output stability dependence on temperature variation placed very stringent requirement on the choice of a cooling system for the laser heads. Originally the cooling system employed was that supplied with the Quantel YAG400 system (CG404 cooling group).[72] Although the cooling capacity of this component was sufficient to cool the oscillator and amplifier heads, the stability of the system was insufficient. Observation that the oscillator output energy and pulse train envelope shape fluctuated significantly in a regular pattern corresponding to the opening and closing of a solenoid valve responsible for the heat exchange of the recirculating deionized water led to the replacement of the CG404. The replacement was a Neslab Coolflow Refrigerated Recirculator (Model No. 313231). Upon replacement of the CG404 the recycling fluctuation ceased. The temperature of the cooling water was maintained at $25.0^{\circ}C \pm 0.1^{\circ}C$.

The most important change that was made in the modification of the original Quantel YAG400 design was the addition of an active mode-locker to the oscillator. The use of active mode-locking in combination with passive mode-locking is a necessity if the inherent

instabilities of a purely passive system are to be eliminated,[4-6,58,59] While the establishment of many new alignment procedures was necessary to ensure the proper use and performance of the acoustooptic modulator, when all the "bugs" were worked out the device was instrumental in the stabilization of the laser. A description of the alignment procedure and precautions will take place in the next section.

The acoustooptic modulator of Figure 6 was placed at Brewster's angle inside the laser cavity and located 127.5 cm from the rear reflector. The device acts as a loss modulator (AM mode-locking). Under the proper conditions, part of the input optical beam is diffracted into a new direction while simultaneously being shifted in frequency by an amount equal to the acoustic frequency. The interaction involves two optical fields at frequencies ω_i and ω_d, such that $\omega_d = \omega_i \pm \omega_s$ where ω_s is the frequency of the sound field. Thus sidebands are generated at $\pm\ \omega_s$ that are in phase with ω_i. If the frequency of the sound field is chosen to correspond to the spacing of the axial modes of the cavity, then phase locking occurs (recall previous discussion on active mode-locking). However, for the case of Nd:YAG, which is a homogeneously broadened system, only one mode can normally oscillate. One way to reconcile this fact with an understanding of mode-locking is prescribed by Yariv.[73] In the presence of internal modulation power is continuously transferred from the high gain mode to those of lower gain (ones that are not above threshold for oscillation). Therefore in the case of a homogeneously broadened system, the phenomenon of sideband formation

is not one of mode-locking but one of mode generation. The net result, however, is that a large number of modes oscillate with equal frequency spacing and fixed phase as in the inhomogeneous case discussed previously. The end result is the same.

The interaction between the light wave and sound wave can be viewed as is the case with all nonlinear phenomena, in terms of energy and momentum conservation. A photon with energy ω_i and momentum K_i is incident on a sound wave of frequency ω_s and momentum K_s. The incident photon is annihilated producing a new photon with ω_d, K_d and a phonon with ω_s, K_s. Figure 10[73] shows the situation for the diffraction of light from both a retreating and oncoming sound wave. The loss modulation occurs because the light is diffracted out from the beam propagation direction at a frequency equal to the reciprocal of the round trip transit time of the cavity.

If in the analysis of energy and momentum conservation the assumption that the acoustic frequency is much less than the optical frequency is to be made (i.e., $\omega_s << \omega_i$), which is certain to be true, then $n_i \approx n_d$ and $K_i \approx K_d = K$. Therefore, the vector triangle of Figure 10a[73] gives

$$K_s = 2K \sin\theta. \tag{20}$$

Using $K_s = 2\pi/\lambda_s$, $K = 2\pi n/\lambda$, equation 20 becomes

$$2\lambda_s \sin\theta = \frac{\lambda}{n} . \tag{21}$$

Equation (21) is the first order Bragg condition for x-ray scattering in crystalline structures. The periodicity of the sound wave is analogous to the periodicity of atomic planes in a crystal. The only

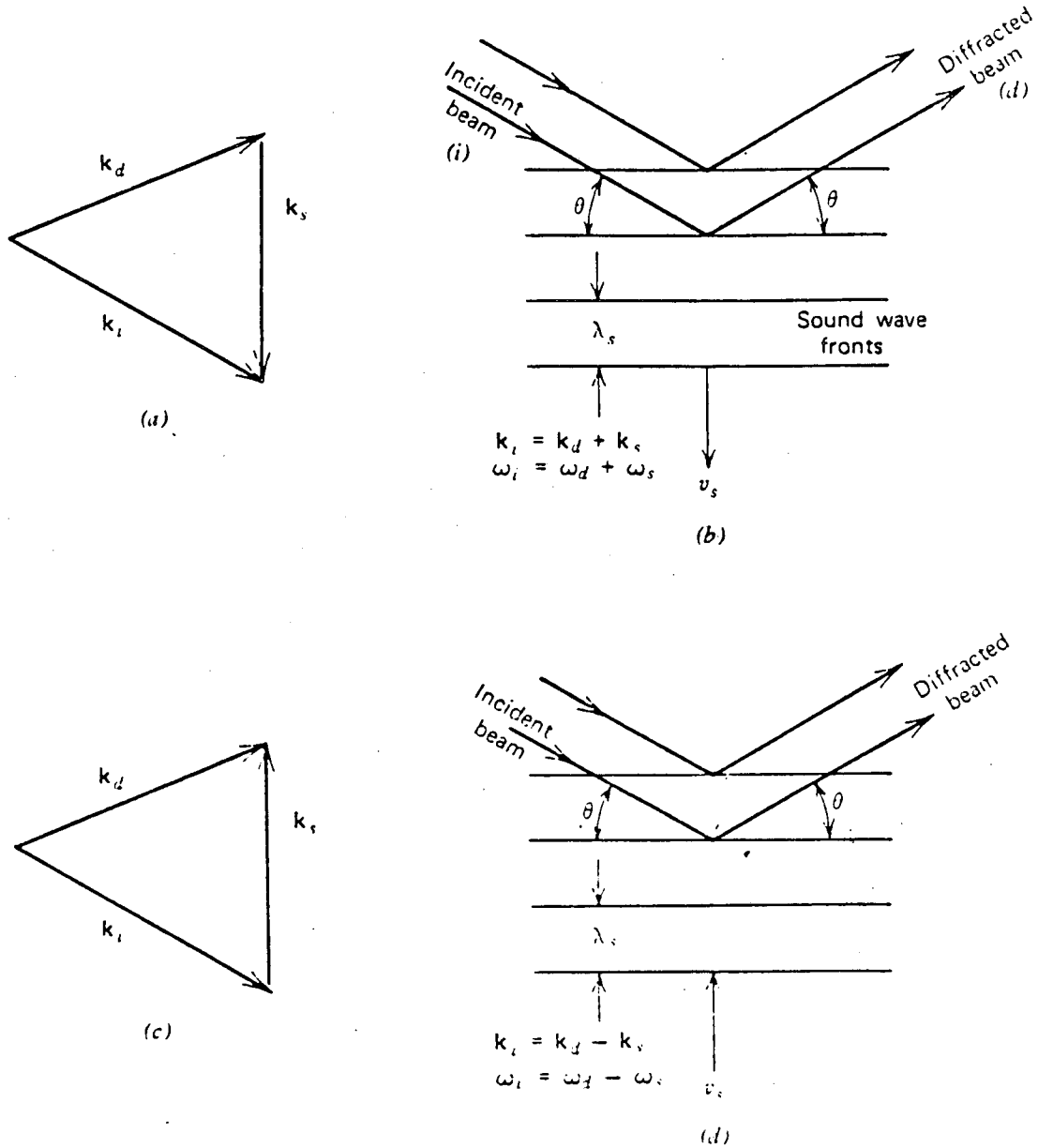

XBL 863-978

Fig. 10. (a) The Bragg vector diagram and (b) corresponding physical picture for the diffraction of light from a retreating acoustic wave. (c-d) The same as (a) and (b) but for an oncoming acoustic wave (from reference 73).

differences are the lack of higher order diffraction angles in equation (21) due to the sinusoidal nature of the sound waves, and the frequency shift (Doppler shift) due to the acoustic planes movement with a velocity equal to the speed of sound in the medium, V_s.

The acoustooptic mode-locking device used was an IntraAction Corporation Model No. ML-505Q. The device is constructed from a 2.75 in. long piece of fused quartz (SiO_2) with a 5mm sound field aperture. The transmission of the RF power is through standard, 50 ohm coaxial cable. A lithium niobate ($LiNbO_3$) transducer bonded to the crystal is used to change the electrical signal into a sound wave. The sound wave travels along the height axis of the crystal. The modulator was mounted on a modified NRC 600A-2 mirror mount. The mount provided adjustments for Brewster's angle (x-axis, if z-axis = beam propagation axis) and more importantly for the Bragg angle (y-axis, if z-axis = beam propagation axis) defined by equation (21).

The RF drive power for the mode-locker is supplied by an Intra-Action Corporation Model No. MLE-6B Frequency Synthesizer. The synthesizer can be used to supply either continuous or pulsed RF output. Use in the continuous mode required cooling of the mode-locker due to the large thermal load. Even though pulsed operation is reported to enhance stability of the laser due to greater modulation depths achievable,[5,6] use of the device discussed presently was in the continuous mode. Output stabilities observed with continuous mode operation[4] were equivalent to those observed with pulsed mode operation.[6] At the large value of RF powers used (8 watts) a

modulation depth at 1064nm of approximately 0.95 was routinely achievable. This is in the range of the modulation depth reported in pulsed mode and is accountable for the high degree of energy stability reported.

Cooling the device was accomplished with a HAAKE FE2 Temperature Controller. The temperature was maintained at 28.0°C ± 0.1°C. The modulation frequency used was 50.145 MHz. Because there are two extrema for every cycle of the RF signal, there are two maxima in the transmission function per period. Therefore a drive frequency of 50.145 MHz corresponds to the radiation field experiencing a frequency of 100-290 MHz. This larger value was used to match the cavity length. Cooling the device serves two purposes. First, heat removal from the crystal is essential if operation in continuous mode is chosen. Second, the RF resonances of the crystal are extremely sensitive to temperature. The steady-state operating temperature depends not only on what the bath temperature is set at, but also on the drive power. Therefore having a variable, temperature controlled bath proved to be essential in "temperature tuning" the crystal to the appropriate resonant frequency. RF resonances were determined by minimizing the ratio of reflected power to transmitted power incident on the crystal. The reflected and transmitted power were measured by a Bird Mode No. 43 Wattmeter. For 8 watts of transmitted power at 50.145 MHz, less than 0.5 watts of reflected power was measured when the crystal was held at 28°C.

The output coupler used for this resonator design was a 30 percent reflector at 1064nm. The non-reflective side was AR coated at 1064nm and had a 30 min. of arc wedge. The output coupler was placed 138.6 cm away from the back mirror and mounted in a home designed mirror mount for one inch diameter optics. The mirror mount, used throughout the laboratory, allowed for both horizontal (θ) and vertical (ϕ) tilt adjustments that were essential for cavity alignment. The mirror mount was rigidly attached to a NRC 430-1 Linear Travel Translation Stage. Proper cavity length matching to the acoustooptic modulation frequency could therefore be accomplished.

The distance from the active mode-locker to the output coupler is an important consideration upon initial setup of the resonator. It is well known[6] that for CW mode-locked lasers it is necessary to place the active mode-locker extremely close to one of the cavity mirrors in order to minimize cavity losses. This criterion is not as important when the laser is pulsed because of the higher peak gains attainable.[6] A distance of 11 cm from the output coupler is well within the critical distance to ensure minimal fluctuations, shortest pulse durations, and minimal resonator losses for this cavity configuration.

The output of the laser oscillator just described is a mode-locked pulse train consisting of between 8 and 10 pulses (FWHM) separated by 2L/c, the round trip cavity transit time (10ns). Typical outputs look like Figure 4. Most experiments utilizing the output of this type of laser require just a single pulse. Depending on experimental

requirements of energy, pulse durations, and spectral purity, the ability to select a single pulse from various parts of the pulse train is an essential part of a pulsed mode-locked system. As was mentioned previously, having a linearly polarized output and an interpulse separation of 10ns allows the use of the Pockels effect as the external gating technique.

Figure 11 depicts the external gating technique used for single pulse selection. A -10.0 cm focal length lens and 16.0 cm focal length lens are paired together to form a telescope which expands the beam by a factor of 1.6. Both lenses are AR coated at 1064nm on both sides to prevent back reflections into the oscillator. The increased beam size is necessary to decrease the optical intensity passing through the Pockels cell in order to avoid optical damage. The single pulse selector is a slightly modified Quantel PF302 pulse slicer.[72] The optical system of the PF302 consists of two crossed Glan-Taylor calcite polarizers. Between the two polarizers is a three terminal, double crystal Pockels cell. The laser output is not perfectly p-polarized (horizontal). Any S-polarized (vertical) light is rejected by the first polarizer (extinction ratio of 10^4). P-polarized light passes through the first polarizer and the Pockels cell. The p-polarized light is deflected upward to a photodetector that generates a fast (< 1ns rise time) trigger signal which activates the Pockels cell after a delay time of approximately 15ns. The Pockels cell s activated for several nanoseconds (depending on a delay cable length). At the moment of activation, the fast high voltage

Fig. 11. Schematic diagram of the optical arrangement for single pulse selection including beam expansion, Glan-Taylor polarizers, and Pockels cell.

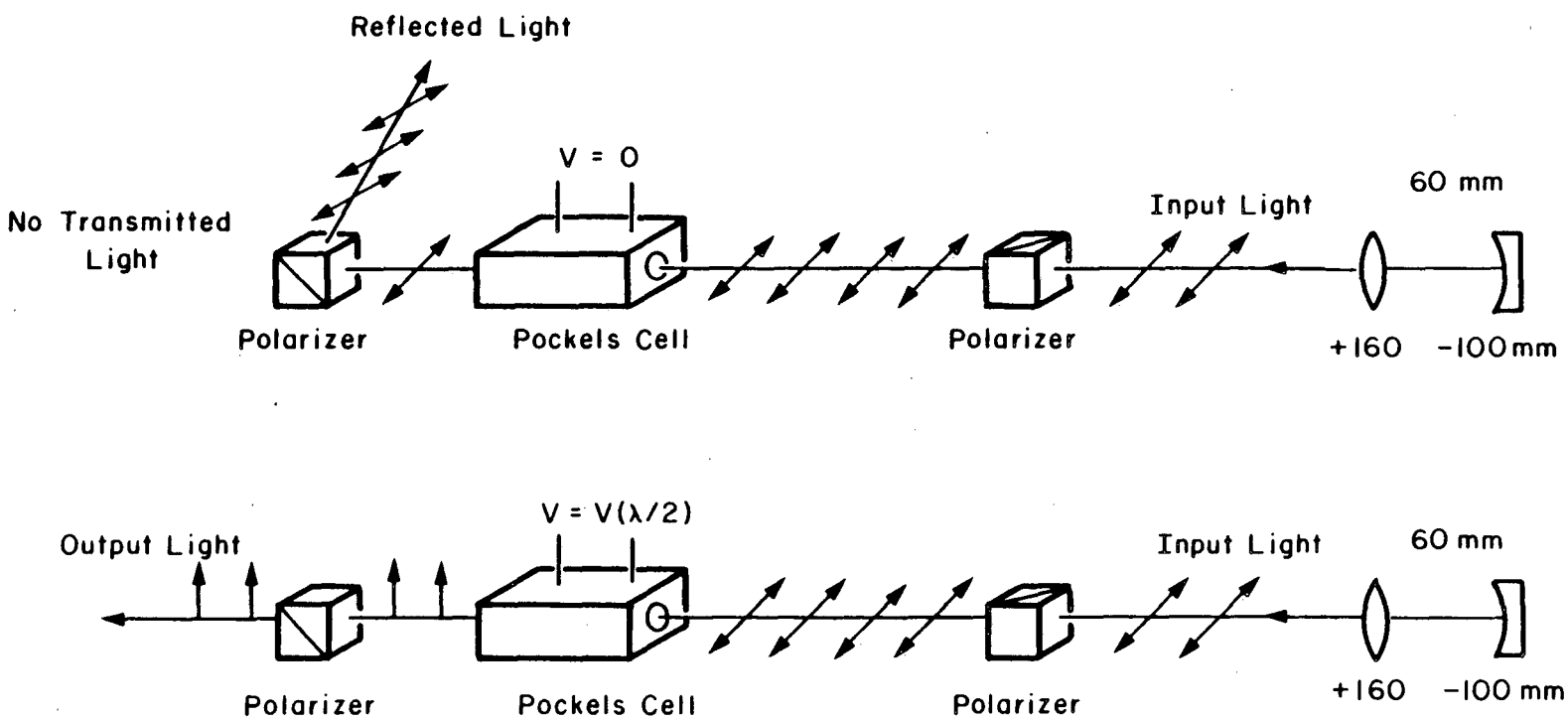

Fig. 11

XBL 863-987

switching electronics apply the half-wave voltage to the KD*P (deuterated potassium dihydrogen phosphate) crystals. This causes a polarization rotation by 90 degrees of the desired pulse. The rotated pulse is thereby transmitted by the second polarizer.

A voltage applied to the optic axis of the KD*P crystals induces birefringence in the material due to the electrooptic effect. By selecting the proper voltage it is possible to obtain a path difference equal to a half wavelength which follows from[72,73]

$$V_{\lambda/2} = \frac{\lambda}{2n_o^3 r_{63}} , \tag{22}$$

where λ is the laser wavelength (1064nm) n_o is the ordinary index of refraction of KD*P (1.47) and r_{63} is the electrooptic coefficient for KD*P (80×10^{10} cm/V_oH). KD*P is used due to the lower value of its absorption coefficient at 1064nm and higher electrooptic coefficient than KDP. The induced optical path difference makes the Pockels cell equivalent to a half-wave plate for light propagating along the crystal axis.

The PF302 is equipped with a Pockels cell which has two crystals in optical series. Therefore the required voltage is one half $V_{\lambda/2}$ (or $V_{\lambda/4}$), which is 3300 volts according to equation (22). When combined with the two crossed polarizers, the Pockels cell acts as a shutter, opening and closing when the high voltage is applied.

The high voltage pulse to the Pockels cell is formed by discharging two 50 ohm coaxial cables of different lengths through their characteristic impedances when a Krytron switch closes. The Krytron

is triggered by an avalanche transistor Marx multiplier train.[74] The transistor chain is triggered by the photodetector output. Variation of which part of the pulse train the pulse is selected from is determined by a threshold condition. Establishment of the threshold condition is achieved by varying the aperture size of an iris placed before the photodetector. The exact duration of the square wave high voltage pulse applied to the Pockels cell is derived from the difference in length of the two cables to be discharged. Twenty centimeters of 50 ohm coaxial cable corresponds to one nanosecond delay. Therefore a suitable delay cable length considering the interpulse separation of 10ns is 60 cm corresponding to 3ns.

Modifications of the PF302 included placing the first polarizer outside the PF302 housing, replacing the Quantel Pockels cell mount with an NRC RSA-2 rotation stage, and placing the whole assembly on a home designed three point kinematic tilt adjust system. All three optical modifications facilitated the alignment procedure which will be discussed in the next section. Electrical modifications included replacing the 47 ohm, one watt resistors which the pulse forming cables were discharged through to 47 ohm 2 watt resistors. Chronic burning out (resulting in an open circuit) of these resistors led to erratic pulse selection. Once the heftier resistors were exchanged, the problem never repeated itself. Also, placing sockets on the PC board for the Krytron connections facilitated changing of the Krytron which typically was necessary for every 10^7 shots of the laser. Prior to the sockets, the Krytron was soldered directly to the PC

board. Finally, provisions were made to delay the trigger pulse to the Marx Multipliers avalanche chain so that pulses well beyond the peak of the pulse train could be routinely selected for amplification. This was essential to the characterization and utilization of the intracavity pulse compression technique to be described in Chapter III.

E. Operation and Performance: (Oscillator and single pulse selector)

Proper alignment of the laser cavity is critical if optimum performance is to be expected. No systematic method of alignment for the cavity existed prior to the time that the work to improve and stabilize the laser was initiated. The inclusion of active mode-locking forced more stringent requirements on intracavity beam propagation. Owing to the fact that the cavity length had become an adjustable parameter, the beam propagation direction needed to be exactly perpendicular to the flat 30 percent reflecting output coupler (i.e., parallel to the optical rail system).

Prior to the implementation of active mode-locking the alignment procedure consisted merely of adjustments of the end mirrors and intracavity lens while only solvent flowed in the dye cell. Tweaking continued until a maximum output power was obtained using the voltage on the flashlamps prescribed by Quantel. Mode-locking dye was then added until the number of pulses in the mode-locked pulse train reached the prescribed number. Use of a power meter to aid the procedure was nearly impossible because the energy fluctuations and percentage of missed shots were so large that a relevant steady-state reading was unattainable at the 10Hz repetition rate of the oscillator. The use of active mode-locking required a more sophisticated and systematic alignment procedure.

Incorporation of a separate alignment laser into the system proved to be invaluable. A Uniphase 1103P Helium-Neon (HeNe) laser (1.8mW, TEM_{00} at 6328Å) with accompanying power supply was used. The HeNe

laser was mounted in an NRC Model number 810 Laser Mount that provided the necessary vertical (ϕ) and horizontal (θ) tilt adjustments. Provisions for vertical and horizontal translational adjustments were made by incorporating two NRC Model number 430-1 translation stages into the post holder for the laser mount. Both angular and translational adjustments were necessary to ensure that the HeNe beam propagation direction was parallel to the optical rail system at the proper laser beam height and lateral position. In retrospect, a more cost effective method would be to use a stationary HeNe laser in conjunction with two aluminum coated mirrors mounted in mirror mounts with vertical (ϕ) and horizontal (θ) tilt adjustments. Parallel propagation and positioning could be achieved in this way as well.

Upon the initial setup of the resonator, the mode-locking dye cell with only solvent flowing was positioned on the optical rail system. The HeNe laser was then adjusted so that its beam passed through the cell and travelled straight down the rail system a distance of approximately eight feet (the laser table distance). This was accomplished by adjusting the first 1.5mm transverse mode selecting aperture to the exact vertical and horizontal position corresponding to where the laser beam was to pass through the Nd:YAG rod. To assure the HeNe beam was parallel to the optical rail system the aperture was then moved up and down the rail system while the HeNe beam was tilted and translated in both vertical and horizontal directions to ensure it passed through the aperture. This procedure was repeated until the

beam no loner walked off the aperture over the full eight foot length of the optical rail system.

The laser head was then placed 73.3cm from the rear mirror and positioned so that HeNe beam passed through the center of the laser rod. The second aperture was then positioned so the beam traverses it clearly and concentrically. It is important to note that once the apertures were initially set, they were never adjusted in either the horizontal or vertical directions. Not only were they used as transverse mode selectors, but also to define the beam propagation axis that alwyas needed to be maintained parallel to the optical rails and orthogonal to the output coupler.

The active mode-locker was then placed 127.5cm from the rear reflector and positioned so the beam passed through the center of the crystal. The output coupler was then placed approximately 140cm from the back mirror. Finally, the intracavity lens was placed between 25.4cm and 27.9cm from the back reflector. The lens position in the plane normal to the beam propagation direction was adjusted so the HeNe beam travelled undisturbed through the two apertures and the laser rod.

With the high voltage on the flashlamps set to 1.16 kV (approximately 10J per lamp per pulse) lasing was achieved by adjusting the rear reflector and output coupler so that the back reflections of the HeNe beam from the reflective surfaces travel back colinear with the beam. Observation of the infrared radiation

(1064nm) was facilitated by viewing the phosphorescence from a Kodak IR Phosphor Card.

Once lasing was achieved, steps were taken to ensure the 1064nm beam travelled straight through the apertures that define the resonator optic axis. The beam was "walked" through the two apertures while monitoring the output energy with a Scientech Laser Power Meter (Model No. 360001) that was displayed by a Scientech Power Energy Meter (Model No. 362). The procedure of walking the beam through the apertures is as follows. The output coupler is tilted in either the horizontal (θ) or vertical (ϕ) direction, resulting in a decrease in energy. Then the rear reflector is tilted in the same direction until a maximum is observed. This is done repeatly in both dimensions until an output energy of between 8mJ and 10mJ is obtained. If this value has not been reached after the beam has been "walked", the intracavity lens should be adjusted. The required adjustments include translation in both the horizontal and vertical dimensions as well as a translation along the propagation direction. Lens adjustment should take place after the beam has been "walked", and not between iterations, since the way the two adjustments affect the beam propagation is closely coupled.

Once the prescribed energy level was reached, it was important to make sure that the beam was travelling straight through the apertures and, therefore, perpendicular to the output coupler. This was accomplished by a translation of the output coupler over a one inch distance. If the output energy did not decrease by more than 10 or 15

percent, then the beam was parallel. If this was not the case, then the beam needed to be "rewalked". This was very important if the active mode-locker was to be aligned properly. Finally, a Brewster angle adjustment was made on the acoustooptic modulator to assure maximum output of p-polarized light.

Once satisfied with the output energy of the free-running (nonmodelocked) laser (8-10mJ), the threshold for lasing was checked by reducing the voltage to the flashlamps and observing when lasing ceased. A threshold value of 0.9 KV or less indicated proper alignment. Threshold valves higher than 0.9 KV indicated either improper alignment or old flashlamps. If flashlamps were the problem, then at the pumping voltages mentioned (1.14 KV - 1.16 KV) output energies below 8mJ were generated. While true that energy insufficiencies with old flashlamps could be compensated for by increasing voltages, use of old flashlamps resulted in erratic mode-locking and beam profile distortions. Flashlamp lifetimes were typically 10^7 shots.

Once satisfied with the general alignment of the resonator and the output performance of the free-running laser, the active mode-locker was turned on. Approximately fifteen minutes were required to allow the mode-locker to reach its steady-state operating temperature. For 8 watts of RF power, it was necessary to maintain the mode-locker at 28°C to keep the crystal in resonance at 50.145 MHz. Once the mode-locker was "warmed up", alignment could proceed. The two adjustments involved in this procedure were Bragg angle and cavity length. Improper Bragg angle adjustment resulted in ineffective

modulation. Cavity length mismatch resulted in energy instability and reduction. If the mismatch was great enough, lasing ceased completely.

It was therefore important upon initial resonator setup to calculate the approximate resonator length. This was done by multiplying the speed of light by twice the modulation frequency. When matching this number to the resonator length, both the index of refraction of the solvent, output window, intracavity lens, laser rod, and acoustooptic modulator as well as their respective lengths had to be taken into account. The output coupler was then placed within one inch of this calculated value from the reflective surface of the rear mirror. The HeNe beam was used to coarsely adjust the Bragg angle. Even though the respective wavelengths of Nd:YAG and HeNe are different (10641Å and 6328Å) and therefore give different values of the Bragg angle according to equation (22), the difference is small enough so that upon initial alignment, the HeNe is adequate. The HeNe output on passage through the modulation becomes three spots. The central spot is the main beam and the spots above and below the central spot correspond to the deflected beams. Crude adjustment of the Bragg angle is accomplished by maximizing the intensity of one of the deflected spots. The intensity of the central spot always remains the brightest, it is still easy to tell when you have reached a maximum in the deflected intensity.

The oscillator was turned on again after the Bragg angle and laser cavity length were coarsely adjusted. Fine adjustment of the Bragg angle required the resonator length to be detuned by approximately one

centimeter. If this was the case, the output energy was in the range between 1.0mJ and 2.0mJ. Proper Bragg angle alignment and cavity length adjustment required the output energy to be approximately 3.0mJ to 3.5mJ at this point. This would be the case, however, when the acoustooptic modulator is turned on, the main beam is slightly deflected resulting in a perturbation of the alignment of the cavity. This can be corrected for simply by adjusting the intracavity lens in both the vertical and horizontal directions. The output energy should then be between 3.0mJ and 3.5mJ.

Fine adjustment of the Bragg angle required viewing of the laser output on a white index card with an FJW Industries Find-R-Scope Infrared Viewer. Observation of the laser output following the beam expanding telescope (factor of 1.6) before the single pulse selector helped to spatially resolve the deflected spots. With the cavity length mismatched by at least one centimeter, fine adjustment of the Bragg angle was accomplished by tilting the modulator (vertical adjustment) until a maximum in the intensity of one of the deflected spots was found. The deflected spot was either above or below the central spot depending on how the light was incident upon the sound wave plane according to Figure 10 (i.e., the direction the modulator is tilted).

Once confidence was established in the Bragg angle adjustment (the intensity monitoring with the eye is subtle and may require a few repeat attempts before being convinced that Bragg angle is correct), the cavity length was matched to the acoustic frequency. The

oscillator energy output was continuously monitored with the power meter while translating the output coupler. Observation of a maximum in energy indicated cavity length matching was complete. It was very important, however, to determine that the value recorded was actually a maximum and not just an artifact that the cavity was improperly aligned (i.e., laser beam not perpendicular to the output coupler). Determination that a maximum was achieved was accomplished by translating the output coupler back and forth through the maximum several times ascertaining that it was a true extremum. Optimum performance from the oscillator was observed when the Bragg angle was correct to within 0.05 degrees and the cavity length was matched to twice the modulation frequency to less than 0.003 in. (~ 75 μm).

The amplitude stability of the laser output (when only actively mode-locked) was measured at this point. This measurement was accomplished in one of two ways. First the output energy was monitored by large area quadrant detector silicon photodiode (Silicon Detector Corp. Model No. DS-380-23-21-251) used in photovoltaic mode. The output of the photodiode was sampled and held and displayed on a storage oscilloscope (Tektronix Model No. 7834 with a 7A24 or 7A26 Dual Trace Amplifier and a 7B92A Dual Trace Time Base) using a slow sweep rate. This allowed a visual determination of the shot-to-shot reproducibility. Second, the output of the photodiode fed into a sample and hold circuit and then digitized and averaged by a DEC LSI11/2 microcomputer. Typically, 100 shots were accumulated and averaged. If the laser output had an energy amplitude stability of

better than ± 2 percent, it was time to add mode-locking dye solution. If not, the alignment procedure or a portion of it was repeated.

The procedure just described was very time consuming. Major maintenance on the oscillator was necessary only every three or four months. Complete realignment was not required every time the laser was remode-locked. Hence, instead of performing the major realignment procedure upon routine remode-locking, short cuts were developed to expedite alignment while maintaining proper performance. If no major problems had occurred and no optical components had been "bumped" (displaced), then upon remode-locking necessary check points were energy and output characteristics of the oscillator. The energy checkpoints were the same as those described previously. The output characteristics observed were the relaxation oscillations and the shape, reproducibility, and modulation depth of one of the relaxation oscillations that would become the mode-locked pulse train upon addition of mode-locking dye.

The discovery that the relaxation oscillations were a good indication of how well the laser was aligned[75] made the procedure much easier. Figure 12 shows the output of an ITT 4014 Bi-Planar Vacuum Photodiode in an ITT F4542 holder displayed on a Tektronix 7834 Storage Oscilloscope (with 7A26 amplifier and 7B92A time base) to demonstrate this point. As seen in Figure 12b, for a small cavity length mismatch (greater than 75 μm) the relaxation oscillations are quite irregular and do not exhibit the nice exponentially damped behavior expected when the cavity length is correct. Figure 12a shows

Fig. 12. Oscilloscope photographs (horizontal scale is 10 μsec/div.) of relaxation oscillation when (a) the cavity length is in resonance with the modulation frequency, and (b) when the cavity length is slightly off resonance. Oscilloscope photgraphs of (horizonal scale is 10 ns/div.) the first relaxation oscillation when (c) the Bragg angle is correctly adjusted, and (d) when the Bragg angle is off by greater than 0.05 degrees. (e) Oscilloscope photograph (horizontal scale is 100 ns/div.) of the first relaxation oscillation with the modulator turned off.

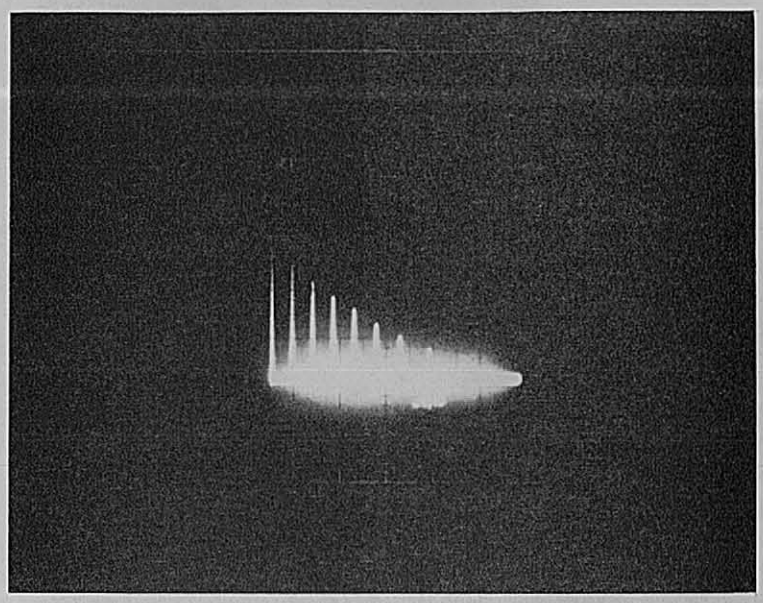

Fig. 12(a)

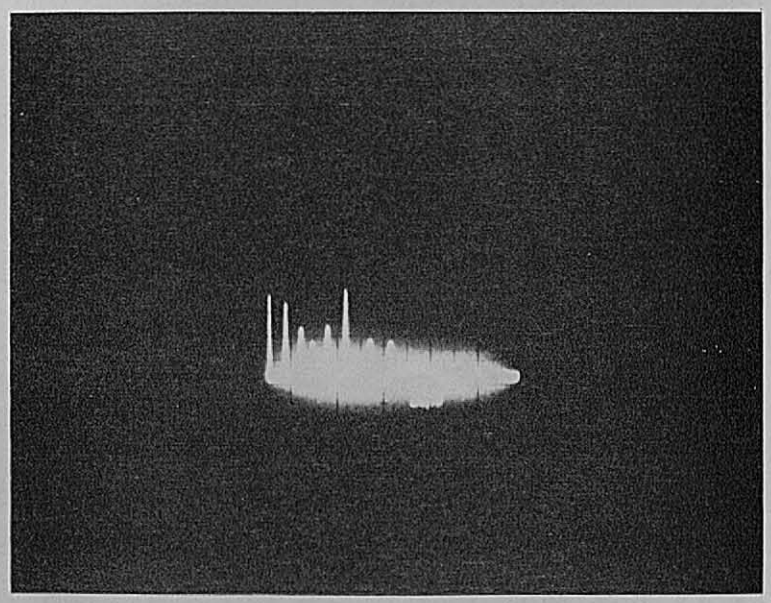

XBB 863-1635

Fig. 12(b)

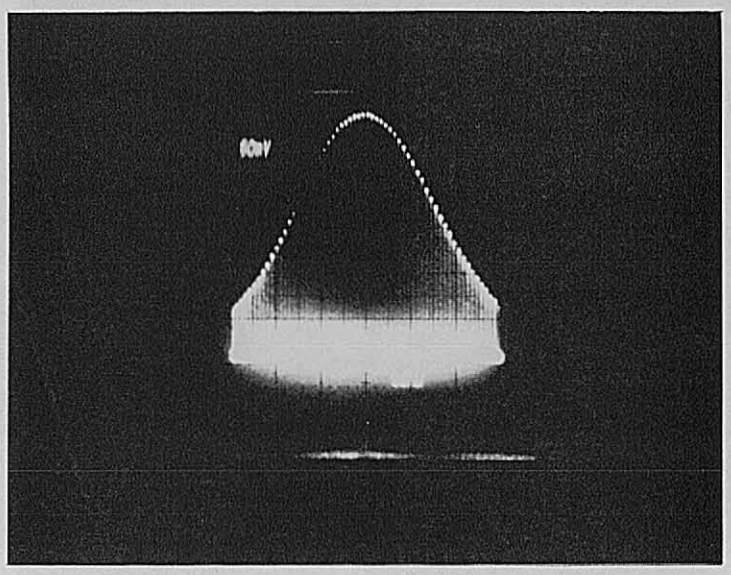

Fig. 12(c)

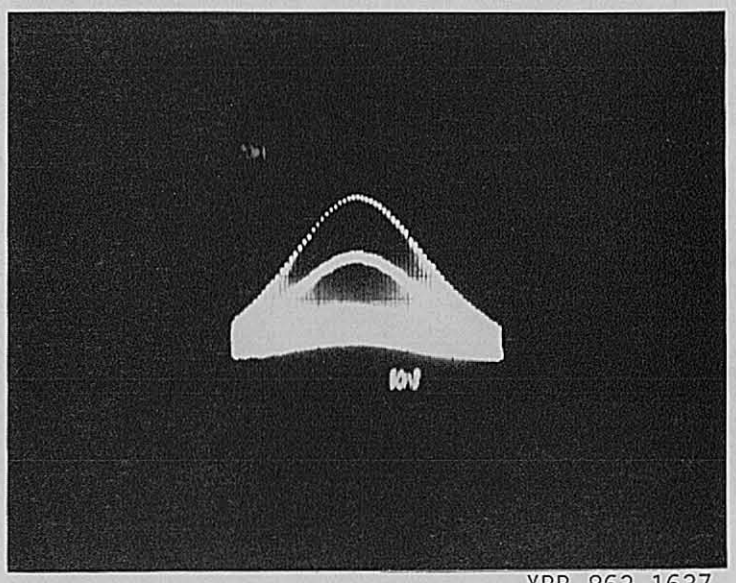

XBB 863-1637

Fig. 12(d)

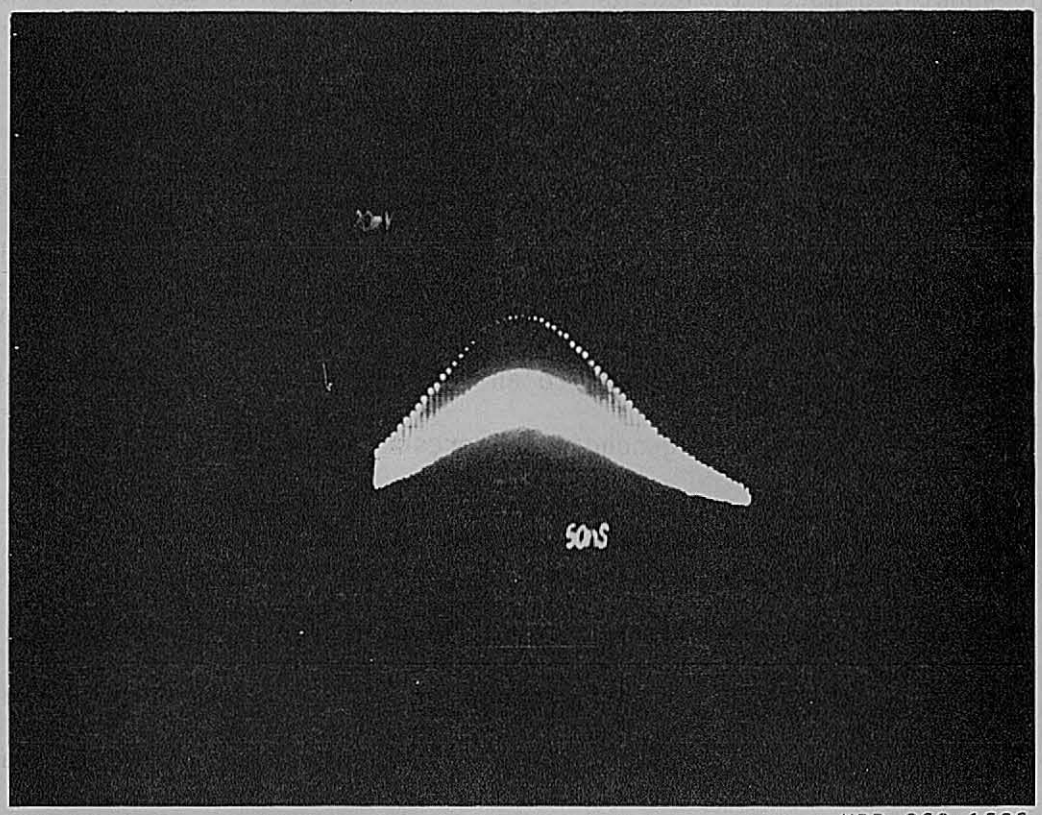

XBB 863-1636

Fig. 12(e)

the smooth, regular, exponentially damped oscillations that occur when the cavity length is properly adjusted. The oscillations are separated by about 7.5 μsec, indicating that it takes approximately 750 round trip cavity transits before pulsing occurs. A buildup time of 750 round trip transits implies pulse durations of approximately 150ps according to equations (10), (15), and (16) for the purely active mode-locked pulse train. The pulse width value quoted does not apply to each relaxation oscillation, which are actually individual actively mode-locked pulse trains, but to an individual pulse of the relaxation spike. At the operating conditions prescribed, there are between seven and ten oscillations per laser firing.

By expanding the time base (from 10 μs/div. to 10ns/div.) the first spike of the relaxation oscillation is displayed. This spike eventually develops into the mode-locked pulse train upon addition of the mode-locking dye. The behavior of this spike is a good indication of how well the Bragg angle has been adjusted. Figure 12c,d, and e demonstrate this point. In Figure 12c the Bragg angle is properly adjusted. The purely actively mode-locked pulse train has a nice Gaussian profile and has an amplitude stability of better than ± 5 percent. There are approximately 65 pulses per train (measured from the 10 percent point). Each of these pulses are about 150ps in duration. Proper Bragg angle adjustment is manifested by the fact that these pulses are well modulated with zero interpulse energy. Figure 12d shows the same relaxation spike when the Bragg angle is improperly adjusted. There is evidence of only slight "ripple"

modulation. Actually, even when the modulator is completely turned off, the same "ripple" modulation is present due to the interference (photon bunching effect) of the laser cavity etalon (defined by the end mirror separation). This is seen in Figure 12e.

Interesting points to compare about Figure 12c,d, and e are that from these pictures it is clear how important the Bragg angle adjustment is. The entire stabilization effect of active/passive mode-locking is due to the fact that mode-locking can be initiated from a well defined pulse (Figure 12c), defined by the transmission function of the modulator. Therefore pulse formation is no longer subject to the fluctuation in the noise spikes associated with the spontaneous emission of the lasing medium. If the modulator is improperly adjusted the modulation is not complete (Figure 12d) and no well-formed pulse results. There is therefore no effect of having the modulator in the cavity (compare Figures 12d and 12e). Therefore, an empirical way exists to adjust the Bragg angle. While monitoring the first relaxation spike by displaying the photodiode output on an oscilloscope, the observation of the modulation depth growing in down to the baseline indicates proper Bragg angle adjustment. Also, the energy in the relaxation spikes of Figure 12c and 12e are approximately equivalent. However, in Figure 12e the energy is distributed over a longer duration because there is no 2L/c structure. The power of the individual actively mode-locked pulses (~ 150ps) is thus much greater than the average power of the free running laser.

The last item to check before the addition of mode-locking dye is the laser threshold with the active mode-locker turned on and properly adjusted. Proper alignment and 8 watts of RF power with no mode-locking dye should result in a sharp threshold at approximately 10 volts above the threshold of the free-running laser.

There was no a priori dye concentration used to optimize passive mode-locking. The concentration eventually decided upon was empirically determined and, in fact was never measured. The decision as to the proper dye concentration was based upon the characteristics of the mode-locked pulse train. These characteristics included the number of pulses per train, energy per pulse train, lasing threshold, and energy amplitude stability of the pulse train.

The Eastman Kodak Q-switch dye 9740 was refrigerated when not being used. One hour prior to mode-locking, the dye was removed from the refrigerator and allowed to warm to room temperature. This prevented the condensation of moisture from the atmosphere into the dye container. When it was finally opened an unmeasured quantity of dye was then dissolved in approximately 50 mls of Eastman Kodak Q-switch Grade 1,2-Dichloroethane. Both the dye and the solvent were used as received. This solution was used as the "concentrate" that was added to the solvent already flowing in the dye cell-reservoir system during alignment.

The dye concentrate was slowly added using a syringe to the reservoir while the laser was running. The number of relaxation oscillations were monitored. As the dye was added, the number of

oscillations decreased, and the intensity of each remaining oscillation increased. As dye is added, the regular, exponentially damped pattern exhibs a loss of cohesiveness. The dye solution reservoir was swirled periodically to enhance mixing and prevent a surge of dye concentrate from passing through the cell. This was done to prevent the generation of a "giant" pulse that could result in optical damage. Concentrate was added until only one oscillation remained.

Addition of dye caused the threshold for lasing of the oscillator to increase. Only the strongest relaxation spike remained. However, the single oscillation contains almost the same amount of energy that was in all the oscillations present prior to the addition of dye. Therefore, the average power does not decrease significantly and the peak power is substantially increased. The oscillation that persists is the last oscillation of the original relaxation oscillations present. Therefore, the addition of dye acts not only to shorten the individual pulses of the pulse train, but also acts as a passive Q-switch. The dye spoils the Q of the laser cavity until the intracavity energy circulation is large enough to completely bleach the dye. In this way almost the same amount of energy is extracted in a single Q-switched pulse train as is the case when the laser is free running.

When only one relaxation spike remained, the time base of the storage oscilloscope was expanded (from 10 μs/div. to 100ns/div.) so the 2L/c structure of the mode-locked pulse train was observable. At

this point, the laser output typically consisted of a pulse train that contained between 25 and 30 pulses. The output was not very stable at this point exhibiting large peak-to-peak amplitude fluctuations (as high as 20 percent). The fluctuations implied that a well defined threshold condition had not been established yet.

Addition of dye concentrate was contained until the pulsed train contained approximately 12 to 15 pulses (measured from the 10 percent intensity points), as shown in Figure 13. At this point the low-level light transmission of the dye cell was between 60 and 70 percent. Between two and fifteen minutes were allowed for thorough dye mixing. The output energy and lasing threshold were measured. The output energy was between 5mJ and 6mJ and the lasing threshold was 1.10KV.

Operation of the laser 30 or 40 volts above threshold resulted in the best performance. Table I shows the effect of flashlamp energy on full train amplitude stability. There is an apparent contradiction present since according to equation (3), the pulse duration is inversely proportional to the number of oscillating axial modes. Therefore there exists the temptation to increase pump power in an effort to excite more modes. However, if the pump energy is too high, the possibility exists for more than one train of mode-locked pulses to develop during the pump cycle.

Frequency of mode-locking (which should be 100 percent) as well as the spatial characteristics of the beam were checked using Kodak Linograph Direct Print Type 2202 paper. If everything was working correctly the beam looked like a TEM_{00} Gaussian intensity profile.

Table I. Effect of flashlamp voltage (energy) on ocillators full train amplitude stability (threshold for lasing ≈ 1.10 kV).

Voltage (kV)	Flashlamp Energy (J)	Amplitude Stability (percent)
1.10	18.15	± 10.0
1.11	18.48	± 4.0
1.12	18.82	± 3.5
1.13	19.15	± 2.3
1.14	19.49	± 1.7
1.15	19.84	± 2.5
1.16	20.18	± 3.3
1.17	20.53	± 3.9
1.18	20.89	± 4.2
1.19	21.24	± 5.3
1.20	21.60	± 8.1

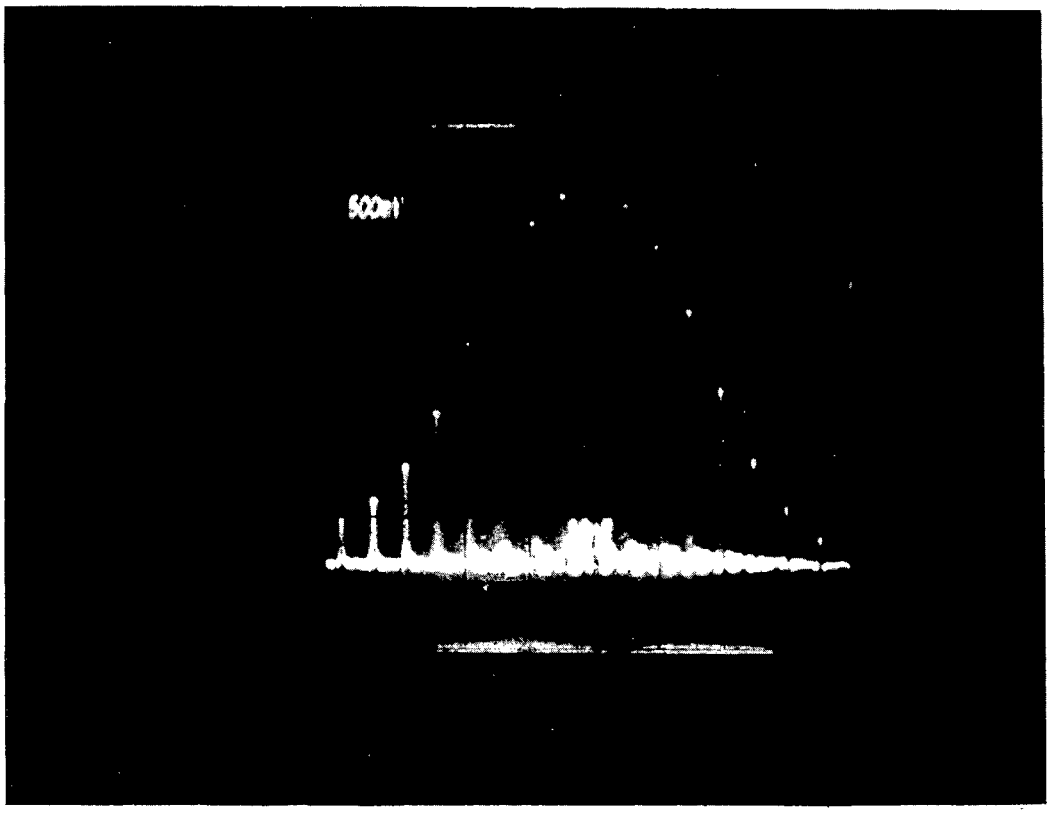

XBB 863-1638

Fig. 13. Oscilloscope photograph (horizontal scale is 10 ns/div.) of a mode-locked pulse train consisting of 12-15 pulses per train (measured from 10 percent intensity points) with individual pulses separated by 2L/c = 10 ns.

Qualitatively, this means more intensity in the center, and smoothly tapered intensity toward the perimeter. The beam was round and perfectly symmetric. Observation of irregularities in the beam profile was facilitated if the burn was taken following the expanding telescope before the single pulse selector. Sometimes a faint side burn was apparent either above or below the main central spot. The side burn was the result of the deflected beam from the acoustooptic modulator. The observation of the side burn depended or how intense the pulse train was and the sensitivity of the burn paper being used. If the side burn had an appreciable intensity compared to the central spot, then most probably the Bragg angle or cavity length were improperly adjusted. If a hole existed in the center of the beam profile, then it was likely more dye concentrate was needed. Asymmetric beam profiles often implied that a fine adjustment of the intracavity lens was necessary.

The occurrence of missed shots indicated one of two problems. Either too much dye concentrate had been added, or the cavity length needed to be adjusted. Addition of too much dye causes the lasing threshold to be higher than expected. To determine if this was the problem the lasing threshold was checked. If the threshold was higher than expected, either the voltage to the lamps was increased or solvent was added to the dye reservoir for dilution. The latter method was preferred to prevent pulse trains with too great an intensity from being generated. If the threshold seemed to be correct, then a fine adjustment of the cavity length was in order.

The addition of dye causes a small change in cavity length due to the increase of the index of refraction in the dye cell. The output coupler was thus translated to shorten the cavity length. Typical micrometer movements to shorten the cavity were between 0.003 in. and 0.006 in. (78 μm to 156 μm).

The importance of matching the cavity length to the acoustooptic driving frequency is demonstrated in Figure 14. At zero cavity length mismatch a maximum in energy and minimum in amplitude fluctuations exist. Better than 2 percent shot-to-shot energy stability was common if careful alignment procedure was followed. Mismatches of ± 0.005 in. (127 μm) led to an energy reduction of approximately 10 percent and increased the amplitude instability to about ± 5 percent. Movement of the output coupler away from resonance by distances greater than 0.015 in. (381 μm) yielded a reduction in energy of 75 percent and fluctuations increased to the point where the output energy could no longer be monitored by a power meter (greater than 40 percent). At mismatches greater than 0.015 in., missed laser firings occurred frequently.

The output of the oscillator was a TEM_{00}, diffraction-limited beam. The divergence of the beam was measured using the frequency doubled output (532nm) of the oscillator. Second harmonic generation was accomplished by passing the mode-locked pulse train through a Type II phase-matched KDP crystal. The green beam was used so that visual determination of the divergence was possible. The diameter of the second harmonic beam was measured immediately following the

Fig. 14. Effect of cavity length mismatch on output energy.

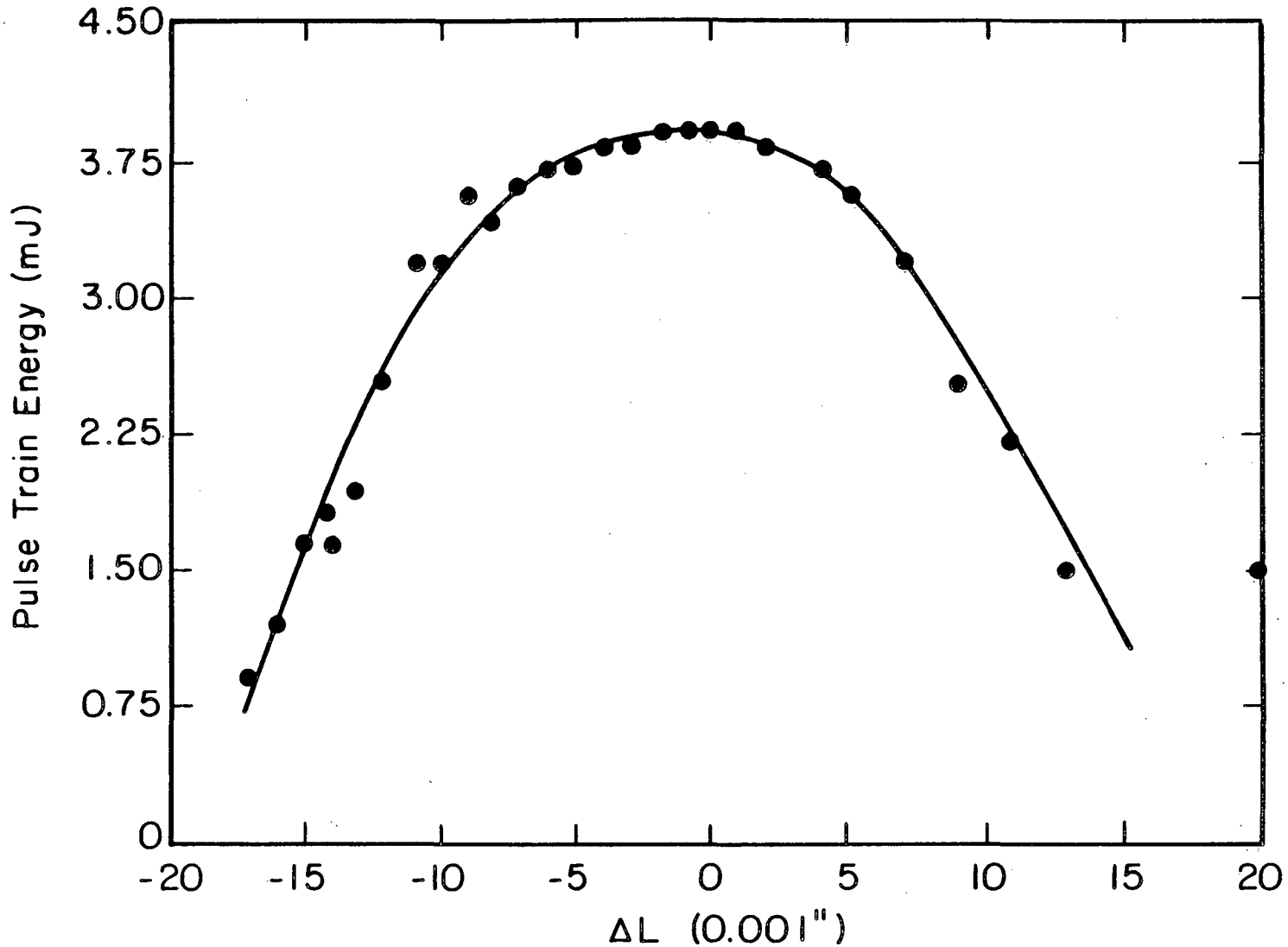

Fig. 14

XBL 863-986

doubling crystal (approximately at the output coupler, where the beam waist should be) and 33 feet away. The measured beam wastes were 0.060 in. and 0.140 in. respectively. The divergence was calculated by taking the difference between the spot sizes at the two distances and dividing by the difference in distances. This is a correct assumption for small angles of divergence ($\sin\theta \approx \theta$, for small θ). The measured divergence of the 532nm beam was 0.2 mrad.

Theoretically, the divergence of a diffraction-limited beam is (see Figure 15)

$$\theta = \frac{\lambda}{\pi w_0} , \tag{23}$$

where w_0 is the beam waist (half diameter) and λ is the wavelength of light under consideration. In the case described here, the beam waist was assumed to be 1.5mm (determined by the aperture defining TEM_{00} operation) and the wavelength of light was 532nm. Using these values with equation (23) yields a calculated diffraction-limited divergence of 0.22mrad. Therefore the laser exhibited diffraction-limited behavior.

Further proof of a diffraction-limited Gaussian laser beam was evident on two occasions. The 1064nm fundamental output was directly measured using a General Electric Model Number GE4TN2505 two dimensional CID (charge injected device) camera. The measured divergence was 0.4mrad. This corroborated diffraction-limited behavior if λ = 1064nm and w_0 = 1.5mm in equation (23). Direct observation of the fundamental beam with the camera displayed on a

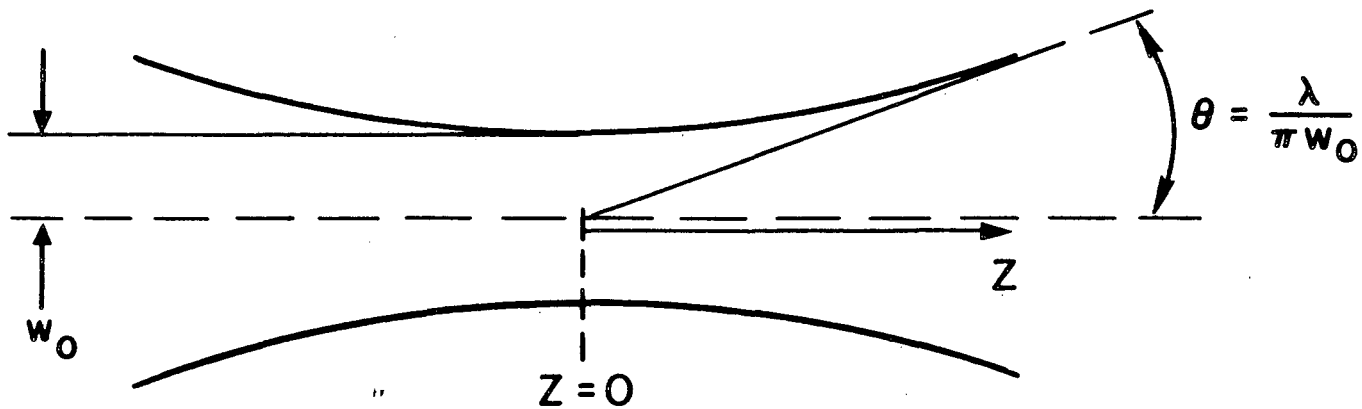

w_o = Beam Waist

Fig. 15. Explanation of divergence of output beam.

XBL 863-985

television monitor also verified TEM_{00} Gaussian spatial quality. The divergence of the third harmonic beam (355nm) was calculated to be 0.15mrad by using the limiting values of spectral widths measured for the OPS (see Chapter IV). This calculated value confirms the results of the two measurement according to equation (23).

For acceptable performance of the single pulse selector, both stable output from the oscillator and proper alignment of the pulse selector were necessary. It was essential to proper alignment of the pulse selector that the laser beam traveled straight through the Pockels cell. Therefore, after oscillator alignment was completed, it was good practice to measure that the beam was travelling parallel to the optical rail system. This was accomplished using a piece of IR phosphor paper taped to a T-square attached to an optical rail plate. The phosphor was marked three inches above the rail plate indicating the appropriate beam height. The rail plate was moved up and down the remaining portion of the rail system. If the beam appeared to be tilted, then a compensating adjustment was performed with the beam expanding telescope placed after the oscillator. Either a vertical (ϕ) or horizontal (θ) tilt adjustment of the one inch mirror mount holding the telescope was sufficient to straighten the propagation of the beam.

Proper alignment of the pulse selector required a "lab standard" Glan-Taylor prism polarizer set for maximum transmission of p-polarized (horizontal) light. The polarizer was set by minimizing the transmission of the laser output (greater than 90 percent

p-polarized) and then rotating the prism by 90 degrees. In general, the observation of minima was always used to set all polarizing optics, since it is always easier to observe a small change in a small signal than a small change in a large signal. In other words the percent variation in a small signal is greater than that in a large signal.

The prism used was a 12.5mm calcite Glan-Taylor polarizer purchased from the Karl Lambrecht Corp. It was mounted in an NRC RSA-1 rotation stage. The transmitted energy measured with the Scientech Laser Power Meter (Model No. 360001) displayed or the Scientech Power Energy Meter (Model No. 362) was monitored while the prism was rotated. Once the prism was set, it was maintained at that position (which maximized transmission of p-polarized light) and used both for Pockels cell alignment and as an analytical polarizer to determine polarization in other experiments.

The Quantel PF302 housing was then placed in position with the Pockels cell removed. The box was positioned so the 1064nm beam passed through the second Glan-Taylor prism clearly and was directed upward to the triggering photodiode. Using the ITT 4014 vacuum photodiode as an energy detector (i.e. displayed on a Tektronix 2215 Oscilloscope with a slow sweep speed) the second Glan-Taylor prism was rotated in the plane around the beam propagation axis to yield a minimum of transmitted p-polarized light. The "lab standard" prism was replaced with another prism identically mounted. The transmission

through the prism pair was again minimized. This resulted in the two Glan-Taylor prisms being set as a pair of crossed polarizers.

Once the prisms were crossed, the Pockels cell was placed inside the PF302 housing between the two polarizers. At this point no voltage was applied to the KD*P crystals in the Pockels cell. The light transmitted through the polarizer-Pockels cell-polarizer system was a minimum if the beam travelled straight through the Pockels cell. However, if this was not the case the minimum was perturbed because of the birefringence of the KD*P crystals. Linearly polarized light propagated parallel to the optic axis of a birefringent material experiences no polarization scrambling or mixing. However, the slightest deviation from colinear propagation of the beam along the optic axis of the crystals causes polarization rotation and scrambling. The polarizers therefore do not act as if they are crossed. For this reason, a home designed three point contact, kinematic mount was constructed for the PF302 housing. The mount allowed for the tilt and lateral adjustments necessary to ensure straight beam propagation through the Pockels cell. Using these adjustments, the light transmission through the prism-Pockels cell-prism system was minimized. The optical system should act as if there was no Pockels cell present when no voltage is applied and should give the same transmitted energy as the two crossed polarizers alone.

The next step was to apply the half wave voltage with the delay cable open circuited and to place a piece of lens paper directly in

front of the Pockels cell to act as a beam diffuser. The transmitted light was then viewed using a Kodak IR phosphor card with the lights turned off. Indication of proper alignment included the observation of a darkened cross, symmetrically located within a diffuse light background as seen in Figure 16. The appearance of a crossed null is evidence of any two crossed polarizers for linearly polarized, incident light. If the contrast between the cross and background was not great enough, or the cross was not centered on the diffuse background, then the alignment was incorrect and was repeated.

If the appearance of the cross was acceptable, then the connection was made to complete the Pockels cell drive circuit and the lens paper was removed. If the rejected pulse train was correctly incident upon the triggering photodiode, then pulse selector triggering was accomplished by opening and closing the iris in front of the photodiode. Observation of Krytron flashing indicated triggering. If the Krytron is flashing, and the firing can be turned on and off by iris adjustment, then monitoring of the rejected train and selected pulse took place. The selected pulse was observed using the ITT F4014 vacuum photodiode displaced on the Tektronix 7834 Storage Oscilloscope. The rejected train was monitored using an HP5082-5220 p-i-n photodiode placed in a circuit shown in Figure 17 also displayed on the Tektronix 7834 oscilloscope. The photodiode-circuit combination has a risetime of less than one nanosecond into a 50 ohm load. The resistor is a current limiting biasing resistor. The smaller capacitor provides the current necessary for short pulse operation and the larger capacitor

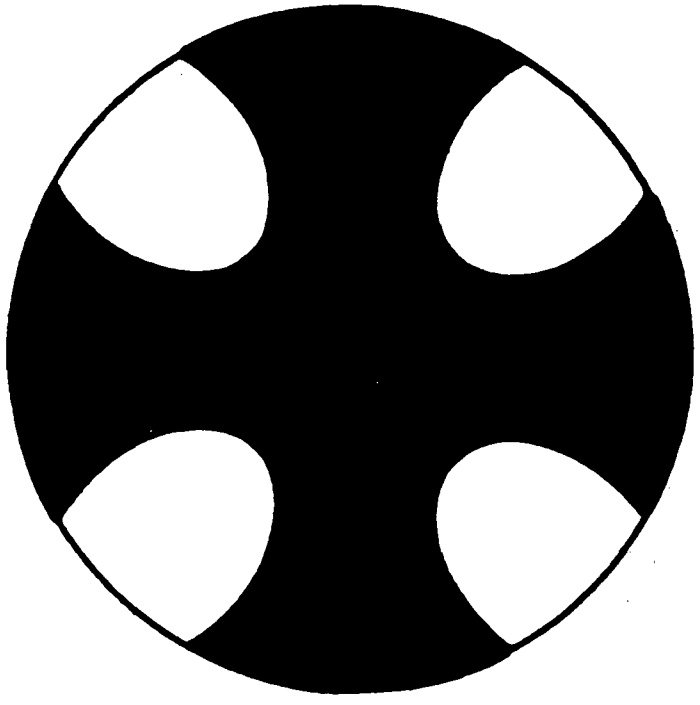

XBL 863-980

Fig. 16. Cross observed with diffuse light input indicating proper alignment of Pockels cell.

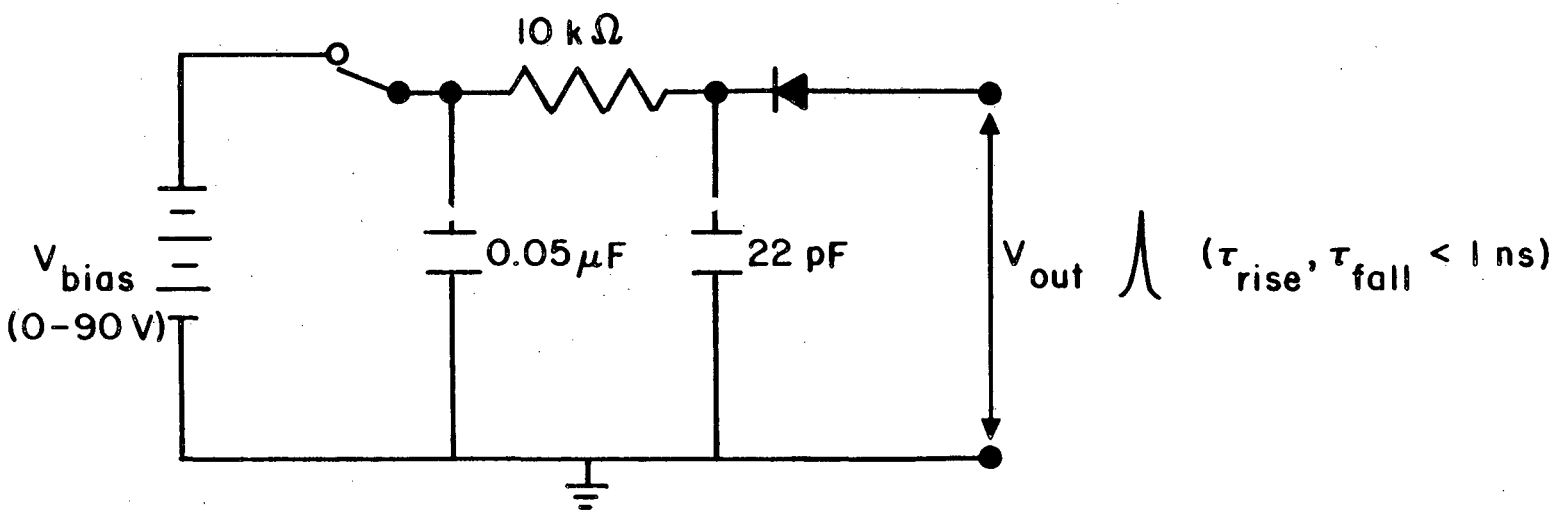

Fig. 17. HP 5082-5220 p-i-n photodiode circuit.

XBL 863-984

serves as a charge storage bank and surge spike filter in case of longer pulse irradiation. A few percent of the rejected pulse train is directed to the photodiode by a beam splitter inside the PF302 housing.

Improper optical alignment resulted in rejected pulse trains and single pulses like those shown in Figure 18a. Proper optical alignment resulted in output from the single pulse selector such as that of Figure 18b. Figure 18c demonstrates a rejected train where only part of the pulse was picked. Improvement of operation like that shown in Figure 18c was attained by either adjusting voltages on the Krytron, avalanche transistors, or the threshold conditions of triggering (small negative bias, 0-5 volts on the base of the first avalance transistor preceding the Marx Multiplier chain). Further improvement was achieved by adjusting the presensitization current of the Krytron (get ready current) or the flashlamp light level to the light pipe that triggered the get ready current to the Krytron. For further details, see reference 72. When properly adjusted, single pulse energy stabilities were between 5 and 10 percent (assuming incident pulse train energy stabilities of better than ± 3 percent).

Fig. 18. Rejected mode-locked pulse train and single pulse selected when (a) alignment is incorrect, (b) alignment is correct, and (c) when alignment is correct, but only part of the pulse is being selected due to improper voltage adjustments.

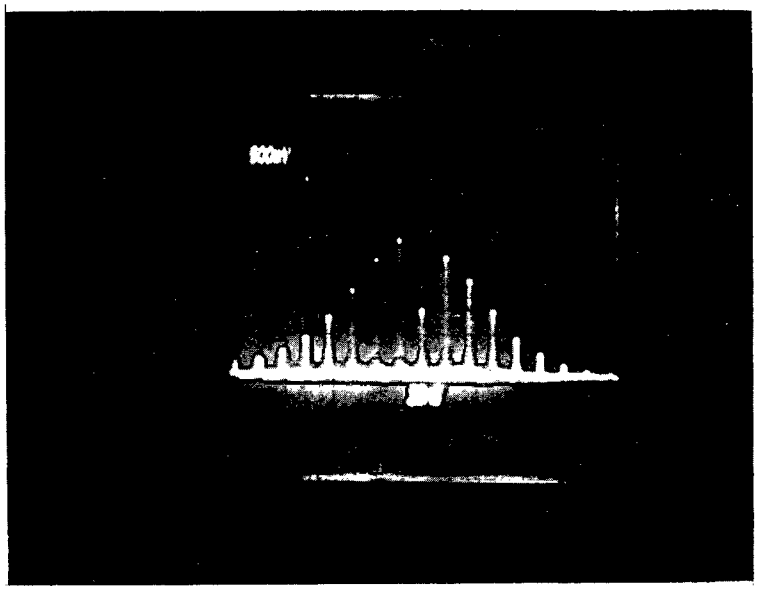

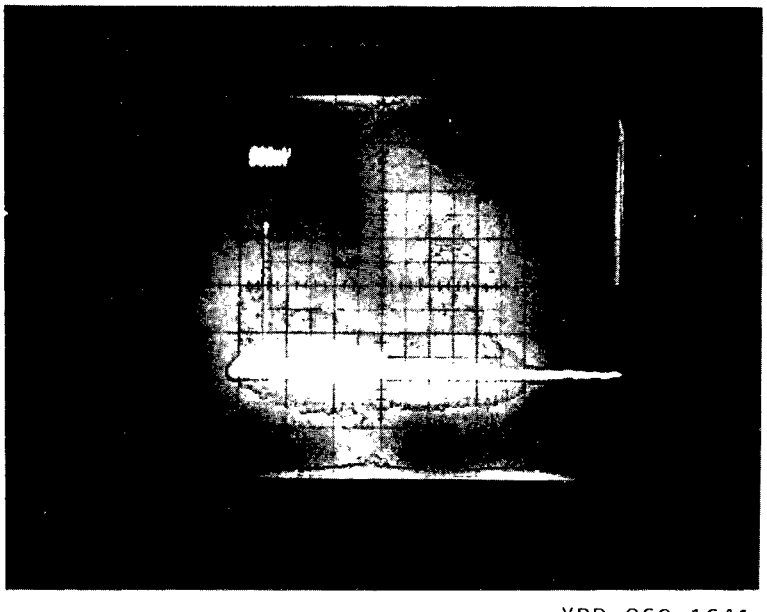

XBB 863-1641

Fig. 18(a)

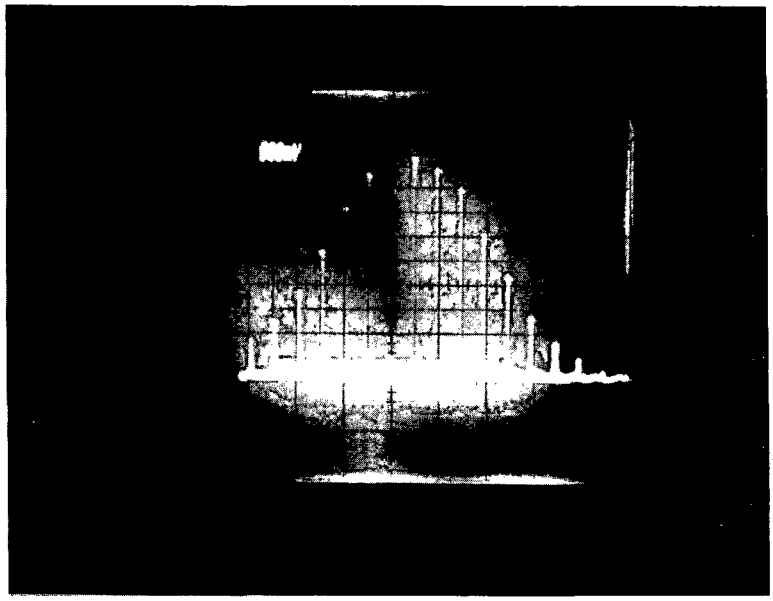

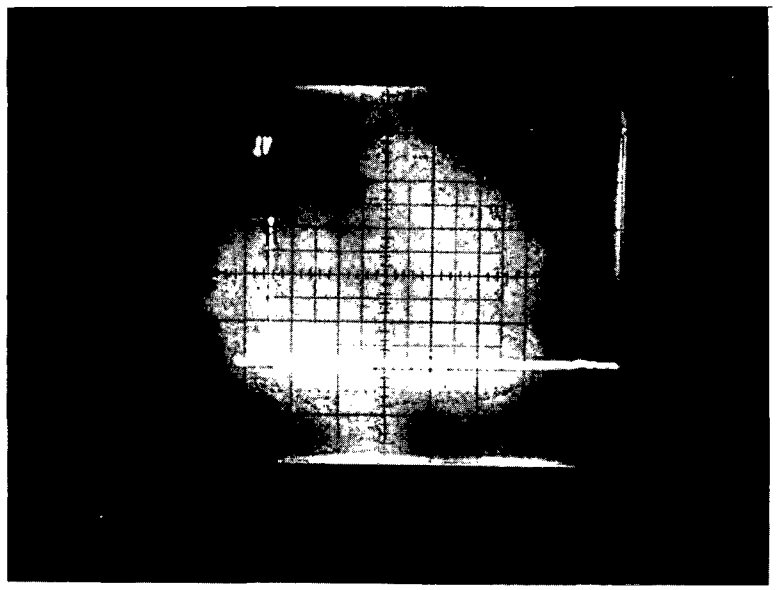

XBB 863-1639

Fig. 18(b)

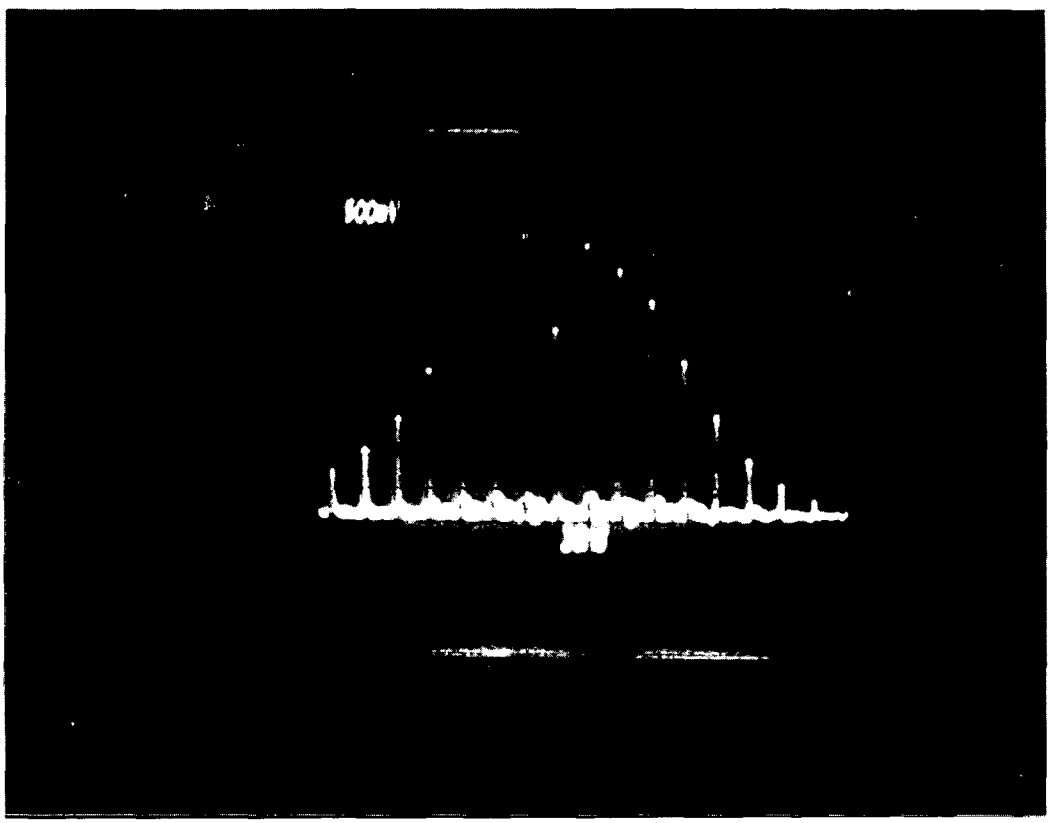

XBB 863-1640

Fig. 18(c)

F. Amplification

Single pulse energies from the oscillator ranged from 10μJ to 400μJ depending on which part of the mode-locked pulse train the single pulse was being selected from, and the operating conditions of the oscillator. These energies were not large enough to guarantee good conversion efficiencies from harmonic generation or optical parametric amplification. Nor were they sufficient to generate signals for various nonlinear optical experiments such as CARS, MPI, and picosecond x-ray generation from laser-initiated plasma formation. All of these projects required very high ($1GW/cm^2$ - $10TW/cm^2$) single pulse peak intensities and well controlled laser beam spatial profiles.

In order to boost the energy content of the single pulses from the oscillator, Nd:YAG amplifiers were utilized. For many experiments the use of a single amplifier was sufficient. However, the original idea was to generate a large quantity of third harmonic (355nm) light for efficient pumping of the tunable OPS. Passage of the pulse through two amplifiers in optical series would have been adequate. However, due to the lack of more than one amplifier for the system, a novel, colinear, double-pass amplifier was developed.

Figure 19 is a schematic diagram of the oscillator-amplifier system. Prior to amplification the single pulse beam was expanded by a factor of 1.6 using a 475mm focal length and a 760mm focal length lens pair. Both lenses were AR coated at 1064mm on both surfaces. The beam was expanded for two reasons. First to better use the gain

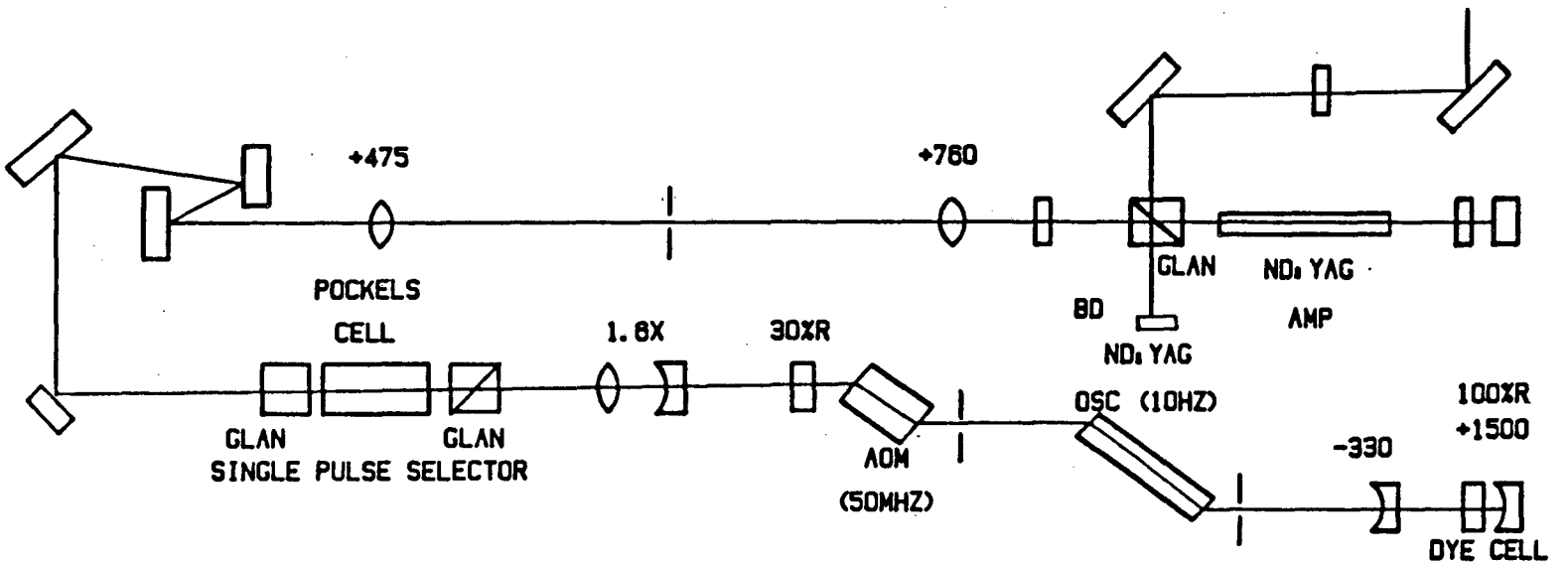

Fig. 19. Schematic overview of the pulsed, active/passive mode-locked Nd:YAG laser-double pass amplifier including single pulse selection.

XBL 866-2185

potential of the amplifier (fill factor), and second to avoid optical damage by reducing the intensity. The large separation required for proper beam expansion and collimation using this lens pair required an eight foot set of optical rails solely for the amplifier stage. The large values of focal lengths for the lenses of this telescope were chosen so that a small aperture could be placed between the two lenses and used as a spatial filter. The milder focus of the long focal length lenses permitted the spacing between the two lenses to be an adjustable parameter both in placement of the spatial filter and beam size incident on the amplifier. Positioning of the aperture could take place along a large portion of the separation distance giving rise to good resolution with respect to aperture location. The beam size could be adjusted by sliding the 760mm focal length lens along the rails. Due to the mild focus, beam size was only a slowly varying function of lens location. Therefore the lens could be moved without much worry about how small the beam was getting in the far field (after the thermal lensing effects of the amplifier).

The double-pass amplifier is depicted in detail in Figure 20. The variable output amplifier consisted of a $\lambda/2$ plate for 1064nm operation that was AR coated at 1064nm, a Glan-Taylor prism polarizer, a 1064nm $\lambda/4$ plate which was AR coated at 1064nm, a Nd:YAG amplifier head (Quantel Model No. SF410-07) equipped with a 7mm diameter by 115mm long, 2 degree cut, AR coated Nd:YAG rod (1.2 percent atomic weight doping), and a normal incidence 1064nm reflector arranged in a colinear, double-pass configuration.

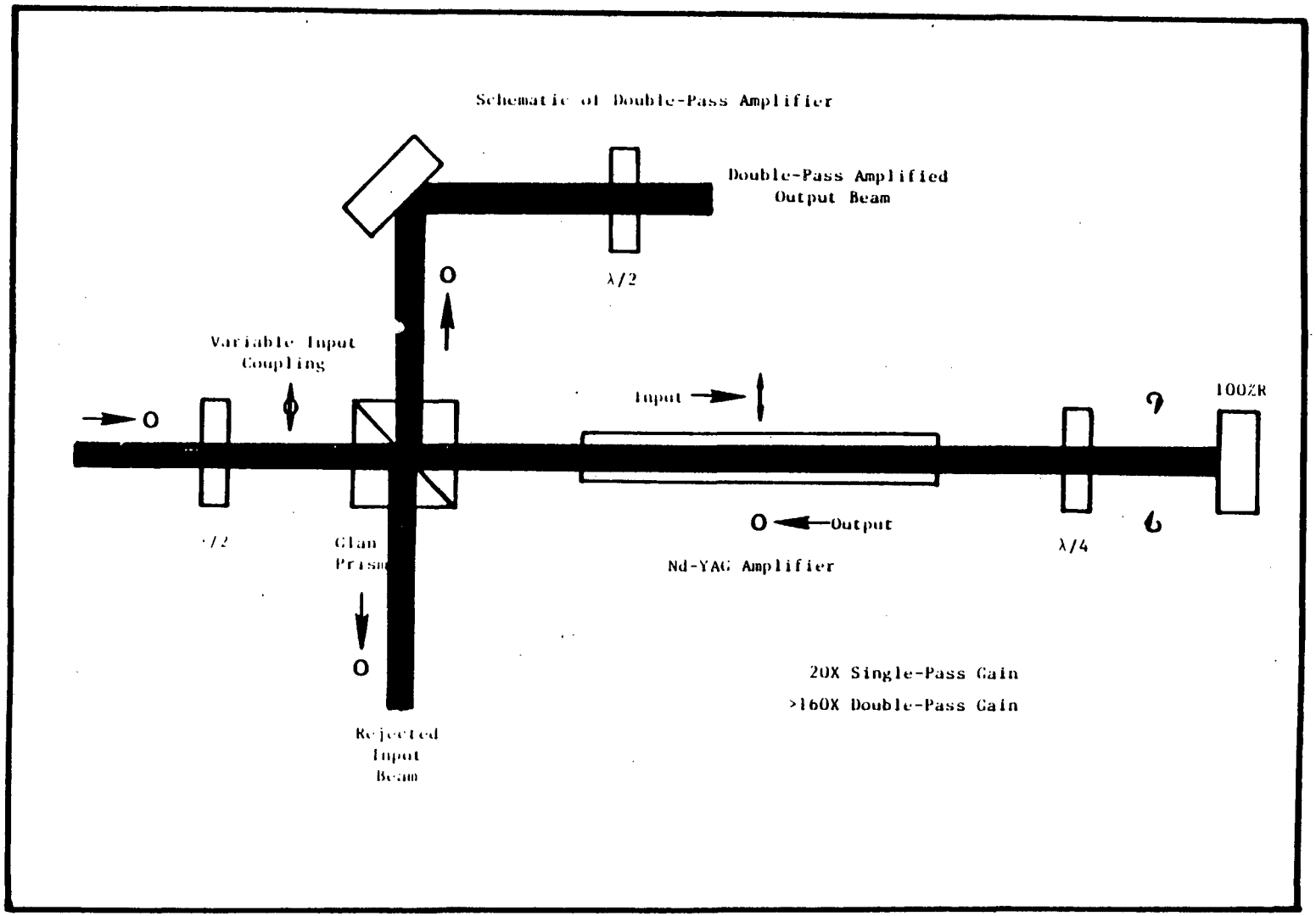

Fig. 20. Detailed schematic diagram of the colinear double-pass amplifier.

XBL 863-981

Variable input coupling to the amplifier was achieved via rotation of the $\lambda/2$ plate preceding the Glan-Taylor prism. The single pulse exiting the pulse selector was s-polarized (vertical). When the $\lambda/2$ plate was rotated, the ratio of the vertical and horizontal components of the pulse were continuously changed. The Glan-Taylor prism was set to transmit only p-polarized (horizontal) light. The s-polarized component was reflected by the prism out of the beam path according to the relation

$$R = \frac{\text{energy rejected}}{\text{incident energy}} = \cos^2(2\theta) \ , \tag{24}$$

where R is the normalized reflection and θ is the angle between the incident plane of polarization and neutral line axis of the $\lambda/2$ plate. Rotation of the $\lambda/2$ plate thus allowed continuous variation of the amount of light through the Glan-Taylor prism. Two passes through the $\lambda/4$ plate resulted in a polarization rotation of 90 degrees of the incident radiation. The resulting s-polarized (vertical) light was thus rejected out of the beam path by the Glan-Taylor polarizer after the second pass through the amplifier. The amplified light that was deflected from the beam path was then directed towards harmonic generating crystals. Single pass and double pass amplification factors of 20 and 200 respectively were observed with this setup.

The colinear, double-pass amplifier employing the polarization scheme had two major advantages over the noncolinear double pass scheme. The latter method, which is most commonly used with such systems, relies on the reflected (second pass) beam being spatially

offset from the incident (first pass) beam. Noncolinearity requires larger diameter amplifier rods. Larger diameter Nd:YAG rods are not always readily available and suffer from poor optical qualities due to the difficulties in growing large boules of material. Also, the larger rods require four flashlamps instead of two to ensure uniform pumping.

More important, however, was that the colinear method provided for continuously variable output at constant flashlamp pumping energies. In this way the changing spatial properties of the beam due to the changing thermal lensing characteristics of the amplifier rod at different flashlamp pumping energies were avoided. Damage to optics and nonlinear optical materials placed after the amplifier were minimized. Compensation for the changing thermal lens of the rod by adjusting lenses and telescopes before and after amplification were unnecessary. The amplifier was initially setup with the highest available voltage on the flashlamps. The optics preceding and following the amplifier head were set for maximum performance (including conversion efficiencies and beam spatial qualities) at the voltage setting. The problem of continuously needing to optimize the optical arrangement for different flashlamp energies was thus circumvented.

The other means of amplification of single pulses to high energies was to use two amplifiers in optical series. Either two Quantel SF410-7 or one SF410-07 and one SF410-09 (equipped with a 9mm diameter by 115mm long Nd:YAG rod pumped by four flashlamps) were used in this

arrangement. More energy is available from the larger amplifier, but beam quality suffers due to reasons already mentioned.

The advantages of using two amplifiers in optical series were that setup and alignment were easier. Output energies equivalent to the double-pass configuration were generated. The disadvantages were that an additional amplifier head power supply and capacitor bank were necessary, the cost of which is approximately $13,000. The extra polarizing optics used in the double-pass scheme could be purchased for less than $1000. The other disadvantage was that every time a different output energy was required from the amplifiers, an optimization procedure was required to compensate for the change in the thermal lens of the rod. At the high energies being generated and used, it was very important that the beam was not coming to a focus when passing through any materials or when incident on a reflective surface.

Those optical elements before and after the amplifier heads that needed adjustment when flashlamp voltages were changed were changed in the following way. The 760mm focal length lens before the amplifier was moved up and down the rail system, thereby changing the size and focusing conditions of the incident beam. Telescopes before harmonic conversion and optical parametric conversion could be adjusted as well. However, these adjustments only resulted in changing of the beam size, and often masked the debilitating effects on beam quality of nonlinear processes (self-focusing) and thermal lensing effects in the amplifier rod. Therefore it was always more fruitful and less

catastrophic (due to optical damage) to change the beam conditions before traversal through the amplifier to offset the change in spatial quality of the beam.

III. Temporal and Spectral Characterization of the Pulsed, Active/Passive Mode-Locked, Nd:YAG Laser

A. Background

A major goal in the design and construction of a solid-state, mode-locked laser is the generation of transform-limited pulses. Even with proper design of the optical system constituting the resonator, pulses that are not transform-limited are normally produced. It is now well understood why it is difficult to generate transform-limited pulses from high-powered lasers. The temporal, spectral, and spatial characteristics of the output pulses from mode-locked lasers are often more complex than predicted by simple theories. Pulse width measurements typically yield pulse durations greater than the reciprocal of the bandwidth. During the high intensity stage of pulse development, the characteristics of the pulses are largely determined by the intensity-dependent, nonlinear index of refraction of the various optical components in the resonantor. The interaction of the high-intensity electric field with these materials leads to a time-dependent phase shift in the oscillating pulse, resulting in a frequency sweep and/or break up of the pulse. This phenomena is known as self-phase modulation. If there is limited self-focusing, self-phase modulation will continue, and spectral shifts become significant compared to the laser gain profile.

In order to generate near transform-limited pulses, measurements of both the spectral and temporal widths of individual pulses as a function of position in the pulse train are necessary. The literature

is flooded with such measurements. Results of these studies have contributed significantly to the understanding of the intensity-dependent phenomena occurring in high-powered lasers. Observation and analysis of these phenomena has been instrumental in the understanding of many fundamental and limiting nonlinear optical processes. In the past, these phenomena have been regarded as detrimental to the operation of mode-locked lasers. However, recently, they have been used to generate the shortest optical pulses to date.[21,22,23]

Treacy[15] was the first to suggest that radiation from mode-locked Nd:Glass lasers was self-phase modulated resulting in pulses with temporal widths significantly larger than the Fourier transform of the bandwidth. He detected a quadratic term in the phase, $\phi(t)$

$$-\phi(t) = \omega t + \frac{1}{2}\beta t^2, \tag{25}$$

corresponding to a frequency sweep (chirp) in the pulse. Compression of these pulses was achieved using a negatively dispersive, grating-pair delay line. Starting with pulses of 4ps duration, compression factors of ten, resulting in subpicosecond pulses (0.4ps) were attained. He concluded that the frequency sweep must be positive and linear. The frequency sweep was also determined to be responsible for the discrepancy between the expected pulse width and that actually measured.

Cubeddu and Svelto[76] were the first to attempt a theoretical description of Treacy's observations. They evaluated self-locking (passive mode-locking) of a Nd:Glass laser in the presence of host

dispersion. Dispersion in a passively mode-locked laser cavity is due to the following three reasons: (1) host dispersion from the laser material; (2) dispersion associated with the gain profile of the laser material; and (3) dispersion associated with the absorption of the dye. Dispersive effects arising from (2) and (3) can be neglected compared to (1). They concluded that due to dispersion, the cavity modes are not equally spaced, which results in the observed widening of the pulses and the frequency sweeps. They also pointed out that in the limit of very high intracavity fields, the leading edge of each mode-locked pulse will completely saturate the dye so that the remaining part of the pulse will pass through the dye without being altered. In this limit the effect of host dispersion (which is positive) will not be compensated for by the negative dispersion associated with the absorption of the dye. There should therefore exist a minimum value for the pulse width and frequency chirp in such a system.

The behavior predicted by Cubeddu and Svelto's theoretical models were experimentally observed by Glenn and Brienza.[77] While testing a new, high-speed energy correlation technique (second-harmonic-generation autocorrelation) to measure the pulse width of ultrashort pulses generated from a mode-locked Nd:Glass laser, they observed pulses of 8ps duration very early in the pulse train. Longer pulses were measured later in the pulse train. They attributed the behavior to the fact that the dye causes shortening of the initial, low amplitude pulses to some limiting value (determined by the dye

relaxation time). Once the pulse amplitude begins to grow rapidly, the dye will bleach completely and therefore no longer be effective in shortening the pulses. The width of subsequent pulses is therefore determined by the physical parameters of the laser cavity such as dispersion in the rod and dye cell and effects of the gain profile. These results were reported before there was evidence of nonlinearities occurring in the cavity due to the high intensity field interacting with the nonlinear index of refraction of the lasing material.

Subpicosecond components and structure in the output of mode-locked Nd:Glass lasers were first reported by Shapiro and Duguay[78] and subsequently by Bradley et.al.[79] Using a two-photon fluorescence technique they observed pulses that consisted of a 0.25ps duration spike superimposed on a broad 6ps duration pulse. The shape of the two-photon fluorescence curve, however, does not uniquely determine the shape of the laser pulse. The narrow spike was thought to imply that within the 6ps pulse there was one or more component with a duration of between 0.2ps and 0.6ps. The observed narrow structures were however close to the theoretical limits set by the 100 cm^{-1} to 200 cm^{-1} spectral widths of these pulses. This work could not be corroborated with that of Treacy[15] because the two-photon fluorescence technique is insensitive to the phase modulation he observed.

Bradley et al.,[79] using a two-photon fluorescence technique in a different configuration from that of Shapiro and Dugyay, also observed a spike superimposed on a broad background pulse. The duration and

intensity of the spike varied from shot to shot. The duration of these spikes varied from 0.2ps to 1.0ps. The pulse durations of the sharp spikes were correlated with the simultaneously recorded spectral widths of 150Å to 30Å. However, because of the nature of the two-photon fluorescence measurement, it could not be determined whether the fine structure originated from isolated subpicosecond pulses or from noise fluctuations. In contrast to what Glenn and Brienza[77] observed, Bradley et al.[79] found no systematic variation of pulse duration throughout the pulse train. Using the third harmonic conversion efficiency of the full pulse train envelope as an indicator of variations in the fundamental pulse durations, they observed that the third harmonic closely followed the fundamental in shape. The total amount of third harmonic light was consistent with a train of pulses each having a 10ps duration.

Duguay et al.,[8] using the two-photon fluorescence method, observed pulses in a mode-locked Nd:Glass laser of approximately 8ps with substructure consisting of peaks between 0.4ps and 0.8ps long. Spectral widths of pulses were less than 20 cm^{-1} at the beginning of the pulse train and up to 80 cm^{-1} near the middle of the train. Because the method of autocorrelation used in these measurements is insensitive to the spectral structure of the pulses, time-resolved spectra were recorded to measure the frequency spectrum of the pulses and to determine whether the pulses were self-phase modulated. The conclusion was that the broadened spectra were a result of self-phase modulation, and an estimation of the value of the nonlinear index of

refraction (n_2) of the Nd:Glass rod was made. Limitations of such lasers imposed by self-focusing could thus be predicted. They concluded that the nonlinear index of the laser glass sets an upper limit to the power density that can be generated in practical laser-amplifier chains. The limitations set by the large value of n_2 for a Nd:Glass laser rod have both a negative and positive aspect. The negative aspect already mentioned is the limitation on energy density extraction due to self-focusing. The positive side results from the benefits produced by limiting the gain of a high-power, short pulse laser system. Because of the spectral broadening due to self-phase modulation, energy gets shifted out from under the peak of the gain curve. The resulting gain limitation gives rise to longer mode-locked trains (Q-switched envelope of between 100ns and 200ns) versus 10ns to 40ns of a typical Q-switched laser. The reduced gain also results in a smoothening of the spatial profile of the pulse (no hot spots, inhomogeneities), which inhibits self-focusing.

The time variation of the spectral composition of radiation from a mode-locked Nd:Glass ring resonator was investigated by Korobokin et al.[7] using a diffraction spectrograph coupled to an electron-optical camera operating in the linear sweep mode. They observed the development of structure in the spectrum as the pulse train developed in time. The measurements agreed in full with their calculated spectrum of self-phase modulated pulses. Investigations of the field intensity distribution[7] were also conducted. By imaging the through-put of a diaphragm onto the photocathode of the camera used in a

framing mode, the time development of spatial profiles was recorded. The resulting images demonstrated significant nonuniform redistribution of the radiation intensity at large values of intracavity power densities, as opposed to the uniform distributions observed at lower power densities. They concluded that self-phase modulation is responsible for the structure of the spectrum in mode-locked, solid-state lasers, and that the discrepancy between the experimentally observed pulse durations and spectral widths could be accounted for solely on the basis of self-phase modulation.

In similar experiments Eckardt et al.[9] showed that mode-locked pulses from a Nd:Glass ring cavity had narrow bandwidths of 3Å at early stages of the pulse train when intensity was well below its peak. As the intensity grew, the bandwidth of the pulses grew to 80Å due to self-phase modulation caused by the intensity-dependent nonlinear index of refraction. They emphasized the importance of understanding self-phase modulation because of its effects on using such pulses in the study of other nonlinear effects.

All the experiments discussed thus far involved measurements on entire pulse trains. Von Der Linde[10] pointed out the importance of studying the properties of single pulses extracted from the mode-locked Nd:Glass pulse train. Using a number of different experimental techniques, he investigated the duration, spectral structure, energy distribution, and shape of the single picosecond light pulses. Pulse durations and spectral structure were measured using two-photon fluorescence techniques and a grating spectrograph respectively. The energy

content of the pulses was determined by photoelectric (photodiode-oscilloscope) measurements, two-photon fluorescence contrast ratios, and measurements of the efficiencies of three-photon induced fluorescence. When used in conjunction with each other, these three methods are well suited for determining both the relative energy distributions amongst the individual pulses in the mode-locked pulse train, as well as the magnitude of the background energy between the pulses.

To determine the shape of individual pulses, an optical sampling technique was devised utilizing stimulated Raman scattering. The observations indicated transform-limited pulses were formed in the leading part of the pulse train. Single pulses between 4ps and 8ps duration with proper two-photon fluorescence ratios (3:1) with no indication of substructure were measured early in the pulse train. The time-bandwidth product of the pulses was reported to be between 0.6 and 0.7, excluding the possibility of self-phase modulation. Observations of pulses later in the train showed distinct spectral and temporal broadening, as well as evidence of the formation of subpico-second components.

Von Der Linde's observations stressed the importance of selecting single pulses for investigations and experimentation. It is conceivable that when the total pulse train is used, the true behavior of pulses is masked by the weighting factor that the higher energy pulses have. He concluded that self-phase modulation becomes significant near the maximum of the pulse train. Using the optical sampling

technique, a pulse asymmetry was detected. The leading edge of the pulse seemed to be sharper (exponential) than the trailing edge of the pulse (Gaussian). Reasons similar to those of Cubeddu and Svelto were[76] given to explain the asymmetry.

The direct measurement of picosecond pulse shapes and durations requires the use of a picosecond streak camera. All investigations discussed to this point used two-photon fluorescence or second harmonic generation autocorrelation measurements to determine pulse durations. These techniques suffer from the problem of misinterpretation unless special care is taken. The only determination of pulse shape was by Von Der Linde.[10] Bradley and Sibbet[11] systematically studied the temporal and spectral development of single pulses as a function of position in tne pulse train. Using a streak camera with an S-1 image tube (near infrared sensitivity) and 2.5ps time resolution in conjunction with a grating spectrograph coupled to a streak camera operating as an image converter, they simultaneously recorded pulse durations and spectral bandwidths of individual pulses within the mode-locked pulse train of a Nd:Glass laser. The fifth pulse of the train was found to be 3.8ps long and had a spectral width of 7.4Å. The corresponding time-bandwidth product was 0.83, demonstrating that the initial pulses were near transform-limited. Observation of frequency broadening later in the pulse train was attributed to self-phase modulation, which built up at a rate of 10 cm^{-1} per cavity round trip. At the end of the pulse train, the pulses had spectral widths of approximately 50Å and were between 5ps and 13ps

long. These measurements, obtained using direct linear measurement techiniques helped to clear up many of the discrepancies and much of the mystery associated with earlier investigations.

Using the same experimental setup as previously, Eckardt et al.[9] systematically studied pulses in various stages of development in the pulse train of a mode-locked Nd:Glass ring resonator. Computer calculations were carried out simulating the evolution of a simple, mode-locked, 0.3nm bandwidth, 6ps duration pulse as it bounced back and forth in the laser cavity. Pulse propagation through the cavity was subject to saturable absorption, self-phase modulation due to the intensity dependent refractive index change, amplification by the inverted medium, and dispersion of the laser medium. Fourier analysis and transformation was used so the intensity-dependent saturable absorption and self-phase modulation could be treated in the time domain, and amplification and dispersion could be treated in the frequency domain. Both a qualitative and quantitative comparisons were made between spectral and temporal structure at various stages of development. Time-resolved spectrograms showed that the original, single component, pulse broadened from 0.3nm to 4nm and acquired periodic structure as the intensity of the pulse grew. Continued development of the pulse resulted in further broadening of the bandwidth to 8nm with a gradual smearing of the periodic structure. The observed and calculated spectra were in excellent agreement.

Eckardt et al.[9] also pointed out that the intensity-dependent refractive index causes both spatial and temporal variations. The

temporal and spatial variation result in self-phase modulation and self-focusing respectively. For nanosecond lasers, the spatial variation is more important. For picosecond lasers the temporal variation is more significant. For a complete analysis both effects should be considered, but due to the complexity of the problem, Eckardt et al.[9] only considered the temporal variation.

Self-focusing in mode-locked Nd:Glass lasers was treated by Eckardt[80] separately. He pointed out that self-focusing in these lasers was responsible for the limitation of the output power and the distortion of the beam's spatial profile. He also attributed the lack of reproducible operation of mode-locked Nd:Glass lasers without mode selecting apertures and plane (not curved) reflectors to self-focusing. Problems related to self-focusing in the laser oscillator were never experienced in the Nd:YAG laser described in this thesis. Therefore self-focusing will not be considered as a separate subject and will only be discussed in terms of its limiting effect on self-phase modulation.

More recently, Zinth et al.[12] considered the problem of measuring the chirp of a laser pulse correctly. They subsequently developed a method which allowed them to select a picosecond pulse from a mode-locked Nd:Glass laser system that exhibited a negligible chirp. They pointed out that for the quantitative determination of the chirp of a light pulse, it is necessary to know the frequency bandwidth, the time duration, and the temporal shape of the pulse. The interpretation of the measured bandwidth requires the knowledge of the observed portion

of the beam. They demonstrated that the presence of a moderate chirp cannot be inferred from the form of the spectrum when most of the beam is imaged onto the spectrometer. Also, considering the difficulty of determining accurately the pulse duration and shape (without the use of a streak camera), there is a problem in establishing the degree of frequency chirp in a picosecond pulse.

The results of Zinth et al.[12] point out important experimental considerations that must be recognized when characterizing the output of a mode-locked laser. First, it is better to use direct, linear temporal measurements (streak cameras), which absolutely determine the temporal widths and shapes of pulses, instead of indirect, nonlinear (two-photon fluorescence and second harmonic generation) autocorrelation methods. Second, it is extremely important to use the narrowest possible acceptance slit width on the spectrometer used to measure the spectral bandwidth of the pulses. In this way only the central (most intense for Gaussian distribution) portion of the beam is monitored in the spectral determinations. Applying these restrictions, they measured the spectrum of pulses on the leading edge of a mode-locked Nd:Glass pulse train and found that only pulses very early in the train were chirp free. Using two-photon fluorescence measurements, they determined these pulses were transform-limited. These pulses were single, amplified pulses and had sufficient energy content for experimentation. They also noted the importance of transform-limited pulses for coherence experiments and emphasized the higher conversion

efficiencies attainable in the generation of new frequencies via nonlinear optical parametric interactions when working with transform-limited pulses.

Despite the large number of reported studies on the pulse quality of Nd:Glass lasers, there are relatively few reports of how spectral and temporal widths vary as a function of position in the pulse train for mode-locked Nd:YAG lasers. Graener and Laubereau[3] studied the variation of the time-bandwidth product as a function of intracavity pulse energy for a passively mode-locked Nd:YAG laser. Using a Fabry-Perot interferometer and a two-photon fluorescence setup for spectral and temporal measurements of amplified single pulses, respectively, they observed near transform-limited behavior early in the pulse train at intracavity pulse energies less than 250 μJ. They found that pulses of larger amplitude within the rising part of the mode-locked train exhibited larger values of the time-bandwidth product. At the peak of the pulse train, values greater than two times the transform-limit were measured. They concluded that these pulses suffered from a loss of coherence due to self-phase modulation via the nonlinear refractive index of the Nd:YAG rod. They modeled the self-phase modulation and the results of such calculations were in excellent agreement with their observations. They concluded that pulse energies should not exceed 200 μJ for the generation of chirp free pulses and therefore pulses should always be selected from the early portion in the mode-locked pulse train.

The observation and report of Graener and Laubereau[3] that self-phase modulation may be significant in Nd:YAG systems led to the detailed study and characterization of the output of the system described in Chapter II.

B. Experimental

Simultaneous spectral and temporal measurements were performed on the second harmonic (532nm) of single amplified pulses from the pulsed, active/passive mode-locked, Nd:YAG laser-amplifier system described in Chapter II. Individual pulse measurements were recorded as a function of position in the mode-locked pulse train. Variation of the position in the mode-locked train was accomplished by changing the threshold conditions for triggering the single pulse selector (i.e. changing the iris aperture size in front of the trigger photodiode). Operating conditions of the laser system were the same as described in Chapter II. A schematic diagram of the experimental arrangement used in the characterization is shown in Figure 21.

The second harmonic of the fundamental radiation was measured because the streak camera used for the temporal determinations incorporated a streak tube with an S-20 photocathode. The spectral response of this tube decreases significantly at wavelengths longer than 750nm. Second harmonic conversion from 1064nm to 532nm was effected in a 2.0 cm long, Type II phase-matched KDP crystal cut at 58.8 degrees with respect to the optic axis. Two nonidentical, fundamental waves (one ordinary and one extraordinary) interact to generate an extraordinary wave at the second harmonic frequency (eo-e interaction).

In performing these measurements, it was important to consider the consequences of using the second harmonic instead of the fundamental. For Gaussian pulse shapes, the pulse width of the second harmonic

Fig. 21. The schematic diagram of the experimental setup used to measure the temporal and spectral characteristics of single pulses of the second harmonic from the pulsed, activate/passive mode-locked, Nd:YAG laser system.

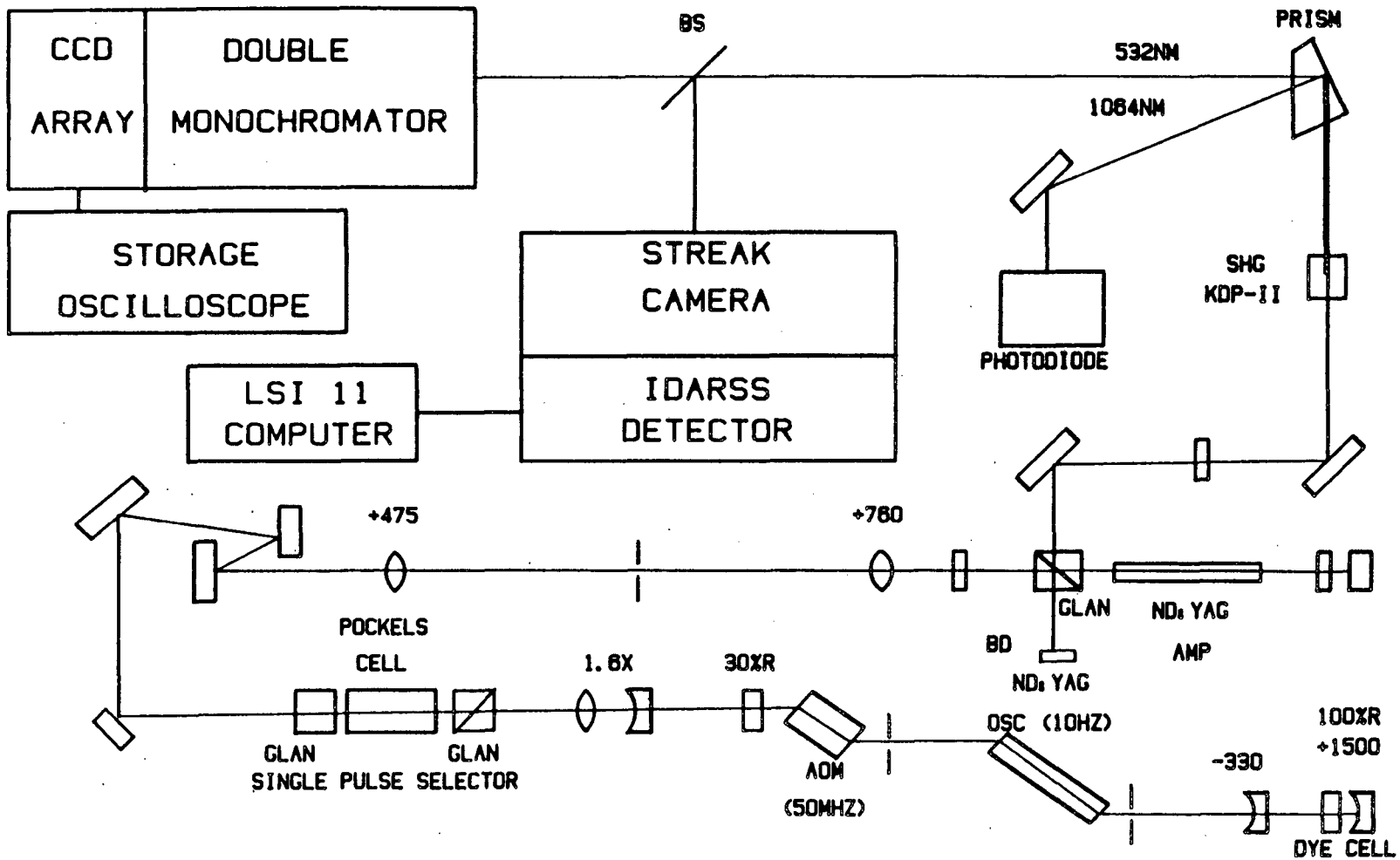

Fig. 21

XBL 864-1264

output should be a factor of $\sqrt{2}$ shorter than the fundamental output if the phase-matching bandwidth is greater than the laser bandwidth. The laser bandwidth cannot be any greater than the gain bandwidth of the amplifying medium which is 6.5 cm^{-1}.[81] The phase-matching bandwidth can be calculated using equation (26)[82]

$$\delta\lambda_1 = 1.39\lambda_1/2\pi \left(\frac{\partial n_1^o}{\partial \lambda_1} - \frac{1}{2}\frac{\partial n_2^e}{\partial \lambda_2}\right), \qquad (26)$$

where n_1^o and n_2^e are the ordinary and extraordinary indices of refraction for the fundamental (λ_1) and second harmonic (λ_2) respectively. The term in parentheses is the expression for the group velocity dispersion of the fundamental and second harmonic. For efficient second harmonic generation (and to observe the expected $\sqrt{2}$ shortening), the phase-matching bandwidth must be at least as large as the laser bandwidth. In KDP at λ_1 = 1064nm, the phase-matching bandwidth for a 2.0 cm crystal is approximately 100Å[82] (88 cm^{-1} at 1064nm), which can readily accommodate the laser bandwidth.

If the fundamental pulse is transform-limited, then the second harmonic pulse duration will be longer than the fundamental if the laser bandwidth exceeds the phase-matching bandwidth.[83,84] The peak intensity of the second harmonic will saturate, and its pulse width will broaden due to the group velocity mismatch between the fundamental and second harmonic pulses. To avoid this pulse stretching, the group velocity delay must be less than the pulse duration. This was certainly the case for the second harmonic generation used in the experimental arrangement described here. In the next chapter, the

effects of group velocity delay will be accounted for and discussed in relation to third harmonic and optical parametric conversion where they cannot be neglected.

The fundamental and second harmonic were separated by a 2 cm aperture, quartz (Suprasil) Pellin-Broca prism (purchased from Optics for Research Corp.). The 1064nm radiation was used to trigger the streak camera via a p-i-n photodiode (HP5082-4220) in a circuit identical to the are shown in Figure 17. The 532nm radiation was split into two beams. One beam was imaged onto the entrance slit of a Hadland Photonics Imacon 500 streak camera optically coupled to a Tracor Northern TN-6100-IDARS (intensified diode array). The temporal profile from the streak camera-IDARS system was collected using a TN1710-21A Optical Spectrometer module in a TN-1710 mainframe. The data was transferred to a DEC LSI-11/2 microcomputer for subsequent signal averaging, display, and analysis. Further details on the performance, construction, and calibration of this system can be found in reference 36.

Spectral data were obtained on a single-shot basis by imaging the other 532nm beam onto a 0.85 meter focal length double monochromator (Spex Industries Model No. 1404) equipped with 1800 lines/mm holographic gratings. A linear charge coupled device array (CCD-Fairchild I-Scan-CCD111-A) was mounted at the image plane of the monochromator. The output of the array was displayed on a Tektronix 7834 storage oscilloscope (equipped with 7A24 dual trace amplifier and 7B92A dual trace time base). This configuration allowed the display of single-

shot spectra measured over a range of 6.7Å (at 532nm) with a resolution of 0.1Å. Each pixel corresponded to 0.026Å (256 pixels total), but the resolution of the monochromator-CCD array combination was approximately four pixels.

A power meter (Scientech Laser Power Meter Model No. 360001 displayed on a Scientech Power Energy Meter Model No. 362) and a calibrated pyroelectric joulemeter (Molectron Model No. J3-05 DW displayed on a Tektronix 2215 Oscilloscope) were used for energy measurements. The energy per pulse train was measured directly after the output coupler of the oscillator. The intracavity pulse energy was calculated using the following expression

$$I.E. = \frac{O.E.}{1-R} \tag{28}$$

where I.E. is the intracavity pulse energy, O.E. is the extracavity measured pulse energy, and R is the reflectivity of the output coupler (R = 0.3).

Subsequent experiments utilized a two-dimensional charge injected device (CID) array (General Electric Model No. TN2505A) placed at the image plane of the monochromator to record spectra. The spectra were digitized with a frame grabber (Poynting Model No. 505-RM), and transferred to a microcomputer (DEC LSI-11/2) for subsequent display and analysis. This configuration provided single shot spectra measured over a range of 15Å (at 532nm) with a resolution of between 0.2Å and 0.4Å. The reason for using the two-dimensional array was check for evidence of spectral inhomogeneity over the spatial profile of the

beam. This configuration required the entrance slits to be opened to a larger degree than in the previous configuration. The resulting resolution was therefore not as good. Also, because a larger portion of the beam was accepted into the spectrometer, some of the chirped character of pulse might have been obscured.[17] Therefore the results in the next section were recorded with the original arrangement.

The experimental arrangement described permitted the simultaneous observation of the pulse duration and spectrum of the second harmonic of single, amplified, picosecond pulse. The direct observation of pulse shapes and durations using a streak camera has many advantages over autocorrelation techniques. Linear streak camera measurements do not mask satellite pulses, pulse break up, or the formation of sub-structure in the pulses as would two photon fluorescence and second harmonic autocorrelation techniques. The use of a high-resolution monochromator coupled to an array detector allowed the measurement of the entire spectrum of a pulse in a single shot. In this way, the observation of the chirped character of the pulse was facilitated. The advantages of this experimental arrangement were very important in the characterization experiments that led to the discovery of intra-cavity nonlinear pulse compression.[4]

C. Results and Discussions

Results are presented with respect to the spectral and temporal development of single, amplified, second harmonic pulses as the position in the mode-locked pulse train is systematically varied. These results are discussed qualitatively in terms of the physical mechanisms thought to be responsible for the observed spectral and temporal characteristics.

A good figure of merit for the quality of pulses from a mode-locked laser is

$$\rho = \Delta\nu_p \times \Delta\tau_p, \tag{28}$$

the product of the spectral bandwidth times the pulse duration. Table 2 gives the values of ρ for transform-limited pulses for several pulse shapes typically encountered in laser physics. For coherent pulse envelopes of Gaussian shape, $\rho = 0.441$. Values of ρ greater than this value indicate a loss of coherence of the laser pulse. The coherence loss may be due to self-phase modulation arising from the interaction of the high-intensity laser pulse with the nonlinear index of refraction of materials inside the resonator. The change in the index of refraction with the electric field,

$$\delta n = n - n_0 = n_2 \langle E(t)^2 \rangle, \tag{29}$$

where δn is the charge in the index of refraction $(n-n_0)$, n_2 is the nonlinear index of refraction of the material and $\langle E(t)^2 \rangle$ is the electric field amplitude, results in a phase change

$$\phi(t) = \frac{\omega_0 Z n_2}{C} \langle E(t)^2 \rangle , \tag{30}$$

Table 2. The values of ρ for transform-limited pulses for several shapes encountered in laser physics.

Pulse Shape	$\rho = \Delta\nu_p X \Delta\tau_p$
$\exp[-1/2(t/\tau)^2]$	0.441
$\exp[-1/2(t/\tau)]$	0.142
$\exp[-1/2(t/\tau)]\theta(t)$[a]	0.11
$1/\cosh(t/\tau)$	0.315
$\sin(t/\tau)/(t/\tau)$	0.892
$\sin^2(t/\tau)/(t/\tau)^2$	0.366
$\mathrm{rec}(t/\tau)$[b]	0.892
$[1+(t/\tau)^2]^{-1}$	0.142

a. $\mathrm{Rec}(t/\tau)$ - rectangle pulse of width $\tau_p = \tau$.

b. $\theta(t)$ - unit step function.

where $\pi(t)$ is the time dependent phase, ω_0 is the central (i.e. carrier) frequency, z is the material pathlength associated with n_2, and C is the speed of light. The instantaneous frequency of the laser pulse

$$\omega(t) = \omega_0 - \partial\phi(t)/\partial t \tag{31}$$

can be calculated from the time dependence of the pulse envelope, E(t). The frequency sweep resulting from the phase modulation is referred to as a chirp (β in equation (4) and (25)).

Figures 22a and 22b show the dependence of ρ on pulse energies inside the laser cavity for the leading edge and the trailing edge of the mode-locked pulse train, respectively. The curves through the experimental data points were drawn for the sake of clarifying the trends and are not a fit to theory. Each experimental point (also given in Table 3) represents the product of the average of 100 shots and a typical single shot to determine the pulse width and bandwidth respectively. Similar behavior to that shown in Figure 22a has been reported in reference 3 for a purely passively mode-locked Nd:YAG laser system.

From Figure 22a it is clear that even very early in the pulse train, at intracavity energies less than 150 μJ, a slight frequency sweep is present in the pulse. The second pulse in the mode-locked pulse train, having an intracavity pulse energy of 143 μJ, exhibits near transform-limited behavior with $\rho = 0.71$ ($\Delta\nu_p = 0.85\ cm^{-1}$, $\Delta\tau_p = 27.9ps$). As pulses later in the leading part of the pulse train are selected, the values of ρ increase substantially. From the

Fig. 22. The dependence of $\rho = \Delta\nu_p X \Delta\tau_p$ on pulse energy inside the laser cavity for (a) the leading edge, and (b) the trailing edge of the mode-locked pulse train.

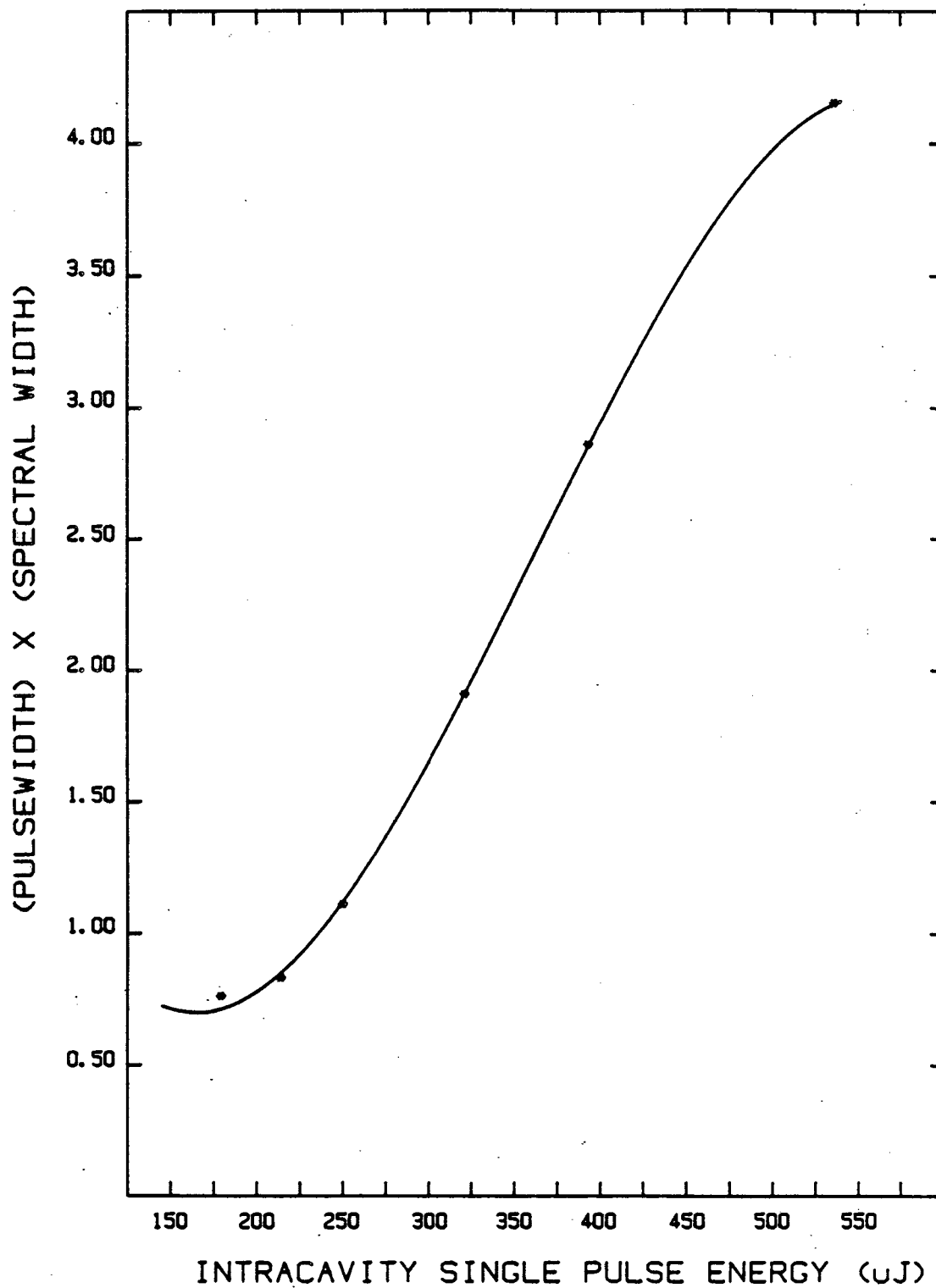

XBL 864-1266

Fig. 22(a)

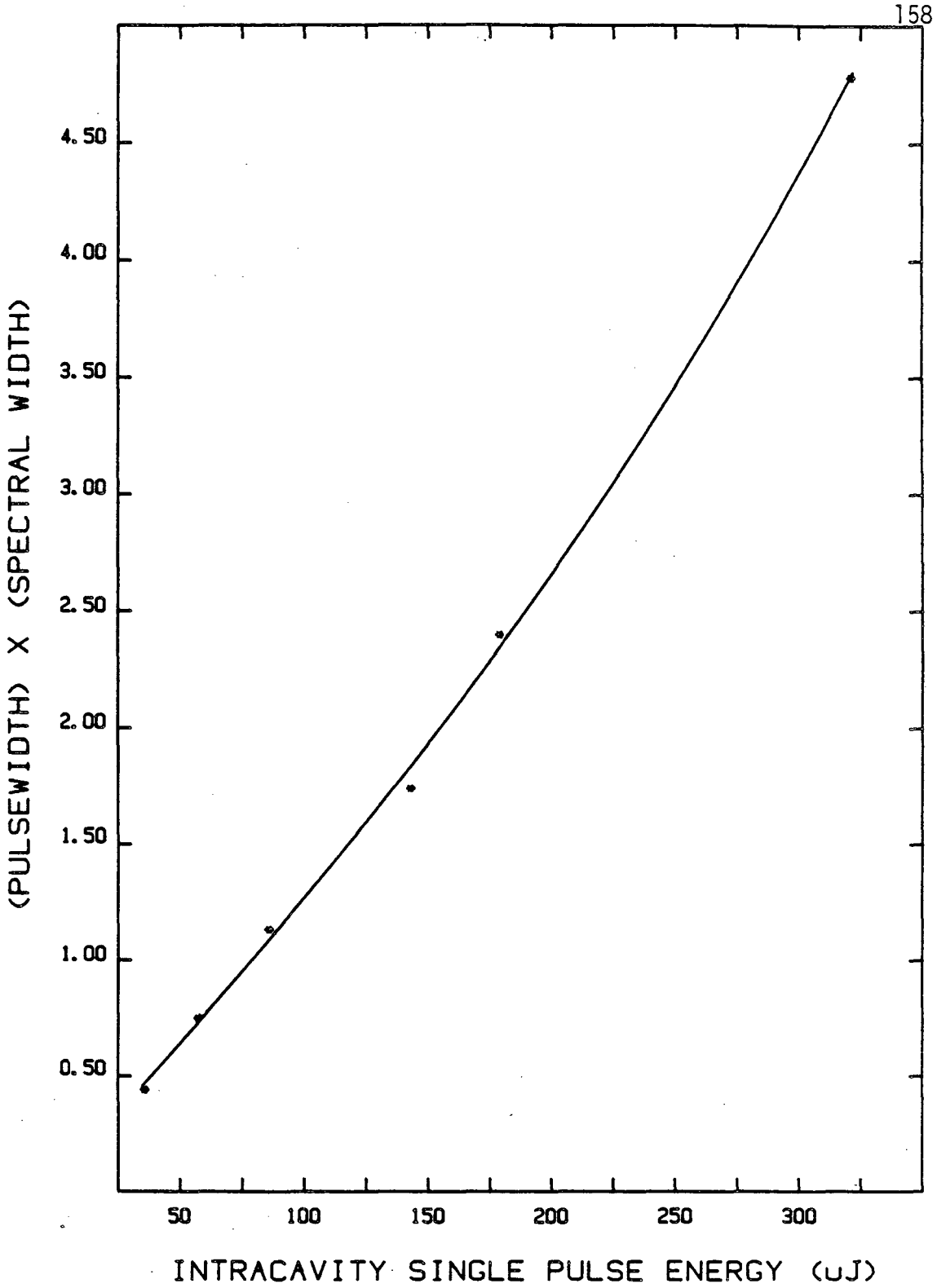

XBL 864-1265

Fig. 22(b)

Table 3. Summary of the results of Figures 22, 26, and 28.

Pulse No.	Energy (μJ)	Intensity (ω/cm^2)	$\Delta\tau_p$(ps)	$\Delta\nu(cm^{-1})$	ρ
1	143	2.90×10^8	27.9	0.85	0.71
2	179	3.82×10^8	26.5	0.95	0.76
3	214	4.59×10^8	26.4	1.05	0.83
4	250	4.37×10^8	32.4	1.14	1.11
5	321	5.44×10^8	33.6	1.47	1.48
6	393	6.06×10^8	36.7	2.60	2.86
7	526	7.61×10^8	39.1	3.53	4.14
8	321	7.12×10^8	25.5	6.25	4.78
9	179	7.91×10^8	12.8	6.25	2.40
10	143	8.70×10^8	9.3	6.25	1.74
11	86	8.08×10^8	4.8	6.25	0.90
12	57	8.08×10^8	3.1	6.00	0.56
13	36	8.60×10^8	2.4	6.25	0.45

third to the seventh pulse in the train (intracavity energies 214 μJ to 536 μJ respectively), the values of ρ rise in a monotonic fashion to a value of 4.15.

From Figure 22a, it is obvious that even with all the care taken in the design and construction of the laser-amplifier system, perfectly transform-limited pulses were not being produced in the early portion of the mode-locked pulse train. True transform-limited behavior can be obtained early in the pulse train with use of a suitable intracavity etalon.[3,4] It is well known that the gain profile of mode-locked solid-state lasers can be shaped and manipulated by proper use of frequency selective elements.[3,12,85-88] Flattening the gain profile which results in an increase in the number of oscillating axial modes aids in the generation of shorter pulses. Conversely, peaking the gain profile leads to sharper spectral bandwidths with longer durations. Variable pulse widths ranging from the picosecond to nanosecond regime can be obtained by combining mode-locking with longitudinal mode selection.[52]

In order to generate shorter, bandwidth limited pulses, the "natural selection" spectral line narrowing effect during the linear amplification stage of mode-locking must be offset.[3] Therefore a suitable Fabry-Perot etalon is placed inside the laser cavity. The transmission through the etalon is given by

$$T(\nu) = 2\{2 + F + F\cos[2\pi(\nu-\nu_1)/\Delta\nu]\}^{-1} . \qquad (32)$$

where ν_1 is the frequency of the transmission minimum, and F and $\Delta\nu$ are the finesse and free spectral range of the etalon given by

$$F = \frac{4r}{1-r^2} \tag{33}$$

$$\Delta\nu = \frac{C}{2ndcos\theta}, \tag{34}$$

respectively. In equations (33) and (34), r is the reflectivity, d is the thickness or spacing and n is the refractive index of the etalon. θ is the adjustable parameter that determines where the minimum (ν_1) lies. Tuning the etalon to a minimum and maximum transmission at the maximum of the spectral gain profile produces flattering and peaking of the profile, respectively. This allows for manipulation of the pulse duration and spectral width depending on the desired application.

The etalon used in the present work was chosen to mimick conditions given in reference 3. Two one-inch-diameter by 0.375-inch-thick, flat reflectors, coated for 10 percent reflectivity at 1064nm, and AR coated at 1064nm on the nonreflective surfaces, were mounted in a Burleigh Instruments VS-25M Etalon. The etalon was held in place by a home-designed, two-inch diameter mirror mount that provided the angular adjustments necessary for tuning. The etalon was placed between the laser head and the second mode selecting aperture.

With 10 percent mirror reflectivities and a mirror separation of 1.21mm, the finesse and free spectral range were 0.494 and 4.13 cm^{-1}, respectively. These conditions were chosen to provide maximum broadening of the laser emission during the linear amplification stage. Spectral and temporal profiles look like Figures 23a and 23b, which are for the etalon tuned to a transmission maximum and minimum respectively at the peak of the Nd:YAG gain profile. In Figure 23a

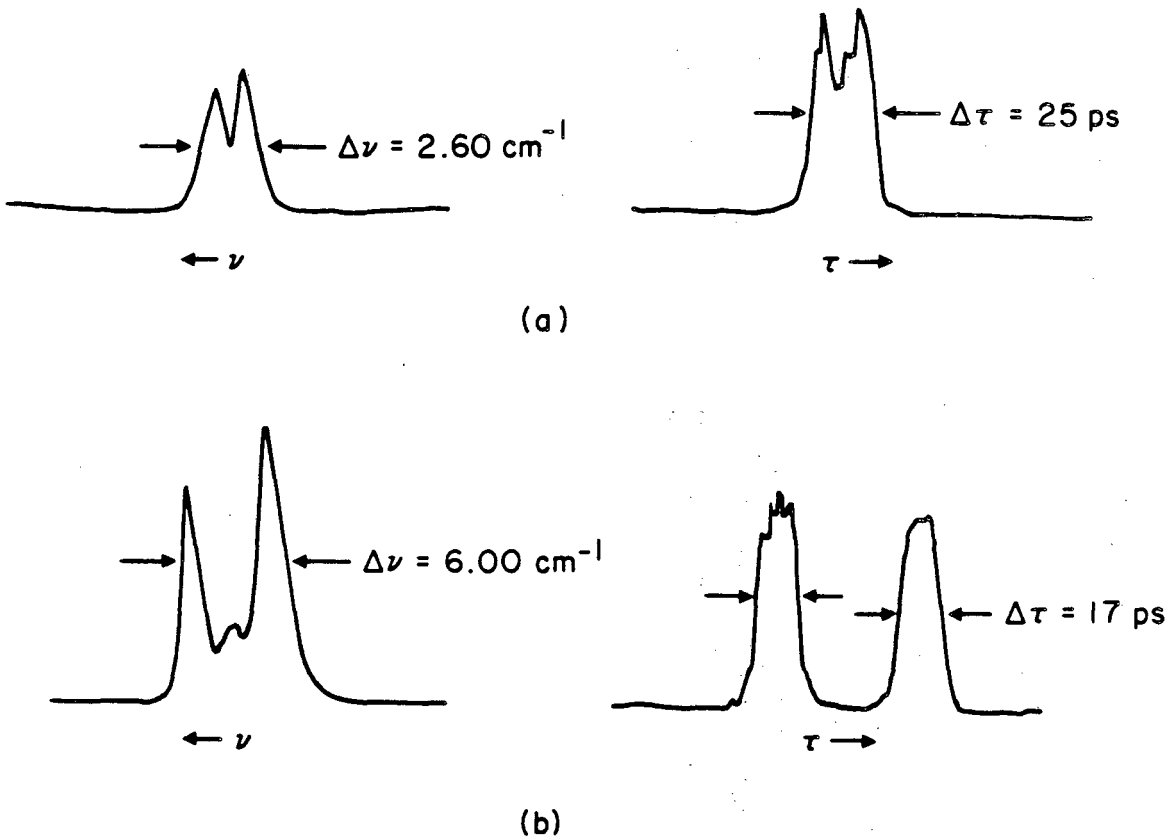

XBL 864-1268

Fig. 23. The spectral and temporal profiles of pulses near the maximum of the pulse with the intracavity etalon acting erratically ($\Delta\nu$ = 4.13 cm^{-1} and F = 0.494) when the etalon is tuned to a (a) transmission maximum, and (b) transmission minimum at the peak of the Nd:YAG gain profile.

there is bimodal character in both the spectral and temporal profile. Figure 23a demonstrates self-phase modulation in the spectral profile and pulse breakup in the temporal profile. Such unstable performance, as predicted in reference 3 for these conditions was due to the fact that a frequency matching of better than 0.01 cm^{-1} was necessary for maximum spectral broadening. Apparently the angular resolution of the etalon configuration was not sufficient or stable enough to meet this strict requirement, resulting in the erratic behavior.

Therefore, a free spectral range of 5 cm^{-1} was chosen that placed less stringent requirements on the resolution of the etalon.[3] The two reflectors were spaced 1.0mm apart. Figures 24a and 24b show the results of measurements of spectral and temporal profiles of pulses selected early in the pulse train with the etalon tuned to a transmission minimum and maximum, respectively, at the center of the gain profile. In Figure 24a true transform-limited behavior is observed (ρ = 0.446) for a pulse with 214 μJ of intracavity energy. Figure 24b demonstrates near transform-limited behavior (ρ = 0.670) for a pulse with 143 μJ of intracavity energy. Both situations depict sharp, single-component spectra with no evidence of self-phase modulation. Pulse durations shorter than normal from this type of laser (17.3ps) result when gain flattening is employed. Pulses with sharper bandwidths (0.57 cm^{-1}) result when gain peaking is employed. The versatility of this system is thus enhanced by using an intracavity etalon. Depending on whether greater temporal or spectral resolution

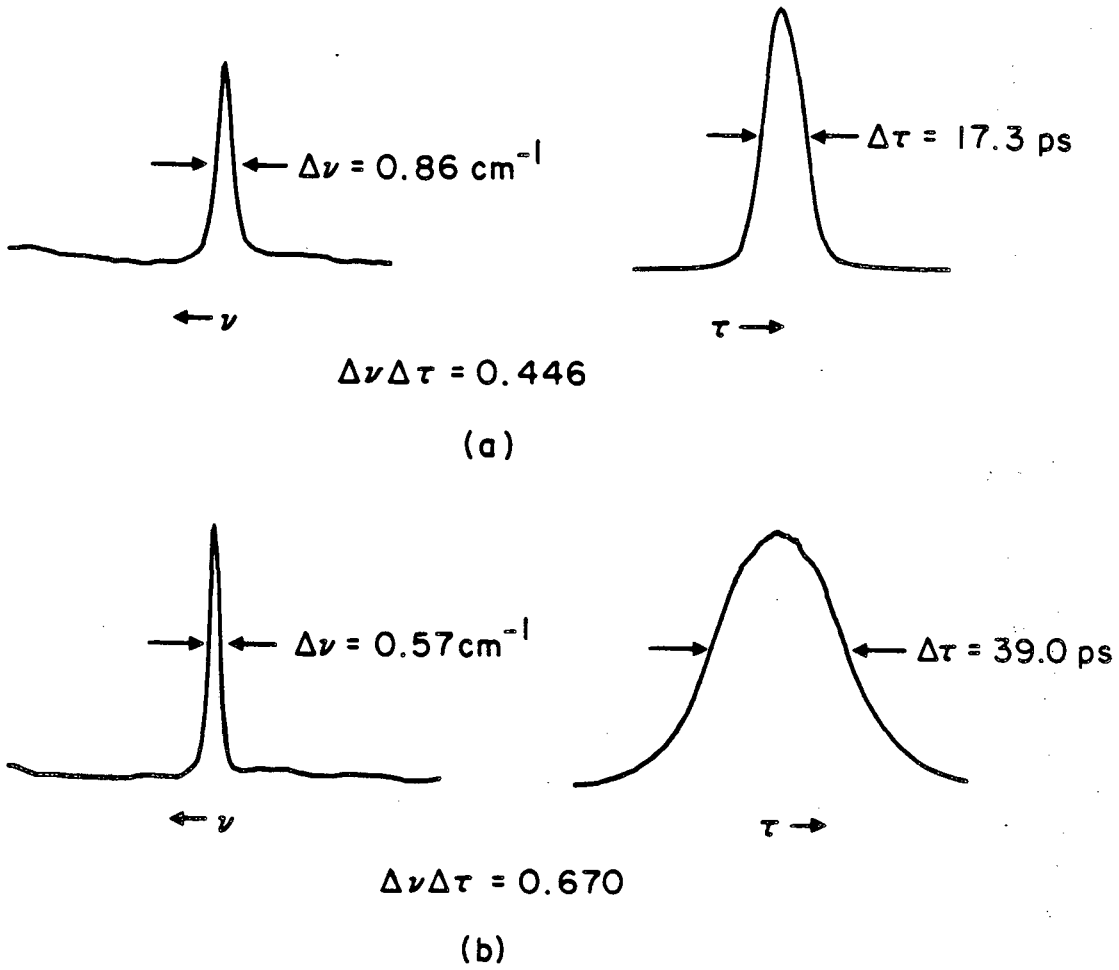

XBL 864-1267

Fig. 24. The spectral and temporal profiles of pulses early in the pulse train with the intracavity etalon acting correctly ($\Delta\nu$ = 5.0 cm^{-1} and F = 0.494) when the etalon is tuned to a (a) transmission maximum, and (b) transmission minimum at the peak of the Nd:YAG gain profile.

is desired for a given experiment, the etalon can be adjusted accordingly.

While looking for transform-limited output with the use of an intracavity etalon, the discovery of very short (8.4ps) pulses was made by looking at pulses after the peak of the pulse train. The behavior of pulse durations and bandwidths for pulses on the trailing edge of the mode-locked pulse train of a Nd:YAG laser had not been previously reported. Therefore a study of such behavior (without an intracavity etalon) was conducted. The results of the pulse width-bandwidth measurement versus intracavity single pulse energy are presented in Figure 22b. The spectral width of the pulses seems to clamp at between 6.0 cm^{-1} and 6.5 cm^{-1}. However, the structure of the individual pulses changes drastically from the middle to the end of the pulse train. The temporal widths of the pulse begin to narrow after the peak of the train, accounting for the monotonic decrease in values of ρ. Eventually, at the extreme end of the pulse train pulses between 2ps and 7ps are encountered. The shorter pulses are very near transform-limited and are the shortest pulses ever reported from a mode-locked Nd:YAG system.

Initially, the explanation for the observation of the pulse shortening included chirp generation (positive frequency sweeping) by self-phase modulation and subsequent pulse compression by negative dispersion in the laser cavity. Negative group velocity dispersion in the system could be associated with the dye absorption and the population inversion of the active medium. However, upon careful

analysis of the spectral characteristics of the pulses along with the corresponding temporal profiles, an alternate interpretation and explanation was put forth.

The best way to understand the pulse evolution and to demonstrate how the self-phase modulation and subsequent pulse compression occur is to show the spectral and temporal profiles of the single amplified second harmonic pulses as a function of position in the train. Figure 25 represents a typical mode-locked pulse train as it appears on a vacuum photodiode (ITT F4014) displayed on a Tektronix 7834 storage oscilloscope (with 7A26 amplifier). The photodiode-oscilloscope combination has a risetime of approximately 0.8ns. The spectral and temporal profiles shown in Figure 26 correspond to the numbered pulses of Figure 25.

Clearly, during the first three round-trip cavity transits (Figure 26a-c), the spectrum remains a single peak, with no sub-structure indicative of self-phase modulation. The pulse intensity is low enough that the saturable absorber still has pulse shortening capabilities and the refractive index change (according to equation (29)) in the Nd:YAG rod and other optical elements is small. During this stage, nonlinear absorption is responsible for pulse shortening from 27.9ps to 26.4ps. The amplification of the inverted medium is also very effective in this stage because the bandwidth of the pulse is narrow and lies completely under the peak of the laser gain curve.

The slight pulse sharpening and amplification allow the intensity of the pulse to grow rapidly until the intensity-dependent refractive

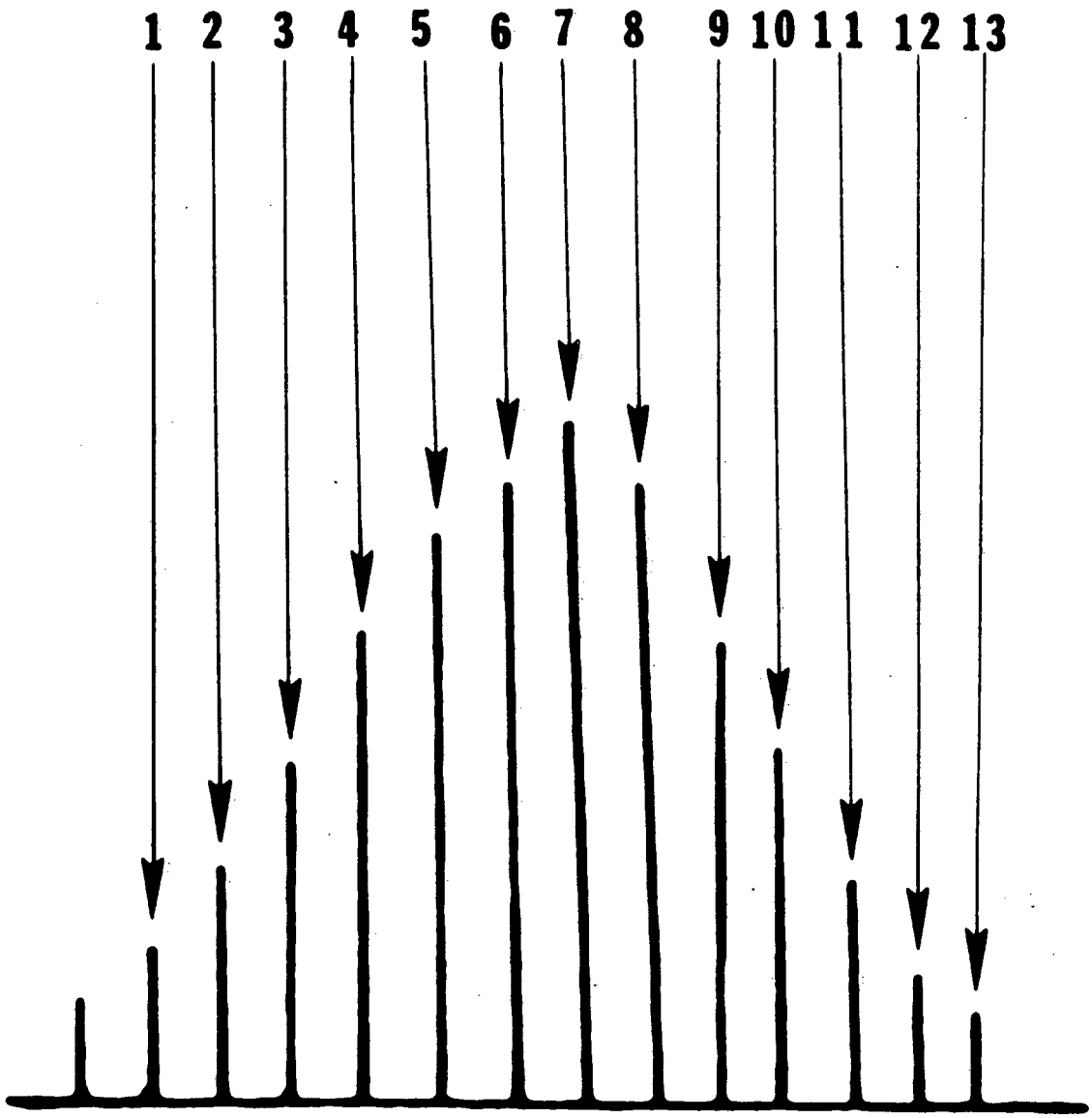

XBL 864-1254

Fig. 25. The number of sequencing of pulses in the mode-locked pulse train corresponding to which pulse in the train is being referred to with respect to its spectral and temporal characteristics (Figure 26).

Fig. 26. The spectral and temporal profiles of single, amplified, second harmonic pulses throughout the mode-locked pulse train of Figure 25.

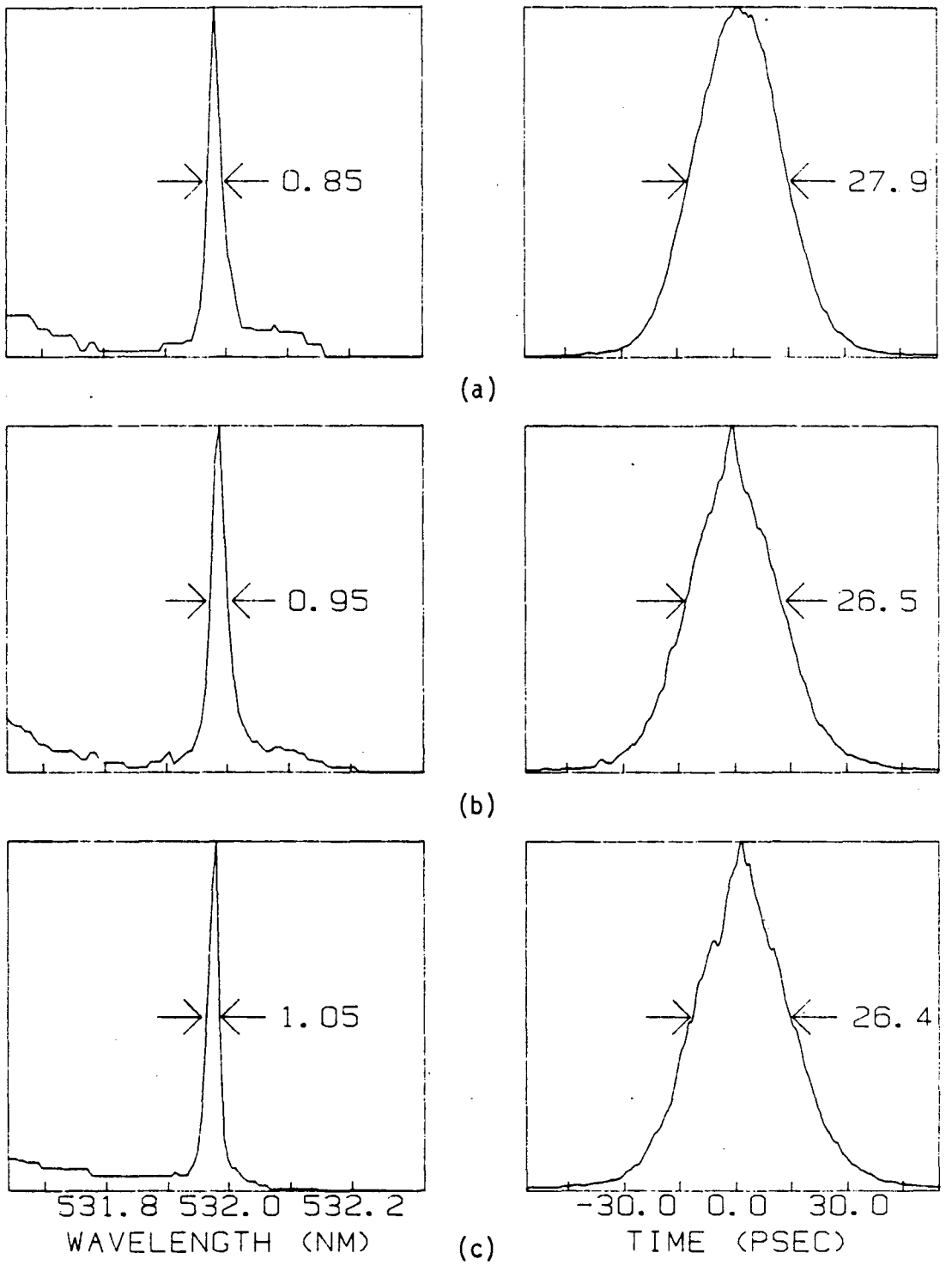

NOTE: ARROWS=FWHM

XBL 866-2175

Fig. 26

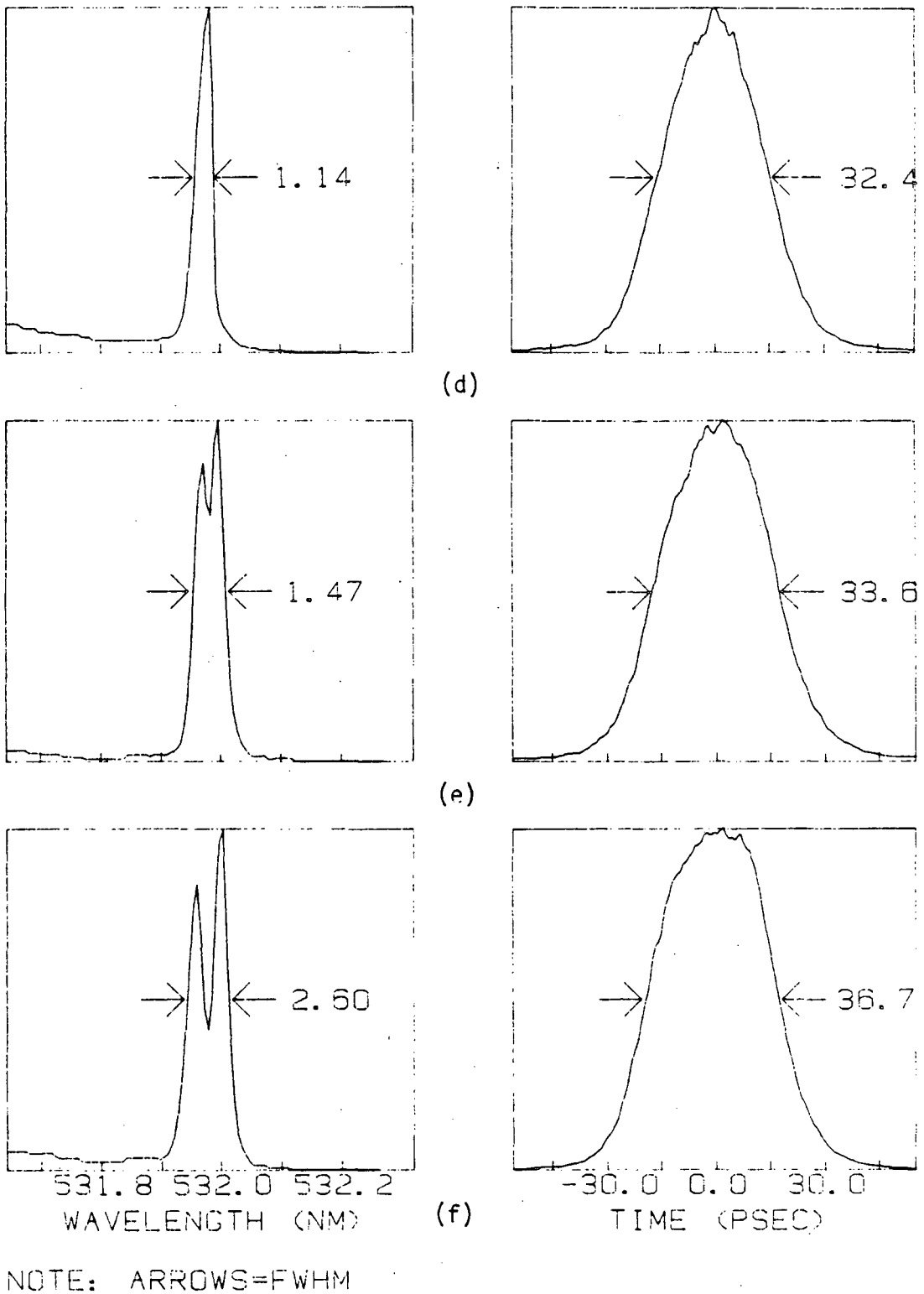

XBL 866-2176

Fig. 26

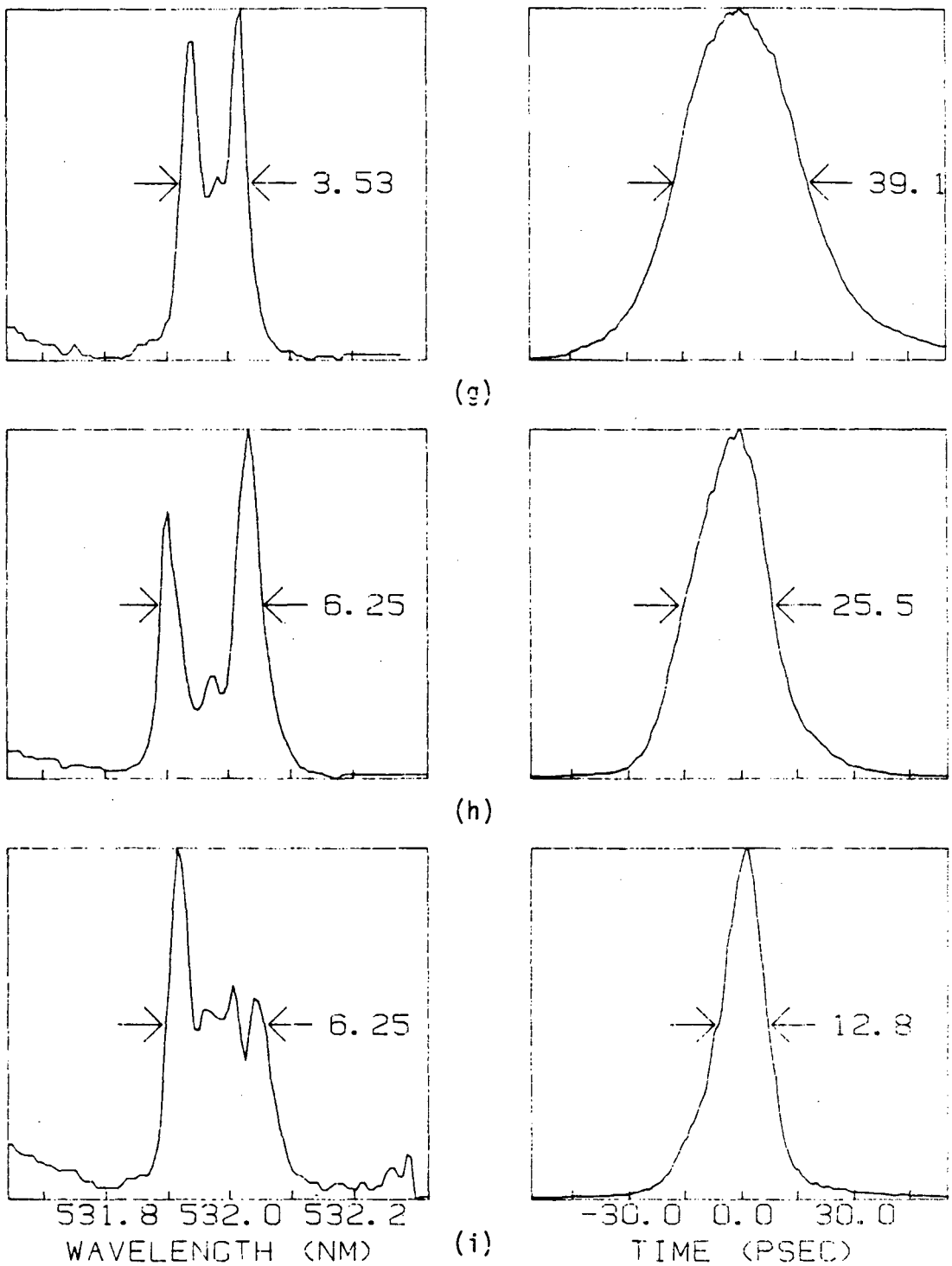

NOTE: ARROWS=FWHM

XBL 866-2177

Fig. 26

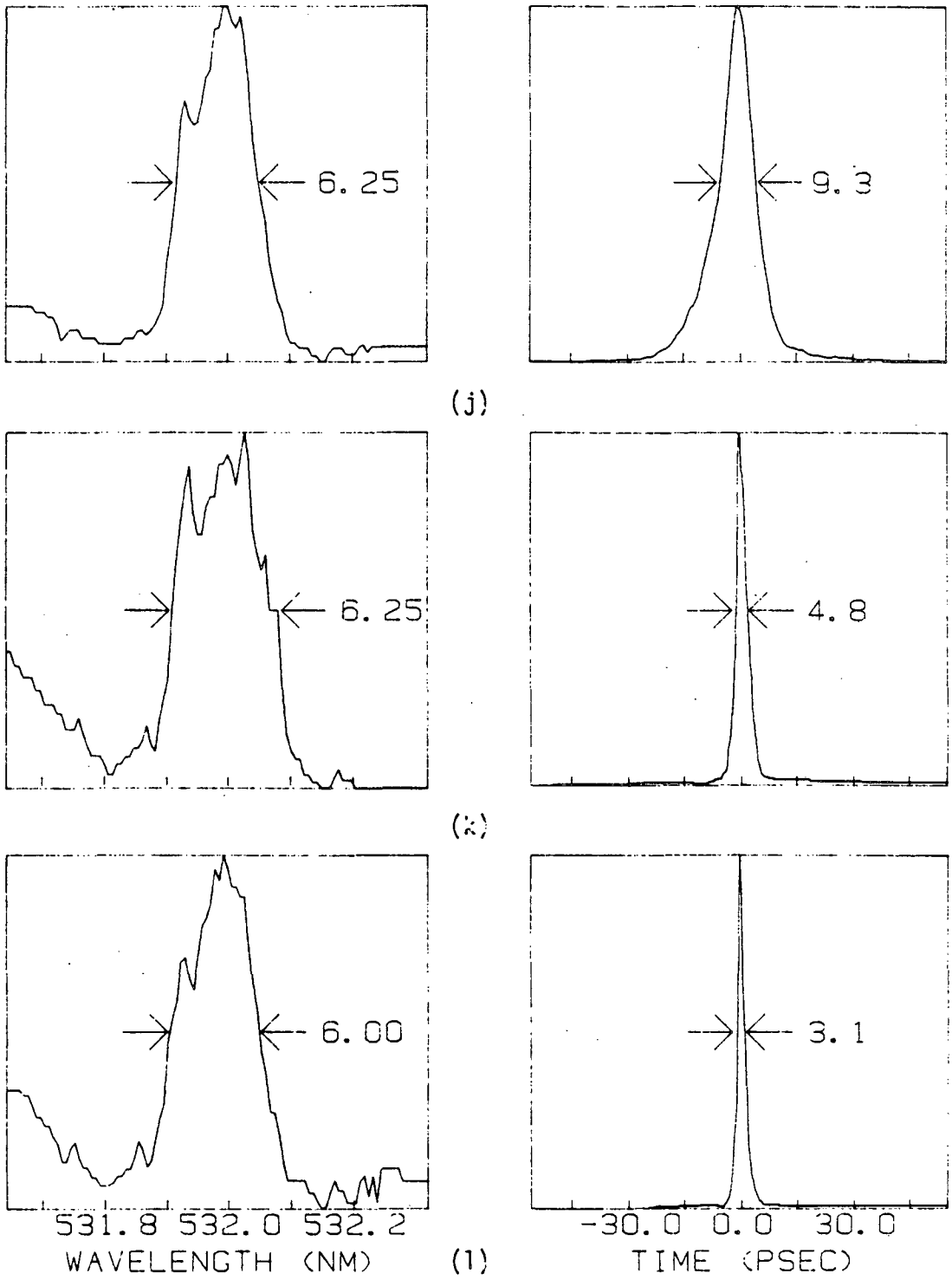

NOTE: ARROWS=FWHM

XBL 866-2178

Fig. 26

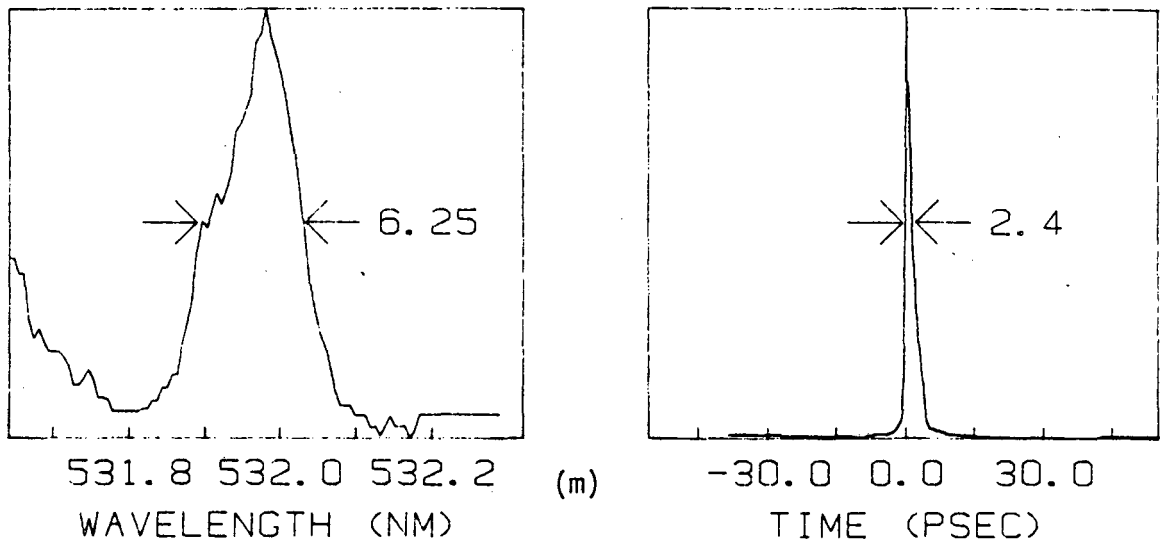

NOTE: ARROWS=FWHM

XBL 866-2174

Fig. 26

index change can no longer be neglected. The fourth pulse (Figure 26d) in the train undergoes spectral broadening and doublet formation centered around the central frequency (λ_0 = 532nm, ω_0 = 18,797 cm^{-1}) due to the phase delay of equation (30). The spectra of pulses five through seven (Figures 26e-g) continue to broaden from approximately 1.9 cm^{-1} to 3.5 cm^{-1} and triplet formation is observed at the peak of the mode-locked pulse train (pulse number seven).

The reason for the Stokes (negative sweep) and anti-Stokes (positive sweep) with respect to the central frequency in the spectra depicted in Figures 26d-m (pulses 4-13) can be inferred by examining equation (35)

$$\omega(t) = \omega_0 - \frac{\omega_0 Z}{C} n_2 \frac{\partial \langle E^2 \rangle}{\partial t} , \qquad (35)$$

which is obtained by substituting equation (31) into equation (30). For $n_2 > 0$, which is the case for Nd:YAG and other optical elements in the cavity, the frequency shift will be negative on the leading edge of the pulse ($\frac{\partial \langle E^2 \rangle}{\partial t} > 0$) and positive on the trailing edge of the pulse ($\frac{\partial \langle E^2 \rangle}{\partial t} < 0$). The frequency sweep with respect to time is depicted graphically in Figure 27. The central frequency crossover occurs at the peak of the pulse because the relaxation of the non-linearity is instantaneous compared to the pulse duration.[89-91] Therefore the phase delay does not become integrated. The self-phase modulated pulses of Figure 26 therefore contains frequency components lower in energy (Stokes) and higher in energy (anti-Stokes) than the

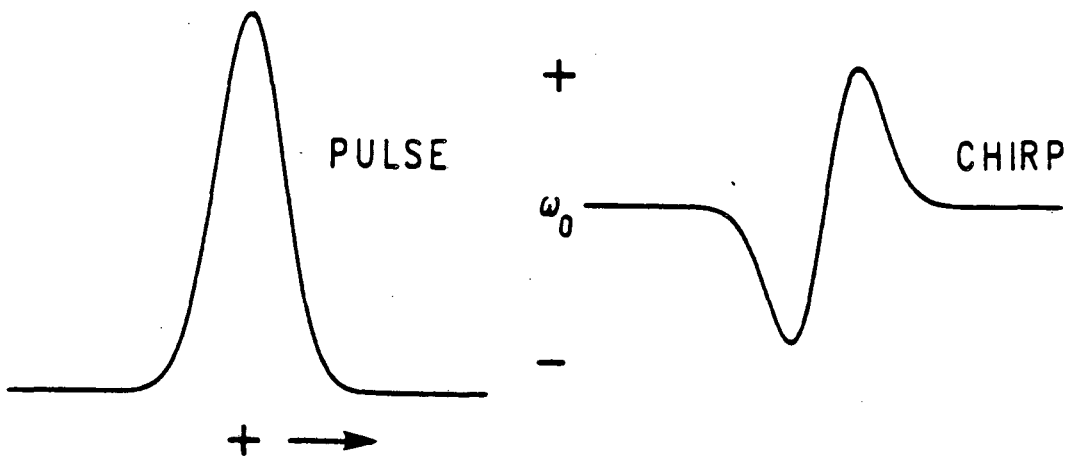

XBL 864-1263

Fig. 27. Graphical interpretation of the frequency sweep impinged on a Gaussian pulse due to self-phase modulation.

central frequency (ω_0) in the leading and trailing edges of the pulse, respectively.

The temporal broadening encountered in pulses 4 through seven (Figures 26d-g) is the result of two effects. First, due to the self-phase modulation, there is more than one frequency group in the pulse. Therefore, positive group velocity dispersion of optical elements within the laser cavity causes the different frequency groups to travel at different velocities. Second, the "natural selection" of spectral components at the center of the gain profile causes narrower bandwidth pulses resulting in longer pulse durations. Even though it appears that there is gain saturation at the central frequencies, the "natural selection" imposed by the shape of the gain profile of the Nd:YAG medium forces frequencies towards the center of the profile, leading to a small increase in the pulse width.

Those pulses that exhibit spectra typical of self-phase modulation also exhibit temporal asymmetry. The leading edges of these pulses are not as sharp as the trailing edges. The asymmetry can be due to a variety of things. Amongst them are self-steepening or nonlinear group velocity dispersion. Self-steepening of picosecond pulses results if the relaxation time of the nonlinearity is on the order or greater than the pulse width. The pulse intensity thus will have an integration effect on the nonlinearity. This results in the phase perturbation being bunched later than the peak of the pulse. The peak of the pulse is retarded with respect to the leading edge of the pulse, resulting in a slowly rising and sharply falling pulse envelope. How-

ever, in glasses and crystalline solids, which constitute all the elements in the cavity, the relaxation of the nonlinear index of refraction is very rapid (10^{-14} to 10^{-15} sec) because the nonlinearity arises from electronic motions in the material.[83-85] Therefore the lifetime effect is not likely to be causing the asymmetry unless there are some other unknown relaxation processes occurring.

The other mechanism that can account for the pulse asymmetry can be understood by looking at Figure 27. Clearly, the frequency shifts for the leading edge and the trailing edge of the pulse are negative and positive, respectively. If the effect of the negative dispersion in the cavity associated with the mode-locking dye is considered, then the negatively swept (leading edge) and positively swept (trailing edge) spectral components will be expanded and compressed respectively. This interpretation qualitatively agrees with the observed asymmetry.

The most interesting and novel observations of pulse behavior occur for the pulses (numbers 8 through 13) after the peak of the mode-locked pulse train. As seen in Figure 26h, the spectral bandwidth of such pulses is between 6.0 cm^{-1} and 6.5 cm^{-1}. This corresponds to the limit imposed by the gain bandwidth of the Nd:YAG lasing medium. On the trailing edge of the pulse train it is apparent that the spectral width of the pulses never exceeds this limit. However, the shape and structure of the spectral profiles change dramatically. Immediately following the peak of the pulse train multiplet structure is observed. As pulses later in the train are

selected, the multiplet structure smoothens and eventually disappears. These spectral profiles seem to be significantly more homogeneous. This would be expected for a nearly transform-limited pulse. For pulses very late in the pulse train, the homogeneous spectrum uniformly fills the entire gain bandwidth of the lasing medium.

The shortest pulses (between 2ps and 3ps) observed, with spectral widths close to 6.5 cm^{-1}, are at or near the transform-limit. These pulses are also referred to as gain bandwidth-limited pulses because they are as short and spectrally broad as the Nd:YAG active medium permits them to be. The self-phase modulation of the pulses is responsible for the pulse narrowing observed on the trailing edge of the mode-locked pulse train. Hence the name intracavity nonlinear pulse compression.

In general, it is thought that due to the narrow laser gain curve in Nd:YAG lasers, spectral broadening due to self-phase modulation cannot extend very far since any frequency outside the laser gain curve cannot be amplified. Mode-locked pulses from Nd:YAG lasers should therefore have simple temporal and spectral structures.[9] On the contrary, because the laser gain curve is so narrow, a spectral filter is imposed on the spectrally broadened pulse. In effect, the pulse continues to broaden in the frequency domain on each round trip cavity transit, but the amplifying medium only amplifies the central portion of the pulse in the time domain.

The nonlinear index of refraction of the lasing medium and other optical components feeds energy into frequencies outside the gain

bandwidth by means of a frequency sweep due to self-phase modulation. Therefore only the middle portion of the laser pulse (in time) has frequency components within the gain bandwidth of the laser medium and only this portion is amplified. The spectrum continues to be broadened upon each round trip through the cavity and, hence, a smaller fraction of the pulse (in time) is amplified. The physical manifestation of this phenomenon is seen by looking at the pulse durations of the pulses in the trailing edge of the pulse train in Figures 26h-m. Pulse durations decrease monotonically from 25.5ps to 2.4ps. The last pulse in the train of Figure 25 (pulse number 13) is at the transform-limit. This is the shortest pulse ever generated from a mode-locked Nd:YAG laser without external pulse compression techniques.

Pulses selected extremely late in the pulse train exhibit durations ranging between 2ps and 8ps. The variation most likely arises from the nonlinear nature of the compression. The pulse shortening is a direct result of the spectral expansion on each transit through the cavity. The spectral broadening due to self-phase modulation is directly related to the pulse intensity. Therefore, the slightest variation in pulse intensity will manifest as a variation in the pulse duration of the shortest pulses.

The fact that these gain bandwidth-limited pulses were observed at all should be attributed to the stability of the laser system. The pulse trains were extremely stable and had very reproducible envelopes, (better than ± 2 percent energy amplitude stability) that in turn

yielded better performance from the pulse selector. Thus, there was little jitter in the pulse selection and these observations were facilitated.

Crucial to the interpretation of the observations presented here is the fact that for pulse compression to be occurring on the trailing edge of the pulse train, the chirp must be continually propagated on each successive round trip transit through the cavity. The question arises, how does the chirp continue to grow after the peak of the mode-locked pulse train if each successive pulse has less and less energy. The answer lies in equation (35). The frequency sweep is proportional to the pulse intensity, not the energy. As can be seen in Figure 28, the peak intracavity pulse power is clamped at approximately the same value (~ 15 MW) at and after the peak of the pulse train due to the pulse shortening.

Fig. 28. A plot of the peak pulse intracavity power versus round trip cavity transit showing that at and after the maximum of the pulse train, the peak power is clamped, ensuring the continuation of the chirp build up, despite the decrease of pulse energy on each successive roundtrip through the cavity.

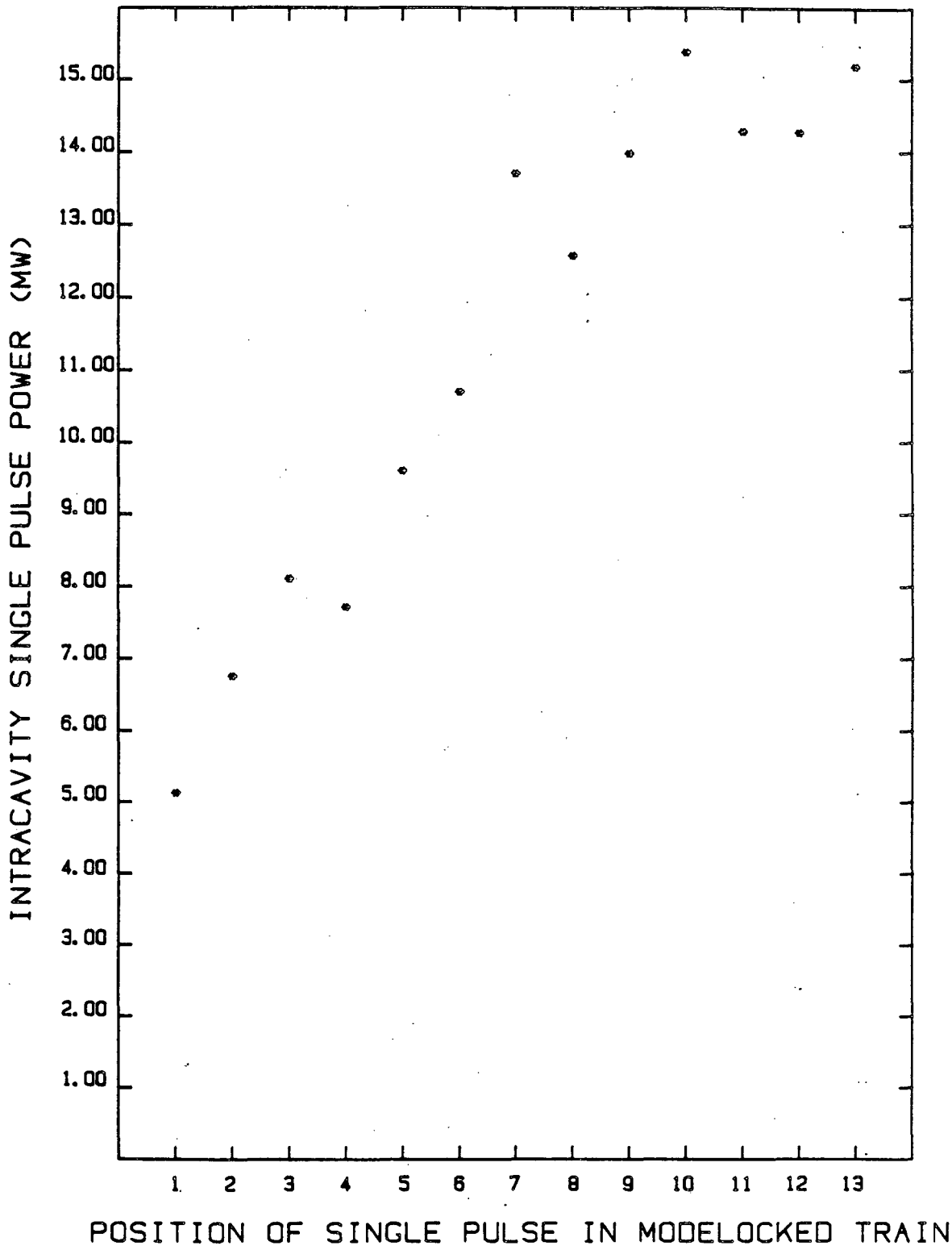

Fig. 28

XBL 864-1255

D. Interpretations, Conclusions, and Comparisons

The idea of intracavity nonlinear pulse compression is not an entirely new one. Applying various optical pulse compression schemes[14-23] outside the laser cavity to intracavity techniques has been a desire of researchers for a long time. The optimal situation would be to have a well-controlled, monotonic, positive frequency sweep impressed upon a pulse circulating inside a laser resonator due to the intensity dependent nonlinear index of refraction of materials in the cavity. Subsequent pulse compression would take place if a suitable negatively dispersive element could be incorporated into the cavity. This could take the form of a Gires-Tournois interferometer[18,19] as one of the laser end mirrors or placement of a grating-pair, negatively-dispersive delay line[15] inside the optical resonator.

Fischer and Bischel[92] applied these principles to obtain more efficient operation of solid-state laser amplifier chains. However, the nature of the spectral modulation and subsequent compression led to temporal sidebands preceding and following the main pulse with about 1/20th the intensity of the main pulse. Recently, Fork[93] has successively used a network of prisms inside a colliding pulse mode-locked laser as a negatively dispersive element to offset the positive chirp inherent in the laser.

Duerinckx et al.[94] had a similar idea. By combining an intracavity optical Kerr cell (to frequency sweep the pulse) with a

Gires-Tournois interferometer as the laser end mirror, they hoped to achieve pulse compression inside an actively AM mode-locked Nd:YAG laser. However, the interferometer could not produce sufficient negative dispersion to do any significant compression on chirped pulses encountered in the Nd:YAG cavity.[95] What was discovered however, was the Nd:YAG amplifying medium was acting as the pulse compresser. Not as a negatively dispersive element, but as a spectral aperture. This is very similar to the discovery of intracavity non-linear pulse compression presented here, however in the present case the Nd:YAG amplifying medium as well as other cavity elements are responsible for the chirp generation. Similar effects have been used to describe the concept of passive FM mode-locking, originally described by Laussade and Yariv,[96] and by Comly, Yariv, and Garmire.[97] They presented an interesting correlation between the appearance of picosecond fine structure in a ruby laser and the matching of the dielectric relaxation time of the Kerr liquid to the reciprocal gain bandwidth of the laser medium. The Kerr liquid was used as the passive FM mode-locker.

Fischer, Kelly, and Gustafson[98] used a similar idea to generate subpicosecond pulses using the optical Kerr effect. Physically, the Kerr medium feeds energy into frequencies outside the gain bandwidth. The Kerr cell chirps the pulse over frequencies much broader than the gain bandwidth and by an amount proportional to the pulse intensity. In a laser with a very broad gain profile (i.e. Nd:Glass, $\Delta\nu_L \approx$ 100–200 cm^{-1}), intensities exceeding that which would induce

self-focusing would be necessary to chirp the spectral width of the pulse to overfill the gain bandwidth of the laser medium. Therefore in Nd:Glass systems, limited bandwidth amplification is necessary for such a scheme to be feasible. This can be achieved in two ways. First, a sufficiently large, constant loss can be coupled to the laser medium raising the threshold level of all frequency elements other than line center. Alternatively, the gain profile can be provided by the gain medium plus a bandwidth limiting device (i.e. etalon) having a linewidth narrower than the laser gain. This second method has been recently used successfully to generate shorter pulses from an actively mode-locked and Q-switched Nd:Glass laser.[99,100] These researchers used the ideas developed presently to choose pulses late in the mode-locked pulse train which exhibited high degrees of self-phase modulation. They limited the gain bandwidth of the laser with use of an intracavity etalon.

In Nd:YAG, where the gain bandwidth is relatively small ($\Delta\nu_L$ = 6.5 cm^{-1}), intensities need not be as great to induce self-focusing, and etalons need not be used unless desired. Also, very low loss, stable cavities can be constructed and used for this scheme. In what follows, it will be seen that the laser system described presently is very well suited for stable production of pulses shorter than those normally generated from a mode-locked Nd:YAG laser system. The use of active mode-locking ensures stable formation of mode-locked pulse train envelopes. The high intensity pulses necessary to cause sufficient self-phase modulation are the result of combining passive

mode-locking with active mode-locking. The importance of having Nd:YAG as the amplifying medium cannot be only stressed. The relatively narrow amplification bandwidth of the medium enables the chirp to grow fast enough at the pulse intensities encountered so that the pulse compression occurs before other competing nonlinear effects take place. Also, the narrow bandwidth allows construction of a very reliable, low loss cavity so the entire gain bandwidth can be used in the compression technique.

Reviewing Table 3, and plotting pulse width and spectral width versus cavity round-trip transit number (Figure 29) demonstrates evidence of three regions of behavior.

(1) Initially there is conventional pulse shortening due to the nonlinear absorption of the mode-locking dye. This occurs for the first four round trip transits.

(2) Region (1) is followed by slight pulse broadening due to the spectral mode selection at the center of the gain profile along with positive group velocity dispersion of the spectrally broadened pulse due to the development of a chirp. Both occur during the nonlinear amplification stage (round trips 5-8) when the laser intensity has built up sufficiently.

(3) The conversion of the chirp into a very narrow pulse occurs during round trips 9 through 14. The narrowing occurs when the chirped bandwidth begins to exceed the amplification bandwidth of the Nd:YAG laser medium. Because spectral elements outside the amplification bandwidth are not amplified, the spectral width is essentially clamped

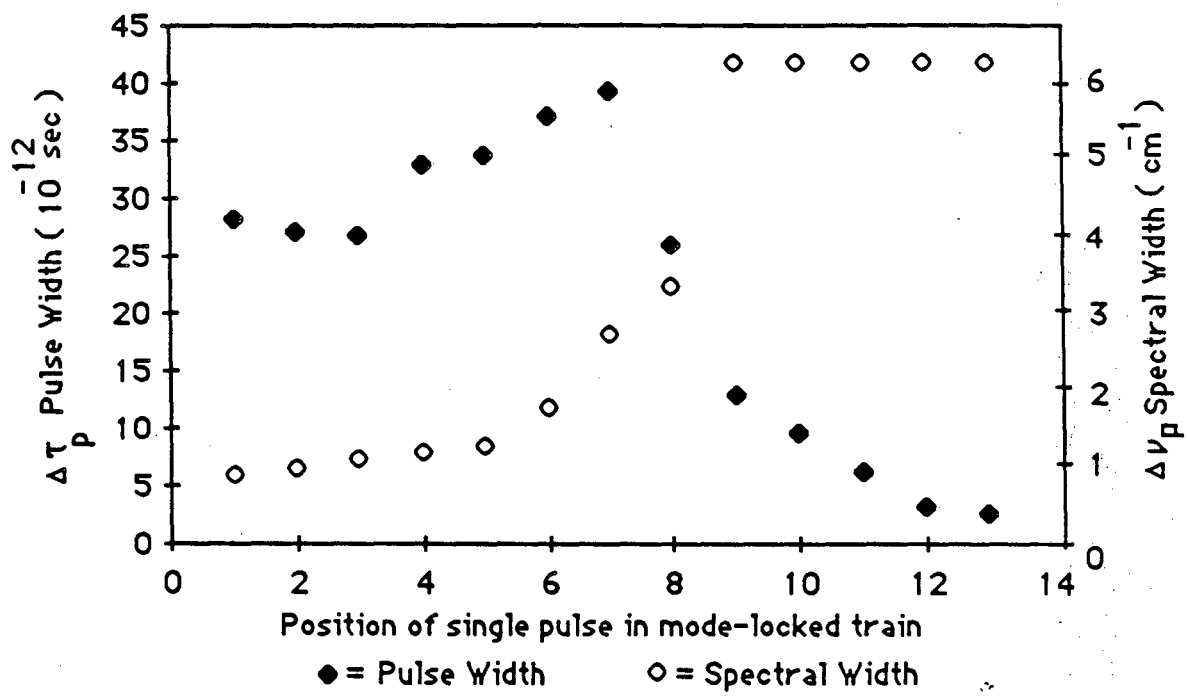

XBL 866-2238

Fig. 29. A plot of pulse width and spectral width versus cavity round trip transit number.

during this regime. However, the substructure of the spectra changes dramatically. The structure smoothens considerably on each round trip transit through the cavity until a homogeneous profile is observed (Figure 26m).

To understand this mechanism it helps to employ the graphical interpretation given in Figure 30. The abscissa and ordinate represent time and frequency respectively. The dashed lines through the ordinate (parallel to the abscissa) correspond to the spectral aperture imposed by the gain bandwidth of the amplifying medium. The dotted lines through the abscissa (parallel to the ordinate) are a transformation of the spectral components that can be amplified in time. For simplicity only three representations are shown. They are early, immediately following the peak, and late in the mode-locked pulse train (Figures 30a-c respectively). Early in the pulse train there is slight evidence of a frequency sweep. According to equation (35) the instantaneous frequency shifts are negative and positive for the leading and trailing portions of the pulse respectively. At this point in the pulse train however, all the frequency components of the pulse are within the spectral bandwidth of the amplifying medium. Therefore the entire pulse can be amplified in time.

Immediately following the peak of the pulse train (Figure 30b) the frequency spread is larger than the gain bandwidth. Certain frequency components are swept outside the spectral aperture. There is a monotonic positive frequency sweep across the maximum of the pulse. However, there are also smaller regions that are negatively swept at

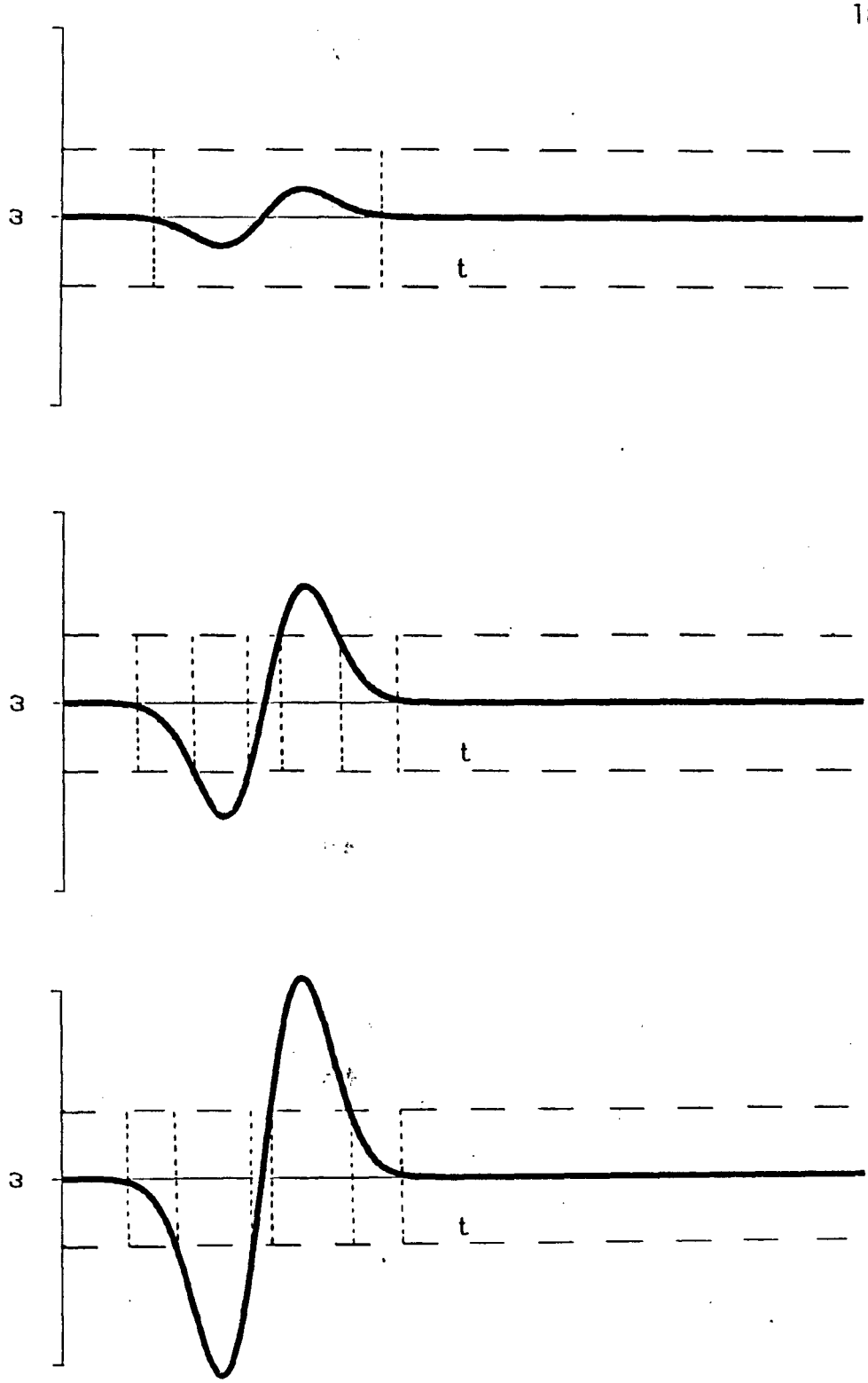

XBL 866-2400

Fig. 30. A graphical interpretation of the pulse compression scheme. (a) Early, (b) after the peak, and (c) late in the mode-locked pulse train.

the extrema of the pulse. The observation of side lobes preceding and following the amplified central portion of the pulse is expected. The side lobes, corresponding to the negatively swept part of the pulse, contain spectral components within the amplifying bandwidth. This phenomena would manifest itself as a form of pulse breakup. However, the observation of side lobes is not typical. This effect is attributed to the presence of a saturabale absorber inside the laser cavity. The nonlinear absorption of the dye effectively acts as a discriminator against the lower energy, negatively chirped portions of the pulse. Hence, the only portion of the pulse that normally gets amplified is the middle portion.

The pulse shortening and energy content of the pulse is directly and inversely proportional to the time derivative of the frequency shift ($|\frac{\partial\omega}{\partial t}|$) respectively. Very late in the pulse train (Figure 30c) the frequency sweep is even greater. The pulse gets shorter until the transform-limit is reached. The energy content of the pulse and wings is decreased. The wings are thus more effectively absorbed by the saturable absorber. The pulse intensity, however, stays the same (Figure 28) due to the pulse shortening. This mechanism is also partially responsible for the reduction of net energy amplification because less energy is extracted from the gain medium.

In their intracavity pulse compression experiment, Duerinckx et al.[94] observed compression from 300ps to 70 ps and from 300ps to 30ps using a 1 cm and 2 cm cell filled with CS_2, respectively. However, they never reached the predicted theoretical limit of 5ps.

Reasons for their inability to realize the shorter pulses were that the intensities available from an actively, AM mode-locked Nd:YAG laser were not sufficient to produce a large enough chirp. Even if the intensities were sufficient, the effects of self-focusing could render the technique useless for the Kerr cell length necessary to observe maximum compression. For example, the self-focusing propagation distance can be approximated using[98]

$$Z_{focus} = \frac{1}{4}\, d\, (n_0/\delta n)^{1/2} \,, \tag{36}$$

where[7,94]

$$\delta n = n_2 \langle E^2 \rangle = \delta I \tag{37}$$

is the change in refractive index due to the intensity dependent non-linear index of refraction and d equals the initial beam diameter. In the second part of equation (37), $\gamma = 4\pi\, n_2/Cn_0$ (or $\gamma = 4.19\times10^{-3}\, \frac{n_2}{n_0}\left[\frac{cm^2}{W}\right]$) and I is the pulse intensity in $\frac{watts}{cm^2}$. The value of n_0 and n_2 for CS_2 at 25°C are 1.62 and 1.3×10^{-11} esu respectively. For pulse intensities encountered in their laser (~1Gw/cm^2) at the peak of the Q-switched pulse train and an initial beam waist of 300 μm (600 μm diameter), a maximum value of 3.36×10^{-5} for δn is calculated. Using equation (36) yields Z_{focus} = 3.29 cm. Therefore, the cell lengths used (1 cm and 2 cm), taking into account the double pass through the cell, are near the length limit that would lead to self-focusing. The longer cell lengths and/or higher pulse intensities that would be necessary for maximum pulse compression would result in beam distortion. Self-focusing effects would probably become important at the

same time as the self-phase modulation effects,[101] rendering the method impractical.

Fortuitously, the pulsed, active/passive mode-locked Nd:YAG laser combines all the features necessary to carry out effiient, gain bandwidth-limited, intracavity nonlinear pulse compression. Table 4 summarizes the calculated results, assuming a uniform beam spatial distribution, of changes of refractive indices in the Nd:YAG rod and quartz acoustooptic modulator and the change in optical pathlength due to the index variation ($\delta n x Z$, Z = 18 cm for Nd:YAG rod, Z = 12.7 for quartz block). Finally, the calculated values of the chirped bandwidth are presented using these factors. Contributions to the chirp, $\Delta\nu$ can be estimated using[12]

$$\Delta\nu = 3\nu_0 \delta n Z / c\tau_p, \tag{38}$$

where ν_0 is the carrier frequency (ν_0 = 9398 cm^{-1}), $\delta n x Z$ is the optical path length change due to the refractive index variation, C is the speed of light, and τ_p is the pulse duration. The values of the bandwidth presented in Table 4 represent the accumulated chirp and therefore are calculated as the sum of the initial bandwidth plus the chirp on each successive round trip transit through the cavity. A uniform intensity distribution is assumed for these calculations. The beam diameter is 1.5mm. The initial bandwidth of the pulse was taken to be the transform-limit ($\Delta\nu_0$ = 0.527 cm^{-1}) of the 27.9ps pulse duration initially observed.

Table 4. Calculated values of changes of indices of refraction in the Nd:YAG rod and quartz acoustooptic modulator, changes in the optical pathlength due to the index variation, and the calculated value of the accumulated chirped bandwidth assuming an uniform beam spatial distribution.

Pulse Number	δn(YAG)	δn(Quartz)	δnxz(YAG)	$\delta nrxz$(Quartz)	Calculated Chirp $\Delta\nu$ (cm^{-1})
1	2.72×10^{-7}	8.26×10^{-8}	4.89×10^{-6}	1.05×10^{-6}	0.727
2	3.58×10^{-7}	1.09×10^{-7}	6.45×10^{-6}	2.38×10^{-6}	1.005
3	4.30×10^{-7}	1.31×10^{-7}	7.74×10^{-6}	1.66×10^{-6}	1.339
4	4.09×10^{-7}	1.24×10^{-7}	7.36×10^{-6}	1.58×10^{-6}	1.599
5	5.10×10^{-7}	1.55×10^{-7}	9.17×10^{-6}	1.97×10^{-6}	1.912
6	5.68×10^{-7}	1.73×10^{-7}	1.02×10^{-5}	2.19×10^{-6}	2.257
7	7.13×10^{-7}	2.17×10^{-7}	1.28×10^{-5}	2.76×10^{-6}	2.632
8	6.67×10^{-7}	2.03×10^{-7}	1.20×10^{-5}	2.58×10^{-6}	3.170
9	7.42×10^{-7}	2.26×10^{-7}	1.34×10^{-5}	2.86×10^{-6}	4.35
10	8.15×10^{-7}	2.48×10^{-7}	1.47×10^{-5}	3.15×10^{-6}	6.16
11	7.57×10^{-7}	2.30×10^{-7}	1.36×10^{-5}	2.93×10^{-6}	8.754
12	7.57×10^{-7}	2.30×10^{-7}	1.36×10^{-5}	2.92×10^{-6}	12.642
13	8.06×10^{-7}	2.45×10^{-7}	1.45×10^{-5}	3.11×10^{-6}	19.684

It is clear from Table 4 that this crude estimate is sufficiently accurate for early pulses (pulses 2-6) to predict the chirped bandwidths of the pulses. However, the region where the chirp should be building up at a rate sufficient to fill the entire gain bandwidth (middle of the train) is not described sufficiently by this approximation.

Recalling that for a Gaussian intensity distribution 90 percent of the energy is contained in 25.6 percent of the beam area (see Appendix I) leads to the results of Table 5, where a beam diameter of 0.76mm is employed for the calculation of the pulse intensities. The calculated chirps of Table 5 overestimate the observed bandwidths of pulses 2 though 8, but do account for sufficient chirp propagation to account for the pulse shortening observed on the trailing edge of the pulse train (pulses 9-14). The final chirped bandwidth (pulse 14, $\Delta\nu = 75.73\ cm^{-1}$) is a factor of twelve times the gain bandwidth of the active medium. The maximum compression ratios observed late in the pulse train are approximately factors of sixteen. Therefore the smaller beam sizes are in qualitative agreement with the observed pulse shortening, and the actual discrepancies may suggest self-focusing is occurring.

Athough these crude estimates are only qualitatively correct, they do point out that even when the energy per pulse is on the decline, the chirp continues to grow due to the pulse narrowing. The observed chirp bandwidth is of course clamped at the gain bandwidth for these

Table 5. The same as Table 4 but assuming a Guassian beam spatial distribution (see Appendix I).

Pulse Number	δn(YAG)	δn(Quartz)	δnxz(YAG)	δnrxz(Quartz)	Calculated Chirp $\Delta\nu$ (cm^{-1})
1	1.06×10^{-6}	3.22×10^{-7}	1.90×10^{-5}	4.09×10^{-6}	1.306
2	1.39×10^{-6}	4.24×10^{-7}	2.51×10^{-5}	5.38×10^{-6}	2.386
3	1.67×10^{-6}	5.09×10^{-7}	3.01×10^{-5}	6.46×10^{-6}	3.395
4	1.59×10^{-6}	4.84×10^{-7}	2.87×10^{-5}	6.15×10^{-6}	4.614
5	1.98×10^{-6}	6.03×10^{-7}	3.57×10^{-5}	7.66×10^{-6}	5.867
6	2.21×10^{-6}	6.72×10^{-7}	3.98×10^{-5}	8.53×10^{-6}	7.120
7	2.78×10^{-6}	8.44×10^{-7}	5.00×10^{-5}	1.07×10^{-6}	8.579
8	2.60×10^{-6}	7.90×10^{-7}	4.68×10^{-5}	1.00×10^{-6}	10.672
9	2.88×10^{-6}	8.77×10^{-7}	5.19×10^{-5}	1.11×10^{-6}	15.303
10	3.17×10^{-6}	9.64×10^{-7}	5.71×10^{-5}	1.23×10^{-6}	22.310
11	2.95×10^{-6}	8.96×10^{-7}	5.31×10^{-5}	1.14×10^{-6}	33.210
12	2.95×10^{-6}	8.95×10^{-7}	5.30×10^{-5}	1.14×10^{-6}	48.336
13	3.13×10^{-6}	9.53×10^{-7}	5.64×10^{-5}	1.21×10^{-6}	75.736

pulses. However the increasing value of $|\frac{\partial\omega}{\partial t}|$ ensures pulse narrowing until the transform-limit is reached.

The failings of the results of Tables 4 and 5 to describe accurately the chirped bandwidths of pulses in the middle of the pulse train indicate a more sophisticated analysis is necessary. The estimations of beam size in these tables places an upper and lower limit on the actual beam size. However, the spatial intensity distribution is probably changing upon successive round trip transits in the cavity in this region. This can also be attributed to the nonlinear indices of refraction. Self-focusing is occurring to some extent, but not enough to cause beam breakup and/or large diffraction losses rendering the pulse compression impractical. Again, using equations (36) and (37), the self-focusing propagation distances are estimated to be 29 cm and 47 cm in the Nd:YAG rod and quartz block respectively. Recalling the rod is 9 cm (18 cm double pass) long and the quartz block is 6.35 cm (12.7 cm double pass) long, large scale self-focusing is not expected to be a problem, and indeed,has not been observed. However, as indicated by this analysis, the spatial intensity distribution must be changing (concentrating) so that values of the chirped bandwidth become large enough to comply with the observed compression ratios. Obviously there is a need to study the beam spatial distribution as a function of round trip cavity transit in order to better understand the role of small scale self-focusing.

The observation that the entire gain bandwidth of the Nd:YAG medium can be filled (and exceeded) by the chirped bandwidth implies that the cavity has extremely low losses. An interesting experiment would involve the use of an intracavity etalon with its transmission peaked at the center of the gain profile (effectively narrowing the gain profile). Desired results would be to observe pulse compression earlier in the mode-locked pulse train. Of course there would be a tradeoff in the maximum pulse shortening attainable with the effectively reduced gain bandwidth. Recently,[99,100] 4ps second harmonic pulses have been generated in an actively mode-locked and Q-switched Nd:Glass laser by selecting single pulses very late in the mode-locked pulse train. The authors attribute the dramatic pulse shortening (100ps to 4ps) to self-phase modulation caused by the nonlinearities in the rod and two acoustooptic elements. They utilized an etalon ($\Delta\nu$ = 15 cm^{-1}) to effectively reduce the gain bandwidth of the Nd:Glass ($\Delta\nu_L$ = 40 cm^{-1}). The pulse compression mechanism is very similar to that which had been described earlier,[4] but suffers from poor signal-to-noise ratio (interpulse background energy), that could be improved with the use of saturable absorbers.

In conclusion, a comparison between the system described presently and other techniques used for short pulse generation from mode-locked Nd:YAG lasers is in order to emphasize the ease and simplicity of this method. Two elegant techniques for short pulse production from Nd:YAG laser have been developed, however they require complexed electronic timing sequences, intricate cavity configurations, and implementation

of passive mode-locking and passive FM modulation methods to attain the very shortest pulses. The regenerative amplifier originally developed by Murray, Kuizenga, and Lowdermilk[102,103] generated 15ps pulses starting with 120ps pulses. Short pulse production required repeated passage of the pulses through an amplifier cavity containing a saturable absorber, an electrooptic Q-switch, and a cavity dumper. Precise timing and therefore complicated electronic circuits were required to ensure that the effects of dye saturation and gain saturation were properly balanced. Compression occurred only while the pulse intensity was in the nonlinear transmission range of the dye and therefore amplification of the pulses had to be slow. However, the net gain of the amplifier increased as the dye saturated which accelerated pulse growth. Therefore to achieve large compressions, gain saturation was used to hold down pulse amplification. This necessitated precise timing between injection of the seed pulse from the actively mode-locked and Q-switched oscillator, the flashlamp triggering of the amplifier head, and the triggering of the Q-switch and cavity dumping circuit. Although this system provides stable production of short pulses synchronized (±5ps jitter) to longer pulses, it is not easily set up.

Choi and Topp[50] using a ring cavity version of the regenerative amplifier, allowing for simple input and output coupling using polarization methods, and generated 5ps pulses using Nd:YAG as the active medium. To obtain these extremely short pulses it was necessary to use a saturable absorber in conjunction with a liquid

phase modulation cell inserted in the cavity. With only the dye, they reported output of between 17ps and 19ps pulse durations. Experiments conducted to reproduce their work[104] showed that Choi and Topp were not regeneratively amplifying the injected pulses, but actually were off-axis multipass amplifying the injected pulse. This resulted in the long, uniform pulse amplitude pulse trains that were observed. Inclusion of passive FM modulators, such as a cell containing CS_2, while resulting in short pulse generation also caused beam profile distortion.[104]

Recently another form of regenerative amplification has been described and experimentally verified. The self-injected, nonmode-locked picosecond laser developed by Brito Cruz, De Martini, and Malaloni[105] uses a single Q-Switched cavity for generation and amplification of subnanosecond pulses.[106] These subnanosecond pulses are then self-injected and compressed by multiple passage through an intracavity saturable absorber resulting in the generation of 15ps pulses.[51] This method bypasses the instabilities associated with purely passively mode-locked systems in the same way active mode-locking helps. Because the pulse is the result of the amplification of a well defined Q-switched pulse and not quantum noise associated with passive mode-locking, statistical fluctuations are avoided.

Six picosecond pulses were generated when a Nd:YAG rod generated the seed pulse and a flashlamp pumped Nd:Glass rod was inserted in the cavity to provide broadband amplification for further pulse compression.[105,107] Generation of these pulses requires precise

cavity configuration including proper placement of elements with respect to end mirrors and exact control over the ratio of the beam size in the saturable absorber and the amplifying medium. The intra-cavity Pockels cell is used as a Q-switch for self injection and a cavity dumper for output coupling. The timing for the triggering of the respective processes requires an intricate circuit for the Krytron driving circuit to the Pockels cell.

In comparison, the configuration of the laser system described presently is an ordinary pulsed, active/passive mode-locked Nd:YAG laser that combines commercially available electronics with a carefully designed optical system. Generation of pulses under 5ps (between 2ps and 3ps), the shortest ever reported from such a system, is achieved simply by selecting single pulses very late in the mode-locked pulse train. Most of the work is done passively by the Nd:YAG amplifying medium. The nonlinear index of refraction imposes a frequency sweep on the pulse, and the spectral aperture due to the narrow gain bandwidth is responsible for the pulse compression. Since the observed pulses are at or near the transform-limit of a Gaussian pulse with a spectral width equal to the gain bandwidth, they represent the shortest pulses achievable using Nd:YAG as the active medium.

IV. Optical Parametric Source

A. Background

Much of the utility of laser sources for experimental studies in the physical and life sciences is derived from their wavelength specificity. Tunable lasers afford the researcher the luxury to be able to excite specific electronic, vibrational, and/or rotational modes of the material under study. In the field of picosecond dynamics and spectroscopy the dye laser has been the most popular choice for tunable ultrashort pulses in the past. Recent advances in synchronously pumped,[46-48] short cavity,[40] and colliding pulsed mode-locked[108] dye laser technology have generated shorter, more stable, amplified tunable light with moderate to high repetition rates.

An alternative method of producing tunable, coherent light is optical parametric generation.[24-34] In contrast to dye lasers, where the limited tuning range of any given dye requires the use of many different dyes and pumping wavelengths to completely cover the visible and near-infrared spectrum, an optical parametric source (OPS) pumped with one wavelength can completely cover these spectral regions. An OPS can have a tuning range of five times that of the most broadly tunable dyes. A single OPS can provide continuous tunability throughout the entire visible spectrum.[32] Various optical parametric sources using different nonlinear optical crystals, pump frequencies, and phase-matching methods have been used to cover spectral regions ranging from the ultraviolet[43,44] (215nm) to the infrared[24,25] (10μm).

Optical parametric interactions involve the second order polarizability

$$P^{(2)} = \chi^{(2)} \cdot EE, \tag{39}$$

of the nonlinear material in use, where $P^{(2)}$ is the second order polarizability, $\chi^{(2)}$ is the second order susceptibility, and EE is the electric field amplitude. The process (see Figure 31) entails the annihilation of a photon of the pump beam at frequency ω_3 having wave vector $\vec{K}_3$ and the simultaneous creation of a photon pair at ω_2 having wave vector $\vec{K}_2$ (signal) and ω_1 having wave vector $\vec{K}_1$ (idler). Phase-matching occurs when both energy and momentum are conserved according to

$$\omega_3 = \omega_1 + \omega_2 \tag{40}$$

$$\vec{K}_3 = \vec{K}_1 + \vec{K}_2. \tag{41}$$

Any photons at frequencies ω_1 and ω_2 can be used as weak input signals (seed photons). However, in the absence of any seed photons, spontaneous parametric emission at the signal and idler frequency will build up from quantum noise in a cone around the forward direction upon passage through a nonlinear crystal. Amplification of the weak spontaneous parametric fluorescence into useful output energies requires a gain of approximately 10^{13} (e^{30}). Since the parametric gain increases exponentially with pump beam intensity, the use of an OPS is particularly attractive when a high peak power picosecond laser is used as the pump source. Using pump intensities in the GW/cm^2 range, which are easily attainable with the laser system described previously (at harmonics up to and including the fourth harmonic), the

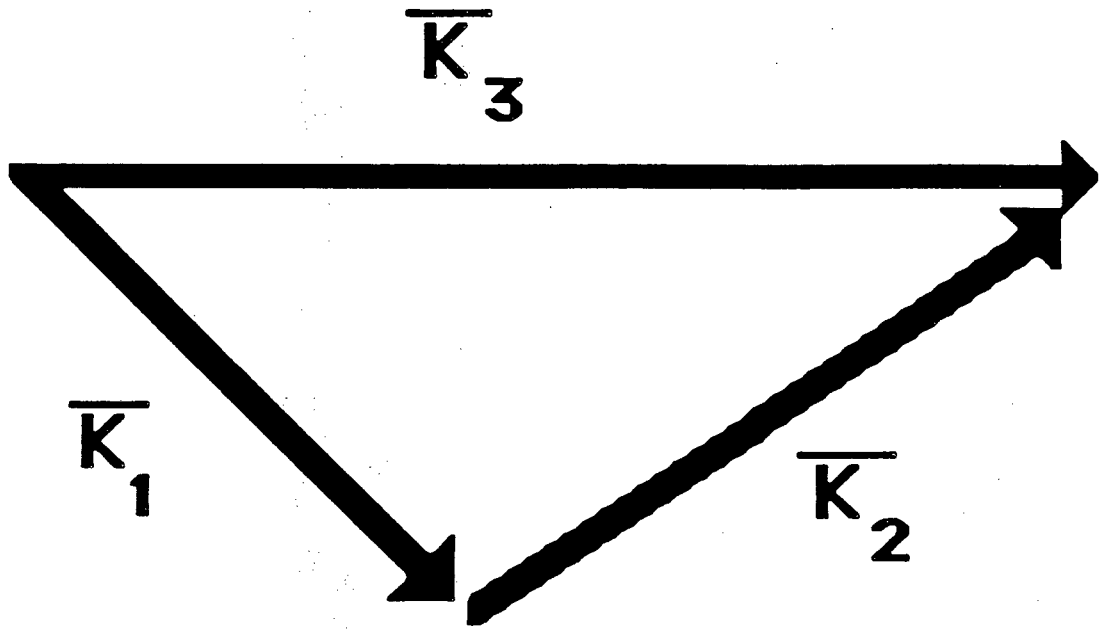

$$\overline{K}_3 = \overline{K}_1 + \overline{K}_2$$

$$\omega_3 = \omega_1 + \omega_2$$

XBL 866-2304

Fig. 31. The vector diagram of phase matching in an optical parametric process.

required gain of 10^{13} can be achieved in a single pass through several centimeters of a nonlinear crystal. The use of these high peak intensities obviates the construction of the external resonator commonly used with Q-switched nanosecond pump pulses when building an optical parametric oscillator (OPO).[24,25,34] Therefore threshold conditions associated with OPO's are relaxed, and a simple, single-pass, travelling-wave OPS can be constructed. The absence of an external resonator permits easy tuning of the device over a broad spectral range (~7000 cm^{-1}) simply by counter rotating the two crystals about the plane normal to the pump beam propagation direction.

The first report of a tunable, coherent optical parametric oscillator was in 1965,[25] in which nanosecond pulses were used to pump lithium niobate ($LiNbO_3$). Since then the literature is filled with reports of nanosecond-pumped OPOs and picosecond-pumped OPSs. Depending on the frequency range of interest, many different nonlinear materials have been used for optical parametric generation. Materials such as lithium niobate ($LiNbO_3$),[29,32,109,110] lithium iodate ($LiIO_3$),[111] alpha-hydrogen iodate (α-HIO_3),[112] and proustite (Ag_3AsS_3)[113,114] have been used to generate tunable picosecond coherent radiation in the mid-infrared region. Ammonium dihydrogen phosphate ($NH_4H_2PO_4$, i.e. ADP),[27,31,42] potassium dihydrogen phosphate (KH_2PO_4, i.e. KDP) and its deuterated analog (KD_2PO_4, i.e. KD*P),[29,43,115] cesium dihydrogen arsenate (CDA),[116] deuterated rubidium dihydrogen arsenate (RD*A),[117] and barium sodium niobate ($BaNaNbO_3$)[118] have been used to generate tunable picosecond coherent radiation in the visible and near-infrared range.

KDP and ADP are excellent materials for this application due to their high damage thresholds (10^{10}-10^{11} W/cm^2) compared to that of other materials such as $LiNbO_3$ and $LiIO_3$ (10^7-10^8 W/cm^2). KDP and ADP are also very attractive because large crystals of excellent optical quality are readily available.

Previous ADP optical parametric sources have utilized Type I (e-oo) phase-matching. Phase-matching has been achieved by both temperature and angle tuning. Pump frequencies have either been the third[42] of fourth[27,31,33] harmonic of a pulsed, mode-locked, Nd:YAG or Nd:Glass laser system. Most previous picosecond optical parametric devices using KDP as the nonlinear material have utilized Type II (e-oe) phase-matching and were pumped with the second harmonic of a mode-locked Nd:YAG laser.[43,45,115,118-122] Spectral and temporal characterization of the output of these devices typically have shown pulses at least a factor of six from the transform limit. For example, with a 27ps pump pulse, an output pulse duration of 21ps and spectral widths of 4 cm^{-1} to 8 cm^{-1} were obtained when conversion efficiencies were between 5 and 12 percent.[118] Conversion efficiencies as high as 50 percent have been reported, however the spectral characteristics of these pulses suffer considerably.[120] Third harmonic (355nm) pulses from mode-locked Nd:YAG lasers have also been used to pump Type II KDP optical parametric generators.[43,122] However, little work has been carried out to characterize the performance of such a device. Spectral bandwidths of 10 cm^{-1}, conversion efficiencies of 10 percent, and continuous tunability from

448nm to 640nm and 792nm to 1687nm[122] (460nm to 600nm and 900nm to 1400nm[43]) have been reported.

What follows is a description of a systematic study of the simultaneous temporal, spectral, and spatial characteristics of single pulses from a picosecond, Type II, KDP, travelling-wave OPS pumped with the third harmonic of the pulsed, active/passive mode-locked, Nd:YAG laser described in Chapters II and III. Proof that the OPS output can be very near the transform-limit will be demonstrated. Pulses of 8ps duration with a spectral width of approximately 2 cm^{-1} have been routinely generated at low conversion efficiencies (less than 5 percent). This is a significant improvement over results previously reported.[43,122]

Energy conversion efficiencies of approximately 25 percent into visible photons have been obtained from the 355nm pumped, KDP OPS. The spectral and temporal profiles become considerably broadened at these high efficiencies. Other performance characteristics under various operating conditions will be presented. Also, reasons for the observations will be given and discussed in detail.

The enhanced performance of the device presented here over that which has been reported previously is attributed to improvements in the characteristics of the pump laser. The use of a highly stable, pulsed, active/passive mode-locked, Nd:YAG oscillator-amplifier system minimized both fluctuations in the OPS output and damage to the OPS crystals. The diffraction-limited beam of the pump laser contributed to the excellent spectral quality of the OPS output.

B. Nonlinear Optical Crystal Configurations

A schematic (top view) of the two crystal OPS with input and output polarizations indicated is shown in Figure 32. The OPS consisted of two, 37mm long KDP crystals cut for Type II phase-matching at an angle of 59 degrees with respect to the optic axis. The KDP was purchased from Cleveland Crystal Corp. in bulk form and cut and polished by the users. Thirty seven millimeters (74mm total length) was chosen as a compromise between two factors. The first consideration was the length dependence of parametric amplification. Under the pump beam intensity conditions allowable by the laser system, a 74mm crystal length was sufficient to generate useful output energies. Due to the length dependence of the parametric gain, there is a tendency to think that increased lengths lead to increased output energy. This is true to a certain point until the effects of group velocity dispersion become significant, which is the second consideration. Due to the wavelength dependence of the indices of refraction the beams of the three wavelengths involved in the parametric interaction, the beams walk off each other in time. This leads to output pulse width broadening. Eventually, if the crystal length is long enough the different wavelength pulses walk off each other completely and no further parametric amplification occurs. Both these mechanisms will be discussed in more detail in the discussion of our experimental observations.

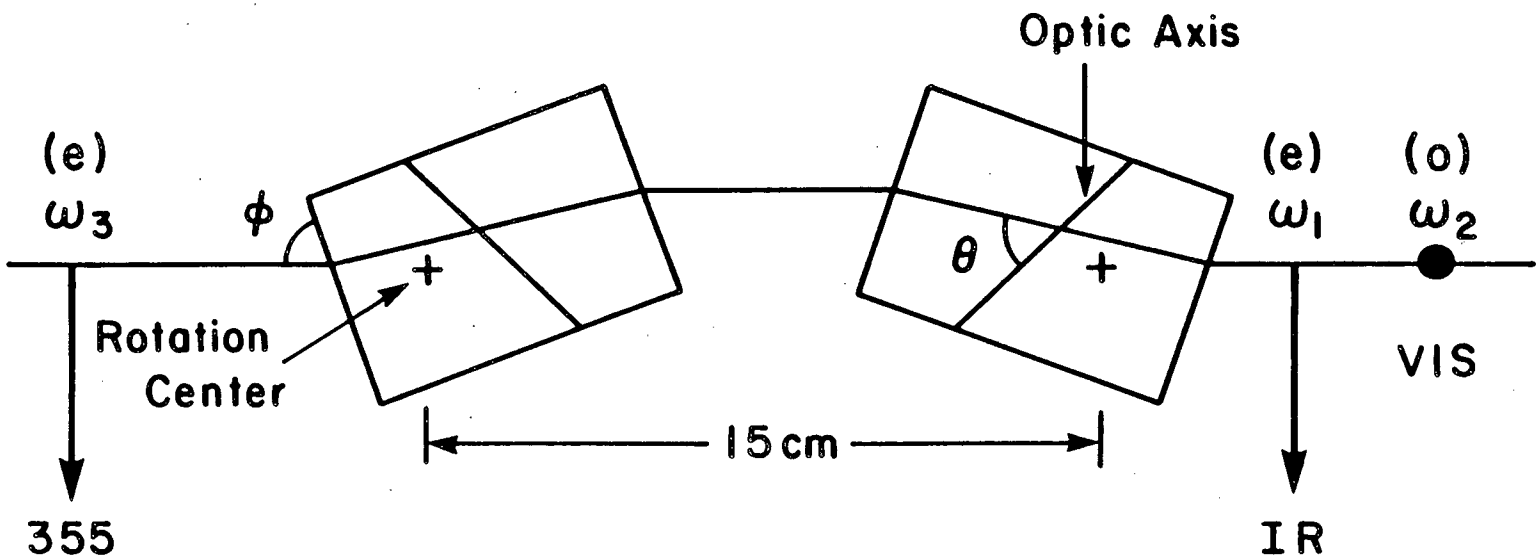

Fig. 32. The crystal orientations and the polarizations of the radiation fields for a Type II phase-matched OPS.

XBL 853-1467

The crystals were placed 14 cm to 15 cm apart. As will be shown later, because there is a trade off between output energy and spectral width for a given crystal spacing, this spacing was chosen to give the greatest output energy along with the smallest spectral width.

In Figure 32 the cross is the rotation center. The two crystals were counter rotated through these points to achieve tuning. Counter rotation throughout the entire tuning range produced no significant deflection in the direction of the output or the pump beam. Any dispersive effects are compensated for by the counter rotation. Tilting the device in the plane formed by the crystal faces orthogonal to the tuning plane had no significant effect on the performance of the OPS. Rotation about the beam propagation axis changed the effective input polarization and therefore had substantial effects on the output energy. The angles θ and ϕ denote the angle formed by the propagation direction and the crystal optic axis and crystal face respectively.

The pump beam ω_3 (355nm) propagates as an extraordinary ray (e-ray). Upon incidence of this beam onto the first crystal, broad band parametric fluorescence is produced at any frequency which satisfies energy and momentum conservation (equations (40) and (41) respectively). All parametric fluorescence frequencies that are colinear with the pump beam get amplified via optical parametric amplification. At the crystal/air interface, the various frequency components get spatially dispersed (according to Snell's Law) and further amplification in the second crystal only occurs for those

frequency elements which overlap the pump beam. Therefore the space between the crystals acts as a spatial and thus spectral filtering element.

The output from the second crystal consists of an infrared and visible beam travelling as an extraordinary (e-ray) and ordinary (o-ray), respectively. The e-oe interaction is known as Type II phase-matching. Tunability (and phase-matching) of the device stems from the angular dependence of the extraordinary index of refraction of a birefringent crystal. Using equations (40) and (41) and the expression for the wave vector,

$$\vec{K} = \left(\frac{\omega}{C}\right)n, \tag{42}$$

where ω is the frequency, C is the speed of light and n is the index of fraction, gives for a negative uniaxial crystal ($n_e < n_o$)

$$\begin{aligned} n_e^{\omega_3}(\theta) &= \left[\left(\frac{\cos\theta_m}{\omega_3}\right)^2 + \left(\frac{\sin\theta_m}{\omega_3}\right)^2\right]^{-1/2} \\ &= \frac{\omega_1 n_e^{\omega_1}(\theta_m) + \omega_2 n_o^{\omega_2}}{\omega_3} \end{aligned} \tag{43}$$

where n_e and n_o are the extraordinary and ordinary indices of refraction, respectively, and θ_m is the angle formed by the propagation direction and the crystal optic axis.

Since the device was to be pumped with the third harmonic of the Nd:YAG laser (355nm), it was natural to use a harmonic generating scheme to achieve maximum energy at the third harmonic (up to OPS

crystal damage thresholds) with the available energy at the fundamental frequency. Besides conversion efficiencies, the other considerations in the choice of a harmonic generating scheme was to use a minimum of optical components due to cost and effects on beam quality, and to be fairly insensitive to laser beam divergence.

The method of choice for third harmonic generation with the foregoing considerations in mind was the polarization mismatch scheme,[123,124] developed at the University of Rochester's Laboratory for Laser Energetics. The scheme is depicted in Figure 33. The scheme employs one $\lambda/2$ plate for 1064nm operation and two identical KDP crystals. In the polarization mismatch scheme the incident electric field is linearly polarized at an angle $\theta_p = \tan^{-1}(1/\sqrt{2})$ (35 degrees) to the ordinary crystalline axis. This is accomplished by placing a $\lambda/2$ plate in the beam at the proper orientation which ensures two ordinary 1064nm photons for each extraordinary 1064nm photons incident upon the first crystal. One extraordinary photon at ω interacts with one ordinary photon at ω in Type II phase-matching to generate an extraordinary photon at 2ω, leaving one ordinary photon at ω unconverted. The output of the second harmonic generator is thus suitably polarized for direct input to a Type II third harmonic generator, which has been rotated by 90 degrees about the propagation axis with respect to the first crystal.

This setup obviates the need for intermediate polarizing optical components. For high efficiency third harmonic generation, a 1:1 photon mix of the fundamental and second harmonic should enter the

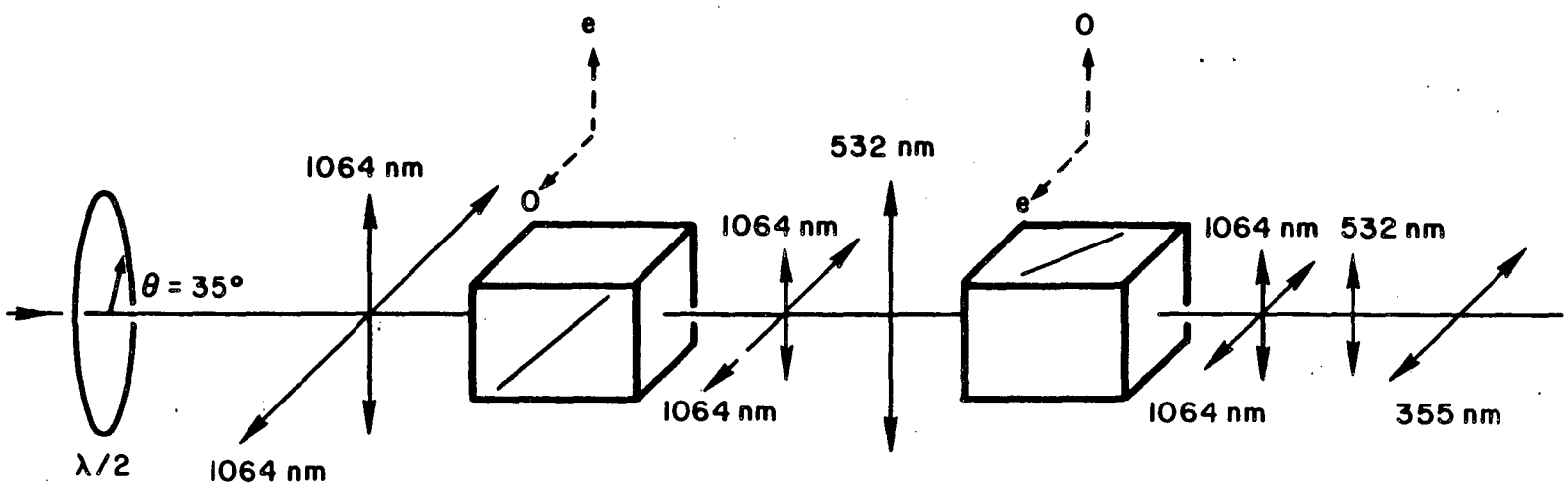

(2,o−1064 nm : 1,e−1064 nm) (1,e−1064 nm : 1,o−532 nm)

XBL 864-1256

Fig. 33. The polarization mismatch scheme for efficient third harmonic generation.

second crystal with polarizations shown in Figure 33. The corresponding optimum energy input mix is 1:2 (infrared:green). The remaining, fundamental, extraordinary photons pass through the third harmonic generator without any further interaction.

Optimum doubling would occur for a 1:1, e:o fundamental photon mix ($\theta_p = \tan^{-1} 1 = 45$ degrees). In the polarization mismatch scheme second harmonic conversion is purposely generated with less than optimum efficiency so that a more favorable mix of polarizations enters the tripling crystal. One advantage of this system is that both crystals are tuned to the peak of the phase-matching angles. Therefore there is an inherent insensitivity to angular mismatch arising from improper alignment and laser beam divergence. Another advantage is that in the case of limited nonlinear optical crystals, the entire tripling process may take place in a single crystal used in a double pass configuration. The output of the doubling stage would be reflected back with a normal incidence reflector, colinearly through the crystal. Passage through a suitable $\lambda/4$ plate placed between the crystal and the normal reflector would rotate each component 90 degrees so that the second harmonic beam returns to the crystal polarized along the ordinary crystal axis as required for tripling. This is possible because the phase-matching angle for Type II doubling and tripling are the same (59 degrees).

C. Experimental

The first experiments carried out to characterize the performance of the OPS were configured in a similar manner to the way the second harmonic output of the laser system was characterized (see Figure 21). The only difference was the inclusion of third harmonic and optical parametric generation. The pulsed, active/passive mode-locked, Nd:YAG laser has been described previously. The laser was operated at 10 Hz, produced pulse trains of between 12 and 15 pulses with energy amplitude stability of approximately ±2 percent, and emitted a diffraction-limited, TEM_{00} 1064nm beam. A single, approximately 30ps duration pulse was selected from the pulse train with a Pockels cell (Quantel PF302) and was amplified to an energy of approximately 7mJ. The second and third harmonics were generated in a pair of Type II phase-matched KDP crystals in a configuration to maximize the third harmonic conversion efficiency.[123,124] Third harmonic conversion efficiencies were routinely between 20 and 25 percent. Energy conversion efficiencies were measured as the total 355nm generated energy divided by the total 1064nm energy incident upon the crystal pair.

The first second and third harmonics were dispersed in a 2 cm aperture quartz (fused silica) Pellin-Broca prism (Optics for Research Corp.). The resulting third harmonic had an energy of approximately 1.5mJ, an energy stability of ±15 percent, a spectral width of between 2 cm^{-1} and 3 cm^{-1}, and a pulse duration of between 30ps and 40ps. The beam had a far field divergence of 0.14mrad when collimated to a

1.8mm beam diameter. The OPS consisted of two Type II KOP crystals, 37mm long, which were mounted on either rotation stages (NRC Model No. RSA-1) or in home-designed, large-aperture, one inch mirror mounts. In these experiments the crystals were spaced by 14 cm, as measured from the rotation centers. The peak power densities of the pump beam incident upon the crystals was between 2 GW/cm^2 and 3 GW/cm^2.

Temporal and spectral measurements were conducted exactly in the same way as in Figure 21. Briefly, pulse durations were measured using an ultrafast streak camera (Hadland Photonics Imacon 500) which was triggered with the residual 1064nm light. The output of the camera was imaged onto an intensified linear photodiode array (Tracor Northern TN-6100 IDARRS) and transferred to a microcomputer (DEC LSI11-73) for signal processing and storage. The overall temporal resolution of this apparatus was 2ps.[35,36]

The output spectrum was measured with a 256 channel charge-coupled-device (CCD) array (Fairchild CCD111A) that was placed at the image plane of a 0.85 meter focal length double monochromator (Spex 1404) equipped with 1800 lines/mm holographic gratings. The CCD output was displayed on a storage oscilloscope (Tektronix 7834). Single shot spectra could be measured with a resolution of 0.01nm over a spectral range of 0.67nm. Energy measurements were made with a calibrated thermopile (Scientech 36001) and with a calibrated pryoelectric detector (Molectron J3-05DW).

Eventually a more sophisticated configuration was arranged to do simultaneous single shot spectral, temporal, spatial, and energy measurements. The new arrangement allowed for the determination of whether there were spectral variations within different spatial portions of the visible OPS output. A schematic diagram of the new setup is shown in Figure 34. Everything up to third harmonic conversion is the same as previously described.

The first, second, and third harmonic were separated using a 2 cm aperture quartz (fused silica) Pellin-Broca prism (Optics for Research Corp.). The first harmonic was used to trigger the streak camera via a p-i-n photodiode (see Figure 17), and the second harmonic was blocked. The third harmonic beam was split into two parts, with one percent of the beam directed onto a large area calibrated photodiode (Silicon Detector Corp. 50380-23-21-251) for energy measurements. The output of the photodiode was sampled and held and stored on a micro-computer (DEC LSI-11/2). The photodiode was calibrated against a thermopile (Scientech 360001). The remaining 99 percent of the 355nm light was passed through a 0.62 times reducing telescope and directed onto the OPS. After the telescope, the beam typically had an energy of 1.35mJ, a spectral width of between 2 cm^{-1} and 3 cm^{-1}, a pulse duration of 30ps to 40ps, and a beam diameter of 0.136 cm (FWHM). Under these conditions the corresponding peak input intensity was 2.7×10^9 W/cm^2.

The OPS again consisted of two, 37mm long KDP crystals cut for Type II phase-matching (59 degrees with respect to the optic axis).

Fig. 34. The schematic diagram of the more sophisticated experimental setup used for the temporal, spectral, spatial, and energy characterization of the OPS.

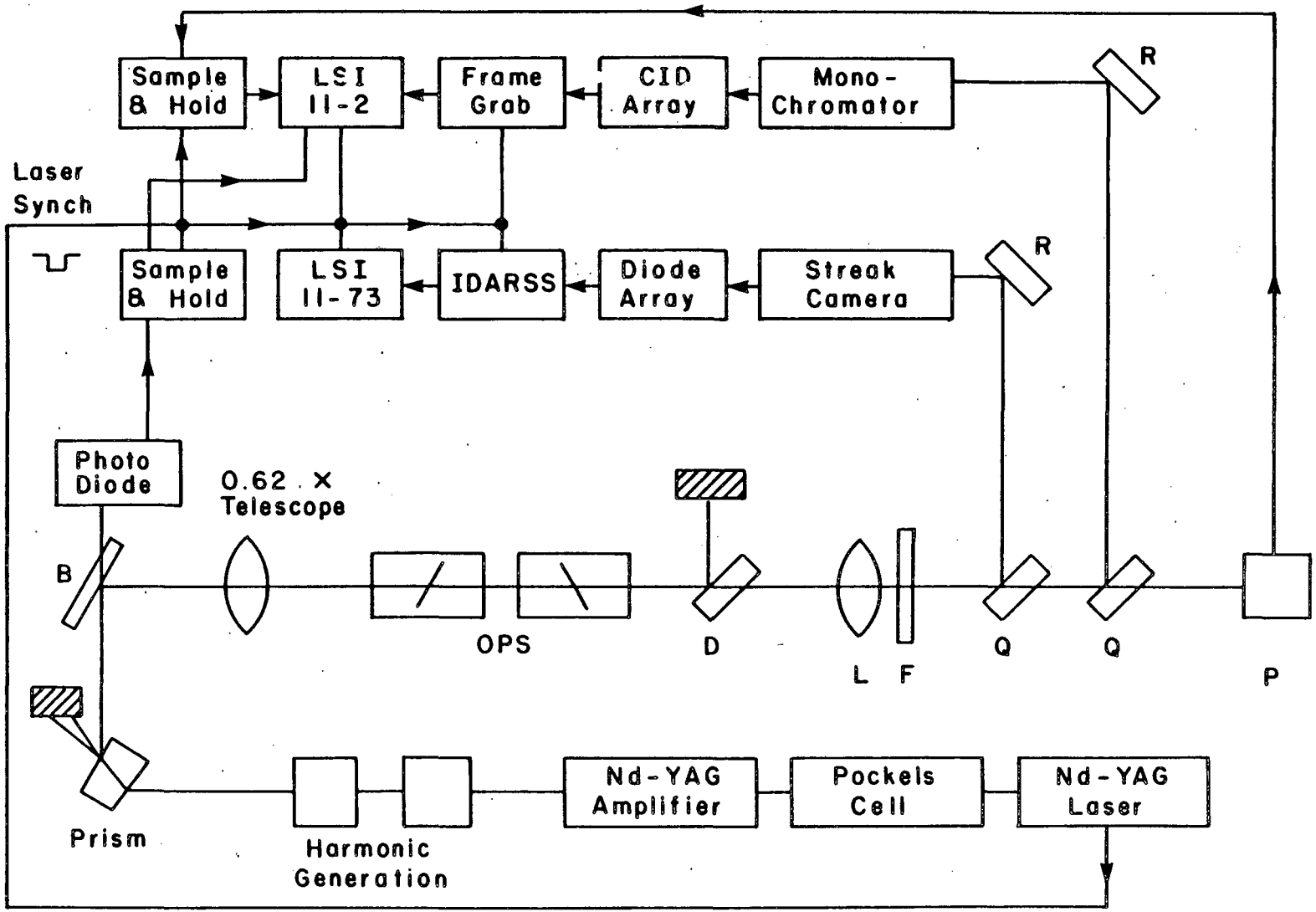

Fig. 34

XBL 853-1468

In this experimental arrangement, the crystals were mounted 15 cm apart (measured from the rotation centers) on stepper-motor-controlled rotation stages. In all mounting configurations the OPS was aligned by rotating the first crystal so that the pump beam was propagating at normal incidence with respect to the crystal face. The second crystal was then rotated until the residual pump beam and the two parametric outputs were colinear. In this configuration a maximum intensity of the parametric outputs were ensured. Tuning throughout the entire tuning range was then achieved by counter rotation of the crystal pair with no significant deflection in the direction of propagation of the parametric outputs or the pump beams.

The remaining 355nm pump beam was separated from the OPS output beam with a 100 percent, 45 degree, 355nm mirror used as a dichroic reflector. The OPS output beams were collimated over several meters distance using a 40 cm focal length lens placed such that its focal length was at the front surface of the first crystal. Colored glass filters (Schott BG18, KG3, GG395, and RG715) were used to select the visible or infrared parametric outputs for characterization. Calibrated glass neutral density filters (Schott) were used to attenuate the OPS output beams. Two uncoated quartz beam splitters were used to send a portion of the tunable outputs to the monochromator and streak camera. The residual output beam was sent to a pyroelectric detector (Molectron J3-05DW) for energy measurements. In what follows the energy values quoted include corrections for the transmission of all optics between the OPS and the pyroelectric detector.

The streak camera system used for temporal measurements was the same one as previously described.[35,36] Spectral measurements were carried out using the same monochromator, a 0.85 meter focal length double monochromator (Spex Industries 1404) equipped with 1800 lines/mm holographic gratings. The difference in this configuration was that the spectra were recorded with a two-dimensional charge injected device (CID) array (General Electric, TN2505-A) placed at the image plane of the spectrometer. The output of the CID array was digitized with a frame grabber (Poynting 505-RM), and transferred to a microcomputer (DEC LSI-11/2) for subsequent display and analysis. Throughout the visible tuning range single shot spectra could be measured over a range of at least 100 cm^{-1} with a resolution of 1.3 cm^{-1}. Using the two dimensional camera allowed for the observation of spectra inhomogeneities in the beam spatial profile.

D. Results

The crystal separation distance of 14 cm to 15 cm was determined by simultaneously monitoring both the visible and infrared output energies and the visible spectral widths. With the knowledge of the input energy, the tradeoff between conversion efficiency and spectral bandwidth could be optimized. The results are displayed in Table 6. Three visible wavelengths, 614nm, 598.1nm, and 581.5nm were used for this measurement. The wavelengths were measured with a 0.22 meter monochromator (Spex Industries Minimate-2 Model No. 161B) equipped with 1200 lines/mm holographic gratings. The light was detected with a photomultiplier tube (RCA 1P28). The monochromator scanning was accomplished under computer control using a simple stepper motor (Spex Minidrive-2 Model No. 1673C). The spectral widths were measured by the original method described in Section IV.C above. The energy measurements were made by displaying the output of the calibrated pyroelectric detector (Molectron J305-DW) on an oscilloscope (Tektronic 2215).

At each wavelength, three crystal spacings were used to measure spectral bandwidth versus total (visible and infrared) conversion efficiencies. For all wavelengths monitored, the total conversion efficiency decreased as crystal separation increased. Efficiencies were different for different wavelengths. However, none of the wavelengths chosen were near the maximum of the tuning curve. At small crystal separations where the conversion efficiencies were high, spectral widths ranged between 7 cm^{-1} and 20 cm^{-1}. As the inter-

Table 6. The measurement of crystal separation distances versus spectral bandwidths and conversion efficiencies of the OPS at 614nm, 598.1nm, and 581.5nm for 1.35 mJ of input energy.

Wavelength (nm)	Crystal Spacing (cm)	Spectral Bandwidth Range (cm^{-1})	Total Conversion Efficiency (%)
614.0	7	7 - 15	17.9
	14	4 - 8	17.9
	21	2 - 4	12.0
598.1	7	9 - 18	23.3
	14	5 - 10	20.0
	21	3 - 7	15.0
581.5	7	12 - 20	30.0
	14	6 - 12	26.7
	21	4 - 10	20.0

crystal distance approached and exceeded 14 cm, the spectral width reduced to between 2 cm^{-1} and 10 cm^{-1} with a corresponding drop in output energy. In this study the smallest spectral width measured was approximately 2.3 cm^{-1}. A discussion of the physical mechanism responsible for this effect is given in Section IV.E below.

The visible and infrared tuning curve for the OPS is shown in Figure 35. The points are measured. The lines drawn through the points are the curves calculated using equation (43). A simple, less than 40 degree crystal rotation yields visible and infrared wavelengths continuously tunable from 450nm to 650nm and 1675nm to 780nm respectively. This corresponds to a total range of 6838 cm^{-1} in both the visible and infrared output leg of the device.

The experimental tuning curve was generated by measuring the visible output wavelength as a function of the rotation angle of the two crystal front surfaces and the beam propagation direction (ϕ in Figure 33). The tuning curves are also shown as a function of internal angle (θ in Figure 32). The infrared tuning curve was calculated from the measured visible and pump wavelengths using equation (40). The existence of the infrared beam was established by blocking the visible beam with appropriate colored glass filters and viewing the phosphorescence of the infrared beam on a Kodak IR phosphor card. Further verification was carried out by direct observation of the infrared beam energy with the pyroelectric detector. The measured tuning curves are in excellent agreement with both previous experimental

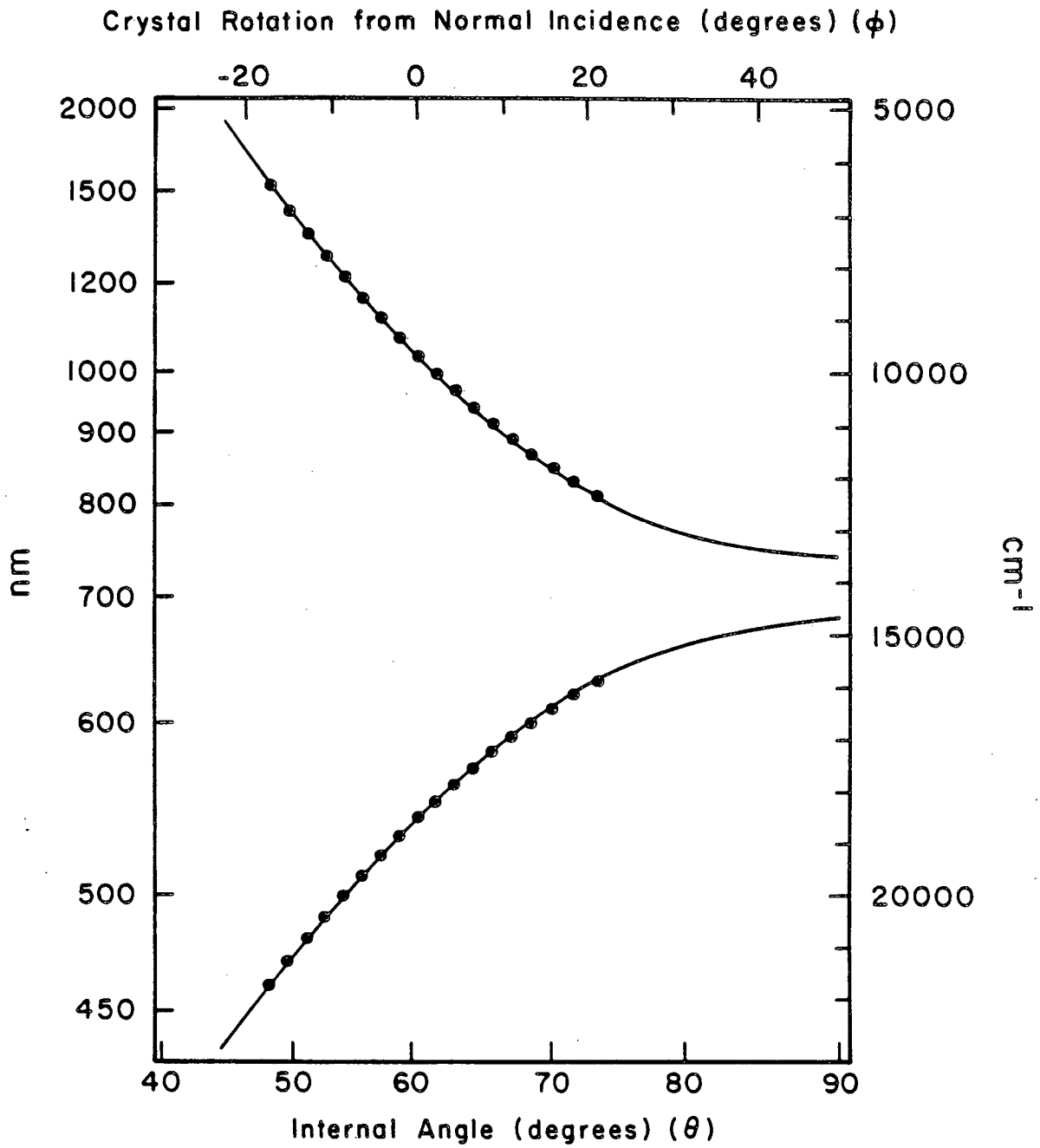

XBL 853-1465

Fig. 35. The measured (dots) and calculated (lines) angle tuning curves of both the visible and infrared OPS outputs.

results[122] and the phase matching curves calculated from the known dispersion constants of KOP.[125]

Figure 36 is a measure of the OPS output energy at 540nm as a function of pump beam energy. This measurement was made by collecting several hundred shots while detuning the doubling crystal to vary the pump energy. The data was sorted into 40 μJ pump energy increments and averaged. Every point is the average of between 5 and 50 shots. The vertical standard deviation is 20 percent at all points. The sharp increase in output energy at 800 μJ pump energy (~1.6×10^9 W/cm^2) demonstrates that the best performance from the device occurs when pump beam energies are within an order of magnitude of the damage threshold of KDP. The sharp increase is the result of the exponential pump intensity dependence of the parametric amplification process. The exponential pump intensity dependence also means that any fluctuations in the pump laser will be greatly amplified in the OPS output. Even the relatively stable pump laser used in these experiments produced a visible OPS output energy fluctuation between 20 and 30 percent.

The energies of the visible and infrared OPS outputs as a function of wavelength are shown in Figure 37. The energies shown in Figure 37 were measured with the pyroelectric detector for laser shots selected such that the 355nm pump energy was in the range of 1.35 ± 0.04mJ. Similarly shaped curves were obtained at other 355nm input energies. Important points to note are that energy conversion efficiencies of greater than 10 percent into visible output can be obtained over the

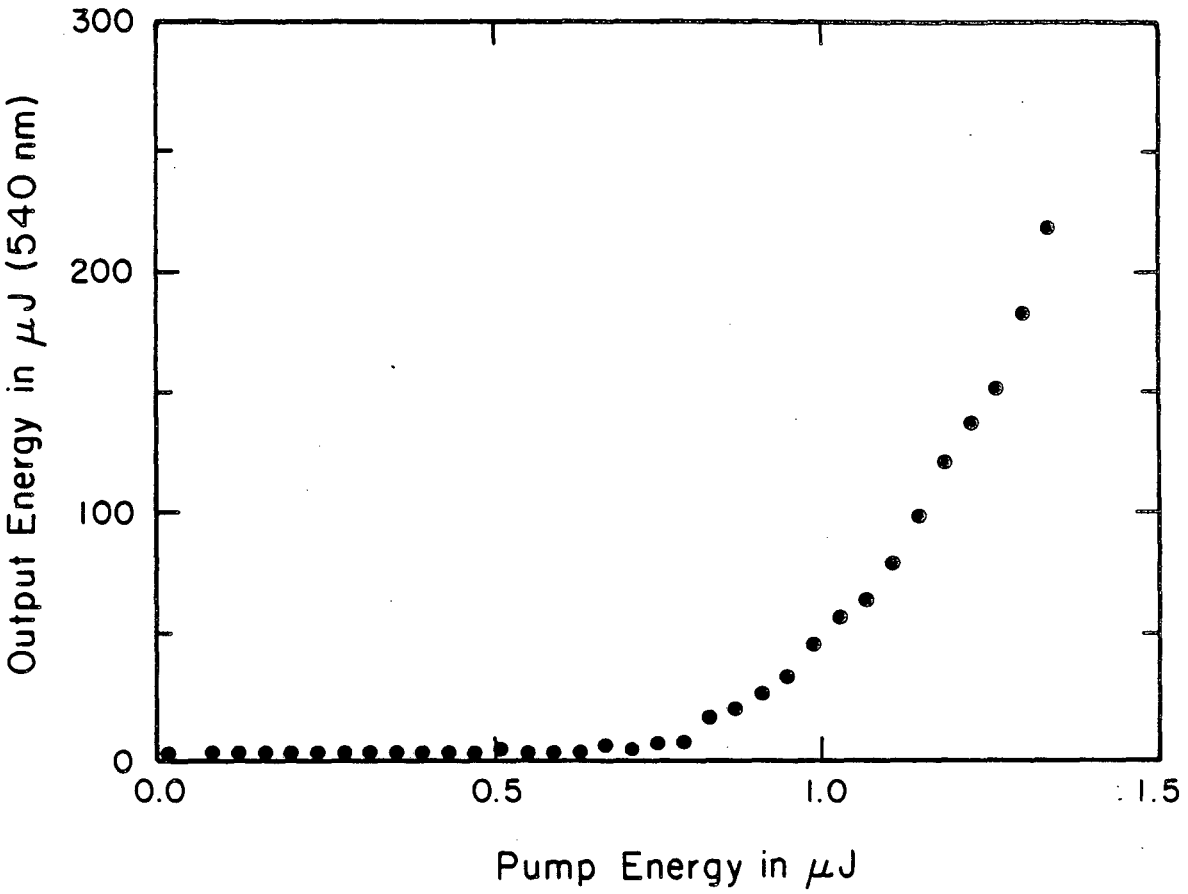

XBL 853-1464

Fig. 36. The visible output energy at 540nm versus the pump energy at 355nm.

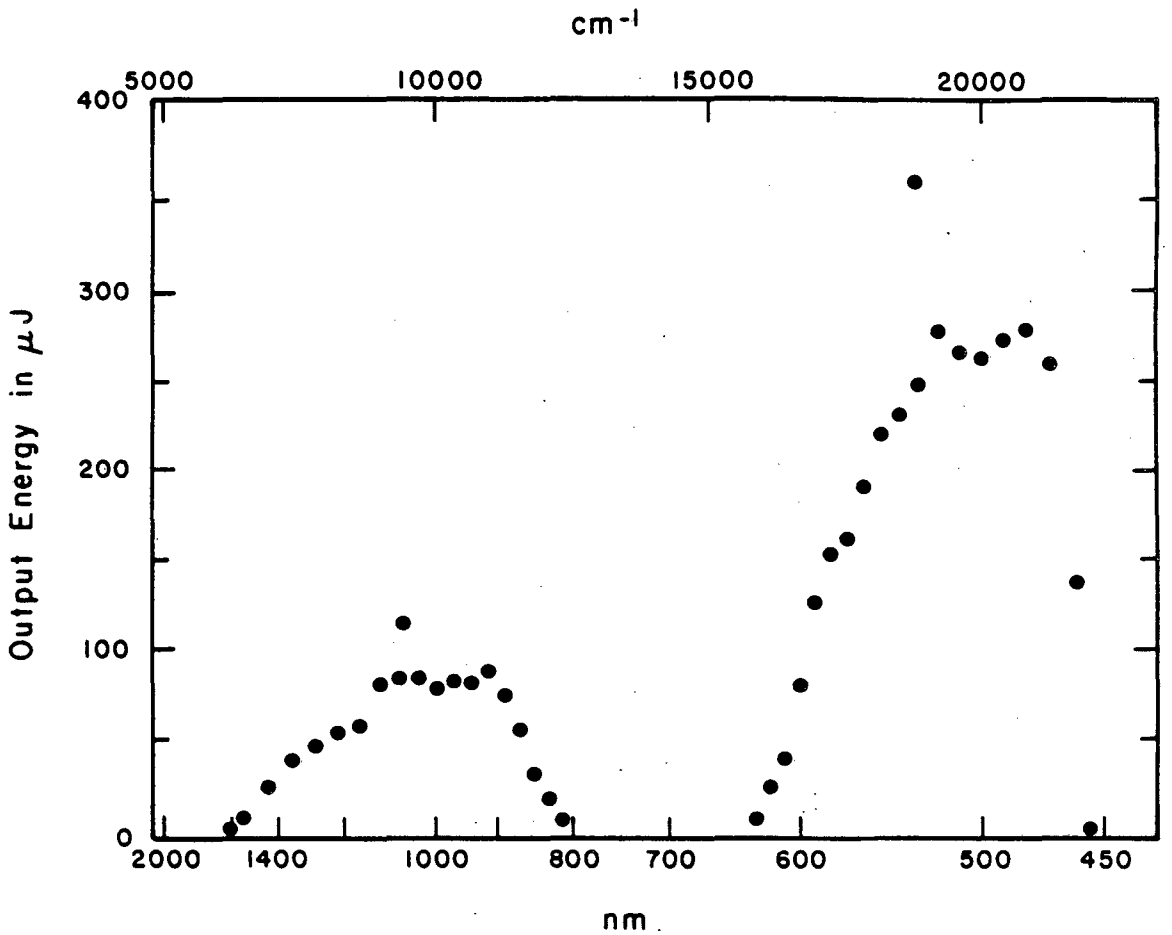

XBL 853-1466

Fig. 37. The output energy of the OPS as a function of wavelength.

spectral range from 470nm to 570nm with a maximum of 26 percent at 532nm. If the energy of the infrared output (1064nm) is included, and losses for reflections at crystal surfaces (~4 percent per surface) are taken into account, then the total conversion efficiency at 532nm is 44 percent. When a few percent scattering loss due to polishing imperfections and minor crystal damage is included, conversion efficiencies near 50 percent are attained. This is near the theoretical limit, considering crystal length and pump beam intensities.

The major thrust of the experimental effort on the OPS was the spectral and temporal characterization of the visible output pulses of the device. Since the tunable radiation was to be used in both picosecond, time-resolved fluorescence measurements and pump-probe experiments utilizing nonlinear optical techniques such as CARS and MPI, it was essential to know both the temporal and spectral profiles of the output pulses.

Figure 38 shows the temporal and spectral profiles of the visible output of the OPS near 600nm measured with the original experimental configuration. The temporal profile is the average of 100 shots, while the spectral profile is a typical single shot. The visible output energy and the 355nm pump energy were approximately 50 μJ and 1.1mJ respectively (~4.5 percent conversion efficiency). Assuming Gaussian pulse profiles, a pulse duration of 8.2ps with corresponding spectral bandwidth of 2.3 cm^{-1} yields a time-bandwidth product of 0.566, which is within a factor of 1.3 of the transform-limit.

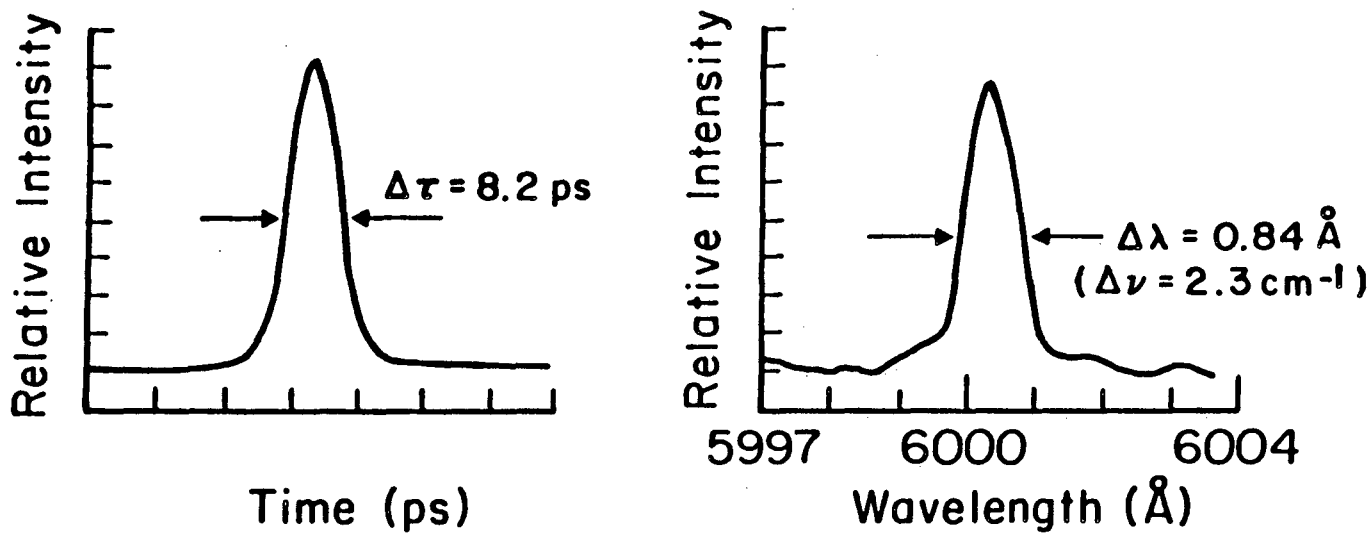

XBL 864-1262

Fig. 38. The temporal and spectral profiles of the visible output of the OPS near 600nm taken with the original experimental configuration.

Similar behavior was observed when the OPS was scanned to the blue edge of the tuning curve. For visible outputs around and beyond 470nm, pulse durations of 7.0ps with corresponding spectral widths of between 3 cm^{-1} and 4 cm^{-1} were routinely observed.

The first experiments involving the output of the OPS as the excitation source were to use visible radiation at approximately 545nm. The pulse durations at this wavelength were typically 20ps to 30ps. Only when the OPS was not working well (i.e. low conversion efficiencies) were the observed pulse widths short (typically between 7ps and 10ps).

The uncertainty in the performance characteristics of the OPS led to the second set of characterization experiments in which conditions could be systematically varied and recorded while simultaneously measuring single shot pulse durations and spectral bandwidths (experimental arrangement of Figure 34). Figures 39 through 43 depict simultaneous spectral and temporal measurements of single visible OPS output pulses measured under a variety of conditions. The pulse durations and spectral widths are given as full widths at half maximum values (FWHM) and the uncertainty relationship, $\Delta\nu_p \times \Delta\tau_p = 0.441$, for Gaussian pulse shapes will be used when discussing transform-limited behavior.

To demonstrate the effect on conversion efficiency versus pulse behavior, visible output at 540nm was chosen because there was sufficient dynamic range to reach the high and low conversion efficiency limits simply by tuning or detuning the doubling crystal

to vary the pump energy. Figures 39 through 43 show the spectral and temporal profiles of the visible output and the 355nm pump temporal profile.

At high conversion efficiencies (15 to 20 percent) the spectral and temporal profiles were typically like those shown in Figure 39. The temporal width is equal to or slightly greater than the pump pulse (between 30ps and 35ps) while the spectral width is between 10 cm^{-1} and 15 cm^{-1}. Under these conditions, the overall shape of the spectral profile remains nearly constant from shot to shot and the center frequency does not shift at all. However, the complex substructure of the output spectrum varies in what seems to be a random manner from pulse to pulse. Pulses produced in this regime are typically a factor of 15 to 30 times the transform-limit.

Figure 40 is a measurement of a single 540nm pulse obtained at low conversion efficiency (~1 percent). Clearly, both temporal and spectral characteristics of the visible output pulses improve significantly at low conversion efficiencies. In this figure a pulse with a duration of 8.4ps and spectral width of 2.6 cm^{-1} is shown. The pulse has a time-bandwidth product of 0.655 which is within a factor of 1.5 of the transform-limit. Such pulses are quite common under these conditions and especially at the ends of the tuning range where the conversion efficiencies are inherently low. This accounts for the observations in the original characterization experiments.

When shorter duration third harmonic pulses are used to pump the OPS, even shorter duration visible output pulses result. Measurements

Fig. 39. The spectral and temporal profiles of the visible output of the OPS at 540nm under conditions of high conversion efficiencies (~20 percent). (a) Spectral bandwidth at 540nm = 12.2 cm^{-1} FWHM. (b) Pulse duration at 540nm = 44.9ps FWHM. (c) Pulse duration of pump at 355nm = 30.4ps FWHM.

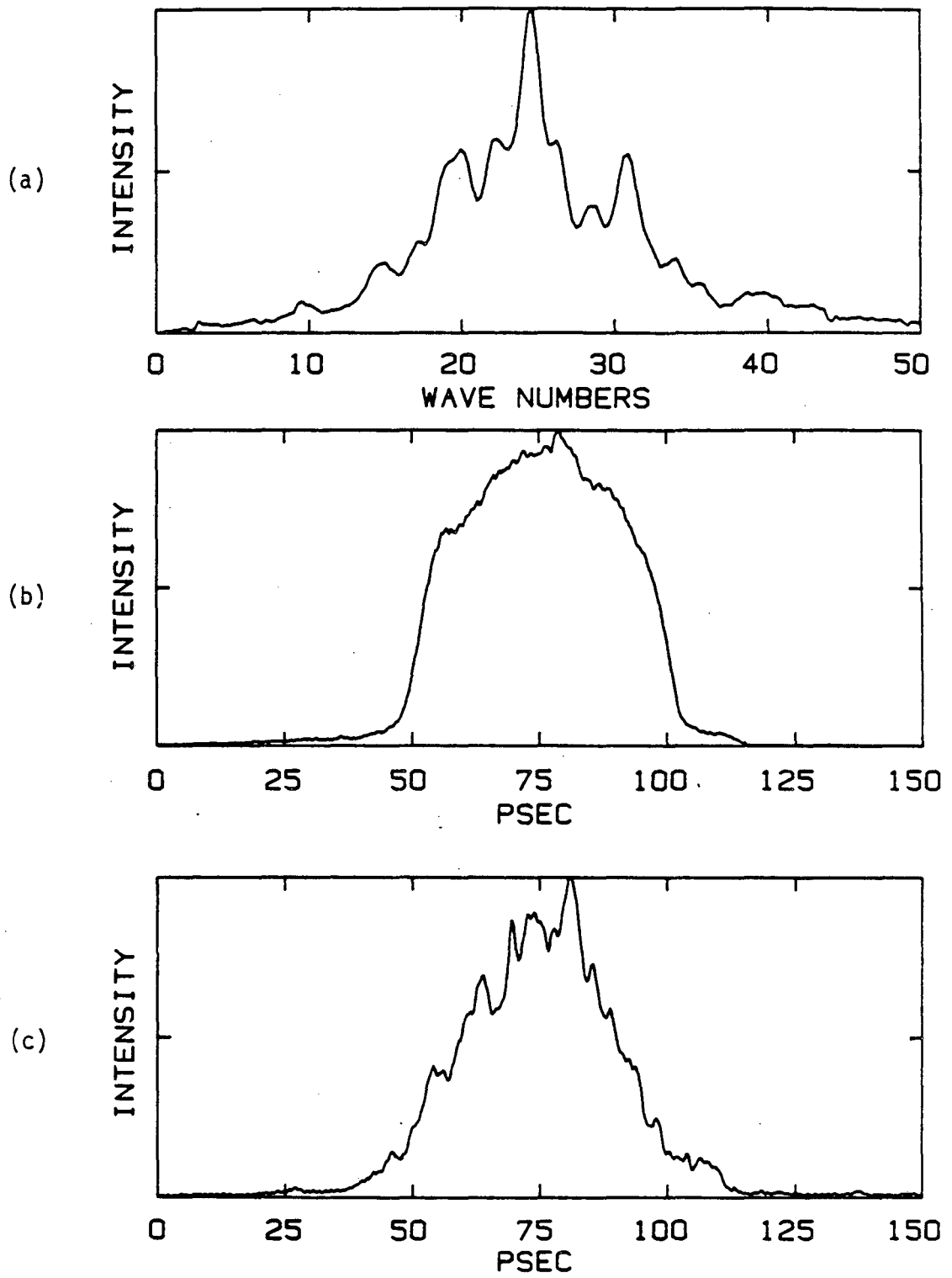

XBL 864-1260

Fig. 39

Fig. 40. The spectral and temporal profiles of the visible output of the OPS at 540nm under conditions of low conversion efficiencies (~1 percent). (a) Spectral bandwidth at 540nm = 2.6 cm^{-1} FWHM. (b) Pulse duration at 540nm = 8.4ps FWHM. (c) Pulse duration of pump at 355nm = 39.6ps FWHM.

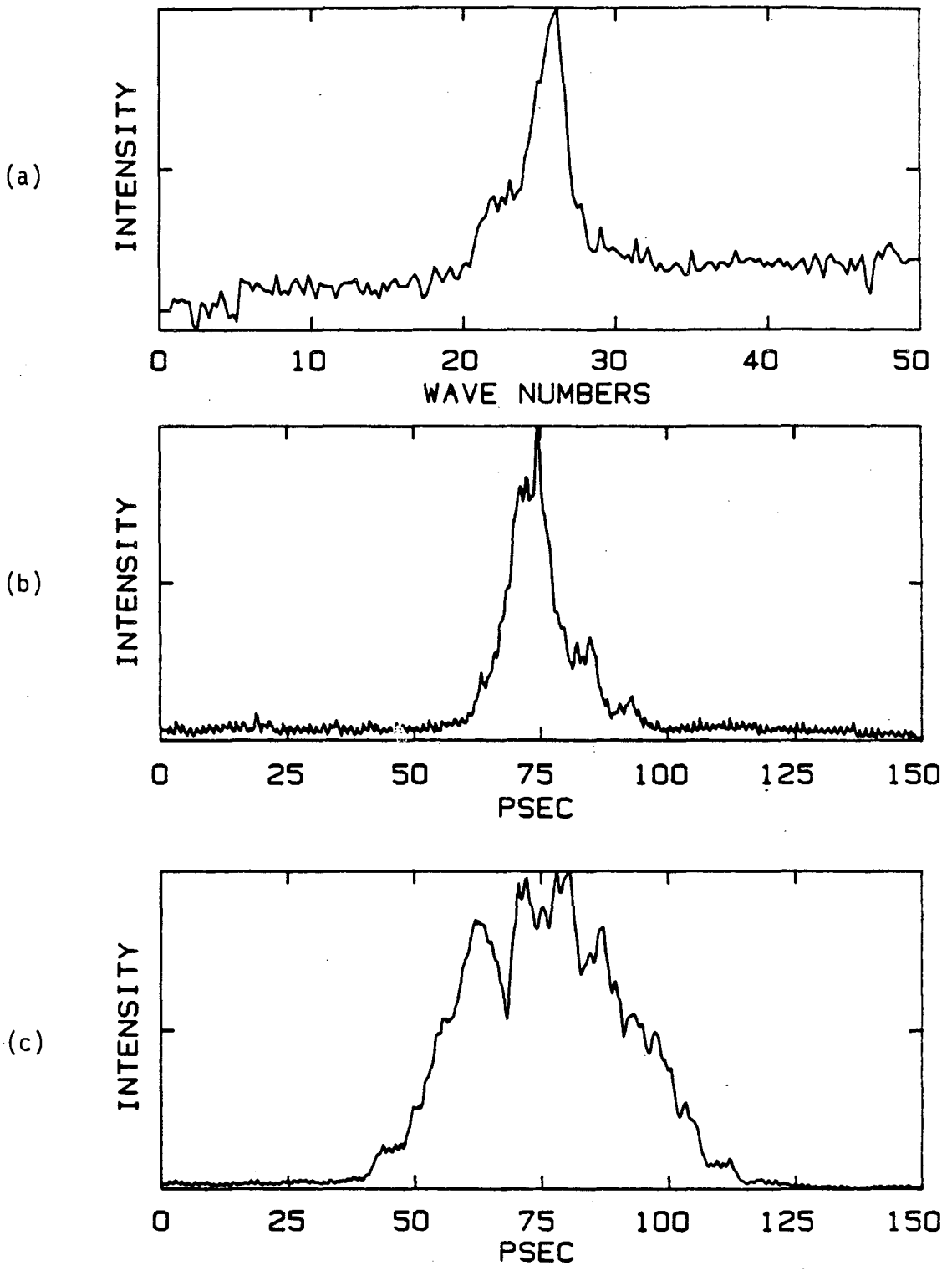

XBL 864-1261

Fig. 40

(again at 540nm) were carried out on OPS pulses that were generated using 355 nm pulses produced via the intracavity nonlinear pulse compression scheme described in Chapter III. This was accomplished by selecting single fundamental pulses after the peak of the pulse train and frequency tripling them. The shorter pump pulses yield approximately 5ps duration visible output pulses with 5 cm^{-1} spectral bandwidths as seen in Figure 41. These pulses are approximately a factor of 1.8 times the transform-limit. It has been predicted (calculated) that shortening the pump pulse to approximately 8ps will result in the generation of approximately 2ps output pulses. Two picoseconds appears to be the limiting value, however, because for crystal lengths used to generate useful output energies, group velocity dispersion broadening effects will become significant for pulses less than 2ps.

Figures 42 and 43 show spectral and temporal profiles obtained when the OPS was tuned to produce visible and infrared output beams at 532nm and 1064nm respectively. The coincidence of this output with the second harmonic and fundamental from the Nd:YAG pump laser seems to produce interesting anomalies. In Figure 42 it is clear that under conditions of high conversion efficiencies (~25 percent), the temporal profile of the visible OPS output remains rather large, approximately 50ps. This result is similar to those attained at nearby wavelengths that are also in the high conversion efficiency regime. However, the spectral width is dramatically reduced to between 2 cm^{-1} and 4 cm^{-1} (3.8 cm^{-1} in Figure 42) even at these high conversion

Fig. 41. The spectral and temporal profiles of the visible output of the OPS at 540nm when shorter duration 355nm pulse are used as the pump. (a) Spectral bandwidth at 540nm = 5 cm^{-1} FWHM. (b) Pulse duration at 540nm = 5ps FWHM. (c) Pulse duration of pump at 355nm = 19.8ps FWHM.

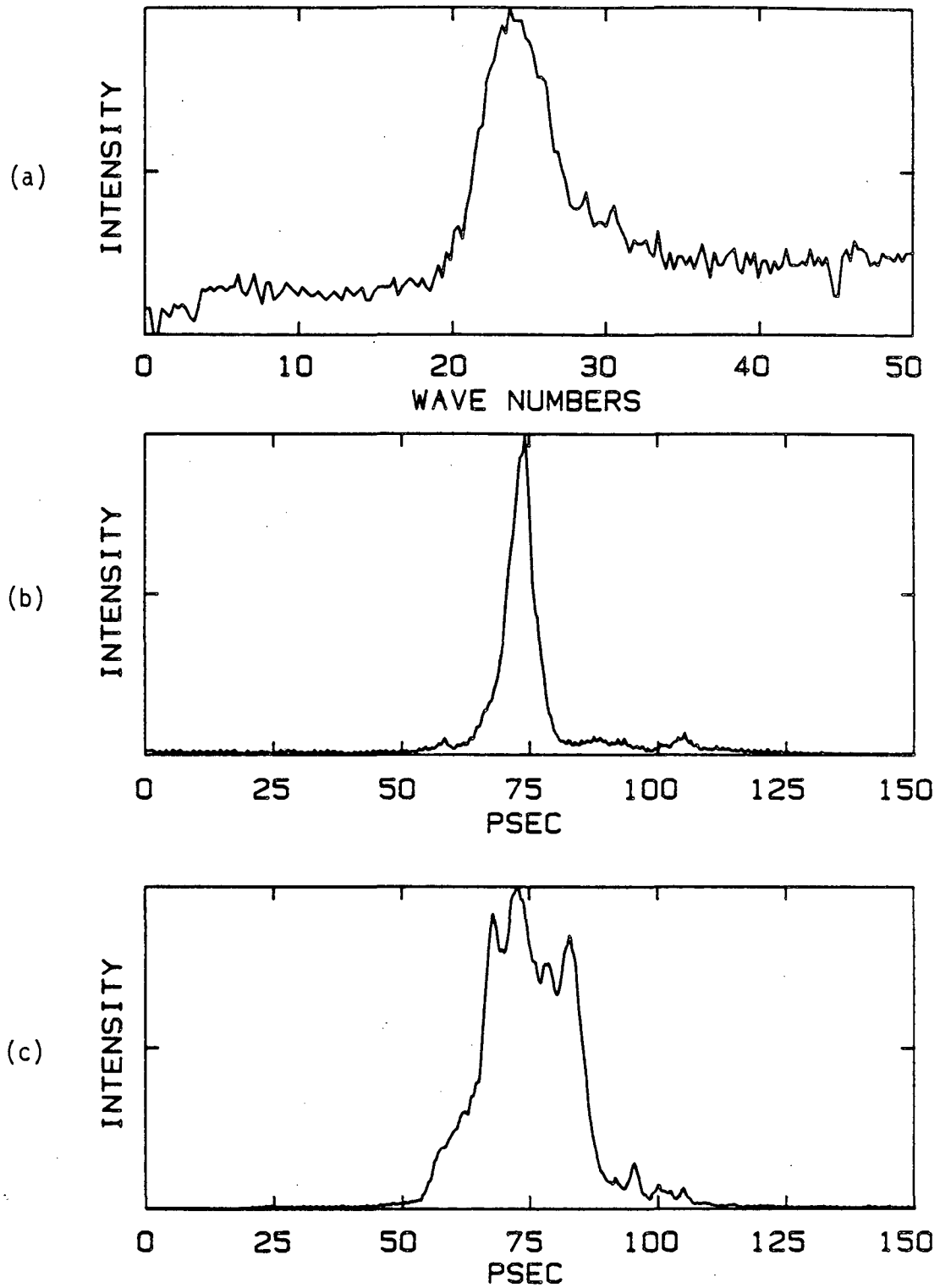

XBL 864-1258

Fig. 41

Fig. 42. The spectral and temporal profiles of the visible output of the OPS at 532nm under conditions of high conversion efficiencies (~20 percent). (a) Spectral bandwidth at 532nm = 3.8 cm^{-1} FWHM. (b) Pulse duration at 532nm = 51.2ps FWHM. (c) Pulse duration of pump at 355nm = 40.0ps FWHM.

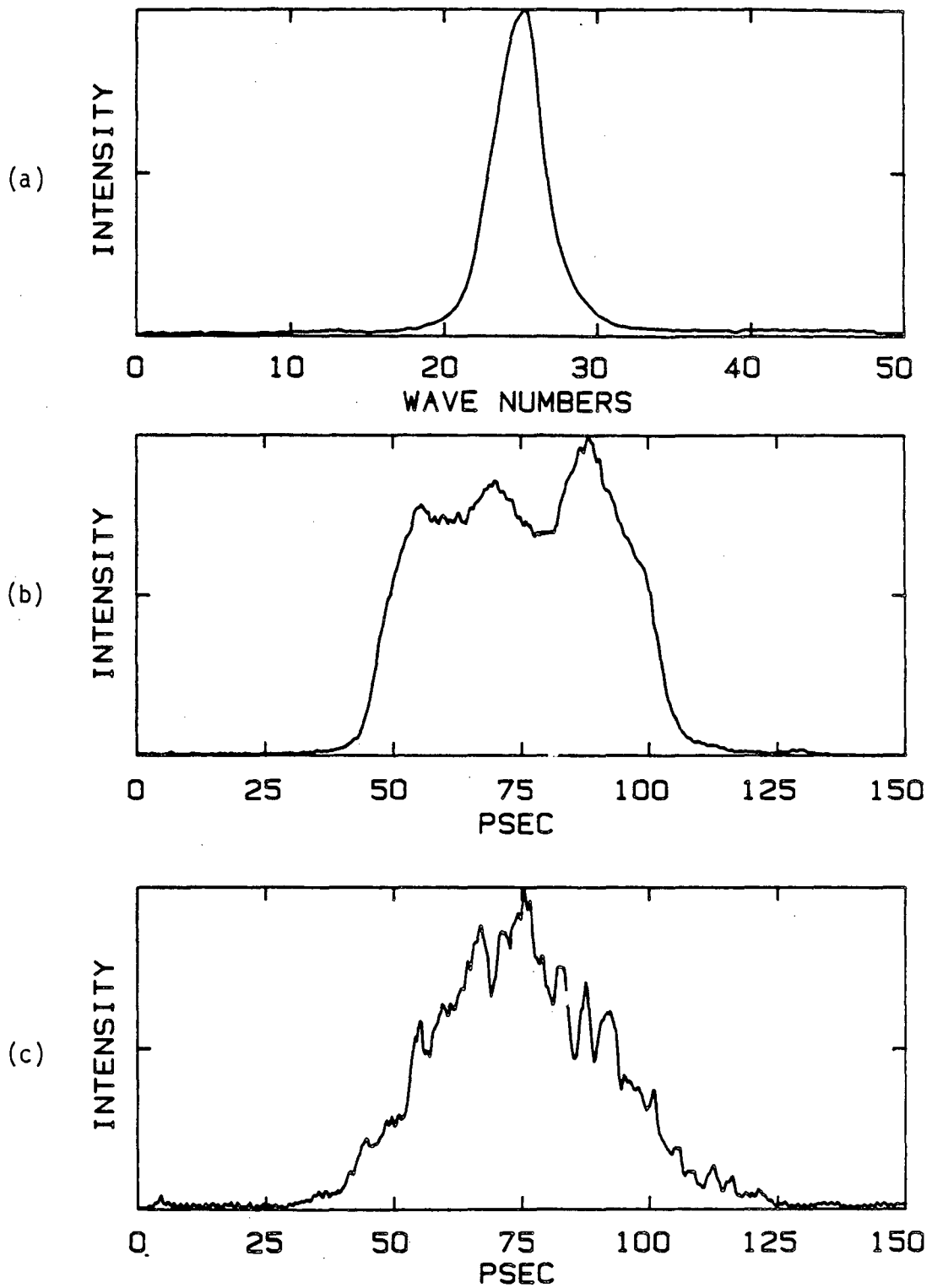

XBL 864-1259

Fig. 42

efficiencies, whereas at neighboring frequencies spectral widths are typically between 10 cm^{-1} and 15 cm^{-1}. When the OPS is tuned to 532 nm, the spectral profiles are very smooth and homogeneous and lack the complex substructure observed at neighboring frequencies.

This result appears to indicate that the scattered laser light is more intense than the spontaneous parametric fluorescence, and that the parametric output results from the amplification of spectrally-narrow, scattered laser light rather than broadband parametric fluorescence. This was confirmed by placing colored glass filters immediately preceding the first OPS crystal to absorb the scattered first and/or second harmonic light at 1064nm (Schott KG3) and/or 532nm (Schott BG1), respectively. As expected, the spectral anomaly persisted if only one of the two harmonics was blocked, but it disappeared completely if both filters were used to eliminate the scattered wavelengths that were acting as "seed" photons. The spectral widths measured when the "seed" photons were not blocked were approximately the same as the spectral widths of the second harmonic measured directly from the mode-locked laser.

It is interesting to note that when the OPS is tuned to generate 532nm output, near transform-limited behavior can be obtained. This is depicted in Figure 43. Using both short pump pulse effects and scattered light "seed" photons simultaneously, spectral bandwidths of 2.4 cm^{-1} and pulse durations of 8.4ps have been measured. These pulses are within a factor of 1.4 of the transform-limit.

Fig. 43. The spectral and temporal profiles of the visible output of the OPS at 532nm when shorter pulse duration 355nm pulses are used on the pump. (a) Spectral bandwidth at 532nm = 2.43 cm^{-1} FWHM. (b) Pulse duration at 532nm = 8.37ps FWHM. (c) Pulse duration of pump at 355nm = 27.0ps FWHM.

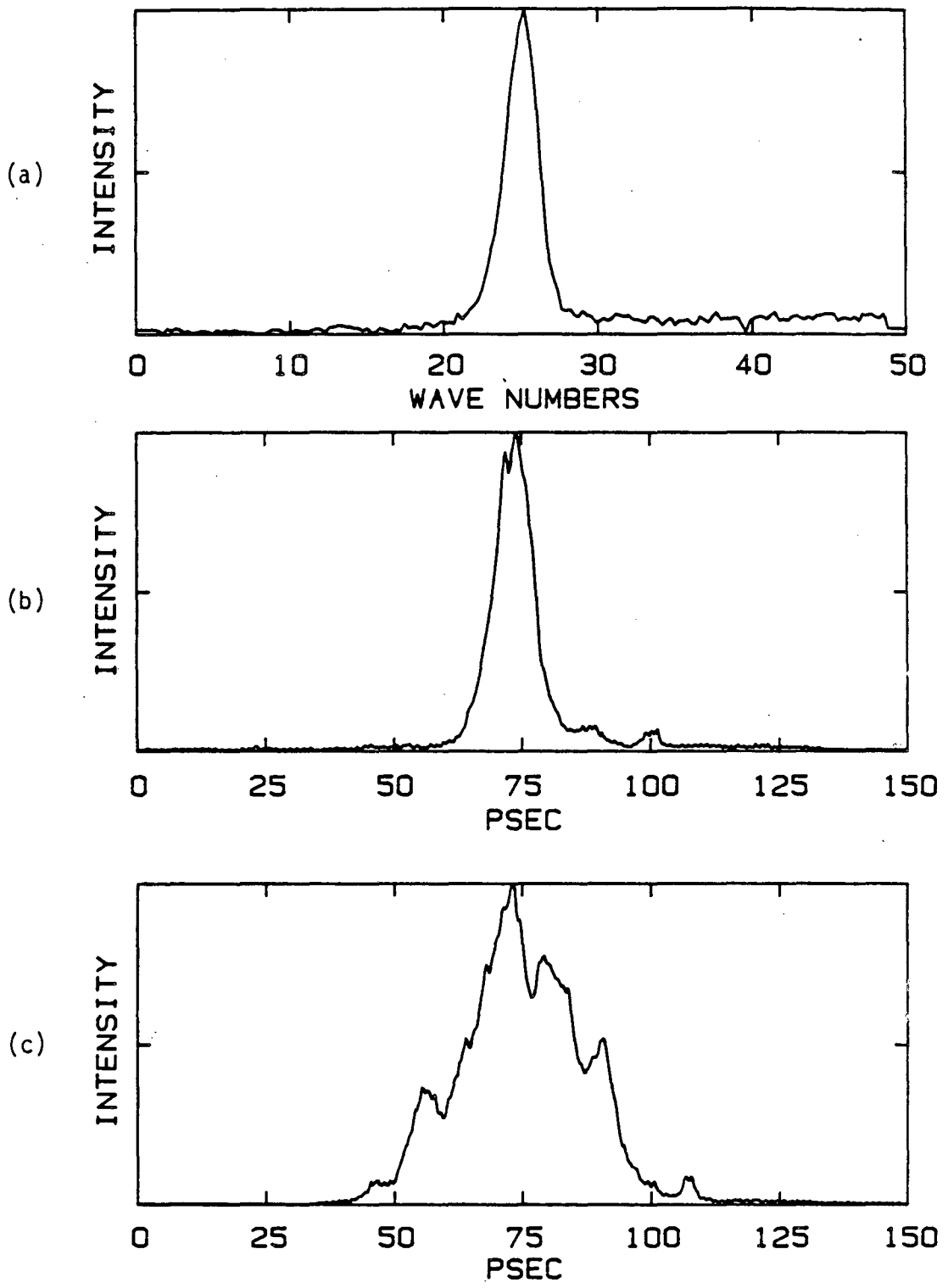

XBL 864-1257

Fig. 43

The idea of seeding the OPS with a spectrally narrow source is very tantalizing. However, efforts to seed the device with fluorescence from coumarin dye solutions or the output of a continuous wave, 2 mW, HeNe laser were unsuccessful. It seems that a relatively intense (possibly ~KW/cm^2), spectrally narrow source may be required for proper seeding.

E. Discussion

Due to the increase in power spectral brightness made possible by the laser, numerous experiments in nonlinear optics have been conducted since 1961.[120] Over the past twenty years, parametric amplification has become an important technique for amplification and power generation over wide frequency ranges. Tunability over these frequency ranges in birefringent, negatively uniaxial crystals is achievable in a variety of ways including angle tuning, crystal heating, and the electrooptic effect. By far the simplest and most widely used method is angle tuning. Because of this simplicity, the theory of parametric amplification has been studied extensively and by now is well understood.[34, 118, 127]

In the non-depleted pump approximation, the equations describing the coupling of three plane waves can be readily solved allowing for finite phase mismatches and the infrared absorption of the nonlinear optical material. For a 355 nm pumped (3rd harmonic of Nd:YAG) Type II phase-matched (e-oe) interaction, use of the conventional notation will be used throughout the discussion. Subscripts 1, 2, and 3 refer to the infrared (idler, e-ray), visible (signal, o-ray), and ultaviolet (pump, e-ray), respectively.

In the case of small signal parametric amplification the single wave intensity can be calculated for[34]

$$I_2 = 2I_2^0 \sinh^2 [(g^2-\Delta K/2)^2 I_3]^{1/2} z , \qquad (44)$$

where I_2 and I_2^0 are the visible output and input intensities respectively, I_3 is the pump intensity, z is the overall crystal length, g is the peak gain coefficient in the absence of any input (i.e., "seed") beam, ΔK is the phase mismatch, and I_2^0 is the signal intensity at the front of the first crystal, corresponding to the intensity of spontaneous parametric fluorescence. In a high gain parametric process (i.e. for large pump intensities, $gzI_2^{1/2} >> 1$) and for the case of colinear phase-matching, the signal and idler intensities grow exponentially according to equation (45)

$$\frac{dI_2}{dz} = 2gI_2 \sqrt{I_3}$$

$$I_2 = I_2^0 \exp[2g\ z\ (I_3)^{1/2}] \ . \tag{45}$$

The peak gain coefficient, neglecting phase mismatches and the infrared absorption of KDP, is given by the expression

$$g = \pi \sqrt{2}\ (16\pi^2/10^{14})^{3/4}\ c^{5/2}\ (1/n_1 n_2 n_3 \lambda_1 \lambda_2)^{1/2}\ \chi_{eff} \tag{46}$$

where c is the speed of light in a vacuum, n_i refer to the effective indices of refraction of the three beams, λ_1 and λ_2 are the wavelengths of the infrared and visible output beams, and χ_{eff} is the effective nonlinear susceptibility for KDP. For Type II phase-matching in KDP, the effective nonlinear susceptibility depends on the phase-matching angle (θ in Figure 32) and the nonlinear optical coefficient, d_{36}, in the following manner[127]

$$\chi_{eff} = d_{36} \sin 2\theta \ . \tag{47}$$

In reality, small phase mismatches and the infrared absorption of the nonlinear material (which acts as an effective loss mechanism in the parametric process) cannot be neglected. Therefore an effective gain coefficient is defined by

$$b = \mathrm{Re}\ \{\tfrac{1}{2}(i\Delta K - \alpha_1/2) + \tfrac{1}{2}[g^2 + (\alpha_1/2 - i\Delta K)^2]^{1/2}\} \tag{48}$$

The phase mismatch, ΔK, is given by

$$\Delta K = K_3 - K_2 - K_1, \tag{49}$$

and α_1 is the effective absorption coefficient for the idler beam. Using the effective gain coefficient, b, in place of the peak gain coefficient, g, transforms equation (45) into

$$I_2 = I_2^0 \exp\,[2bz\ (I_3)^{1/2}]\ . \tag{50}$$

A number of observed performance performance characteristics of the OPS are explained by equation (50). The strong exponential dependence of the output intensity on the pump beam intensity implies that any amplitude fluctuations in the pump beam will be greatly amplified in the output beam. The square root intensity dependence in the exponent of equation (50) means that small changes in the input intensity lead to large changes in the output power, as seen in Figure 37. Both the large vertical standard deviations (20 to 30 percent output energy fluctuations) for essentially constant pump energy and the sharp rise in output energy above 800 μJ pump energy are a result of equation (50). The measured exponential behavior of signal output energy versus pump input energy is in excellent agreement with that predicted by theory.

The variation in the visible and infrared output energies through the tuning range (Figure 38) is also explained by equations (45) through (50). The sharp decrease in energy on the red edge of the visible tuning curve is due to the angular dependence of χ_{eff} and thus g(b). The sin2θ dependence results in reduced values of the gain coefficients for these longer visible wavelengths past 600 nm ($\theta \approx 90^\circ$). The theoretical phase-matching condition can be satisfied for valves of λ_2 up to 680 nm ($\theta = 90^\circ$) as seen in the calculated tuning curve (Figure 36). However, because of the decreasing value of χ_{eff} (and thus g and b), no visible output was observed beyond 650 nm in this work. One possible way to obtain output to the theoretical limit of 680 nm would be to pump the OPS with a higher intensity (I_3) to compensate for the decreased valve of b so that the exponent in equation (50) would remain sufficiently large. The problem is that the intensities required to achieve this condition would exceed the damage threshold of KDP resulting in a rapid degradation in the performance of the device. Tunability out to the degenerate wavelength (710 cm) can be achieved with a 355 nm pumped Type I (e-oo interaction) phase-matched OPS.

As the OPS is tuned to the extreme blue edge of the tuning curve, the increasing values for the infrared absorption coefficients for the corresponding infrared wavelengths generated (beyond 1500 cm) leads to a decrease in the peak gain coefficient, b, according to equation (48). This causes the sharp blue cut off in the visible output energy near 450 cm. When literature values for α_1,[129] n_i,[125] and d_{36},[128]

are substituted into equations (45) through (50), the calculated curves agree only qualitatively with the measured values. The calculated curve is more sharply peaked than the experimentally observed values and falls too rapidly at the red edge of the tuning range. The discrepancies between the calculated and measured curves are not unexpected since the simple view presented presently neglects pump beam depletion, finite beam size, beam walk of in both space and time due to refraction and dispersion respectively, and the wavelength dependence of the nonlinear optical coefficient, d_{36}. For instance, allowing for pump beam depletion would tend to suppress the central peak of the curve and increase the relative intensities at the ends of the tuning range. If the other factors are taken into account it has been demonstrated[130] that for a similar system (532 nm pumped Type II, e-oe interaction OPS) a much more quantitative agreement between the calculated and experimentally observed wavelength dependencies of parametric amplification can be generated.

In order to assess the effects of the different possible factors contributing to both the temporal and spectral characteristics of the OPS, it is important to consider each of them in turn to decide which is the most prominent under a particular operating condition. The observed shortening of the visible OPS pulse relative to the pump pulse at low conversion efficiencies is primarily due to the power dependence of the parametric gain. It has been shown by Glenn[131] that under the assumption that the pump pulse is not appreciably depleted (i.e., low conversion efficiencies), an expression for the

parametrically amplified pulse can be derived in terms of the incident pump pulse shape. If the pump pulse is strong enough to provide appreciable gain, but the gain is not large enough to appreciably deplete the pump pulse, then the visible parametrically amplified pulse will undergo shortening according to

$$\tau_2 = \tau_3 \left[bz(I_3)^{1/2} \right]^{-1/2} , \qquad (51)$$

where τ_2 and τ_3 are the signal and pump pulse width respectively, b is the effective gain coefficient, z is the total crystal path-length, and I_3 is the pump beam intensity.

The maximum shortening that can be achieved is determined by the mismatch in the group velocities of the signal, idler, and pump frequencies. For sufficient amplification such that reasonable output energies can be obtained in a single pass starting from parametric fluorescence, $2bz(I_3)^{1/2}$ must be about 30.[32] This is consistent with the gain calculated from the present results, assuming the entire output energy is the result of the amplification of a single photon of parametric fluorescence. Under these amplification conditions, equation (51) predicts an output pulse duration 0.26 times the pump pulse duration. A pump pulse duration of 35ps would lead to a visible output pulse duration of 9.0ps. This is in excellent agreement with the output pulse durations observed at low conversion efficiencies throughout the entire tuning range (Figures 38, 40, 41, 43).

However, the predictions inherent in equation (51) only hold true if there is no pump pulse depletion. At higher conversion

efficiencies, pulse shortening is completely absent (Figures 39 and 42). Pump pulse depletion has the effect of reducing the gain at the center of the pulse, allowing the relative intensities of the leading and trailing edges of the pulse to grow until the output pulse profile resembles that of the input pulse.

The discussion of the temporal characteristics of the OPS output would not be complete without commenting on dispersive effects. Because of group velocity dispersion, i.e. $n_2 > n_3 > n_1$, the visible and infrared output pulses walk off from the pump pulse in opposite directions. While this allows for more efficient energy conversion, since it permits amplification over a larger portion of the pump pulse envelope and minimizes depletion at the peak of the pump pulse,[120,132] it also tends to broaden the output pulse duration.[133]

Models of the behavior of the OPS using the typical pulse durations normally associated with mode-locked Nd:YAG lasers do not typically consider the effects of group velocity dispersion because of the relatively long pulse widths. However, in the present discussion, the wavelength associated with the OPS vary enough that pulse broadening due to the interaction of the ultrashort pulses with the dispersive material should be considered. Two regimes should be considered, both low and high conversion efficiencies. At low conversion efficiencies, since the majority of the output pulse results from parametric amplification in the last few millimeters of the second crystal, any group velocity dispersion broadening must take

place over a pathlength of a few millimeters. For the known indices of refraction[119] for λ_3 = 355nm, λ_2 = 532nm, and λ_1 = 1064nm in a Type II KDP OPS, which are $n_e^3 = 1.49790$, $n_o^2 = 1.51228$, and $n_e^1 = 1.46899$, respectively, the group velocities can be calculated according to

$$v_i = \frac{d\omega}{dK}. \tag{52}$$

Therefore, when the OPS is tuned to produce visible output at 532nm, $v_3 = 0.9916v$, $v_2 = 0.9535v$, $v_1 = 0.6419c$, resulting in a group velocity difference of approximately 2.0ps/cm. Passage through 10mm of KDP causes pulse broadening of approximately 2.0ps. This is consistent with what is observed at low conversion efficiencies. For instance, when the OPS is tuned to 532nm and is pumped with a 29ps pulse, the output pulse duration is 8.4ps (Figure 44). This pulse width is approximately one picosecond longer than the prediction of equation (51).

At high conversion efficiencies, using the same values as above, if it is assumed parametric amplification occurs through the total crystal length (74mm), the pulse broadening of 15ps would be attributed to group velocity dispersion. Again, this is consistent with observed pulse durations. Figure 43 shows that when a 40ps, 355nm pulse is used to produce 532nm light at high efficiencies, the output pulse is 51ps. In fact, group velocity dispersion is the reason why in a Type II third harmonic generating scheme, the 355nm produced is always slightly longer than the first and second harmonic used.

The effects of group velocity dispersion limit the shortest pulses achievable with the OPS configuration. Without dispersive effects, equation (51) leads to the belief that the shorter the pump pulse, the shorter the output pulses at low conversion efficiencies. Therefore if the ability to pump the OPS with an infinitely short 355nm pulse existed, then the output pulse duration would always be approximately 1/4 the input pulse width (for $2bz(I_3)^{1/2} = 30$). However, the shorter the pump pulse, the more significant dispersive effects become. Therefore, for the arrangement described presently, pumping the OPS with pulses shorter than 8ps (yielding output of 2ps duration) would have no further narrowing capabilities.

Unlike an OPO, the spectral linewidth of a picosecond pumped OPS has nothing to do with the resonance properties of the external resonator. In fact, because of the shortness of the pulses single picosecond pulses are useless for pumping an OPO. However, full picosecond pulse trains can be used to synchronously pump OPO resonators.

The following physical processes can possibly influence the frequency widths of the signal and idler pulses in a single pass, travelling wave OPS: (1) in a colinear geometry, the large parametric gain produces frequency components despite the phase-matching condition (equation (41)) $\Delta K = 0$; (2) because of the finite divergence of the pump beam the parametric pulses are generated in slightly different directions with different central frequencies; (3) off-axis parametric amplification within the beam diameter gives pulses of a

certain frequency spread. The spacing between the two crystals acts as a spatial and therefore spectral filter in colinear parametric amplification due to the refraction of the signal, idler, and pump beams; (4) the spectral width of the pump pulse may have an effect on the bandwidth of the output pulse; and (5) if the pulses are near the Fourier transform-limit, then the Fourier transform of the temporal profile will effect the spectral profile assuming a non-phase (frequency) modulated output pulse.

According to equation (48), in an optical parametric process the effective gain coefficient decreases with increasing phase mismatch, ΔK. The phase mismatch, ΔK, corresponds to a frequency variation, $\Delta\nu$, according to the relation

$$\frac{d\nu}{dK} = \frac{1}{2\pi(n_e^2(\theta) - n_o^1)} , \tag{53}$$

where $d\nu/dK$ is the group velocity dispersion, and $n_e(\theta)$ and n_o are the angle dependent extraordinary and ordinary index of refraction, respectively. The amplification bandwidth for colinear parametric amplification thus corresponds to the range of ΔK for which significant amplification will occur according to

$$\Delta\nu = 2\left|\frac{d\nu}{dK}\right| \; |\Delta K| \; . \tag{54}$$

In the regime of high gain exponential amplification, i.e. $2bz\sqrt{I_3} = 30$, this contribution can become quite significant. Neglecting absorption at the idler frequency, equations (45) through (50) give the full width at half maximum bandwidth by the condition

$$\exp\,(2bz\sqrt{I_3}) = \frac{1}{2}\exp\,(gz\sqrt{I_3}). \tag{55}$$

Neglecting absorption and using equation (48), equation (55) can be solved to yield

$$\Delta K = \left(\frac{2g\ln 2}{2}\right)^{1/2} \tag{56}$$

Again, for high gain, i.e. gz I_3 = 30, and z = 7.4 cm, ΔK = 0.86 cm^{-1}. Therefore, according to equations (52), (53), and (54), the contributions from the phase mismatch to the spectral width can be determined by the group velocities according to

$$\Delta\nu = \frac{\Delta K}{\pi c}\,(\alpha_1\alpha_2/v_1-v_2)\ . \tag{57}$$

From literature data for KDP,[125] values for the term in parentheses in equation (57) have been calculated for λ_1 = 1064nm and λ_2 = 532nm. Using equation (57) an estimation of the frequency spread arising from the phase mismatch given by equation (56). For λ_2 = 532nm is 4.6 cm^{-1}. The expected bandwidth derived above seems is consistent with the observed spectral widths at low conversion efficiencies (excluding the "seed" photon effects). The observed broadening at higher conversion efficiencies can be attributed to pure pulse depletion.

Because tunability of the device arises from the angular dependence of the extraordinary index of refraction of KDP, the divergence of the pump beam will have an effect on the bandwidth of the parametric pulses. The frequency width is estimated from the relationship

$$\Delta\nu = 2|d\nu/d\theta|^{\theta}/n_3^e(\theta) \tag{58}$$

where θ is the angle of divergence of the pump beam defined in equation (23), and $n_3^e(\theta)$ is the index of refraction of the crystal at the frequency of the pump. $|d\nu/d\theta|$ represents the slope of the tuning curve and may be calculated according to the relation

$$|d\nu/d\theta| = \frac{n_3\nu_3}{2(n_2-n_1)} \frac{(n_3^e)^2 - (n_3^o)^2}{(n_3^e\, n_3^o)^2} \sin 2\theta, \tag{59}$$

where n_3^o and n_3^e are the respective ordinary and extraordinary indices of refraction at the pumping frequency, and n_3 and ν_3 are the index of refraction and frequency of the pump beam respectively for the phase matching angle. It is obvious from Figure 35 that over the range of the tuning curve of a Type II, 355nm pumped OPS in which there is measurable output, the slope of the tuning curve changes. $|d\nu/d\theta|$ values at 620nm, 532nm, and 450nm are 8.94 cm^{-1}/mrad, 14.13 cm^{-1}/mrad, and 19.77 cm^{-1}/mrad, respectively. For these three wavelengths, if the appropriate values of $n_3^e(\theta)$ (1.490, 1.499, and 1.507, respectively) are used along with the assumed value of 0.15mrad for the divergence of the pump beam (estimated from the measured first and second harmonic beam divergence), then the frequency spread due to the finite divergence of the pump beam is calculated to be 1.80 cm^{-1}, 2.83 cm^{-1}, and 3.94 cm^{-1} for 620nm, 532nm, and 450nm, respectively. Because of the curvature of the tuning curve, the effect of pump beam divergence on output spectral

width does vary with respect to wavelength. However, at low conversion efficiencies, there is good agreement with observed spectral bandwidths. Therefore pump beam divergence does seem to be an important determining factor at low conversion efficiencies.

In a two crystal OPS, the first crystal emits broadband parametric fluorescence at any frequency and in any direction for which the phase-matching condition is satisfied.[134] Because of ordinary refraction (Snell's Law) at the crystal/air interface of the second surface of the first crystal, the parametric fluorescence and pump beam will be dispersed. The space between the two crystals therefore acts as a spatial filter for spectral components of the parametric fluorescence being dispersed in directions other than that of the pump beam. Only the narrow cone of parametric fluorescence that overlaps the pump beam will be amplified in the second crystal. Therefore the spectral width of the output beam would be expected to decrease as the spacing between the two crystals is increased until the spectral width corresponding to the limit set by the bandwidth for colinear amplification is reached. In the present work (see Table 6), it was found that the spectral width of the output changed very little for crystal spacings greater than 14 cm. Separations greater than 14 cm resulted only in a drop in output energy.

However, because the signal and idler fluorescence walk off the pump beam at the output surface of the first crystal at angles defined by Snell's Law, phase-matching is also possible at other frequencies in these off-axis directions. At an angle α between the pump beam and

signal beam propagation direction, other signal and idler frequencies ($\nu_2(\alpha)$ and $\nu_1(\alpha)$) can be generated. The angle α is estimated from the ratios of the beam diameters to the distance between both crystals, $\alpha \approx d/L$, using the small angle approximation. The frequency difference $\Delta\nu = \nu_2(\alpha) - \nu_2(0)$ may be calculated from equation (60)

$$\Delta\nu = \alpha^2 \frac{\nu_3 n_3 \nu_2}{2(n_2-n_1)\nu_1 n_1 n_2} , \qquad (60)$$

where n, n_2, and n_3 are the indices of refraction of the idler, signal, and pump beams, respectively. For a beam diameter of 0.136 cm and crystal spacing of 15 cm, α = 9.07mrad. At 620nm, 532nm, and 450nm, the values of $\Delta\nu/\alpha^2$ are 0.30 $cm^{-1}/mrad^2$, 0.43 $cm^{-1}/mrad^2$, and 0.64 $cm^{-1}/mrad^2$, respectively. Therefore the corresponding spectral bandwidth contributions at the above wavelengths due to off-axis parametric amplification are 24.7 cm^{-1}, 35.4 cm^{-1}, and 52.7 cm^{-1}, respectively. Spectral widths of this magnitude were never observed in the present work. Off-axis parametric amplification does not seem to have a significant contribution to the spectral quality of the device described here.

The effect of the bandwidth of the pump pulse on the frequency width of the signal or idler pulse is estimated as follows. In the range of large exponential amplification [$(2bz\sqrt{I_3}) \approx 30$], because of the square root dependence or I_3 in the exponent of equation (50), a decrease by five percent in pump intensity leads to a reduction in signal intensity by a factor of two. Also, assuming a Gaussian frequency distribution of the pump pulse, the frequency width at five

percent below the maximum of the distribution is approximately 0.3 times the Gaussian half width, $\Delta\nu_3$. Considering the fact that a change in frequency in the forward beam propagation direction gives a certain phase mismatch ($\Delta K \neq 0$ in equation (48)), with a corresponding reduction in amplification, the following expression can be derived[32]

$$\Delta\nu_2 = \Delta\nu_3 \times 0.3 \times \frac{n_3-n_1}{n_2-n_1} , \qquad (61)$$

where $\Delta\nu_2$ and $\Delta\nu_3$ are the bandwidths of the signal and pump beam, respectively, and n_1, n_2, and n^3 are the indices of the idler, signal, and pump beams, respectively. Values of $\Delta\nu_2/\Delta\nu_3$ for 620nm, 532nm, and 450nm are 0.129, 0.0986, and 0.0634, respectively. If the bandwidth of the pump beam is approximately 3 cm^{-1}, clearly then the contribution of the pump beam bandwidth is clearly negligible over the entire tuning range. At 620nm, 532nm, and 450nm, the effect is 0.39 cm^{-1}, 0.29 cm^{-1}, and 0.19 cm^{-1}, respectively.

All of the above physical mechanisms can contribute to the spectral width of the parametric outputs. However, a lower limit of what the spectral width can actually be must be defined. The lower limit is defined by the uncertainty principle and is the Fourier transform of the temporal profile. Again, for Gaussian pulse shapes, $\Delta\nu\Delta\tau \leq 0.44$. The only pulses observed in the present work near the transform-limit are those attained at low conversion efficiencies. The visible output pulses at higher conversion efficiencies are far from the transform-limit, having both longer pulse durations and

broader spectral bandwidths. The longer pulse duration have already been attributed to pump pulse depletion.

At low conversion efficiencies, the finite divergence of the pump beam, and the phase mismatch, seem to be the dominating factors. The spectral width predicted by these mechanisms agree quite well with what is actually observed throughout the tuning curve. At higher conversion efficiencies, the major contributing factor seems to be the phase mismatch ($\Delta K \neq 0$). The phase mismatches arising only from the large parametric amplification seem to underestimate the observed spectral width by approximately a factor of two, while the off-axis parametric amplification phase mismatch overestimates the frequency spreading by factors ranging from 2 to 5 depending on the part of the tuning range under consideration. From the results of the crystal spacing versus spectral width measurements (Table 6) and from the fact that the spectral widths do broaden at high conversion efficiencies one is lead to the conclusion that these two factors are important in determining the spectral width at high conversion efficiencies. This ties in with the concept of pump pulse depletion playing an important role in determining the output spectrum. The phase mismatch ($\Delta K \neq 0$) at high parametric gains allows frequencies not at the center of the gain ($\Delta K \neq 0$) to be amplified at the expense of the central frequencies. Thus pump pulse depletion results in the enhanced relative amplification of the wings of the spectral distribution.

The phase-matching condition, $\Delta K \neq 0$, not only plays a key role in determining the spectral properties of the OPS output beam, but is

also very important in determining the spatial properties of the beam. From the above discussion it is evident that the spatial divergence of the OPS output beam is determined by both crystal separation and by noncolinear phase-matching. In the first crystal the parametric fluorescence occur as a cone with a relatively large divergence, resulting in a broad frequency spread due to off-axis phase-matching. In the second crystal amplification occurs only for those frequency components of the initial emission which are contained in the narrow pump beam. This results in signal and idler beams of small divergence and a narrow frequency width.

Noncolinear phase-matching appears to be the dominant effect in determining the shape of the final parametric beams. The visible output beam does not have the round shape that would be expected if the spatial filtering effect due to crystal separation were the main factor in determining the beam shape. Instead, the signal beam has a crescent shape characteristic of a section of a noncolinear phase-matching cone. Noncolinear phase-matching effects have been used to explain[135,136] the observance of cones of light produced during second harmonic generation experiments.[137] The mixing of off-axis light rays with the intense on-axis laser beam produces second harmonic rays in a locus of directions corresponding to those for which phase-matching can occur. This results in cones of second harmonic light produced that are observed as rings either concentric with or offset from the central second harmonic beam depending on the phase-matching angle.

The same concepts can be applied to optical parametric amplification to explain the crescent shape of the output beam by assuming the off-axis light results from parametric amplification of light scattered into the phase-matched directions that still overlap the pump beam. A locus of directions defining a noncolinear phase-matching cone can be understood from a geometrical construction based on equation (43).[135,136]

With the above discussion in mind, the expectation of spectral inhomogeneities through the beam profile is not unreasonable if spatial broadening occurred throughout the crystal pair, since off-axis parametric amplification would occur for many of the frequency elements of the broadband parametric fluorescence. However, since careful investigation of the spectrum of selected portions of the OPS output beam showed no evidence of spectral inhomogeneities, it appears that spatial broadening occurs in the second crystal, after the spatial and spectral filtering effects of crystal separation (i.e. aperture effect) take place.

The crescent shape of the OPS output may be pictured as arising from the cross section of the noncolinear phase-matching cone defined by the overlap with the pump beam propagation direction. The crescent shape is observed when viewing the visible output beam in the plane perpendicular to the direction of beam propagation. The more divergent parts of the output beam that define the crescent shape are clearly visible to the eye. However, the energy content of these parts is no more than a few percent of the total power of the output.

Therefore it is safe to conclude that the majority of the output results from colinear parametric amplification and not from amplification of scattered light.

The bulk of the output power is concentrated in an oblong central spot that has a measured divergence of 0.6mrad in the plane defined by the crystal optic axis and the direction of propagation, and 1.2mrad in the perpendicular plane. This is in good agreement with the estimated divergence of $\theta = \frac{a}{L} = 0.73$mrad, where a is the pump beam diameter (0.136 cm) and L is the crystal length including crystal separation (18.7 cm).

Using the value of the measured divergence and extrapolating the beam back through the length of the crystals and crystal spacing implies that the parametric output arises from approximately a point source near the front surface of the first crystal. This is quite a reasonable conclusion considering that the spontaneous parametric emission arises from the annihilation of a 355nm photon at the most intense part of the pump beam. The subsequent amplified parametric output results from the coincidental traversal of the photon pairs with the pump beam along the entire length of both crystals. By placing a lens at one focal length distance from the front surface of the first crystal, it is possible to compensate for the beam divergence. For instance, using a 40 cm focal length lens, a collimated beam was maintained over several meters with a beam diameter of approximately 3mm.

It should be noted that the OPS beam is also very focusable. The tunable visible output, when combined at the focus with the second harmonic output of the mode-locked Nd:YAG laser has produced CARS signals in N_2, O_2, and from various vibrational levels of the ground electronic state of I_2 vapor.

The discussion of the observed performance characteristics of the OPS would not be complete if the origins of the seemingly random fluctuations in energy and the observed temporal, spectral, and spatial substructures were not mentioned. Even though the central frequency of the output spectra stays constant, the complex substructure varies from shot to shot. The temporal profile and spatial properties also vary from shot to shot. This is true even for an essentially constant pump energy, temporal width, and spatial intensity distribution. Only when the OPS is tuned to produce signal and idler beams coincident with the second and first harmonic of the mode-locked Nd:YAG laser do these fluctuation cease to exist.

Other than at 532nm where "seed" photon effects are observed, the amplified parametric output results from amplification of quantum noise associated with spontaneous parametric fluorescence. In a single pass, travelling wave, picosecond pumped OPS, within the limited duration of the pump pulse, the parametric amplifier is not able to achieve a steady-state oscillation (without resonator feedback). The OPS output therefore consists primarily of amplified quantum noise, and is thus proportional to the average intensity of the quantum noise.[26,134] The ultimate stability of the OPS is

limited to the fluctuations of the quantum noise. The fluctuations associated with the quantum noise are zero point fluctuations in the spectral, spatial, and temporal distributions of the spontaneous parametric fluorescence. The fluctuations are readily observable at low and high conversion efficiencies and are manifested as what seems to be the random appearance and disappearance of different modes in the visible output spectrum. Since the zero point fluctuations are a direct result of the quantum mechanical decay process, they are inherent in any optical parametric source, unless a well-formed seed pulse is used, as is observed when the OPS is tuned to produce visible output at 532nm.

The almost periodic substructure in the spectra of the visible output of the OPS at high conversion efficiencies (Figure 39) varies from pulse to pulse, but is always present. The periodicity in the substructure is most probably an interference effect arising from the fact that the pump pulse is self-phase modulated.[137]

F. Conclusion

The OPS described here has proven to be a simple and reliable source of tunable visible and near-infrared light. By taking advantage of the large peak intensities available from the active/passive mode-locked Nd:YAG laser, the spectral versatility of the system has been extended many-fold. The device has already been used in investigations involving time-resolved emission spectroscopy[38,39] and coherent Raman spectroscopy. Tunable ultraviolet light has been produced by simply frequency doubling the visible output in a Type I KDP crystal in the range of 250nm to 325nm. By summing the tunable visible or infrared output with the fundamental or second harmonic of the Nd:YAG laser, respectively in a Type II KDP crystal, the wavelength range between 316nm and 404nm can be generated. With one simple two crystal OPS, the spectral capabilities of a mode-locked Nd:YAG laser have been extended from the four harmonics of the fundamental radiation to nearly continuous tunability from 1670nm to 250nm (a gap exists from 780nm to 650nm and 450nm to 404nm).

The frequency doubled output of the OPS at 266.7nm is currently being used as a two-photon-resonant, three photon ionization probe of bromine atoms in the carbon-bromine bond cleavage occurring in the secondary dissociation of bromo-iodo-ethane (CH_3CHBrI). The CH_3CHBrI is initially excited with the fourth harmonic (266nm) of the laser. By doing a pump-probe experiment, the time-resolved, secondary dissociation dynamics of CH_3CHBrI will be investigated according to

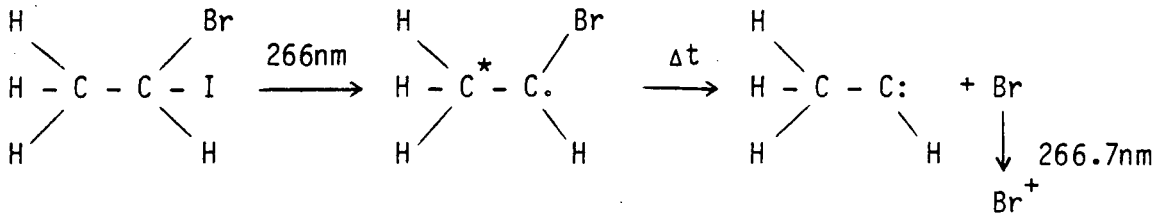

(62)

Besides the experiment discussed above, the laser system is now being used to conduct other experiments on fundamental studies of unimolecular reaction dynamics. In connection with these experiments the versatility of the two crystal OPS has and will be exploited. Using the exact same two crystals in the same phase-matching configuration, high-energy, tunable, near-infrared output in the range of 800nm to 1400nm has been generated by using the second harmonic (532nm) as the pump source. The tuning curves and output energies versus wavelength are shown in Figure 44.[43] Even though the tuning range for this parametric interaction is contained within the range of the near-infrared output attainable from the 355nm OPS, the output energies achievable pumping with 532nm are significantly higher. The two reasons for this are that it is easier to generate second harmonic light than it is to generate third harmonic light because one less conversion step is necessary, and because the handling and manipulation of the visible pump beam is easier than that of the ultraviolet pump since nonlinear materials and optics are less susceptable to damage by visible radiation.

In the study of the unimolecular reaction dynamics of the chloroethyl radical formed by the photodissociation of chloro-iodo-ethane

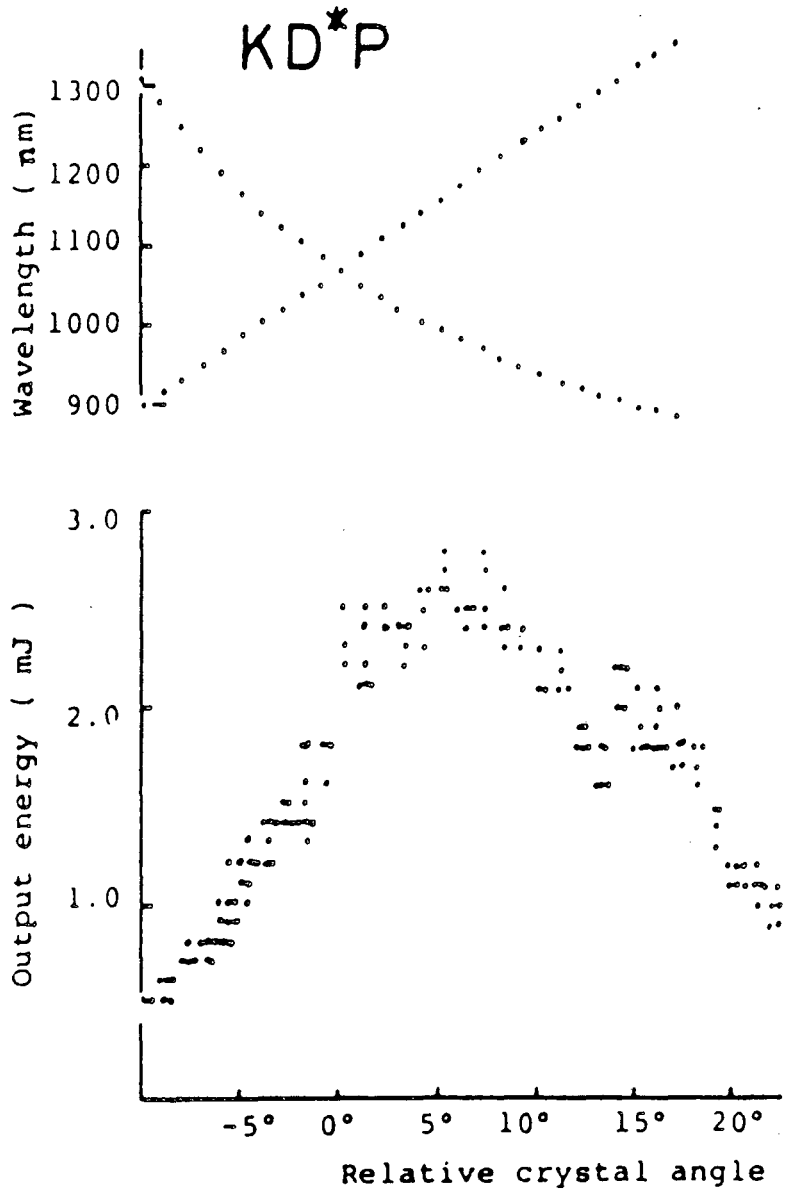

Dependence of wavelengths and spectral widths of SH-OPOA on the rotation angles of KD*P.

XBL 866-2179

Fig. 44. The tuning curve and output energy versus wavelength for a second harmonic (532nm) pumped Type II (e-oe interaction) OPS (from reference 44).

(CH_3CHClI), the utility of the second harmonic pumped OPS is twofold. The experiment involves using the tunable output of the 532nm pumped OPS to excite the second and third overtone of the C-H stretching vibrational mode (ν_3) in the chloroethyl radical. The wavelengths needed for these excitations are approximately 1150nm and 860nm, respectively. Both these excitation wavelengths have sufficient energy to cause cleavage of the carbon-chlorine bond. Then by mixing the output of another second harmonic pumped OPS with the hydrogen Raman shifted fourth harmonic (266nm -> 299nm) in a Type I KDP crystal, tunable ultraviolet radiation in the range 227nm to 245nm can be generated.[45] Ultraviolet light at 234nm will be used for the two-photon resonant, three-photon ionization of the chlorine atom from the dissociation of the radical. By delaying the probe (UV) pulse with respect to the pump (near-infrared) pulse a determination of the dissociation time can be made. This experiment will be a direct measurement of the time it takes vibrational energy to transfer from one part of a molecule to another. Using these results, insight into the possibilities and limitations of mode-selective chemistry might be ascertained. The experiment looks like the following,

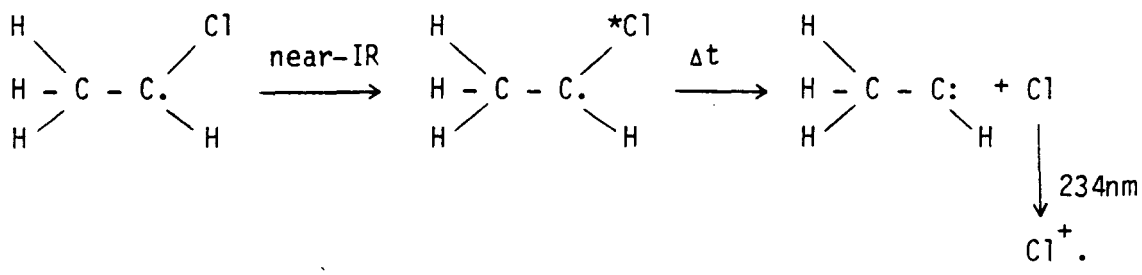

(63)

The ultraviolet range of 222nm to 232nm can be generated in a similar fashion by summing the tunable near-infrared output with the nitrogen Raman shifted fourth harmonic (266nm → 283nm) in a Type I KDP crystal. The extension of the spectral range of the picosecond pulses beyond 266nm to higher energy ultraviolet radiation will have great utility in the study of unimolecular reaction dynamics and vibrational energy transfer in which the tunable ultraviolet radiation can be used as a resonant multiphoton ionization probe. Also, by frequency tripling these wavelengths in rare gases, tunable vacuum ultraviolet (VUV) radiation can be generated for photoionization experiments. The high intensity, picosecond pulses are extremely well suited for VUV generation.[31]

The above discussion concerning the variety of spectral ranges attainable by employing various optical parametric sources and frequency summing schemes using high intensity picosecond sources is very tantalizing. The question arises then of why these tunable sources have not been exploited to the fullest extent in investigations of ultrashort dynamics and spectroscopy. The answer lies not in materials availability or the complexity of the device, but in the fact that until recently, and without a great deal of work, stable, reliable pumping sources have not been available. The key to the reliable operation of the OPS has been the reliability of the active/passive pulsed mode-locked Nd:YAG laser used as the pumping source. This is evidenced by the fact that researchers have been using high intensity, mode-locked solid-state lasers to study

parametric interactions in nonlinear materials since the late 1960's.[29,30,117,121,131,138-141] However, only recently have these devices begun to play an active role in the study of picosecond dynamics,[32,38,39,111-114,132,142-145] primarily due to the advances made in mode-locked solid-state laser engineering. Even with the enhanced performance characteristics of the pump lasers used in optical parametric conversion, use of such devices will be limited due to the advances in commercially available tunable picosecond and subpicosecond dye lasers.[146]

Even for relatively stable pump pulses, the output of the OPS shows some fluctuations in temporal, spectral, and spatial profiles. Since these instabilities are associated with the zero point fluctuations of the quantum noise from the spontaneous parametric fluorescence which is being amplified, they are inherent to the system and unavoidable under the present setup. Therefore future work might be directed at developing a suitable "seed" photon source. The source should have an output consisting of a narrow spectral band, short, KW/cm^2 pulse. One possibility for such a source could be the stimulated emission from a second or third harmonic pumped laser dye which could be grating tuned. Another possibility for seed photons is the Stokes and anti-Stokes components of stimulated Raman scattering occurring in various liquids pumped by the harmonics of the Nd:YAG fundamental. Perhaps even the dispersed output of another OPS could be used as the narrow band source. Any of these devices need only a small pumping energy to achieve the peak intensities needed for the "seed" source.

Besides extending the spectral range of the mode-locked solid-state laser used as the pump, an optical parametric device extends the temporal resolution due to the observed pulse shortening at low conversion efficiencies. However, at the higher conversion efficiencies inherent at the center of the tuning range, the pulse shortening is obliterated by pump pulse depletion. For many experiments shorter pulses with high energies are needed. Therefore it would be convenient to simultaneously achieve high conversion efficiencies and significant pulse shortening. A novel approach to such a problem has been suggested by Fendt et. al.[147] whereby an optical parametric generator-amplifier system is employed. The two crystal generator supplies a well defined input pulse at the signal frequency and is amplified in the one crystal amplifier choosing a judiciously shaped pump pulse. Pulse shortening occurs by adjusting the time delay between the input signal pulse and the pump pulse using a variable delay line. The technique requires properly shaped pump pulses to the amplifier stage. Pulse shaping is achieved by passage of the pump pulse through a saturable absorber.

The method, as is the case for all optical parametric devices, benefits from the steep slopes of the pulses generated in a high gain parametric interaction, but suffers from broadening effects of pump pulse depletion if very large pump intensities are used, and from group velocity dispersion. However, if proper care is maintained, then efficient generation of short pulses can be achieved. For instance, Fendt et. al.[147] generated 0.5ps, nearly transform-limited

pulses with energy conversions exceeding 5 percent when pumping with an 8ps fundamental pulse from a mode-locked Nd:Glass laser. Similar techniques could be employed for optical parametric devices using different harmonics as pump sources to achieve very short, high energy pulses in different spectral ranges, and should be considered to extend the temporal resolution of the OPS considered presently.

The ideas mentioned involving methods of improving the spectral and temporal characteristics of the tunable outputs without significantly increasing the complexity of the device are suggested as future work. Other possibilities also exist. However, it should be emphasized that the device "as is" is a highly reliable, simple method of generating continuously tunable picosecond pulses over a broad range that can be used for many experiments.

V. Rotational Reorientation Dynamics of Rhodamine 6G as a Function of Excitation Wavelength

A. Introduction:

Studies of the rotational motion of molecules in solution have been used in the past to aid in the understanding of the interactions between molecules and their solvent environment.[37,38,148-156] Rotational reorientation measurements have also been used as a probe to elucidate specific solute characteristics such as molecular shape, charge, and vibrational relaxation times and mechanisms.[157-163] Also, because molecular reorientation is the limiting process for low gain laser dye ampliers, knowledge of the rotational reorientation times is important in determining storage efficiencies for dye laser amplifier schemes.[164]

A variety of experimental techniques have been used in these studies including both nanosecond and picosecond time-resolved fluorescence depolarization, absorption recovery, and transient gratings. While these methods are quite different, the solute molecules under investigation have been very similar. Medium size xanthene dye molecules are a popular choice due to their large absorption cross sections, large fluorescence quantum yields, and easy availability. Furthermore, within the xanthene dye family there are various isomers whose absorption and emission wavelengths are within spectral regions which are easily accessible with readily available lasers and detection schemes. While the conclusions drawn from the results of the previous studies have been in agreement, the validity

of making comparisons between studies in which different experimental techniques have been employed has never been thoroughly investigated.

One major bone of contention among the interpretation of previous experiments is the influence of excitation wavelength on the measurements of rotational reorientation kinetics. The possibility exists that certain molecules have rotation times that are sensitive to the excitation wavelength in emission experiments,[153-155,158,162] or to the probe wavelength in absorption recovery experiments.[160,163] It is easy to understand the wavelength dependence if it results from excitation into different electronic states that have transition moments oriented in different directions. In an asymmetric molecule, excitation with different wavelengths would sample different components of the rotational diffusion tensor and anisotropic rotational reorientation times would be measured.

A more subtle and interesting question arises in understanding the variation of rotational behavior with excitation wavelength when excitation occurs to different vibrational levels within the same electronic manifold. Similar to the case of accessing different electronic stats, deviations in the direction of the transition moment with vibrational level would cause changes in measured rotational times for asymmetric molecules. Another mechanism which might result in a wavelength dependence of the rotational dynamics of the solute molecule is the amount of energy being deposited into the local solvent environment due to vibrational relaxation. The sudden energy dissipation could possibly induce a local temperature change resulting

in localized viscosity perturbations. It is well known that viscosity plays an important role in rotational reorientation dynamics.[37]

Previous investigations have not provided sufficient insight to thoroughly evaluate the effect of wavelength or the rotational behavior of xanthene dyes in solution. Therefore the comparisons of different experimental studies is not really valid. The combination of time-resolved emission spectroscopy using an ultrafast streak camera[35,36] with the broadly tunable picosecond source[165] described in the previous chapter as the excitation souce allowed for the systematic investigation of the effect of excitation wavelength on the dynamics of rotational motion of the xanthene dye rhodamine 6G(R6G) in ethanol to be undertaken.

B. Experimental:

The technique of picosecond, time-resolved fluorescence depolarization using an excitation source which was continuously tunable across the majority of the visible spectra ration made this experiment extremely facile and swift. The experimental apparatus is shown in Figure 45 and is described in detail elsewhere.[35,36,165] Briefly, the optical parametric source (see Chapter IV for details) was pumped by approximately 1 mJ of the 355 nm third harmonic of a single, amplified pulse of an active/passive mode-loced Nd:YAG laser system identical to the one described in Chapters II and III. For the present experiments the OPS output pulses typically contained between 50 mJ and 100 mJ in energy and were betwen 10 ps and 15 ps in duration. The excitation wavlengths selected for this study were 464nm, 476nm, 495nm, 503nm, 510nm, 532nm, and 545nm. Figure 46 shows the absorption and emission spectra for R6G in ethanol. Note that the selected wavelengths span the abosprtion spectrum of the ground state of R6G.

An ultrafast streak camera (Hadland Photonics Imacon 500) with linear photodiode array readout (Tracor Northern IDARSS) was used to time resolve the emission. The sample was excited with vertically polarized light and the emission was monitored through a Glan-Taylor prism polarizer to select polarizations at the desired orientation. The emission was measured at polarization parallel, perpendicular, and 54.7 degrees with respect to the vertical input polarization. The latter orientation is chosen because all rotational artifacts

Fig. 45. The schematic diagram of the experimental setup for picosecond time-resolved fluorescence depolarization measurements.

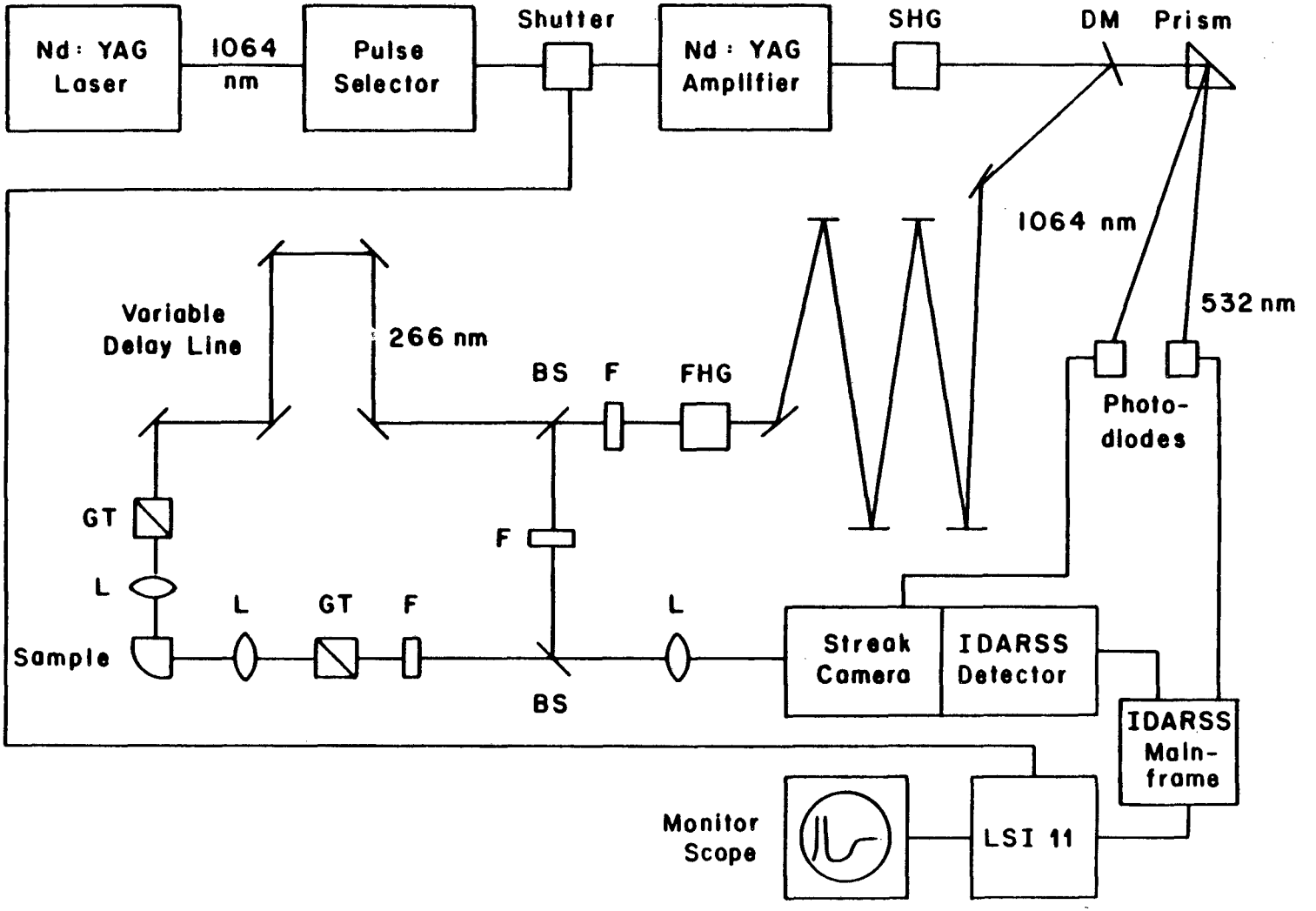

Fig. 45

XBL 866-2237

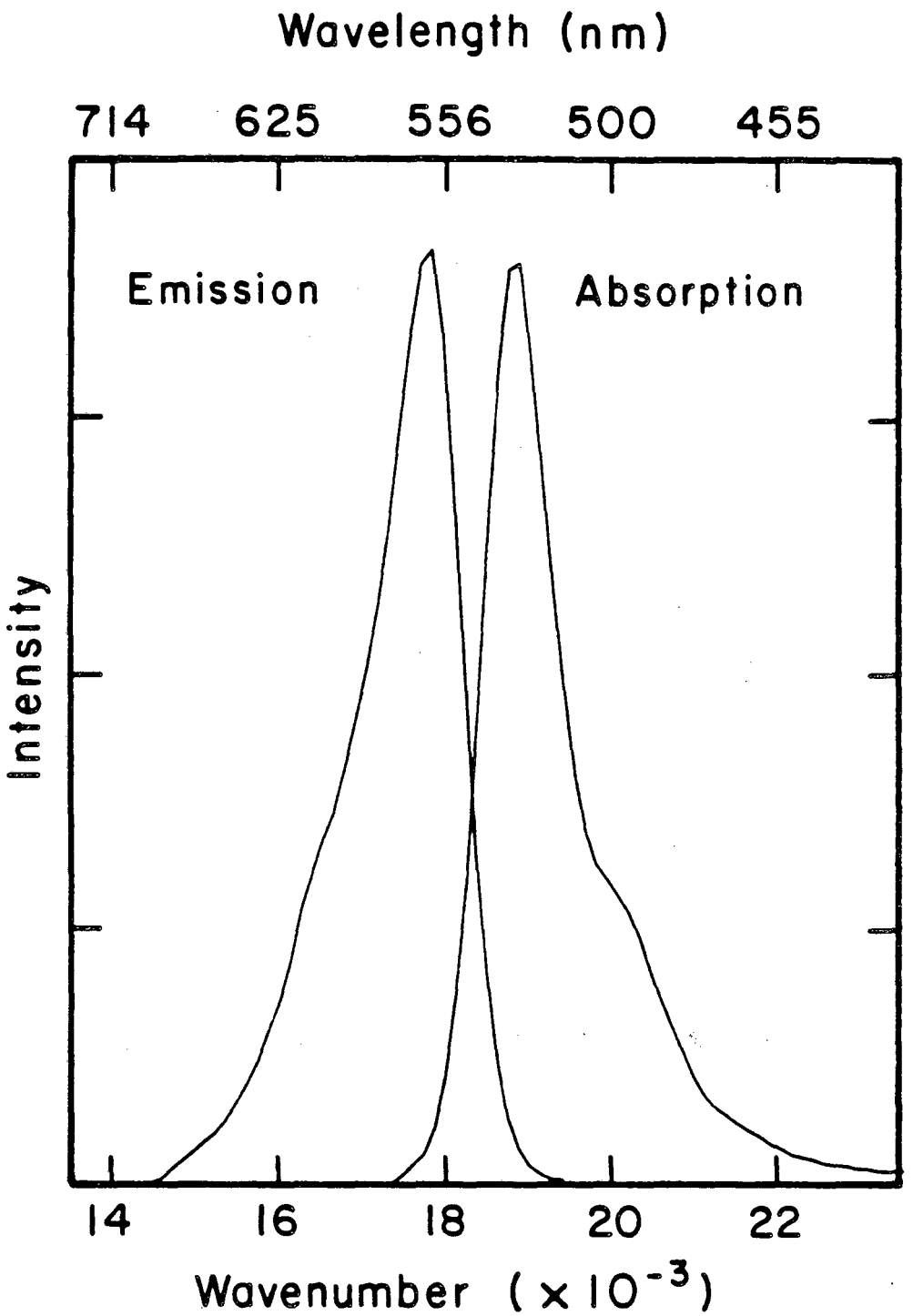

XBL 866-2182

Fig. 46. The absorption and emission spectra of Rhodamine 6G in ethanol.

disappear at this angle (thus denoted the "magic" angle) and therefore can be used as a check to see that no experimental artifacts such as stimulated emission are occurring.

Each data set is an accumulation of between 200 and 500 laser shots. For all excitation wavelengths, the emission was passed through high pass cut off filters (Schott KV550) before detection. An example of the vertical and horizontal components of the emission using 476 nm excitation pulses is shown in Figure 47. The vertical and horizontal components were normalized by the procedure of tail matching[151] at times longer than the given rotational lifetimes. The rotational anisotropy, r(t), was derived from the vertical and horizontal components by standard methods[166] and is given by

$$r(t) = \frac{I_{||}(t)-I_{\perp}(t)}{I_{||}(t)+2I_{\perp}(t)} \tag{64}$$

Using the expression

$$r(t) \propto e^{-t/\tau} \tag{65}$$

the rotational reorietnation time can be established.

A diagram of the fluorescence depolarization concept is shown in Figure 48. Briefly, at time zero (t=0) excitation occurs preferentially to molecules with transition moments oriented vertically resulting in the creation of an anistropic distribution of excited state species. At early time (i.e. times short compared to rotational reorientation times), emission is rich in the vertical component. As the molecules rotate, the horizontal components grows in and the

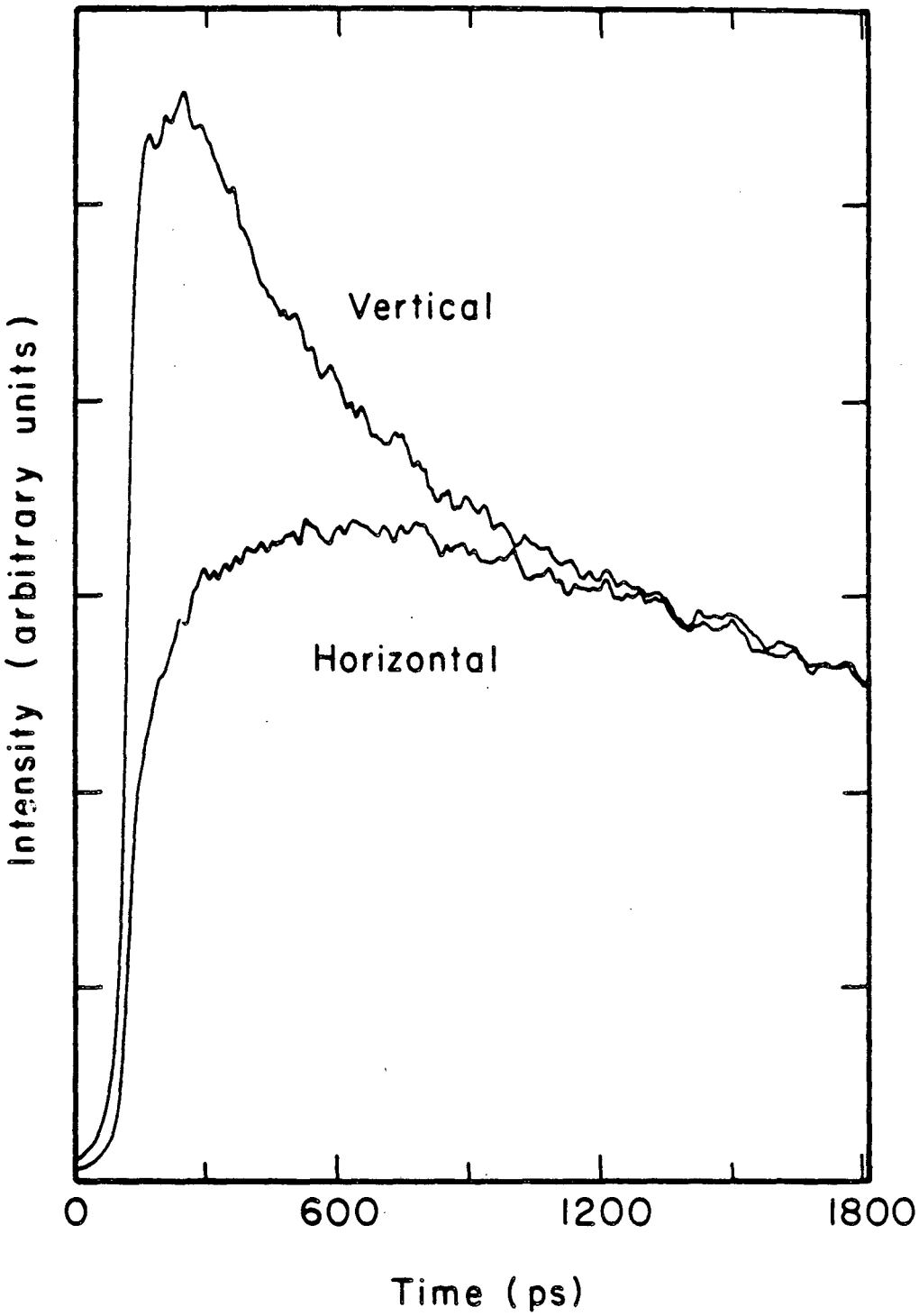

XBL 866-2180

Fig. 47. The vertical and horizontal components of the emission using 476nm as the excitation wavelength.

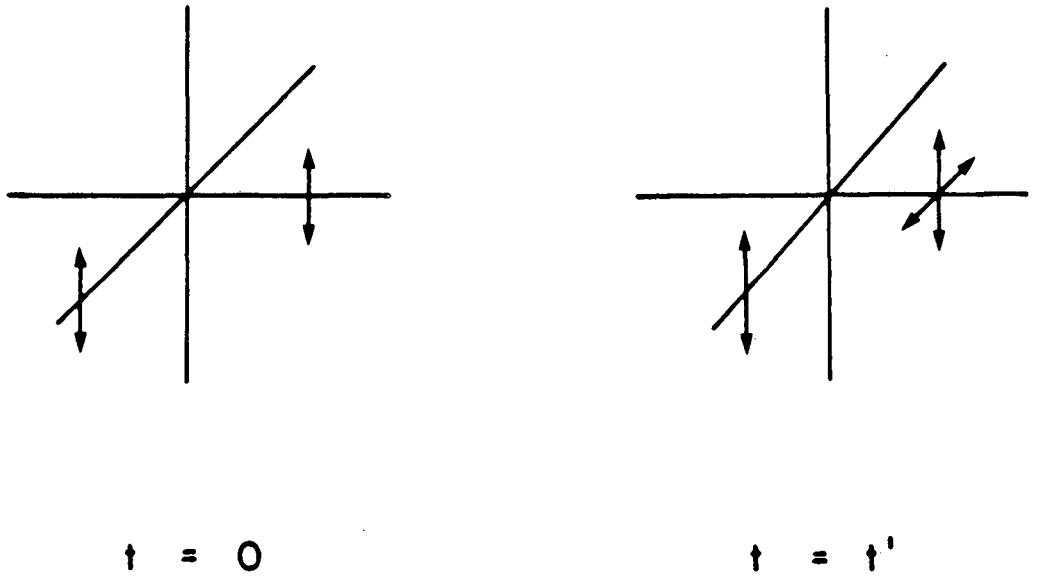

XBL 866-2172

Fig. 48. The time-resolved fluorescence depolarization concept.

vertical component decays. At times long compared to the rotational reorientation time (t=t'), the emission is isotropic.

The solutions used for samples in these experiments were prepared using Eastman Kodak Laser Grade R6G and spectral grade ethanols at concentrations of 10^{-6} M. The laser power was sufficiently attenuated to ensure saturation and/or stimulated emission processes were eliminated.

C. Results and Discussion:

Semi-log plots of rotational anisotropy versus time for all the data sets were linear, indicating a single exponential decay. For a symmetric top molecule with its transition moment parallel to its symmetry axis, a single exponential decay is expected. However, for R6G the structure is approximately that of an oblate ellipsoid (see Figure 49), with the transition moment in the plane perpendicular to the symmetry axis. For an oblate top molecule and stick boundary conditions the two unique diffusion constants would be expected to be quite similar.[159] Therefore, it is not surprising that the decays in this study appear to be a single exponential.

A plot of the rotational reorientation time as a function of excitation wavelength is shown in Figure 50. At all wavelengths the fluorescence lifetime was found to be 3.6 ± 0.2 ns and the rotational lifetime is approximately 300 ps. The plot demonstrates that no systematic variation in the rotational reorientation time with excitation wavelength is observed. The uncertainties denoted in Figure 50 are not the standard deviation from the average, but encompass the total estimated random and systematic errors.

As proposed by Heiss et al.,[153] local thermal effects which occur on the timescale of molecular rotation would result in a decrease in the rotational reorientation time with decreasing excitation wavelength. The observation of this effect has been reported previously for R6G as well as for other molecules.[153-155,163]

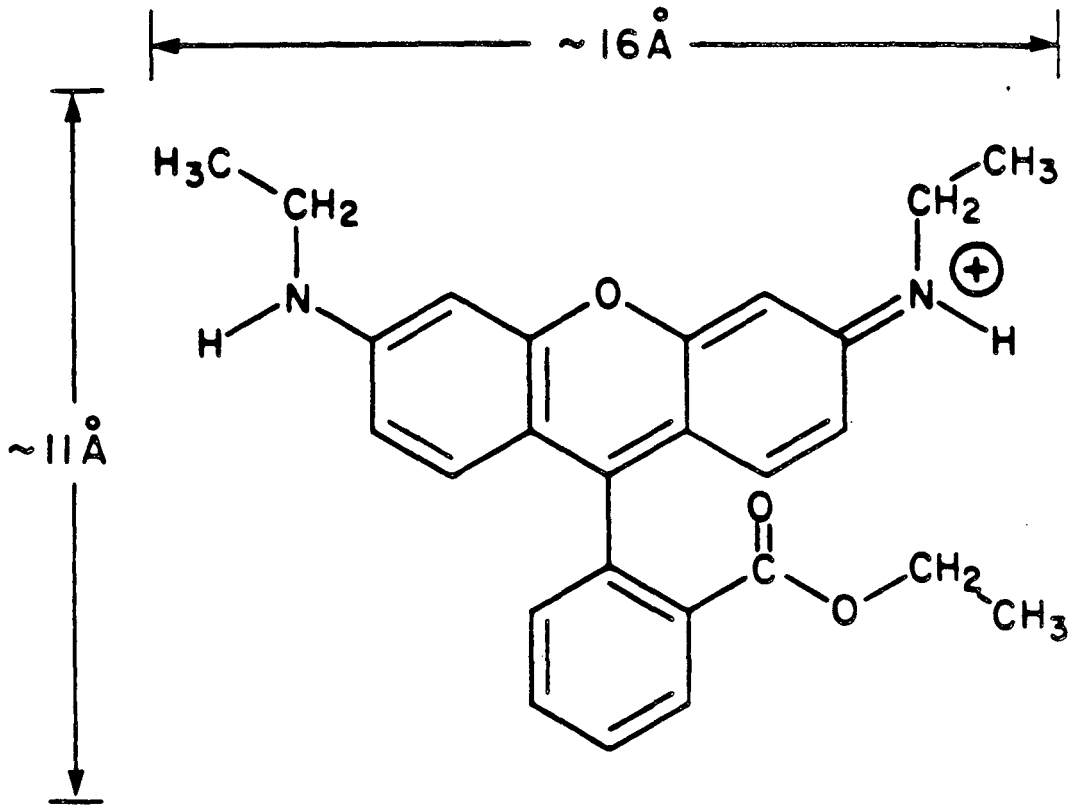

Rhodamine 6G (R6G)

XBL 866-2173

Fig. 49. The molecular structure of Rhodamine 6G.

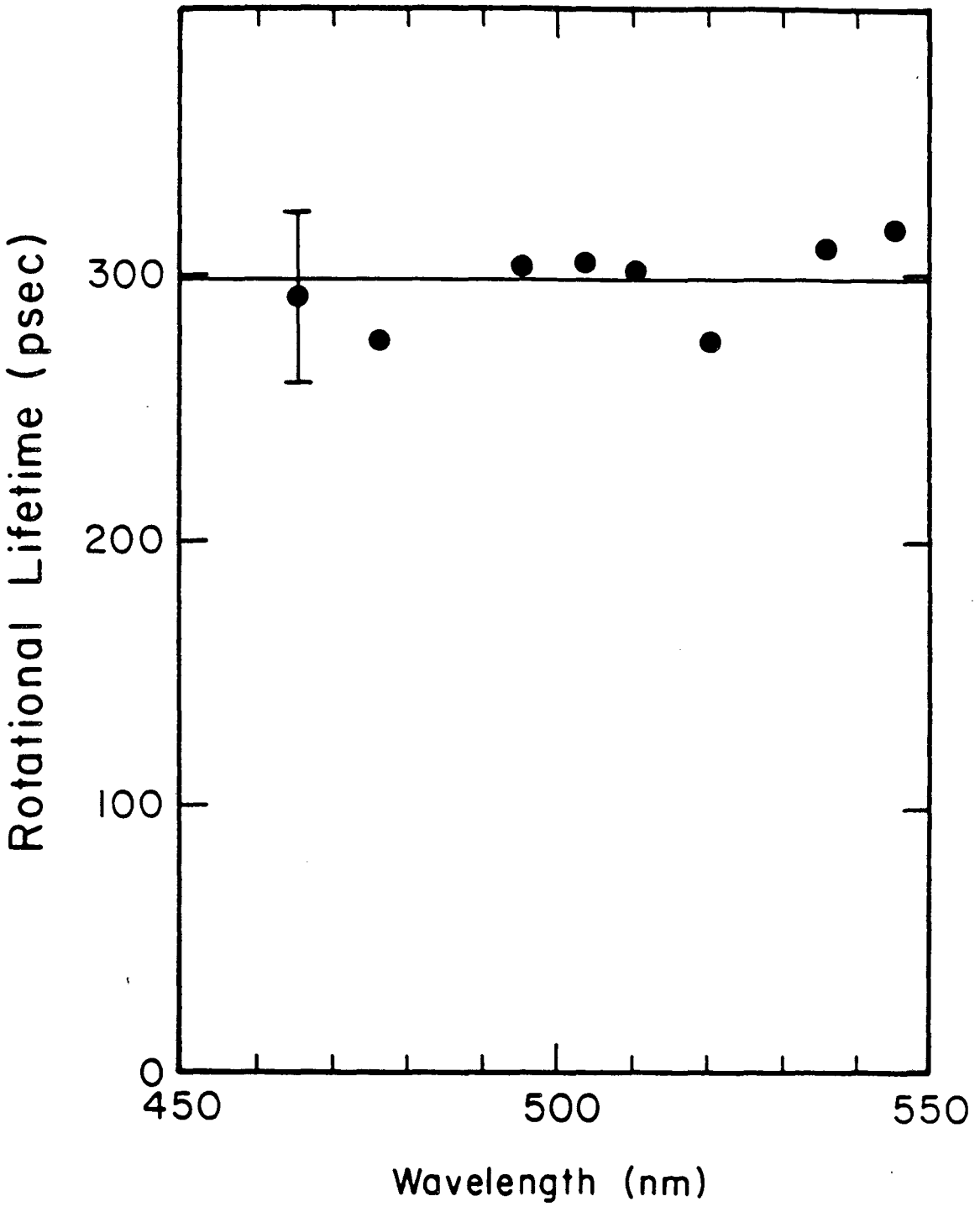

XBL 866-2184

Fig. 50. The plot of the rotational reorientation time versus wavelength.

In earlier investigations however which specifically studied R6G,[153,154] the solvents used had viscosities that were an order of magnitude larger than ethanol. The local heating might be less effective in the less viscous solvents thus leading to the discrepancies reported presently.

In order to understand the disagreement between the present and previous results on other molecules specific molecular geometries must be considered. For example, cresyl violet, studied by Blanchard and Wirth[163] has less symmetry than R6G and must be treated as an asymmetric rotor. For an asymmetric rotor, the function r(t) is described by the sum of these exponentials each of which is a function of the diffusion constants about the different molecular axes. The observed experimental decays however appear to be a single exponential because the sum is dominated by one of the terms. The smaller contributions from the other two terms have the effect of modifying the lifetime of the apparent single exponential decay. Blanchard and Wirth[163] have suggested that different wavelengths access excited vibronic states with varying transition moments. The different transition moments possess different linear combinations of the different exponentials and yield a different measured lifetime for the apparent single exponential decay. However, in R6G the diffusion constants are very similar as mentioned earlier. Therefore when the relative contributions from the two different experimental decays is varied no difference in the measured single exponential decay is detected. Thus variation in anisotropic diffusion would not be

expected to be observed in the measured rotation times of R6G as it is in cresyl violet. The lack of sensitivity of rotational reorientation lifetime of R6G in ethanol to excitation wavelength does not preclude the possibility that the transition moment varies with excitation wavelength. Another measurement was performed to address this issue.

While the results presented in Figure 55 challenge the idea of local thermal melting of the solvent cage on the timescale of molecular rotation, they do not address the effect of heat deposition and dissipation that may occur in a time regime much faster than molecular rotation. If the excess vibrational energy is rapidly released into the local environment and also rapidly dissipated, the rotational lifetimes may not be affected at all. However, the heating caused by the dissipation of the vibrational energy on very short timescales can cause an increased librational motion of the solute. The librational movement looks like a rotational displacement or wag. The effect of this process appears identical to emission from a molecule which has an angle between the absorption and emission transition moments. If librational motion were occurring, the displacement would be greater at shorter wavelengths because more energy would be deposited into the local environment, thus increasing the apparent angle.

An experimental observable which is sensitive to the angle between the absorption and emission dipoles is the value of r(t) at time zero, r(0). Therefore the value of r(0) was measured for the same wavelengths as in Figure 50. A plot of r(0) versus wavelength is

presented in Figure 51. Clearly the value of r(0) is independent of excitation wavelength.

In the case where the absorption and emission transition moments are parallel, the value of r(0) is 0.4.[166] Obviously from Figure 51, the values measured in the present study are below this value. Realize however, that the assignment of time zero is difficult and therefore some systematic error may be present in these measurements. The estimation of the uncertainty in the location of time zero does not exceed ten percent of the measured value. Irregardless of the uncertainty in the measurement, low values of r(0) have been reported previously in the literature,[155,159,161] and have been attributed to angular differences in the excited and ground state transition moments.

Penzkofer and Falkenstein[161] have reported values of r(0) less than 0.4. They claim thay excitation occurs simultaneously to a number of vibronic states that have a distribution of transition moments. Other studies[159] supports the models of Heiss et al.[153] and Zinsli[155] which state that the displacement of the exicted state transition moment is the result of short time librational motion of the solute induced by local thermal effects. However, as is the case for longer time scales, local thermal effects on short time scales would be sensitive to excitation wavelength. At shorter wavelengths, excitation would populate states with higher vibrational energy in the electronic manifold. The excess vibrational energy would be dissipated in the local environment leading to higher local temperatures, and

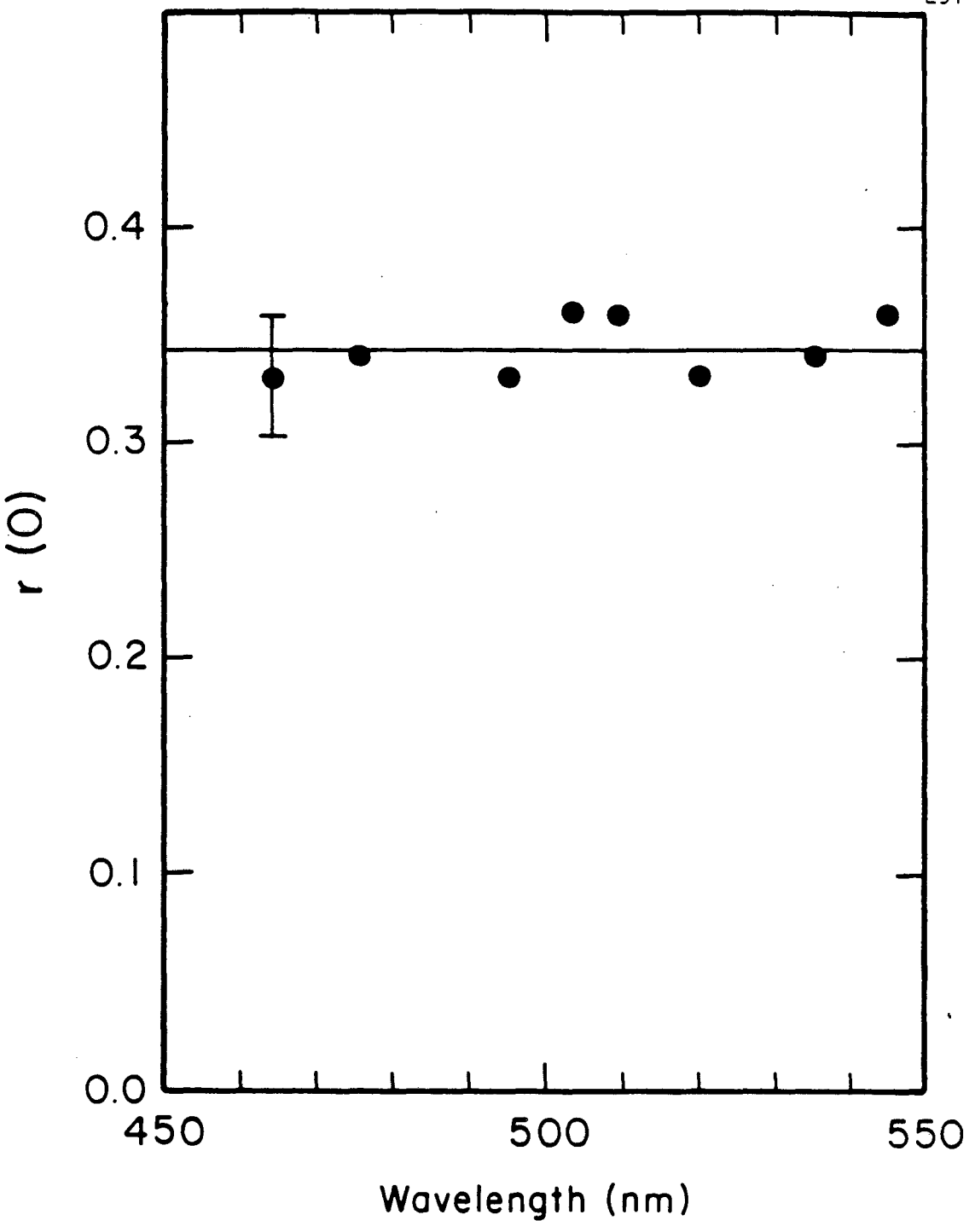

XBL 866-2181

Fig. 51. The plot of the rotational anisotropy at time zero versus wavelength.

therefore larger rotational displacements due to the librational movement. This wavelength dependence of r(0) is not evident in Figure 56.

D. Conclusion:

The results revealed presently demonstrate that the variation of excitation wavelength does not affect the dynamics of rotational motion of R6G in ethanol solutions. Similarities in behavior manifested for symmetric, oblate, cationic, xanthene dyes in solutions suggest that the present results should be applicable to a range of other dye molecules in low viscosity solutions. These results also support the comparability of the results of experimental investigations which involve different excitation wavelengths. Most importantly, the fact that constant values of rotational reorientation lifetime and r(0) with excitation wavelength are measured argues against either long-lived (on the scale of rotational lifetimes) or short-lived local heating effects playing a role in the determination of rotational behavior in solution.

Appendix I.

To calculate energy area under a Gaussian curve, $e^{(-r^2/r^2_o)}$, when

$r = r_o$ $[(1-1/e)x100]\%$ = 63.2% of the energy

$r = 2r_o$ $[(1-1/e^4)x100]\%$ = 98.2% of the energy

$r = 3r_o$ $[(1-1/e^9)x100]\%$ = 99.99% of the energy.

Let $r_{max} = 3r_o$ (assume 10.0 mJ and 9.99 mJ are indistinguishable). Then find r where 90% of energy is located, i.e. $r = nr_o$.

$$[1 - 1/e^{n^2})] = 0.9$$

$$-e^{-n^2} = -0.1$$

$$-e^{-n^2} = 0.1 = 1/10$$

$$-n^2 = -\ln 10$$

$$n^2 = \ln 10$$

$$n = 1.517$$

Therefore, 90% of the energy is contained in a beam with radius $r = 1.517r_o$.

$$\frac{\text{Area}(90\%)}{\text{Area}(\text{max})} = \frac{\pi(1.517r_o)^2}{\pi(3r_o)^2} = \frac{(1.517)^2}{9} = 25.57$$

Thus, for a Gaussian beam, 90% of the energy is contained in 25.6% of the beam's area.

REFERENCES

1. W. Koechner, Solid State Laser Engineering, Springer Series in Optical Sciences, Editor D. L. MacAdam, Vol. 1 (1976).

2. Ultrashort Light Pulses, Picosecond Techniques and Applications, Edited by S. L. Shapiro, Chapters 2 and 4.

3. W. Graener and A. Laubereau, Opt. Commun. 37(2), 138 (1981).

4. H. Nathel, D. M. Guthals, D. W. Anthon, and J. H. Clark, J. Opt. Soc. Amer. 73(12), 42 (1984). H. Nathel, D. M. Guthals, and J. H. Clark, Proceedings from the Conference on Lasers and Electro-Optics (June 1984), Anaheim, California, paper Th144.

5. A. Lewis and J. T. Knudtson, Appl. Opt. 21(16), 2897 (1982).

6. H. P. Kortz, IEEE J. QE-19, 4 (1983).

7. V. V. Korobkin, A. A. Malyutin, and A. M. Prokhorov, ZHETFP Red. 12(5), 216 (1970).

8. M. A. Duguay, J. W. Hansen, and S. L. Shapiro, IEEE J. QE-6(11), 725 (1970).

9. R. C. Eckhardt, C. H. Lee, and J. N. Bradford, Appl. Phys. Lett. 19(10), 420 (1971). R. C. Eckhardt, C. H. Lee, and J. N. Bradford, Opto-Electr. 6, 67 (1974).

10. D. Von der Linde, IEEE J. QE-8(3), 328 (1972).

11. D. J. Bradley and W. Sibbett, Opt. Commun. 9(1), 17 (1973).

12. W. Zinth, A. Laubereau, and W. Kaiser, Opt. Commun. 22(2), 161 (1977).

13. J. R. Taylor, W. Sibbett, and A. J. Cormier, App. Phys. Lett. 31(3), 184 (1977).

14. J. A. Giordmaine, M. A. Duguay, and J. W. Hansen, IEEE J. QE-4(5), 252 (1968).

15. E. B. Treacy, Phys. Lett. 28A(1), 34 (1968). E. B. Treacy, IEEE J. QE-5(9), 454 (1969).

16. M. A. Duguay and J. W. Hansen, Appl. Phys. Lett. 14(1), 14 (1969).

17. A. Laubereau, Phys. Lett. 29A(9), 539 (1969).

18. F. Gires and P. Tournois, Compt. Rend. Acad. Sci. (Paris), Vol. 258, 6112-6115 (June 1964).

19. J. Desbois, F. Gires, and P. Tournois, IEEE J. QE-9(2), 213 (1973).

20. R. W. Lehmberg and J. M. McMahon, Appl. Phys. Lett. 28(4), 2041 (1978).

21. N. Nakatsuki and D. Grischowsky, Appl. Phys. Lett. 42(1), 1 (1983).

22. C. V. Shank, R. L. Fork, R. Yen, R. H. Stolen, and W. J. Tomlinson, Appl. Phys. Lett. 40(9), 761 (1982).

23. B. Nikolaus and D. Grischkowsky, Appl. Phys. Lett. 42(1), 1 (1983).

24. R. L. Herbst, R. N. Fleming, and R. L. Byer, Appl. Phys. Lett. 25, 520 (1974).

25. R. L. Byer, R. L. Herbst, and R. N. Fleming, Proc. Second, Int. Conf. on Laser Spectroscopy, Megeve, France, 1974, Berlin:Springer, 206 (1975).

26. J. A. Giordmaine and R. C. Miller, Phys. Rev. Lett. 14, 973 (1961).

27. D. Magde and H. Mahr, Phys. Rev. Lett. 18, 905 (1967).

28. J. M. Yarborough and G. A. Massey, Appl. Phys. Lett. 18, 438 (1971).

29. K. P. Burneika, M. V. Ignatavichus, V.I. Kabelka, A. S. Piskarskas, and A. Y. Stabinis, JETP Lett. 16(7), 257 (1972).

30. A. Laubereau, L. Greiter, and W. Kaiser, Appl. Phys. Lett. 25, 87 (1974).

31. A. Kung, Appl. Phys. Lett. 25, 653 (1974).

32. A. Selmeier and W. Kaiser, Appl. Phys. 23, 113 (1982).

33. G. A. Massey, J. C. Johnson, and R. A. Elliot, IEEE J. QE-12, 143 (1976).

34. R. A. Baumgartner and R. L. Byer, IEEE J. QE-15, 432 (1979).

35. S. P. Webb, S.W. Yeh, L.A. Philips, M. A. Tolbert, and J. H. Clark, Rev. Sci. Instrum., to be published.

36. S. P. Webb, Ph.D. Thesis, University of California, Berkeley, April 1985.

37. L. A. Philips, Ph.D. Thesis, University of California, Berkeley, April 1985.

38. L. A. Philips, S. P. Webb, H. Nathel, and J. H. Clark, Chem. Phys. Lett., to be submitted.

39. A. N. Glaser, S. W. Yeh, S. P. Webb, and J. H. Clark, Science, 227, 419 (1985).

40. H. P. Kortz, A. J. Cox, G. W. Scott, D. M. Guthals, H. Nathel, S. W. Yeh, S. P. Webb, and J. H. Clark, IEEE J. QE-21(11), 1795 (1985).

41. D. J. Nagel, M. C. Peckerar, H. Nathel, M. S. Helfand, D. M. Guthals, and J. H. Clark, Proceedings of the 1984 International Symposium on Electron, Ion, and Photon Beams (Tarreytown, New York, May 29-June 1, 1984).

42. F. Wondrazek, A. Selmeier, and W. Kaiser, Appl. Phys. B 32, 39 (1982).

43. Y. Takagi, M. Sumitani, N. Nakashima, and K. Yoshihara, Rev. Laser Eng. (in Japanese) 10, 419 (1982).

44. D. A. Agelov, G. G. Gurzadyund, and D. N. Nikogosyan, Sov. J. Quantum Electron. 9, 1334 (1979).

45. Y. Takagi, M. Sumitani, N. Nakashima, D. V. O'Connor, and K. Yoshihara, Appl. Phys. Lett. 42(6), 489 (1983).

46. A. Wokaun, P. F. Liao, R. R. Freeman, and R. H. Storz, Opt. Lett. 7, 13 (1982).

47. T. L. Koch, L. C. Chiu, A. Yariv, Opt. Commun. 40(5), 364 (1982).

48. H. Vanherzeele, H. J. Mackey, and J. C. Diels, Appl. Opt. 23, 2056 (1984).

49. I.N. Duling III, T. Norris, T. Sizer II, P. Bado, and G. A. Morou, JOSA B 2(4), 616 (1985).

50. K. S. Choi and M. R. Topp, Picosecond Phenomena (eds. E. P. Ippen, C. V. Shank, and S. L. Shapiro), Springer Series in Chemical Physics, Vol. 4, pp.12-16 (1980). K. S. Choi and M. R. Topp, J. Opt. Soc. Amer. 75(5), 520 (1981).

51. C. W. Brito Cruz, F. De Martini, H. L. Fragnito, and E. Palange, Opt. Commun. 40(4), 298 (1982).

52. W. Koechner, Solid-State Laser Engineering, Springer Series, in Optical Sciences, Editor, D. L. MacAdam, Vol. 1, Chapter 9 (1976).

53. H. W. Mocker and R. J. Collins, Appl. Phys. Lett. 7, 270 (1965).

54. A. J. DeMaria, D. A. Stetser, and H. Heyman, Appl. Phys. Lett. 8, 174 (1966).

55. J. A. Fleck, Phys. Rev. B 1, 84 (1970).

56. V. S. Letokhov, Sov. Phys. JETP 28, 562 (1969). V. S. Letokhov, Sov. Phys. JETP 28, 1026 (1969).

57. B. C. Johnson and W. D. Fountain, Tech. Digest, Int. Electron Devices Meeting, 322 (1974).

58. S. Kishida and T. Yamane, Opt. Commun. 18, 19 (1976).

59. W. Seka and J. Bunkenburg, J. Appl. Phys. 49, 2277 (1978).

60. A. E. Siegman and D. J. Kuizenga, Appl. Phys. Lett. 14, 181 (1969). A. E. Siegman and D. J. Kuizenga, IEEE J. QE-6, 694 and 709 (1970). A. E. Siegman and D. J. Kuizenga, Opto-Electr. 6, 43 (1974).

61. D. J. Kuizenga, D. W. Phillion, T. Lund, and A. E. Siegman, Opt. Commun. 9, 221 (1973).

62. D. J. Kuizenga, D. W. Phillion, and A. E. Siegman, IEEE J. QE-10, 721 (1974).

63. G. F. Albrecht and J. Bunkenburg, Opt. Commun. 38, 377 (1981).

64. R. Harrach and G. Kachen, J. Appl. Phys. 39,. 2482 (1968).

65. H. Weichel, J. Appl. Phys. 44, 3635 (1973).

66. P. N. Everett, Rev. Sci. Instrum. 41, 1495 (1970).

67. A. R. Clobes and M. J. Brienza, IEEE J. OE-6, 65 (1970).

68. J. P. Letellier, NRL Mem. Report 2684, NRL Washington D.C. (1973).

69. D. J. Bradley, G. H. C. New, and S. J. Caughey, Opt. Commun. 2, 41 (1970).

70. D. Von der Linde and K. F. Rogers, IEEE J. QE-9, 960 (1973).

71. L. M. Osternik and J. D. Foster, Appl. Phys. Lett. 12(4), 128 (1968).

72. Operation and Maintenance Manual for YG400, Quantel International, Santa Clara, California.

73. A. Yariv, Quantum Electronics, Second Edition, Chapters 11 and 14, Wiley, New York (1975).

74. R. C. Hyer, H. D. Sutphin, and K. R. Winn, Rev. Sci. Instrum. 46(10), 1333 (1975).

75. D. J. Kuizenga, Opt. Commun. 22(2), 256 (1977).

76. R. R. Cubeddu and O. Svelto, IEEE J. QE-5, 495 (1969).

77. W. H. Glenn and M. J. Brienza, Appl. Phys. Lett. 10(8) 221 (1967).

78. S. L. Shapiro and M. A. Duguay, Phys. Lett. 28A 20, 698 (1969).

79. D. J. Bradley, G. H. C. New, and S. J. Caughey, Phys. Lett. 30A(2), 78 (1969).

80. R. C. Eckhardt, IEEE J. QE-10(1), 48 (1974).

81. R. B. Cheseler and J. Geusic, Laser Handbook, Vol. 1, editors F. T. Arecchi and E. O. Shulz-Desbois (North Holland, Amsterdam, 1972) p.325-368.

82. R. C. Miller, Phys. Lett. 28A(5), 177 (1968).

83. J. Comly and E. Garmire, Appl. Phys. Lett. 12(1), 7 (1968).

84. W. H. Glenn, IEEE J. QE-5(6), 289 (1969).

85. M. W. McGeoch, Opt. Commun. 7, 116 (1973).

86. D. Von der Linde and K. F. Rodgers, Opt. Commun. 8, 91 (1973).

87. P. C. Magnante, J. Appl. Phys. 40, 4437 (1969).

88. G. I. Kachen and J. O. Kysilka, IEEE J. QE-6, 84 (1970).

89. R. R. Alfano and S. L. Shapiro, Phys. Rev. Lett. 24(11), 592 (1970).

90. R. R. Alfano, L. L. Hope, and S. L. Shapiro, Phys. Rev. A6(1), 433 (1972).

91. W. Yu, R. R. Alfano, C. L. Sam, and R. J. Seymour, Opt. Commun. 14(3), 344 (1975).

92. R. Fischer and W. Bischel, Appl. Phys. Lett. 24, 468 (1974). R. Fischer and W. Bischel, IEEE J. QE-11, 46 (1975).

93. J. A. Vladmanis, R. L. Fork, and J. P. Gordon, Opt. Lett. 10(3), 131 (1985).

94. A. J. Duercinckx, H. A. Vanherzeele, J. L. van Eck and A. E. Siegman, IEEE J. QE-14(12), 983 (1978).

95. A. J. Duercinckx, J. Opt. Soc. Amer. 66, 1074 (Abstract TuC18) 1976.

96. J. P. Laussade and A. Yariv, Appl. Phys. Lett. 13, 2 (1968).

97. J. C. Comly, A. Yariv, and E. M. Garmire, Appl. Phys. Lett. 15, 5 (1969).

98. R. A. Fisher, P. L. Kelley, and T. K. Gustafson, Appl. Phys. Lett. 14, 4 (1969).

99. T. Tomie and M. Yano, Technical Digest of the Conference on Lasers and Electro-Optics (CLEO), 126 (1985).

100. T. Tomie, Japan J. Appl. Phys. 9, 1008 (1985).

101. A. E. Siegman, private communication.

102. J. E. Murray and W. H. Lowdermilk, Picosecond Phenomena, edited by C. V. Shank, E. P. Ippen, and S. L. Shapiro, 281-283 (Springer, New York, 1978).

103. J. E. Murray and D. J. Kuizenga, Appl. Phys. Lett. 37(1), 27 (1980).

104. D. M. Guthals, L. A. Philips, and J. H. Clark, private communication.

105. C. H. Brito Cruz, F. De Martini, and P. Matoloni, IEEE J. QE-19(9), 573 (1983).

106. C. H. Brito Cruz, E. Palange, and F. De Martini, Opt. Commun. 39(3), 331 (1981).

107. D. Huppert and P. M. Rentzepis, Appl. Phys. Lett. 32(4) 241 (1978).

108. R. L. Fork, B. I. Greene, and C. V. Shank, Appl. Phys. Lett. 38, 671 (1978).

109. Z. I. Ivanova, V. Kabelka, S. A. Magnitski, A. Piskarskas, V. Smilǵyavichyus, N. M. Rubinina, and V. G. Tunkin, Sov. J. Quant. Electron. 7(11), 1414 (1977).

110. A. Fendt, W. Kranitzky, A. Laubereau, and W. Kaiser, Opt. Commun. 28(1), 142 (1979).

111. P. G. Kryukov, Y. A. Matveets, D. N. Nikogosyan, A. V. Sharkov, E. M. Gordeev, and S. D. Franchenko, Sov. J. Quant. Electron. 7(1), 127 (1977).

112. R. Danelyus, G. Dikchyus, V. Kabelka, and A. Piskarskas, Sov. Phys. Tech. Lett. 22(5), 642 (1977).

113. B. Bareika, G. Dickchyus, E. D. Isyanova, A. Piskarskas, and V. Sirutkaitis, Sov. Tech. Phys. Lett. 6(6), 301 (1980).

114. T. Elsaesser, A. Seilmeier, and W. Kaiser, Opt. Commun. 44(4), 293 (1983).

115. G. A. Massey and R. A. Elliot, IEEE J. QE-74, 899 (1974).

116. K. Kato, IEEE J. QE-11, 939 (1975).

117. T. A. Rabson, J. J. Ruiz, P. L. Shah, and F. K. Tittel, Appl. Phys. Lett. 21(4), 129 (1972).

118. R. Danelyus, A. Piskarskas, and V. Sirutkaitis, Sov. J. Quantum Electron. 12, 1616 (1982).

119. P. Kryukov, Yu. Matveets, D. Nikogosyan, and A. Sharkoy, Sov. J. Quantum Electron. 8, 1319 (1978).

120. V. Kabelka, A. Kutka, A. Piskarskas, V. Smilǵyavichyus, and Ya. Yasevichyute, Sov. J. Quantum Electron. 9, 1022 (1979).

121. A. Akmanov, S. Akmanov, R. Khokhlov, A. Kovrigin, A. Piskarskas, and V. Sukhorukov, IEEE J. QE-4(11), 828 (1968).

122. R. Danelyus, V. Kabelka, A. Piskarskas, and V. Smilgyavichyus, Sov. J. Quantum. Electron. 8, 398 (1978).

123. R. S. Craxton, Opt. Commun. 34, 474 (1980).

124. W. Seka, B. D. Jacobs, J. E. Rizzo, R. Buni, and R. S. Cruxton, Opt. Commun. 34, 469 (1980).

125. F. Zernike, J. Opt. Soc. Amer. 54, 1215 (1964).

126. P. A. Franken, A. E. Hill, C. W. Peters, and G. W. Weinreich, Phys. Rev. Lett. 77, 118 (1961).

127. J. A. Armstrong, N. Bloembergen, J. Ducuing, P. S. Pershan, Phys. Rev. 14, 1918 (1962).

128. A. Yariv, Quantum Electronics, Second Edition, Chapters 16 and 17, Wiley, New York (1975).

129. V. I. Bespalov, I. A. Batreva, L. A. Dmitrenko, V. V. Korolikhin, S. P. Kuznetsov, and M. A. Novikov, Sov. J. Quantum Electron. 7, 885 (1977).

130. H. Bergner, V. Brückner, and B. Schröder, Sov. J. Quantum Electron. 11(7), 952 (1981).

131. W. H. Glenn, Appl. Phys. Lett. 11(11), 333 (1967).

132. R. Danelyus, G. Dikchyus, V. Kabelka, A. Piskarskas, A. Stabinis, and Ya. Yasevichyute, Sov. J. Quantum Electron. 7, 1360 (1977).

133. A. M. Wiener, IEEE J. QE-19, 1276 (1983).

134. T. Gallorenzi and C. L. Tang, Phys. Rev. 166, 225 (1968).

135. H. E. Bates, J. Opt. Soc. Amer. 61(7), 904 (1971).

136. H. E. Bates, J. Opt. Soc. Amer. 63(2), 146 (1973).

137. B. Schroder, Opt. Commun. 49(1), 75 (1984).

138. S. A. Akmanov, A. I. Kovrigin, A. P. Sukhorukov. R. V. Khoklov, and A. S. Chirkin, JETP Lett. 7(7), 237 (1968).

139. S. A. Akmanov, A. S. Chirkin, K. N. Drabovich, A. I. Kovrigin, R. V. Khokhlov, and A. P. Sukhorokov, IEEE J. QE-4(10), 598 (1968).

140. J. A. Armstrong, S. S. Jha, and N. S. Shiren, IEEE J. QE-6(2), 123 (1970).

141. G. A. Bukavkas, V. I. Kabelka, A. S. Piskarskas, and A. Yu. Stabinis, Sov. J. Quantum Electron. 4(3), 290 (1974).

142. G. Dikchyus, R. Danelyus, V. Kabelka, A. Piskarskas, T. Tomkyavichyus, and A. Stabinis, Sov. J. Quantum Electron. 6(4), 425 (1976).

143. R. Gadonas, R. Danelyus, and A. Piskarskas, Sov. J. Quantum Electron. 11(3), 407 (1981).

144. R. Danelyus, A. Piskarskas, and V. Sirutkaitis, Sov. J. Quantum Electron. 12(12), 1626 (1982).

145. P. G. Kryukov, Yu. A. Matveets, D. N. Nikogosyan, and A. V. Sharkov, Sov. J. Quantum Electron. 8(11), 1319 (1978).

146. Spectra-Physics Series 3000 CW Mode-locked and Mode-locked Q-switched Nd:YAG laser and Spectra-Physics Model 375B Synch Pumped Dye Laser Brochure.

147. A. Fendt, W. Kranitzky, A. Laubereau, and W. Kaiser, Opt. Commun. 28(1), 142 (1979).

148. K. G. Spears and L. E. Cramer, Chem. Phys. 30, 245 (1979).

149. D. P. Millar, R. Shah, and A. H. Zewail, Chem. Phys. Lett. 66, 345 (1979).

150. T. J. Chuang and K. B. Eisenthal, Chem. Phys. Lett. 11, 368 (1971).

151. G. R. Fleming, J. M. Morris, and G. W. Robinson, Chem. Phys. 17, 91 (1976).

152. R. S. Moog, M. D. Ediger, S. G. Boxer, and M. D. Fayer, J. Chem. Phys. 86, 4694 (1984).

153. A. Heiss, F. Dorr, and I. Kuhn, Ber. Bunsenges. 79, 294 (1975).

154. M. Schulz, K. Teuchner, M. Nather, W. Becker, and S. Dahne, ACTA Phys. Pol. A54, 823 (1978).

155. P. E. Zinsli, Chem. Phys. 20, 299 (1977).

156. A. von Jena and H. E. Lessing, Chem. Phys. 40, 245 (1979).

157. A. von Jena and H. E. Lessing, Chem. Phys. Lett. 78, 187 (1981).

158. E. R. Pantke and H. Labhart, Chem. Phys. Lett. 23, 476 (1973). E. R. Pantke and H. Labhart, Chem. Phys. Lett. 23, 482 (1973).

159. A. von Jena and H. E. Lessing, Ber. Bunsengens., Phys. Chem. 83, 181 (1979).

160. V. Sundstrom. T. Gillbro, and H. Bergstrom, Chem. Phys. 73, 439 (1982).

161. A. Penzkofer and W. Falkenstein, Chem. Phys. Lett. 44, 547 (1976).

162. M. D. Barkley, A. A. Kowalczyk, and L. Brand, J. Chem. Phys. 75, 3581 (1981).

163. G. J. Blanchard and M. J. Wirth, J. Chem. Phys. 82, 39 (1985).

164. T. Sizer II, J. D. Kafka, I. N. Duling III, C. W. Gabel, and G. A. Morou, IEEE J. QE-19(4), 506 (1983).

165. D. M. Guthals, H. Nathel, D. W. Anthon, C. C. Hayden, and J. H. Clark (to be submitted).

166. T. Tao, Biopolymers 8, 609 (1969).

This report was done with support from the Department of Energy. Any conclusions or opinions expressed in this report represent solely those of the author(s) and not necessarily those of The Regents of the University of California, the Lawrence Berkeley Laboratory or the Department of Energy.

Reference to a company or product name does not imply approval or recommendation of the product by the University of California or the U.S. Department of Energy to the exclusion of others that may be suitable.

TECHNICAL INFORMATION DEPARTMENT
LAWRENCE BERKELEY LABORATORY
UNIVERSITY OF CALIFORNIA
BERKELEY, CALIFORNIA 94720